Report No. FHWA-KS-14-02 ▪ FINAL REPORT▪ August 2014

Verification of Mechanistic-Empirical Design Models for Flexible Pavements through Accelerated Pavement Testing

Stefan Romanoschi, Ph.D., P.E.
Paul Lewis
Daba Gedafa
Mustaque Hossain, Ph.D., P.E..

Kansas State University Transportation Center

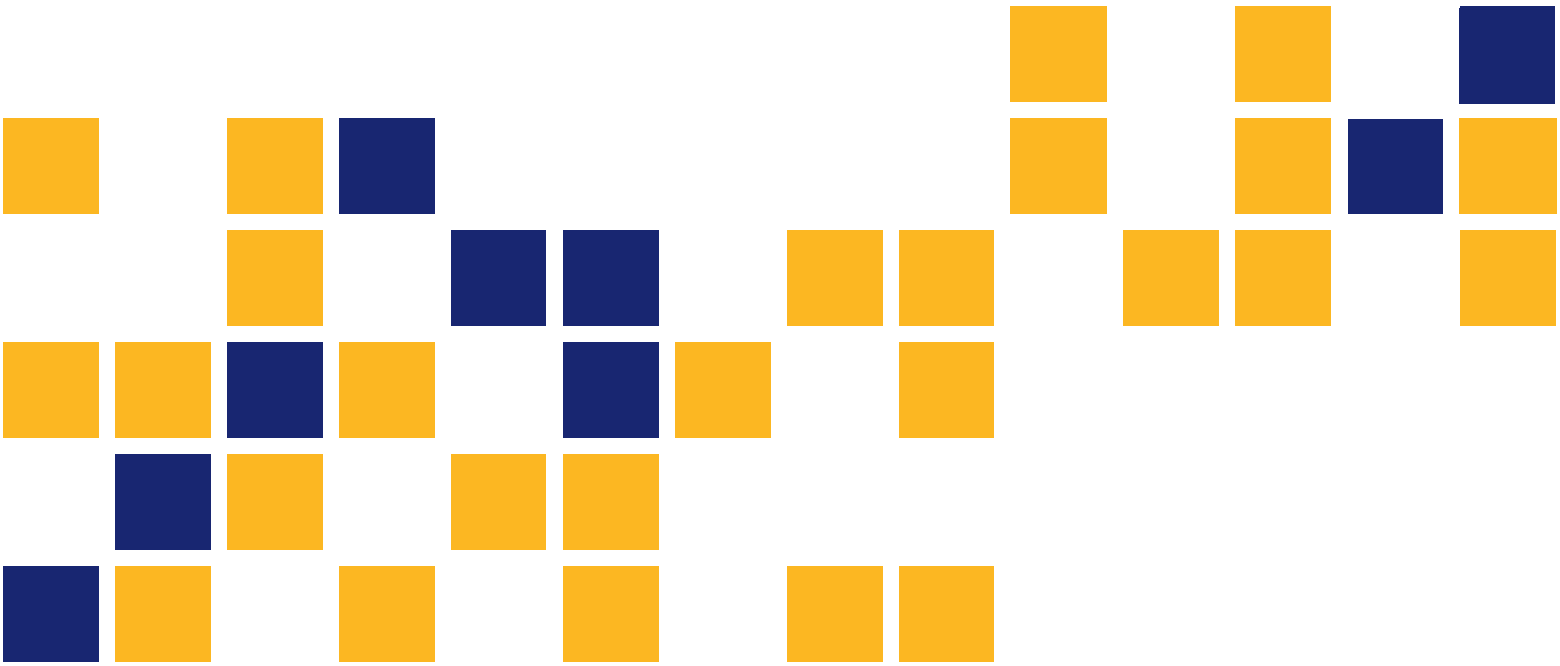

Kansas Department of Transportation

This page intentionally left blank.

1 Report No. FHWA-KS-14-02	**2 Government Accession No.**	**3 Recipient Catalog No.**
4 Title and Subtitle Verification of Mechanistic-Empirical Design Models for Flexible Pavements through Accelerated Pavement Testing		**5 Report Date** August 2014 **6 Performing Organization Code** TPF-5(048)
7 Author(s) Stefan Romanoschi, Ph.D. P.E., Paul Lewis, Daba Gedafa, and Mustaque Hossain, Ph.D., P.E.		**7 Performing Organization Report No.**
9 Performing Organization Name and Address Kansas State University Transportation Center Department of Civil Engineering 2118 Fiedler Hall Manhattan, Kansas 66506		**10 Work Unit No. (TRAIS)** **11 Contract or Grant No.** C1516
12 Sponsoring Agency Name and Address Kansas Department of Transportation Bureau of Research 2300 SW Van Buren Topeka, Kansas 66611-1195		**13 Type of Report and Period Covered** Final Report April 2005 – December 2010 **14 Sponsoring Agency Code** RE-0508-01/RE-0328-01
15 Supplementary Notes For more information write to address in block 9. Prepared for Midwest States Accelerated Pavement Testing Pooled Fund Program under TPF-5(048). Sponsored by Iowa, Kansas and Missouri DOTs.		

The Midwest States Accelerated Pavement Testing Pooled Fund Program, financed by the highway departments of Kansas, Iowa, and Missouri, has supported an accelerated pavement testing (APT) project to validate several models incorporated in the NCHRP 1-37A design method, popularly known as Mechanistic-Empirical Pavement Design Guide (MEPDG) for flexible pavements. The following models were investigated: the dynamic modulus estimation model, the relationship between the dynamic modulus and the pavement response; and the relationship between the pavement response (strains) and pavement performance. In addition to these, the experiment aims to compare the performance of the coarse and fine Superpave mixes, and to validate and calibrate the Asphalt Pavement Analyzer (APA) and Hamburg Wheel-Tracking Device Tester as screening tools for estimating rutting performance of Superpave asphalt mixes.

The experiments were conducted at the Civil Infrastructure Systems Laboratory at Kansas State University. The test program consisted of constructing 12 flexible pavement structures and subjecting them to full-scale accelerated loading tests. The experiment found that the revised Witczak model predicts the dynamic modulus of asphalt concrete mixes with reasonable accuracy. The MEPDG structural response model under-predicted the longitudinal strains at the bottom of the asphalt concrete layers, while the MEPDG over-predicted the permanent deformation in the asphalt layer. The comparison between the results of the laboratory rutting tests performed at 35°C indicate that results of the Hamburg Wheel Rut Test correlate best with results of the APT experiment, followed by those from the APA.

17 Key Words Mechanistic-Empirical Pavement Design Guide, MEPDG, Superpave, Asphalt Pavement Analyzer, Testing, Mix Design		**18 Distribution Statement** No restrictions. This document is available to the public through the National Technical Information Service www.ntis.gov.	
19 Security Classification (of this report) Unclassified	**20 Security Classification (of this page)** Unclassified	**21 No. of pages** 194	**22 Price**

Form DOT F 1700.7 (8-72)

This page intentionally left blank.

Verification of Mechanistic-Empirical Design Models for Flexible Pavements through Accelerated Pavement Testing

Final Report

Prepared by

Stefan Romanoschi, Ph.D. P.E.
Paul Lewis
Daba Gedafa
Mustaque Hossain, Ph.D., P.E.
Kansas State University Transportation Center

A Report on Research Sponsored by

THE KANSAS DEPARTMENT OF TRANSPORTATION
TOPEKA, KANSAS

and

KANSAS STATE UNIVERSITY TRANSPORTATION CENTER
MANHATTAN, KANSAS

August 2014

NOTICE

The authors and the state of Kansas do not endorse products or manufacturers. Trade and manufacturers names appear herein solely because they are considered essential to the object of this report.

This information is available in alternative accessible formats. To obtain an alternative format, contact the Office of Public Affairs, Kansas Department of Transportation, 700 SW Harrison, 2nd Floor – West Wing, Topeka, Kansas 66603-3745 or phone (785) 296-3585 (Voice) (TDD).

DISCLAIMER

The contents of this report reflect the views of the authors who are responsible for the facts and accuracy of the data presented herein. The contents do not necessarily reflect the views or the policies of the state of Kansas. This report does not constitute a standard, specification or regulation.

Abstract

The Midwest States Accelerated Pavement Testing Pooled-Fund Program, financed by the highway departments of Kansas, Iowa, and Missouri, has supported an accelerated pavement testing (APT) project to validate several models incorporated in the NCHRP 1-37A design method, popularly known as Mechanistic-Empirical Pavement Design Guide (MEPDG) for flexible pavements. The following models were investigated: the dynamic modulus estimation model, the relationship between the dynamic modulus and the pavement response; and the relationship between the pavement response (strains) and pavement performance. In addition to these, the experiment aims to compare the performance of the coarse and fine Superpave mixes, and to validate and calibrate the Asphalt Pavement Analyzer (APA) and Hamburg Wheel-Tracking Device Tester as screening tools for estimating rutting performance of Superpave asphalt mixes.

The experiments were conducted at the Civil Infrastructure Systems Laboratory at Kansas State University. The test program consisted of constructing 12 flexible pavement structures and subjecting them to full-scale accelerated loading tests. The experiment found that the revised Witczak model predicts the dynamic modulus of asphalt concrete mixes with reasonable accuracy. The MEPDG structural response model under-predicted the longitudinal strains at the bottom of the asphalt concrete layers, while the MEPDG over-predicted the permanent deformation in the asphalt layer. The comparison between the results of the laboratory rutting tests performed at 35°C indicate that results of the Hamburg Wheel Rut Test correlate best with results of the APT experiment, followed by those from the APA.

Acknowledgements

The research project was selected, designed, and monitored by members of the Midwest States Accelerated Pavement Testing Pooled-Fund Technical Committee. The committee included Mr. Andy Gisi, Kansas Department of Transportation, chair; Mr. John Donahue, Missouri Department of Transportation; and Mr. Mark Dunn, Iowa Department of Transportation. The authors acknowledge the cooperation and supervision of all committee members in this study. Contributions of Mr. Miguel Portillo, Mr. Tito Nyamuhokya, and Mr. Cristian Dumitru in various phases of this study are also gratefully acknowledged. The research team is also grateful to Sergeant Joe French, from the Motor Vehicle Inspection Division of the Kansas Highway Patrol, for his help in the measurement and calibration of the Civil Infrastructure Systems Laboratory (CISL) axle load.

Table of Contents

List of Tables

List of Figures

Chapter 1: Introduction and Background

1.1 Report Organization

This is the final report that describes the research project conducted under the Kansas Department of Transportation (KDOT) Contract titled, "Midwest Accelerated Testing-Pooled Fund – FY 2005 to 2007," also known as Kansas State University's (KSU) Research Project Number 5-34367. This contract is funded by the Midwest States Accelerated Pavement Testing Pooled-Funds Program. States participating in this program are Iowa, Kansas, and Missouri.

The purpose of the project was to conduct the experiment selected by the Midwest States Accelerated Testing Pooled-Funds Technical Committee for Fiscal Year 2005. The experiment titled "Verification of Mechanistic- Empirical Design Models for Flexible Pavements through Accelerated Pavement Laboratory (APT) Testing" is also known as Civil Infrastructure Systems Laboratory (CISL) Experiment No. 14. The first two Accelerated Testing Laboratory (ATL) experiments, ATL-Exp #1 and #2 were reported by Melhem (1997); ATL-Experiments #3 through #6 were also reported by Melhem (1999); ATL-Experiment #7 was reported by Melhem and Sheffield (2000); ATL-Experiment #8 is reported by Melhem, et al. (2003a); CISL Exp #9 and 10 are reported by Melhem, et al. (2003b) and CISL Exp #11, 12, and 13 are reported by Romanoshi, et al. (2003, 2008, 2009).

This report describes the following aspects of CISL Experiment #14:

1. A description of the experiment including experiment objectives, test setup, and testing strategies followed.
2. Material and methods used for pavement construction and the pavement response monitoring instrumentation.
3. A detailed description of the laboratory work conducted to characterize the pavement materials.
4. The experimental work performed in terms of total number of load cycles applied to each specimen, testing conditions (load magnitude, temperature, etc.), and time schedule.

5. A summary of the data collected including results from response monitoring instrumentation and distresses measured at the pavement surface.
6. A comparison of the measured pavement response of the tested pavement structures and the response predicted by linear elastic pavement structure models.
7. A comparison of the measured permanent deformation of the tested pavement structures and that calculated by the MEPDG models.
8. A comparison between the performance of the tested asphalt concrete mixes and the results of the laboratory tests on the asphalt mixes.
9. Conclusions drawn from the results obtained and performance observed.
10. Recommendations to the participating highway agencies for practical implementation.

1.2 Project Overview

The "AASHTO Guide for the Design of Pavement Structures" is the primary document used by state highway agencies to design new and rehabilitated highway pavements. The Federal Highway Administration's (FHWA) National Pavement Design Review conducted from 1995 to 1997 found that some 80% of the states make use of either the 1972, 1986, or 1993 AASHTO Pavement Design Guide. All those design guide versions employ empirical performance equations developed using AASHO Road Test data from the 1950s. The 1986 and 1993 guides contained some state-of-the-practice refinements in material input parameters and design procedures for rehabilitation design. In recognition of the limitations of earlier guides, the AASHTO Joint Task Force on Pavements (JTFP) initiated an effort in the late 1990s to develop an improved guide by the year 2002. The major long-term goal identified by the JTFP was the development of a design guide based as fully as possible on mechanistic principles.

The National Academy of Science, through its National Cooperative Highway Research Program (NCHRP) (specifically NCHRP Project 1-37A), has dedicated significant resources provided by the AASHTO member states to develop a user-friendly procedure capable of executing mechanistic-empirical design while accounting for local environmental conditions, local highway materials, and actual highway traffic distribution by means of axle load spectra.

Since the resulting procedure is very sound and flexible and it considerably surpasses any currently available pavement design and analysis tools, it was adopted by AASHTO as the new AASHTO design method for pavement structures. It is also expected that the Departments of Transportation in the three Midwestern states of Kansas, Iowa, and Missouri will adopt the new AASHTO design method to replace the 1993 AASHTO design method currently in use.

It should be noted that all mechanistic design approaches produce "*theoretical structural designs"* that should be adjusted or *"calibrated***"** to actual conditions using data originated from in-service pavement structures. Although calibration should be incorporated in the new AASHTO design procedure, it is to be remembered that it is a procedure with (i) national correlations to estimate selected inputs, (ii) national default values, and (iii) national calibration factors developed from the LTPP sites (Von Quintus and Scofield 2003). It is clear that all these need to be validated and/or calibrated for each specific state and/or region. Without region/state specific calibration, the new guide will be ineffective and of limited use for design purposes. Also, assessment of the design reliability can only be attempted after the guide has been calibrated and validated.

Products of the NCHRP Project 1-37A are the design software and documentation supporting the design guide. They were released to the pavement engineering community in June 2004. For successful application of the new AASHTO design method to local conditions, this specific calibration strategy should address all main aspects of pavement performance and economic analysis: (1) characterization of pavement materials and soil, (2) traffic loading, (3) environment conditions, (4) field calibration, (5) design reliability, (6) alternative surface-type consideration, and (7) life-cycle cost (LCC) analysis. Even before the final software version and documentation was released, each of the three states had allocated resources to calibrate the models for regional/state conditions. The calibration task is complex, and requires significant resources and time.

The calibration of a design model for flexible pavements encompasses three major tasks:

- Verification of the models to predict mechanical properties of pavement materials from conventional, local material properties as follows:

    - dynamic modulus for asphalt concrete from binder viscosity and aggregate gradation, and resilient modulus
    - resilient modulus of unbound materials from gradation or classification data
    - elastic modulus of stabilized materials from compressive strength data;
- Verification of the mechanistic structural model that calculates the response (stresses, strain, and deflections) of the flexible pavement structure under a given wheel loading for a given pavement structure with known layer thickness and material stiffness; and
- Verification or calibration for local pavement configurations of pavement performance models or transfer functions, the empirical functions that relate the distresses in the pavement structure to the magnitude of the pavement response.

This research work aims to contribute to the first three tasks-the verification and calibration of material characteristics prediction models, mechanistic structural models, and pavement performance models-by conducting APTs at the CISL at KSU. Due to the limited number of pavement sections that can be constructed and tested at CISL, the research work focused on verification of the NCHRP 1-37A models for representative flexible pavement structures in three Midwestern states: Iowa, Kansas, and Missouri.

1.3 Accelerated Pavement Testing at the Civil Infrastructure Systems Laboratory

The APT facility at the CISL at KSU is an indoor facility with about 7,000 ft^2 of floor space. It is owned and operated by KSU. The laboratory allows full-scale accelerated pavement testing on pavement structures. The test pavements are constructed in three, 6-ft test pits of varying width and 20-ft in length.

The accelerated loading is provided by the APT machine that can be moved on rails between the testing pits. The main components of the machine are the steel frame, which has two main girders with a 42-ft center-to-center span; and the bogie, that is supported by the frame (Figures 1.1 and 1.2). The bogie is pulled back and forth by a rubber belt attached to an electric motor fixed on the frame. The wheel-load assembly consists of a single or tandem axle mounted on the bogie. Loading of the axle assembly is accomplished with a hydraulic pump mounted on the bogie, above the axle, and connected to two hydraulic cylinders mounted on top of a single

axle. The hydraulic pump pressurizes the oil in the hydraulic circuit and thus, the two cylinders push the bogie into the steel frame and the axle on the top of the test pavement. The hydraulic pump is also used to raise the bogie when uni-directional loading is applied. The axle load is controlled by the pressure in the hydraulic circuit. Load cells mounted on each wheel are used to measure the instantaneous wheel loads.

The bogie moves with a constant speed of 7 mph above the test pavement; acceleration and deceleration are done outside the test area. The bogie takes approximately 5.8 seconds to complete its travel distance in one direction. In bi-directional loading mode, approximately 650 passes of the bogie are applied in one hour of operation, and about 100,000 passes in one week. The operation is typically stopped for several hours weekly for maintenance of the machine and measurement of pavement response and performance. Typically, two test pavements are constructed in each pit and loaded simultaneously with one wheel of the axle passing above each test pavement.

FIGURE 1.1: Single-Axle Bogie

FIGURE 1.2: Side View of the Single-Axle Bogie

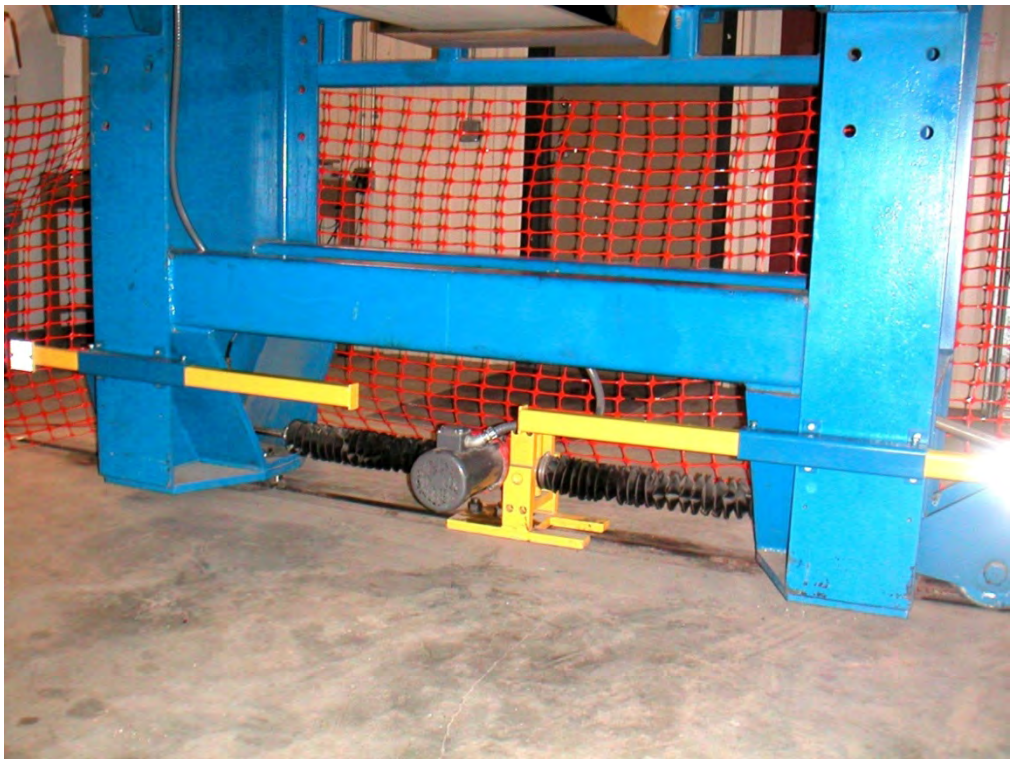

FIGURE 1.3: Lateral Wander System

The machine is equipped with a lateral wandering device that moves the entire frame in a lateral direction, with a maximum lateral wander of ± 24 inch. The lateral movement is applied in steps of 0.5 inch using a screw jack (Figure 1.3). Table 1.1 gives the number of wheel-load passes at each lateral position.

TABLE 1.1: Number of Passes for Each Lateral Position of the Accelerated Pavement Testing Wheel

Lateral position (inch)	Number of wheel passes	Lateral position (inch)	Number of wheel passes
-6	10	0	38
-5.5	12	0.5	38
-5	15	1	37
-4.5	18	1.5	35
-4	21	2	33
-3.5	24	2.5	30
-3	27	3	27
-2.5	30	3.5	24
-2	33	4	21
-1.5	35	4.5	18
-1	37	5	15
-0.5	38	4.5	12
0	38	6	10
Maximum Distance = 6 inches		P = 90% N=640	St. Dev. =3.65”

A temperature-control chamber was built to encase the entire steel frame such that the temperature in the asphalt concrete layers could be controlled within ± 6^{o}F (± 3^{o}C). For the CISL 14 project, target testing temperatures were 68^{o}F (20^{o}C) and 95^{o}F (35^{o}C). Figure 1.4 shows the temperature-control chamber as used in the entire experiment.

FIGURE 1.4: Accelerated Pavement Testing Machine with Temperature-Control Chamber

1.4 NCHRP 1-37A Design Guide and Models for Flexible Pavements

1.4.1 General Framework of the Guide

The design approach to be provided in the guide is summarized in Figure 1.5. The activities are divided into three major parts:

Part 1 consists of the development of input values for the analysis. A key step of this process is the foundation analysis. For new pavements, the foundation analysis consists of strength and stiffness determination and, where appropriate, an evaluation of volume change, frost heave, thaw weakening, and drainage concerns. As part of the foundation analysis, subgrade improvements such as strengthening and drainage are considered.

The foundation analysis for rehabilitation projects also includes a subgrade analysis. However, the most important part of the foundation analysis for rehabilitation projects is the investigation of distress types occurring in the existing pavements and the underlying causes of those distresses. Overall strength/stiffness of the existing pavement is evaluated using deflection testing and back-calculation procedures.

Also during the first stage, pavement materials characterization and traffic input data are developed. The FHWA Integrated Climate Model is used to develop climatic inputs for the foundation and materials analysis, and the pavement response analysis in Part 2.

In the NCHRP 1-37A model, traffic is considered in terms of axle-load spectra. The full spectra for single, tandem, tridem, and quad axles is considered.

Part 2 of the design process is the structural/performance analysis. After the pavement structure or rehabilitation alternative is selected, a structural model that employs the input data prepared in Part 1 is used to estimate pavement response. The structural model for flexible pavement design is the JULEA linear elastic pavement model.

The pavement response computed in critical locations in the pavement structure is then used to estimate pavement performance. The performance is expressed by the evolution of major distresses in time. The distresses considered for new flexible pavement structures are rutting, load-associated cracking, temperature-associated cracking, and roughness of the longitudinal profile. Roughness is considered as a derivative distress; it is computed from the magnitude of rutting and cracking, and not directly from pavement response data. The concept of reliability is introduced when the evolution of distresses are estimated. They are computed based on probabilistic reliability levels and typical standard deviations for each distress type.

The final version of the guide does not allow automatic iterative adjustments of the design alternative if the performance criteria are not satisfactory. The user needs to modify the design pavement structural alternative and rerun the software.

Part 3 of the process was planned to contain those activities required to evaluate the technically viable alternatives: an engineering analysis and life cycle cost analysis of the alternatives. Unfortunately, this part is not included in the final version of the NCHRP1-37A design software, even though in the initial stages of the development of the guide, it was intended to be there. The user needs to successively select technical viable alternatives and to compute pavement performance for each alternative. The pavement performance data obtained from the runs on different alternatives needs to be fed in a life-cycle cost analysis. This will lead to the final selection of the optimum design solution.

1.4.1.1 Hierarchical Design Approach

The NCHRP 1-37A design model uses a hierarchical design approach. Such an approach provides the designer with several levels of "design efficacy" that can be related to the class of highway under consideration or to the level of reliability of design desired. A chosen higher level of design output implies that the inputs also will be of a higher level. The hierarchical approach is employed with regard to traffic, materials, and environmental inputs, and in some cases to the types of analyses used.

While there are many variations throughout the guide where as few as two levels or as many as four are available, the general approach is to provide for three levels. Within the three levels there also are variations, but generally the features of each level are as follows (McGee 2004):

Level 1: Level 1 is a "first-class" or advanced design procedure and provides for the highest practically achievable level of reliability. It typically would be used for design in the heaviest traffic corridors or wherever there are dire safety or economic consequences of early failure. The design inputs also are of the highest practically achievable level and generally require site-specific data collection and/or testing. Examples are dynamic modulus testing of asphalt concrete and site-specific axle-load spectra.

Level 2: Level 2 is the standard design procedure expected to be used for routine design. The inputs typically would be user selected possibly from an agency database, would be derived from a less-than-optimum testing program, or would be estimated empirically. Examples would be dynamic modulus estimated from binder, aggregate, and mix properties or site-specific traffic volume and classification data used in conjunction with agency-specific axle-load spectra.

Level 3: Level 3 typically is the lowest class of design and would be used where there are minimal consequences of early failure and on lower volume roads. Inputs typically would be user-selected default values. Examples would be default dynamic modulus values for given mix classes or default axle-load spectra for functional highway classes.

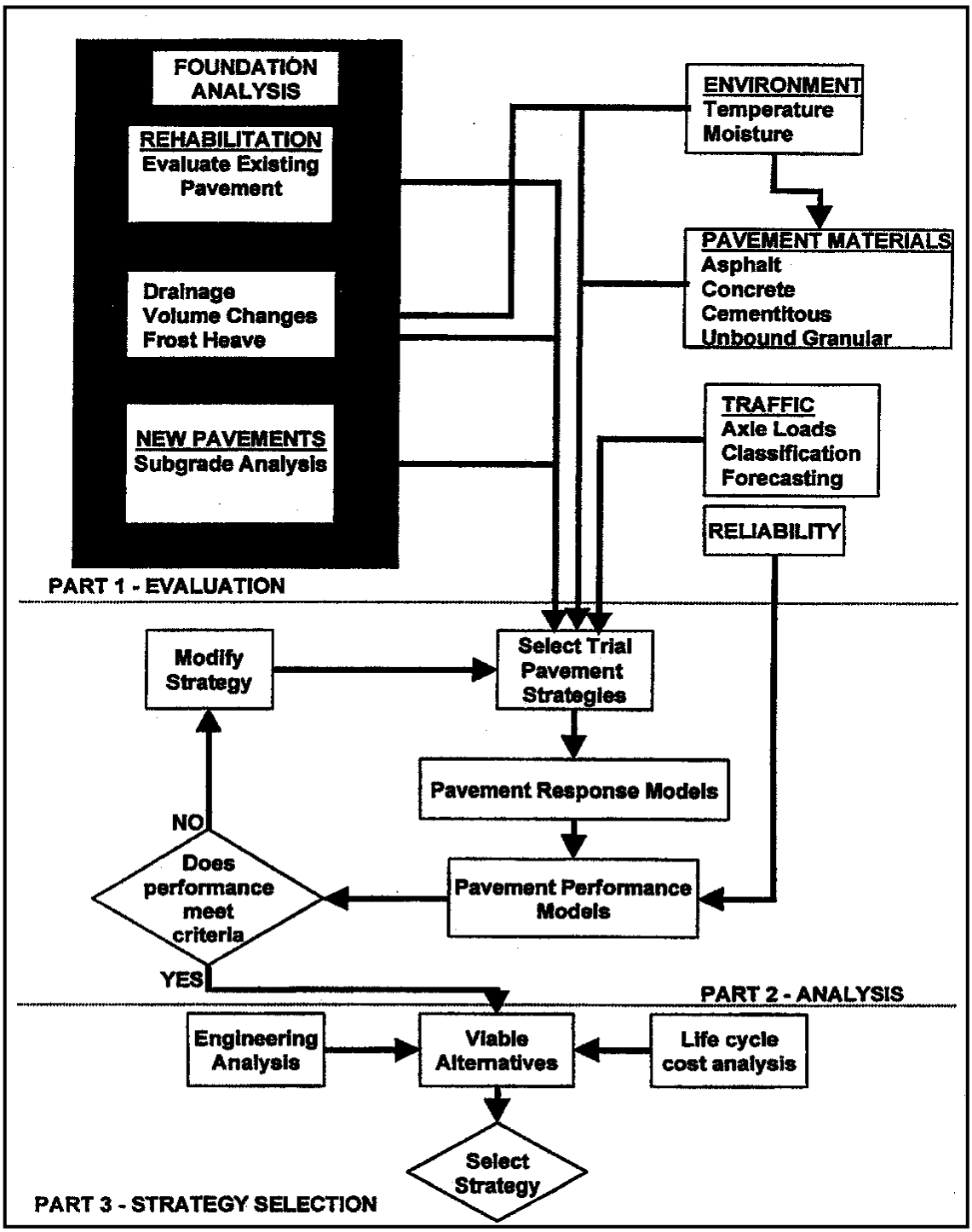

Source: McGee (2004)

FIGURE 1.5: Schematic of the Design Process in Mechanistic-Empirical Pavement Design Guide

1.4.1.2 Pavement Materials Characterization

Materials characterization guidelines are provided so the designer can develop appropriate materials property inputs for use in the analysis portion of the design process. The materials parameters needed for the design process may be classified in one of three major groups (Witczak, et al. 2002):

- pavement-response model materials inputs
- materials-related pavement distress criteria
- other materials properties

Pavement-response model material inputs are related to the moduli and Poisson's ratio used to characterize layer behavior within the specific model. Bound materials such as asphalt concrete (AC), Portland Cement Concrete (PCC), and high-strength stabilized bases generally display a linear or nearly linear stress-strain relationship. Unbound materials such as granular materials and fine-grained soils display stress- dependent properties. Granular materials generally are “stress hardening” and show an increase in modulus with an increase in stress. Fine-grained soils generally are “stress softening” and display a modulus decrease with increased stress. Modulus-stress state relations have been developed for granular materials and for fine-grained soils. In practice, assumed Poisson's ratio values are acceptable for routine mechanistic-empirical pavement design based on isotropic elastic structural analysis models. This is true because the parameter has well-defined limits for specific materials types and because the stress, strain, and displacement outputs of the response model are not particularly sensitive to Poisson’s ratio.

Materials parameters associated with pavement distress criteria normally are linked to some measure of material strength (shear strength, compressive strength, modulus of rupture, etc.). The “other” category of materials properties constitutes those associated with special properties required for the design solution. Examples of this category are the thermal expansion and contraction coefficients of both Portland cement concrete and asphalt mixtures.

1.4.1.3 Classes of Materials

In the NCHRP 1-37A design model, all flexible pavement materials have been classified in one of the following categories:

- hot-mix asphalt - dense graded (HMAC)
- open-graded asphalt treated materials (ATPB)
- cold-mix asphalt (CMA)
- cementitious stabilized materials (CTB, CSB, CTPB)
- non-stabilized granular base/subbase (AB,GAB,CA)
- subgrade soils
- bedrock

1.4.1.4 Levels of Materials Characterization

In keeping with the hierarchical approach, materials characterization is comprised of three levels with level 1 indicative of a design approach philosophy of the highest practically achievable reliability, and levels 2 an 3 of successively lower reliability. Details of hierarchical characterization are given in the materials characterization section of the NCHRP 1-37A model (NCHRP 2004). However, a general tabulation of elastic modulus characterization methods is given in Table 1.2.

TABLE 1.2: Parameters Used in Mechanistic-Empirical Pavement Design Guide for Materials Stiffness

Material	Level 1	Level 2	Level 3
Asphalt Concrete	Measured Dynamic Modulus	Estimated Dynamic Modulus from Binder Viscosity and Gradation Data	Default Dynamic Modulus
Stabilized Materials	Measured Elastic Modulus	Estimated Elastic Modulus from Chemical Content and Soil Type	Default Elastic Modulus
Granular Materials	Measured Resilient Modulus	Estimated Resilient Modulus from Gradation Data	Default Resilient Modulus
Subgrades	Measured Resilient Modulus	Estimated Resilient Modulus from Gradation and Plasticity Data or Soil Classification Data	Default Resilient Modulus

1.4.2 Structural Response Models for Flexible Pavements

Adequate structural modeling of flexible pavement structures is the heart of a mechanistic-based design procedure. Structural response models are used to compute critical stresses, strains, and displacements in flexible pavement systems due to both traffic loads and climatic factors (temperature and moisture). These responses are then utilized in a damage model to accumulate damage, month by month, over the entire design period. Accumulated damage at any time is related to specific distresses such as fatigue cracking, which is then predicted using a field- calibrated cracking model (the main empirical part of a mechanistic-empirical design procedure).

Structural models selected for use in the NCHRP 1-37A design model for flexible pavements include the multi-layer elastic system (JULEA code for linear elasticity). If the user opts to use the level 1 hierarchical approach to characterize the non-linear moduli response of any unbound layer materials (bases, subbases and/or subgrades), then a 2-D finite-element system (non-linear unbound materials) code (DSC2D) can be used. Structural response models require several inputs:

- traffic loading
- pavement cross-section
- Poisson's ratio each layer
- elastic modulus each layer
- thickness each layer
- coefficient of thermal expansion (for HMAC)

Given these inputs, the structural models produce stresses, strains, and displacements at critical locations in the pavement and subgrade layers.

This design procedure is the first to include the capability to accumulate damage on a monthly basis over the entire design period. This approach attempts to simulate how pavement damage occurs in nature, incrementally, load by load, over continuous time periods. By accumulating damage monthly, the design procedure becomes very versatile and comprehensive.

This approach allows use of elastic moduli within a given time period, such as a month, that are representative of that time increment. Thus, in the heat of summer, the dynamic modulus of AC is much lower than in the cold of winter. The resilient modulus of an unbound base course and of the fine-grained subgrade can vary with moisture content. This procedure also allows for the aging of paving materials. For example, AC materials age with time, increasing their stiffness. This has been modeled so that the modulus of asphalt concrete is increasing constantly over time. It is believed that the added capabilities that incremental damage gives far outweigh its main disadvantage of computation time and the inclusion of aging models for paving materials.

1.4.3 Performance Models for Flexible Pavements

1.4.3.1 Permanent Deformation Models

The NCHRP 1-37A pavement design model contains models for predicting permanent deformation in each pavement layer (NCHRP 2004). The average vertical resilient strain in each layer/sublayer is computed for each analysis period of the entire design period with a linear elastic program for each axle-load configuration. Rutting distress is predicted in absolute terms and not computed based on Miner's law; the incremental distress computed for each analysis period is directly accumulated over the entire target design life of the pavement.

The model used for unbound materials has the form:

$$\delta a\,(N) = \beta 1 * (\varepsilon 0 / \varepsilon r) * \varepsilon v * h * EXP[-(\rho/N)\beta] \qquad \textbf{Equation 1.1}$$

Where:

δ_a – permanent deformation for the layer/sublayer;

β_1 - calibration factor for the unbound granular and subgrade materials;

ε_0 , β and ρ – Material properties $\log \beta = -0.6119 - 0.017638 * w_c$;

ε_r – resilient strain imposed in laboratory test to obtain the above listed material properties;

ε_v – average vertical resilient strain in the layer/sublayer;

h – thickness of the layer/sublayer;

w_c – water content in the layer/sublayer; and

N – number of traffic repetitions.

All parameters, except β_1, are computed as functions of the resilient modulus of the layer/sublayer and water content, estimated based on the groundwater table depth. The final calibrated model parameters, derived from the permanent deformation data collected on 88 Long-Term Pavement Performance (LTPP) sections in 28 states, were:

β_{1GB} = 1.673 for unbound granular base and β_{1SG} = 1.35 for unbound subgrade soil.

The relationship used in the NCHRP 1-37A mechanistic design guide to predict rutting of the asphalt mixes is based upon a field-calibrated statistical analysis of repeated permanent deformation laboratory test results. The model is as follows:

$$\varepsilon_p / \varepsilon_r = k_1 * 10^{-3.4488} * T^{1.5606} * N^{0.479244} \qquad \text{Equation 1.2}$$

$$k_1 = (C_1 + C_2 * depth) * 0.328196^{depth} \qquad \text{Equation 1.3}$$

$$C_1 = -0.1039 * h_{ac}^2 + 2.4868 * h_{ac} - 17.342 \qquad \text{Equation 1.4}$$

$$C_2 = 0.0172 * h_{ac}^2 - 1.7331 * h_{ac} + 27.428 \qquad \text{Equation 1.5}$$

Where:

ε_0 , β and ρ – Material properties;

ε_r – resilient strain of the asphalt material as a function of mix properties, temperature and time rate of loading (in/in);

ε_p – accumulated plastic strain at N repetitions of load (in/in);

T – temperature (deg F);

N – number of traffic repetitions; and

h_{ac} – thickness of the layer/sublayer.

The final calibrated model parameters were derived from the permanent deformation data collected on 88 LTPP sections in 28 states.

The models developed above were derived based on observed deformation of in-service pavement structures. The models are empirical. However, a desirable feature is that they include the effect of temperature and moisture content in the computation of permanent deformation directly through their effect on the resilient modulus of the foundation layers or dynamic modulus for the asphalt concrete layers.

1.4.3.2 Load-Associated Cracking Models

Load-associated cracking is one of the most common types of flexible pavement distresses. Repeated vehicle loads induce tensile stresses in the bound layers. Under repeated loadings, fatigue cracks initiate at locations where the largest tensile strains and stresses develop. Location of these critical points depends on many factors like the structural configuration of the pavement, stiffness of the layers, and configuration of the wheel load (area of distribution, magnitude of stresses at the tire-pavement interface). After the cracking initiation at critical locations, the repeated traffic effect causes the cracks to propagate through the entire layer. These cracks allow water infiltration, thereby reducing overall performance of the pavement. Most pavement structural models assume that cracks initiate at the bottom of the asphalt concrete surface layer and then propagate upward. These cracks are named bottom-up fatigue cracks. The NCHRP 1-37A Guide considers the alligator cracking as bottom-up fatigue cracking. In addition to the conventional bottom-up type fatigue cracking, top-down cracking is also taken into account. The NCHRP 1-37A Guide considers longitudinal cracks in the wheel path as top-down cracks. Even though there is no consensus on the cause for the formation of top-down cracking, there is extensive evidence for its existence.

The NCHRP 1-37A model adopted Miner's law to estimate fatigue damage:

$$D = \sum_{i=1}^{T} \frac{n_i}{N_i}$$ **Equation 1.6**

Where:

D = damage,

T = total number of periods,

n_i = actual traffic for period i,and

N_i = allowable repetitions to failure under conditions prevailing in period *i*.

The most commonly used model to predict the number of repetitions to fatigue cracking is a function of tensile strain and mix stiffness. The final relationship used for predicting the number of repetitions to fatigue cracking is the Asphalt Institute Model that is based on constant stress criterion. The final fatigue model used in the design guide obtained by numerical optimization and other modes of comparison is:

$$N_f = 0.00432 * k_1^{'} * C (1/\varepsilon_t)^{3.9492} (1/E)^{1.281} \quad \textbf{Equation 1.7}$$

Where:

$C = 10^M$ and $M = 4.84*[V_b / (V_a+V_b) - 0.69]$

V_b = effective binder volumetric content (%), and

V_a = air voids (%).

The parameter $k_1^{'}$ was introduced to account for different asphalt layer thicknesses and is for bottom-up cracking:

$$k_1^{'} = \frac{1}{0.000398 + [0.003602/(1 + e^{(11.02 - 3.49*h_{ac})})]} \quad \textbf{Equation 1.8}$$

For top-down cracking, it is given by:

$$k_1^{'} = \frac{1}{0.01 + [12.00/(1 + e^{(15.676 - 2.8186*h_{ac})})]} \quad \textbf{Equation 1.9}$$

Finally, the transfer function to estimate fatigue cracking from fatigue damage is expressed as in the equations below for bottom-up and top-down cracking, respectively.

Bottom-up cracking

$$F.C. = \left(\frac{6000}{1 + e^{(C_1 * C'_1 + C_2 * C'_2 * \log 10(D*100))}} \right) * \left(\frac{1}{60} \right)$$

Equation 1.10

Where:

F.C=bottom-up fatigue cracking, percent lane area,

D= bottom-up fatigue damage,

C1 = 1.0,

C2 = 1.0,

C'1= -2 * C'2, and

$C'_2 = -2.40874 - 39.748 * (1 + h_{ac})^{-2.856}$

Top-down cracking

$$F.C. = 1000 * 10.56 / [1 + e^{(7 - 3.5 * \log 10(100 * D))}]$$

Equation 1.11

Where:

F.C.= top-down fatigue cracking, ft/mile; and

D= top-down fatigue damage.

The fatigue cracking model for asphalt concrete was calibrated based on data from 82 LTPP sections located in 24 states, using 441 observations for alligator cracking and 408 data points for longitudinal cracking. The bottom-up cracking is calculated as a percentage of lane area, while the longitudinal cracking is expressed in terms of linear feet per mile of pavement.

An important observation made during the calibration process was that for all levels of asphalt thickness, the alligator cracking increases with decreasing subgrade modulus. It was also

observed that the impact of subgrade support upon alligator cracking is directly dependent on the thickness of the HMA layer, and that the greatest potential for damage is observed for asphalt layers with thickness in the range of 3- to 5-inches.

Fatigue damage lessens below the maximum cracking level in the range of 3- to 5-inches because at the bottom of very thin HMA layers little or no tensile stresses or strains develop. Pavements with thin HMA layers exhibit rutting failure in the foundation layers before exhibiting fatigue cracking in the asphalt concrete layers.

1.5 Research Objectives

The objectives of this research are as follows**:**

- to validate and calibrate the dynamic resilient modulus model used in NCHRP 1-37A for asphalt concrete mixes and to compare it with the field-measured modulus, for two mixes in each of the three Midwestern states: Kansas, Iowa, and Missouri;
- to validate the pavement response model used in NCHRP 1-37A for new flexible pavement structures;
- to validate the relationship used in NCHRP 1-37A to predict the performance of new flexible pavements;
- to compare the performance of coarse and fine Superpave mixes; and
- to validate the Asphalt Pavement Analyzer (APA) and the Hamburg Wheel-Tracking Device (HWTD) Tester as screening tools for evaluating the rutting performance of Superpave asphalt mixes.

To achieve these objectives, 12 experimental pavement structures were constructed for this experiment in six pairs and were subjected to full-scale accelerated testing.

Chapter 2: Description of the Experiment

2.1 Civil Infrastructure Systems Laboratory 14 Experiment

The Civil Infrastructure Systems Laboratory (CISL) 14 research project was funded by Midwest Pooled Fund with the aim to verify the models used in the Mechanistic-Empirical Pavement Design Guide (MEPDG) for the design of new flexible pavements through accelerated pavement testing (APT). Twelve experimental pavement structures were constructed at CISL and tested between 2006 and 2009. Three pairs were “fatigue cracking” sections aimed to study fatigue-cracking behavior of flexible pavements. The remaining three pairs were “rutting” sections aimed to study rutting behavior of asphalt concrete pavements. In total, six hot asphalt mixes were used, two for each of the three states. One “fatigue-cracking” and one “rutting” pavement were built for each mix.

Figure 2.1 shows an example of four test sections, a fatigue-cracking pair and rutting pair of test sections, built in two pits to test the two asphalt concrete mixes of one state. The pavement sections were constructed in three layers: an asphalt concrete surface layer, a 6-inch unbound granular base course, and a 5-ft, A-7-6 clay subgrade. The “fatigue-cracking” sections had a 4-inch nominal thickness for the asphalt concrete (AC) surface layer and were loaded at a pavement surface temperature of 68°F (20°C). The “rutting” sections had a 7-inch nominal thickness for the asphalt concrete surface layer and were loaded at a pavement surface temperature of 95°F (35°C).

The sections were loaded with a 22,500-lbs single axle applied at the uniform travel speed of 7 mph. Lateral movement was provided by a lateral wandering device that moved the entire frame of the APT machine in the lateral direction, with a maximum lateral wander of ±2.0-ft. Transverse profiles at the pavement surface were measured periodically during APT loading to record the evolution of rut depth with the number of load repetitions.

Instrumentation was embedded in the experimental pavement sections during construction. Strain gauges were used to measure horizontal and vertical strains at the bottom of the hot-mix asphalt (HMA) layer. Linear variable differential transducers (LVDTs) were used to measure the dynamic and permanent vertical deformation in each layer. Pressure (stress) cells were used to measure the vertical compressive stress below the base layer. Thermocouples were

used to measure the temperature at the surface and two additional depths in each pavement structure.

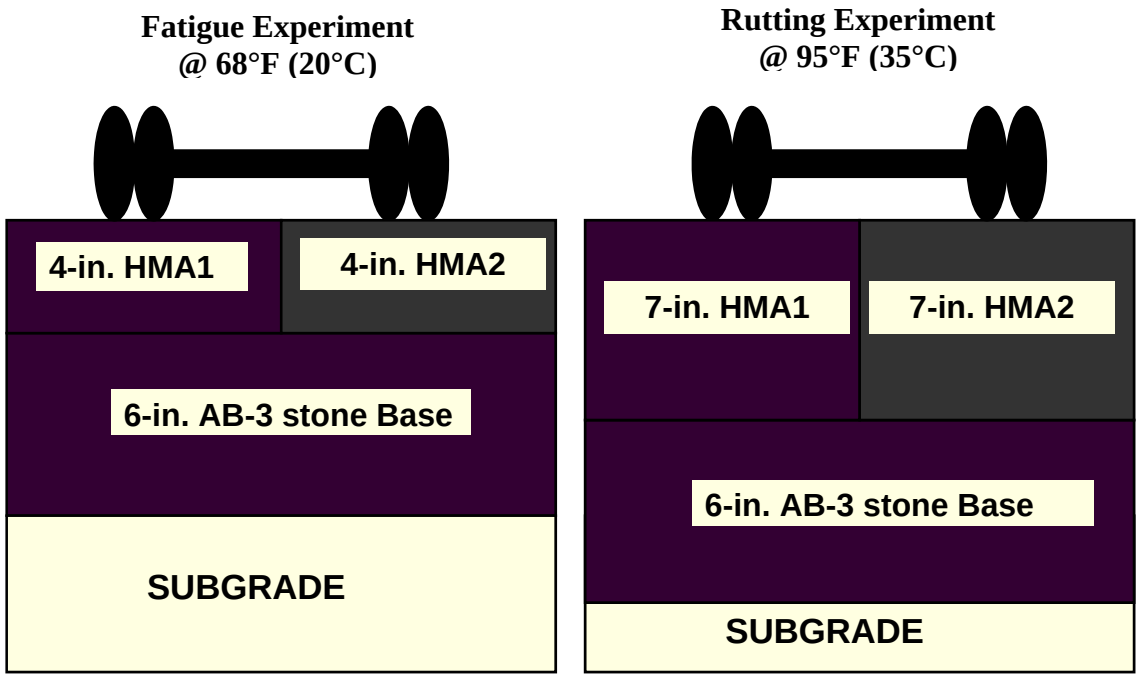

FIGURE 2.1: Cross Section of the Experimental Pavement Sections

The Departments of Transportation (DOTs) of Kansas, Missouri, and Iowa provided the asphalt mix designs of the six asphalt mixes used for verification of mechanistic prediction models. A local contractor, Schilling Construction Inc., constructed the pavement sections at CISL with materials transported from the three states. The six asphalt mixes consisted of a Kansas course mix (KS1) with 19-mm nominal maximum aggregate size (NMAS); a Kansas fine mix (KS2) with 12.5-mm NMAS; two 12.5-mm NMAS Missouri mixes with different binders (PG 70-22 for MO1 mix and PG 64-22 for MO2 mix), and two 12.5-mm NMAS Iowa mixes with the same binder but different design ESALs (30 million ESALs for mix IA1 and 3 million ESALs for mix IA2). The mix design information, including aggregate gradation, PG binder grade, gravimetric binder content, and *in-situ* measured air-void content are given in detail in Chapter 3. Table 2.1 gives the notation used for the six asphalt concrete mixes and the 12 test sections.

TABLE 2.1: Notation Used for the Experimental Test Sections

Mix Notation		Target Test Temperature/ HMA layer thickness	Test Lane Notation	Pit	Lane	Pit/Lane Acronym	Onyango's Notation*
KS Sections							
KS1	19A	35°C / 7.0 in	KS1-7	Middle	South	MS	KS-1
KS2	12.5A		KS2-7		North	MN	KS-2
KS1	19A	20°C / 4.0 in	KS1-4	South	North	SN	KS-3
KS2	12.5A		KS2-4		South	SS	KS-4
MO Sections							
MO1	PG70-22	35°C / 7.0 in	MO1-7	Middle	North	MN	MO-1
MO2	PG64-22		MO2-7		South	MS	MO-2
MO1	PG70-22	20°C / 4.0 in	MO1-4	North	North	NN	MO-3
MO2	PG64-22		MO2-4		South	NS	MO-4
IA Sections							
IA1	30M	35°C / 7.0 in	IA1-7	Middle	South	MS	IA-1
IA2	3M		IA2-7		North	MN	IA-2
IA1	30M	20°C / 4.0 in	IA1-4	South	South	SS	IA-3
IA2	3M		IA2-4		North	SN	IA-4

* Used by Dr. Mbaki Onyango (Von Quintus and Scofield 2003)

2.2 Subgrade Soil

The soil used in the construction of four experimental pavement sections at the CISL laboratory was obtained from Bayer Construction Co. in Manhattan, Kansas. This type of soil is commonly used for construction of embankment layers underneath flexible and rigid pavements in the three Midwestern states.

The soil was a clay soil with 96% passing the No.200 sieve. The soil was classified as A-7-6 according to the AASHTO soil classification system (Onyango 2009). Properties of the untreated soil are given in Table 2.2.

TABLE 2.2: Properties of Subgrade Soil

Percent passing No. 200 sieve (%)	96
Liquid limit	46.5
Plastic limit	22.5
Plasticity index	24.0
MDD (Standard Proctor) (Kg/m^3) / [pcf]	1,630/[101.7]
OMC (%) (Standard Proctor)	21.0
AASHTO class	A-7-6
Unified classification system	CL

2.2.1 Sieve Analysis of Untreated Soil

A sample of soil weighing 500 gm was dried to constant mass and washed through a U.S. No. 200 (0.075 mm opening) sieve. The portion of the soil retained on the sieve was then collected into a bin and dried in the oven to determine mass of the soil retained on the No. 200 sieve. The percentage of the soil passing through the No. 200 sieve was then determined as:

*% passing #200 = 100 – [(mass retained on # 200 sieve)/500]*100*

The percentage of soil passing No. 200 sieve obtained for the studied soil was 96%.

2.2.2 Atterberg Limit Tests of Untreated Soil

The liquid limit, plastic limit, and plasticity index of the soil were determined according to ASTM D 4318-00. Liquid-limit tests were performed according to the multiple-point method. The sample for the test was prepared by thoroughly mixing the portion of the air-dried soil passing a No. 40 sieve with water. Using a spatula, a portion of the sample was spread to form an approximately horizontal surface in the brass cup of the liquid-limit device to a depth of about 10 mm at its deepest point. A groove was formed in the prepared soil surface through the line joining the highest point to the lowest point on the rim of the cup by drawing the grooving tool perpendicular to the surface of the cup throughout its movement. The two halves of the soil on either side of the grove were then allowed to flow together by dropping the cup through a height of 10 mm using the crank of a liquid-limit device. The number of the drops (N) required to close

the groove along a distance of 13mm (0.5 inch) was recorded. The procedure was repeated by mixing different water contents with the soil to obtain three values of N: one between 25 and 35 drops, one between 20 and 30 drops, and one between 15 to 25 drops. A graph was drawn between number of drops and water content. It was found that the water content corresponding to 25 drops, which is recorded as the liquid limit (LL), was 46.5.

The sample for the plastic-limit test was prepared by mixing soil with water, sufficiently to allow the soil mass to roll on a glass plate without sticking to the hands. A portion of the sample (2 grams) was then formed into an ellipsoidal mass and rolled on a glass plate under the pressure of the fingers that was sufficient to roll the mass into a thread of uniform diameter throughout its length. The rolling was continued until the diameter of the thread was 3.2 mm. The thread was then broken into several pieces and formed into ellipsoidal mass and rolled again following the same procedure. The procedure was continued until the thread crumbled and was not possible to be pressed and rolled into 3.2 mm diameter. The water content of the soil mass at this stage was reported as the plastic limit of the soil. The plastic limit for the soil was found to be 22.5.

2.2.3 Moisture-Density Tests

The maximum dry density (MDD) and optimum moisture content (OMC) of the soil were determined according to ASTM D 698-00. The portion of the soil passing a No. 4 sieve was thoroughly mixed with different water quantities and allowed to stand for 6 hours by placing it in trays covered with flat plates to ensure the uniformity of the soil-water mix. The mix was then placed in the standard Proctor mold and compacted into three layers of equal thickness. Each layer was compacted by dropping the standard Proctor rammer for 25 times and was scarified before placing the next layer to ensure good bonding between layers. After compaction, the wet density of the mix was determined from the weight of the mix in the mold, moisture content of the mix, and volume of the mold. Dry density was determined from the values of wet density and moisture content. The process was repeated for several water contents.

The variation of dry density with water content is shown in Figure 2.2. The highest dry density obtained from the graph is recorded as MDD. The moisture content corresponding to MDD is considered as optimum moisture content (OMC).

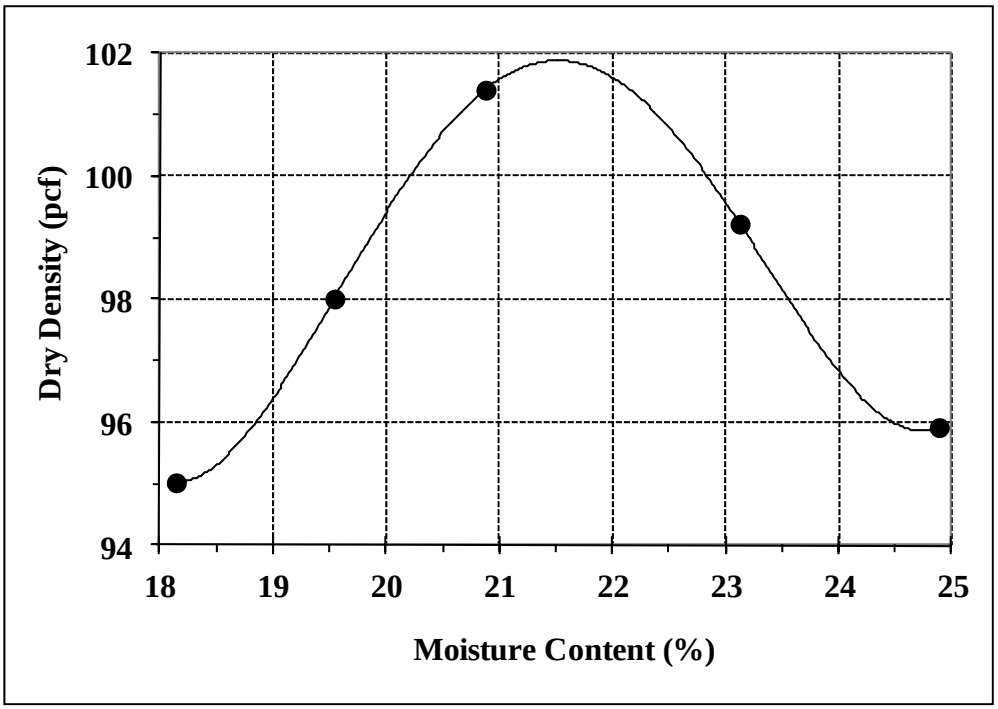

FIGURE 2.2: Results of Standard Proctor Tests on Untreated Soil

2.2.4 Triaxial Resilient Modulus Tests

The triaxial resilient modulus tests were performed on an IPC UTM-25 hydraulic testing machine following the AASHTO T 307-99 test protocol (Onyango 2009). In this test procedure, the soil is tested under one confining pressure level and five deviator stress levels. The soil samples were compacted at three relative dry density levels (90%, 95% and 100% of MDD) and three gravimetric moisture levels (OMC; OMC -5% and OMC +5%).

Results of the triaxial resilient modulus tests are given in Table 2.3 and Figure 2.3. They show that the resilient modulus decreased with the deviator stress and the moisture content, and increased with the compaction level. At high-moisture content, the samples exhibited high deformations and could not withstand all loading cycles for all deviator stress levels; the tests were then stopped.

TABLE 2.3: Laboratory Triaxial Resilient Modulus of Subgrade Soil

Dry Density	Moisture Content (%)		Deviator Stress (kPa)				
			23.8	37.5	50.8	71.2	105.2
90% MDD	OMC - 5%	16.0	94.0	83.7	79.1	75.4	77.3
	OMC	21.0	83.0	69.2	56.2	45.7	
	OMC + 5%	26.0	34.1	27.2			
95% MDD	OMC - 5%	16.0	129.5	132.2	120.2	124.1	126.7
	OMC	21.0	101.9	83.4	71.8	58.0	
	OMC + 5%	26.0	30.7	25.5			
100% MDD	OMC - 5%	16.0	690.4	485.4	405.9	322.9	254.5
	OMC	21.0	690.4	485.4	405.9	322.9	254.5
	OMC + 5%	26.0	220.3	220.9	219.6		

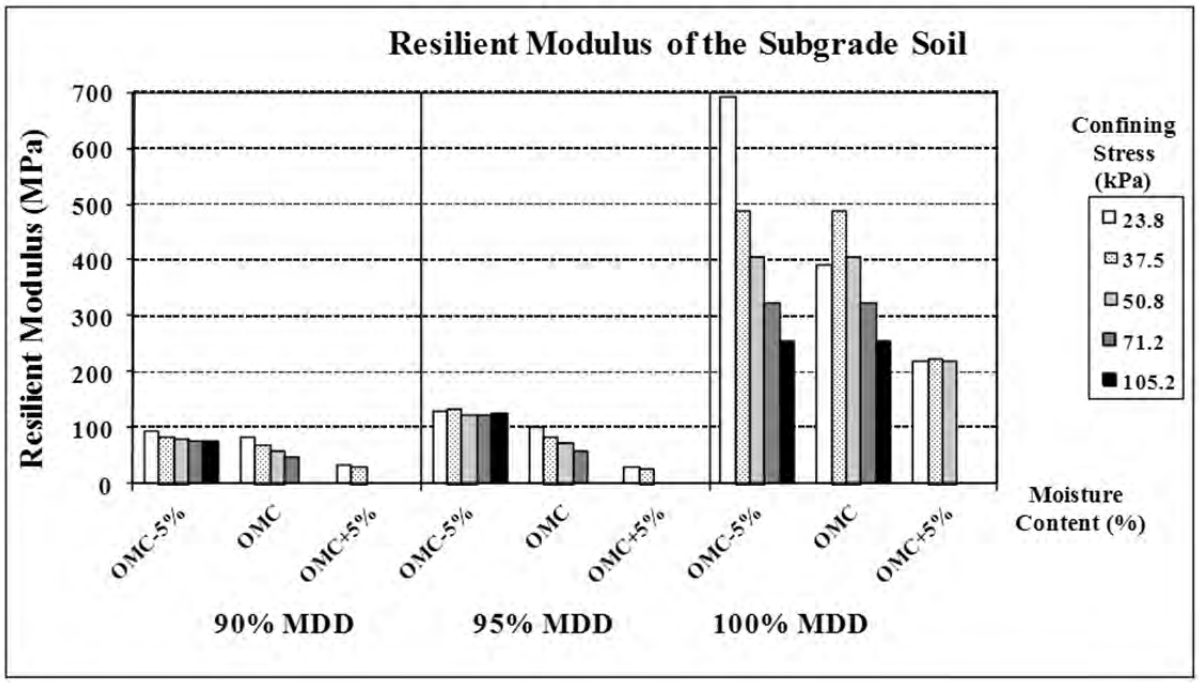

FIGURE 2.3: Triaxial Resilient Modulus of Subgrade Soil

2.3 Construction of Soil Embankment Layer

The top two feet of the soil existing in the pit was removed. Then, the new soil was placed in the pit and compacted to a density greater than 90% of the maximum dry density (MDD) (Table 2.4 and Figure 2.4), at near optimum moisture content. The compaction was done with a “jumping jack”-type vibratory compactor. This subgrade was brought up to the required depth in two-inch lifts. The as-compacted dry density and the moisture content for the soil

subgrade and granular unbound base layer, measured with the Troxler nuclear density gauge, are given in Table 2.4; location of the test points is given in Figure 2.4. Higher densities were achieved for the top 6 inches of the subgrade soil than for the lifts below it. The highest densities were recorded for the Iowa test sections.

Stiffness of the compacted soil was measured with a GeoGage device, following the procedure recommended by the gage manufacturers. Results reported in Table 2.5 suggest the soil in the Missouri sections had the highest as-compacted stiffness.

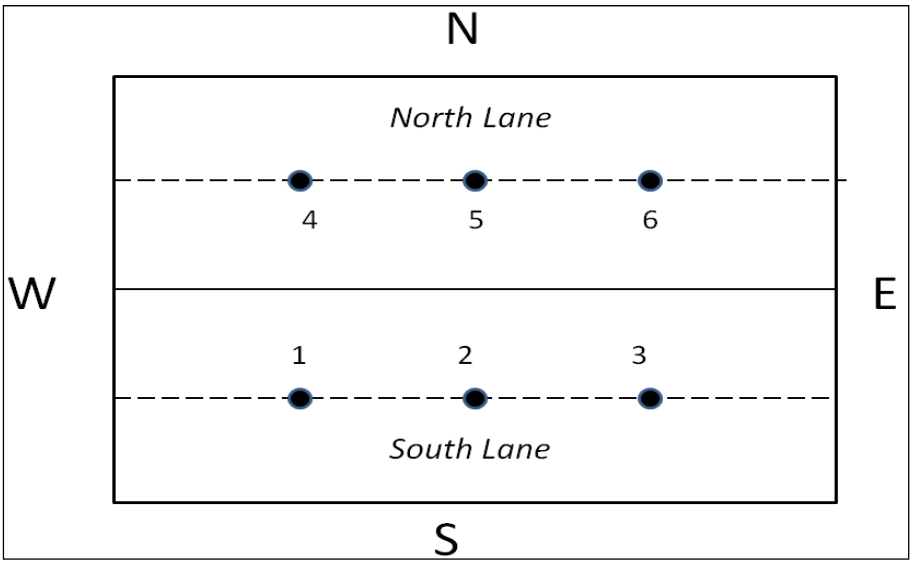

FIGURE 2.4: Location of Nuclear Density Measurements on Soil and Base Layers

TABLE 2.4: As-Constructed Densities for Subgrade and Base Layers

Section	Location	12" below top of subgrade		6" below top of subgrade		Top of subgrade		Top of base	
Kansas Test Sections									
	Date	6/22/2005		6/28/2005		8/10/2005		8/19/2005	
		RDD	MC	RDD	MC	RDD	MC	RDD	MC
KS1-7 MS KS19A	1	94.9	20.6	95.1	22.5	97.4	22.1	139.2	7.8
	2	92.1	25.8	98.3	21.0	95.6	25.1	130.9	8.0
	3	89.0	24.7	97.1	20.2	93.5	23.4	137.3	8.6
	Average	92.0	23.7	96.8	21.2	95.5	23.5	135.8	8.1
KS2-7 MN KS12.5A	4	95.7	20.3	100.7	17.8	99.1	21.3	138.5	7.8
	5	92.5	22.3	96.0	22.6	96.8	22.9	136.7	8.2
	6	93.0	23.0	99.4	19.8	98.5	21.6	135.0	7.4
	Average	93.7	21.9	98.7	20.1	98.1	21.9	136.7	7.8
KS1-4 SS KS12.5A	1	95.5	23.9			95.0	25.1	133.1	7.8
	2	93.5	25.3			94.1	26.6	132.4	7.3
	3	95.2	20.9			92.5	27.3	135.2	7.9
	Average	94.7	23.4			93.9	26.3	133.5	7.7
KS2-4 SN KS19A	4	90.2	27.2			95.3	25.2	134.5	7.8
	5	91.8	27.4			95.4	24.8	130.2	6.7
	6	93.9	24.9			94.3	22.4	132.7	6.6
	Average	92.0	26.5			95.0	24.1	132.5	7.0

RDD - InSitu Relative Dry Density (% of MDD); MC-Insitu Moisture Content (%)

TABLE 2.4 Continued

Section	Depth	12" below subgrade		6" below subgrade		top subgrade		top base	
Missouri Test Sections									
	Date	10/26/2006		11/02/2006		11/16/2006		11/30/2006	
		RDD	MC	RDD	MC	RDD	MC	RDD	MC
	1	88.6	17.1	88.9	23.1	98.3	25.2	129.2	6.0
MO2-7	2	93.7	20.3	97.5	21.0	99.2	22.9	127.0	6.1
MS	3	95.4	21.2	93.2	18.8	92.5	23.5	130.9	6.5
64-22	**Average**	92.6	19.5	93.2	21.0	96.7	23.9	129.0	6.2
	4	99.5	20.0	94.0	20.1	96.2	23.5	132.2	6.3
MO1-7	5	94.9	21.0	92.4	19.4	97.2	23.8	133.4	6.9
MN	6	94.8	21.2	91.9	19.8	95.5	23.9	130.0	6.2
70-22	**Average**	96.4	20.7	92.8	19.8	96.3	23.7	131.9	6.5
	1	87.0	23.3	95.2	22.1	96.2	23.3	131.2	6.1
MO2-4	2	93.2	20.6	91.5	23.7	96.3	24.5	141.4	8.1
NS	3	94.1	18.5	86.2	23.9	99.6	24.0	128.5	6.8
70-22	**Average**	91.4	20.8	91.0	23.2	97.4	23.9	133.7	7.0
	4	92.4	20.4	90.4	22.8	99.0	24.4	132.2	6.5
MO1-4	5	96.3	17.7	91.7	22.4	93.9	24.4	132.0	7.2
NN	6	93.6	21.1	91.6	22.0	98.0	24.0	128.7	6.9
64-22	**Average**	94.1	19.7	91.2	22.4	97.0	24.3	131.0	6.9
Iowa Test Sections									
	Date	10/30/2007				11/20/2007		12/03/2007	
		RDD	MC	RDD	MC	RDD	MC	RDD	MC
	1	94.1	23.0			102.4	19.8	119.7	5.3
IA1-7	2	96.2	22.6			105.1	19.3	121.4	4.8
MS	3	94.2	24.5			104.3	18.7	118.9	5.7
	Average	94.8	23.4			103.9	19.3	120.0	5.3
	4	97.5	21.8			102.8	19.5	117.2	6.2
IA2-7	5	90.4	24.1			105.6	18.7	117.6	5.3
MN	6	91.3	24.3			104.6	19.3	115.3	6.8
	Average	93.1	23.4			104.3	19.2	116.7	6.1
	1	100.2	21.9			106.9	18.3	123.6	4.6
IA1-4	2	99.7	21.9			107.9	18.7	120.2	6.0
SS	3	97.0	22.6			106.0	19.6	121.8	5.5
	Average	99.0	22.1			106.9	18.9	121.9	5.4
	4	101.0	22.2			103.5	20.0	120.7	6.0
IA2-4	5	102.1	20.4			106.8	19.0	122.4	5.6
SN	6	100.1	20.4			106.5	19.4	119.0	5.8
	Average	101.1	21.0			105.6	19.5	120.7	5.8

RDD - Insitu Relative Dry Density (% of MDD); MC – Insitu Moisture Content (%)

TABLE 2.5: As-Constructed Stiffness (MPa) Measured with the GeoGage

Section	Location	12" below top of subgrade	6" below subgrade	Top of subgrade	Top of base
Kansas Test Sections					
Date		6/22/2005		6/28/2005	8/19/2005
KS1-7 MS KS19A	1	5.03		7.26	8.39
	2	5.00		7.69	11.01
	3	9.34		5.26	11.71
	Average				
KS2-7 MN KS12.5A	4	4.21		7.18	12.32
	5	5.45		6.60	10.78
	6	4.18		5.07	10.07
	Average				
KS1-4 SS KS12.5A	1	6.65		4.62	12.06
	2	4.72		4.32	12.30
	3	4.84		3.73	12.18
	Average				
KS2-4 SN KS19A	4	6.33		5.00	11.33
	5	7.31		7.20	11.90
	6	5.33		5.81	14.33
	Average				
Missouri Test Sections					
Date		10/26/2006	11/02/2006	11/16/200	11/30/2006
MO2-7 MS 64-22	1	5.65	7.70	8.86	7.66
	2	7.14	9.50	11.61	9.38
	3	7.25	9.78	7.00	8.52
	Average				
MO1-7 MN 70-22	4	7.83	8.01	12.47	7.49
	5	8.34	10.49	8.75	11.09
	6	7.33	6.10	9.49	6.81
	Average				
MO2-4 NS 70-22	1	8.60	8.18	11.58	8.78
	2	8.75	9.25	7.22	13.68
	3	10.01	4.81	11.69	7.01
	Average				
MO1-4 NN 64-22	4	8.63	9.84	7.64	8.82
	5	10.51	10.88	9.74	10.27
	6	7.62	7.56	9.15	6.69
	Average				

TABLE 2.5 Continued

Section	Location	12" below top of subgrade	Top of subgrade
Iowa Test Sections			
Date		10/30/2007	11/20/2007
IA1-7 MS	1	5.01	5.96
	2	10.75	12.39
	3	8.92	15.34
	Average		
IA2-7 MN	4	7.63	6.76
	5	7.51	13.31
	6	8.63	8.23
	Average		
IA1-4 SS	1	8.36	7.18
	2	6.93	8.67
	3	8.31	12.57
	Average		
IA2-4 SN	4	8.42	
	5	10.02	10.62
	6	9.38	12.59
	Average		

2.4 Construction of the Granular Base Layer

A well-graded aggregate, classified as AB-3 under KDOT Specifications (KDOT 1990), was used as the material for the base layer. AB-3 is classified as an A-1-a aggregate, according to the AASHTO soil classification system. It is an ideal material for roadway base courses. The standard compaction test result of AB-3 is shown in Figure 2.5. Maximum dry density for the material is 131 pcf (2.1g/cm^3), at 10.3 % moisture content. The grain-size distribution of AB-3 base material is shown in Figure 2.6.

Laboratory triaxial resilient modulus tests were conducted on one sample of the AB-3 base material following the AASHTO T 307-99. Results are given in Table 2.6. As expected, the resilient modulus increased with confining pressure, σ_3, and bulk stress, Θ.

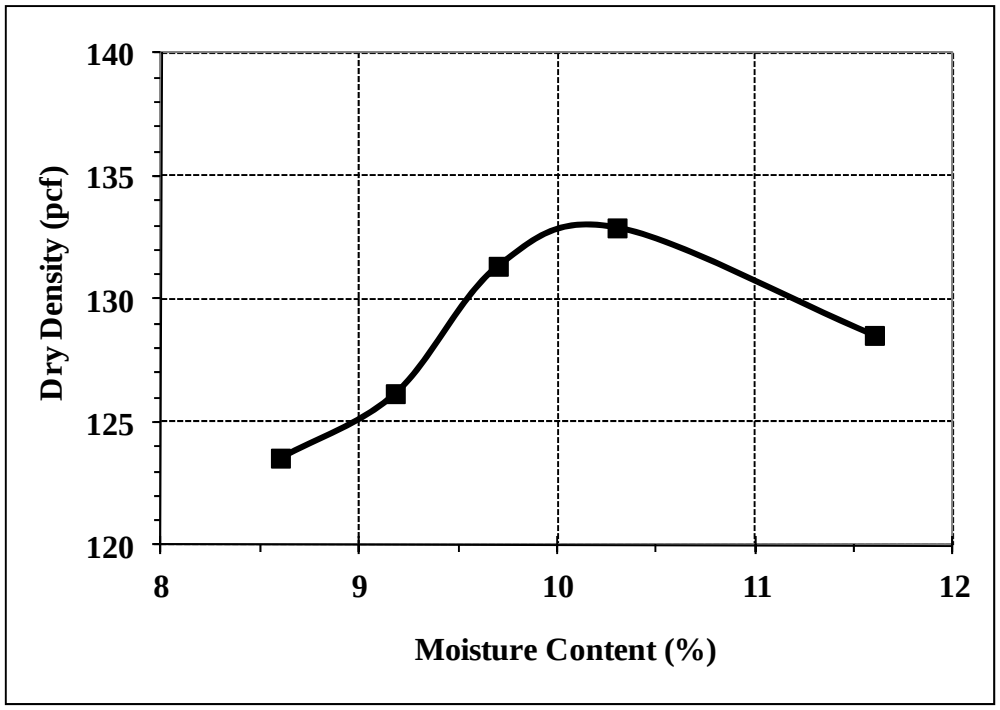

FIGURE 2.5: Moisture–Density Curve for the AB-3 Granular Base Material

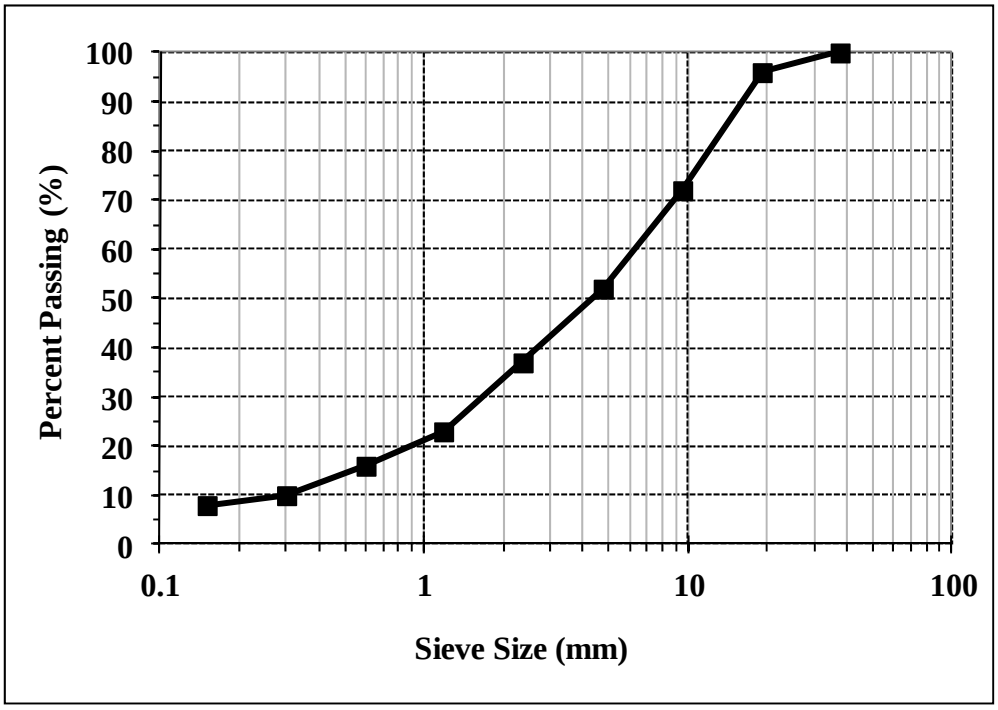

FIGURE 2.6: Gradation Curve for the AB-3 Granular Base Material

TABLE 2.6: Laboratory Resilient Modulus of the AB-3 Base Material

Sequence	σ_3 (MPa)	σ_1-σ_3 (MPa)	Θ (MPa)	τ_{oct} (MPa)	Mr (MPa)
1	20.5	20.6	82.1	9.7	118.1
2	20.5	41.8	103.3	19.7	126.2
3	20.5	61.6	123.1	29.0	134.1
4	34.4	34.9	138.1	16.5	155.1
5	34.6	68.4	172.2	32.2	168.5
6	34.5	102.6	206.1	48.4	168.5
7	68.5	68.7	274.2	32.4	216.9
8	68.5	137.5	343.0	64.8	220.0
9	68.4	206.3	411.5	97.3	205.4
10	102.6	68.7	376.5	32.4	226.2
11	102.4	102.8	410.0	48.5	238.8
12	102.4	206.8	514.0	97.5	254.9
13	137.6	102.7	515.5	48.4	281.7
14	137.4	137.9	550.1	65.0	293.0
15	137.6	275.4	688.2	129.8	301.8

2.5 Construction of the Asphalt Concrete Surface Layer

Paving of the hot-mix asphalt (HMA) layer was done by Shilling Construction Co. of Manhattan, Kansas, with a conventional paver, see Figure 2.7. Compaction was done with a steel-wheeled vibratory roller, see Figure 2.8. At least 50 tons of each mixture type were produced before building the test sections at the CISL, using aggregates and binders transported from the respective states and stored at the asphalt plant.

FIGURE 2.7: Paving of Asphalt Concrete

FIGURE 2.8: Compaction of Asphalt Concrete

Thickness of the as-constructed layers was determined by measuring (with surveying equipment) the elevation on top of each constructed layer at 19 points, spaced at one-foot intervals along a straight line corresponding to the position of the wheel path. The points were numbered from east to west, with the first point being at one foot west of the east wall of the pit. A fixed point at the base of a steel pole near the east gate of the CISL laboratory was used as a reference. Elevations recorded at the top of the compacted subgrade soil, at the top of the granular base layer, and on top of the pavement surface are given in Appendix A. The thickness of the as-constructed layers, computed as the difference between the elevations recorded in the same point, are given in Appendix A and plotted in Figures 2.9 to 2.14.

Figures 2.9, 2.11, and 2.13 indicate that the thickness of the base layer was relatively close to 6.0 inches, the nominal thickness. Figure 2.10 suggests that the thickness of the asphalt concrete layer was relatively close to 4.0 and 7.0 inches, the nominal thicknesses. However, the HMA layer thickness was more than 8.0 inches for the IA2-7 rutting section.

The *insitu* density of the asphalt concrete was measured with the Troxler nuclear gage, to verify the uniformity of compaction. However, it was considered more appropriate to evaluate the as-compacted density based on cores taken outside of the wheel paths at the end of APT loading. Density data as measured on the cores is reported in Chapter 5.

It is important to note that the *insitu* air voids of the compacted mix varied from one mix to the other and from the desired value of 7.0 percent, as discussed in Chapters 3 and 5. In addition to this, the *insitu* binder content for the IA1 and IA2 mixes was higher than the design binder content. Therefore, results of the APT and laboratory tests should not be used to compare the mix design or derive any conclusions on the mix design practice used by the three state DOTs. The values can be used only to compare the mixes as they were produced and constructed for this research project.

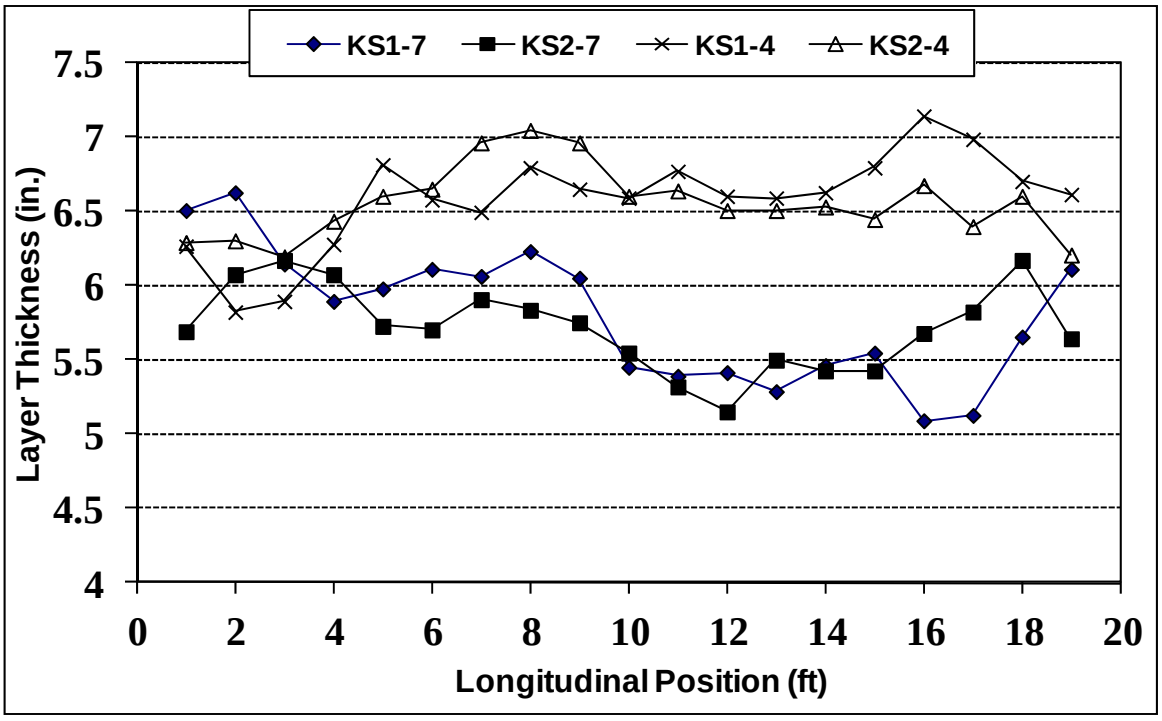

FIGURE 2.9: As-Constructed Thickness of Base Layer for Kansas Sections

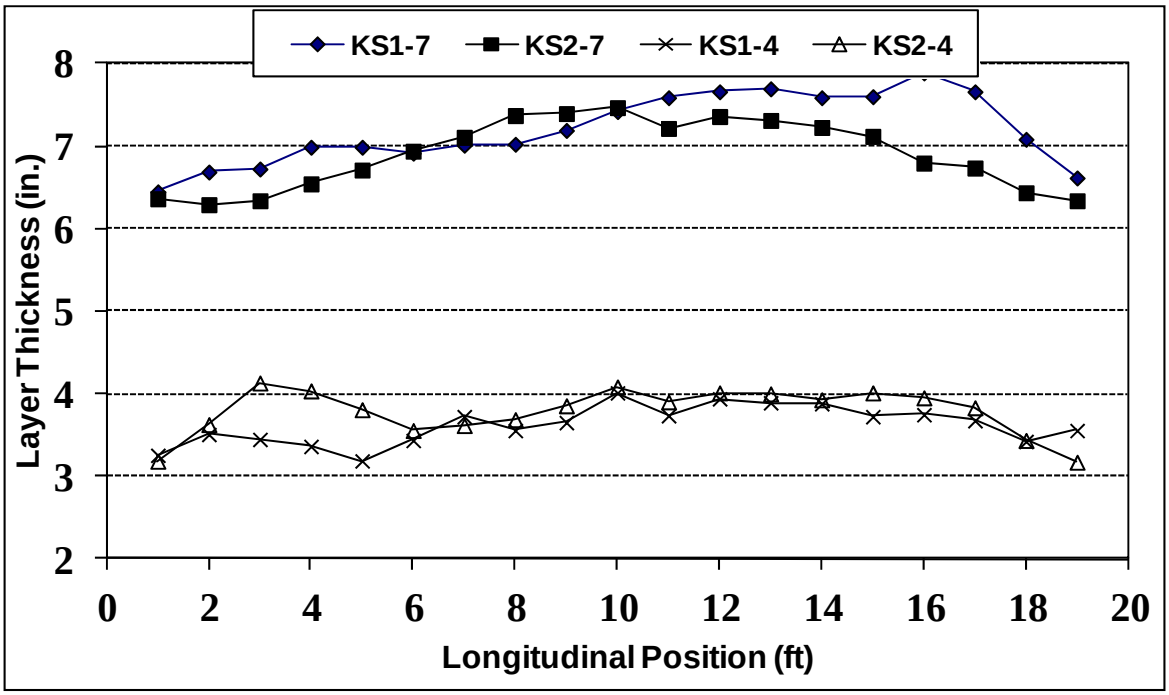

FIGURE 2.10: As-Constructed Thickness of HMA Layer for Kansas Sections

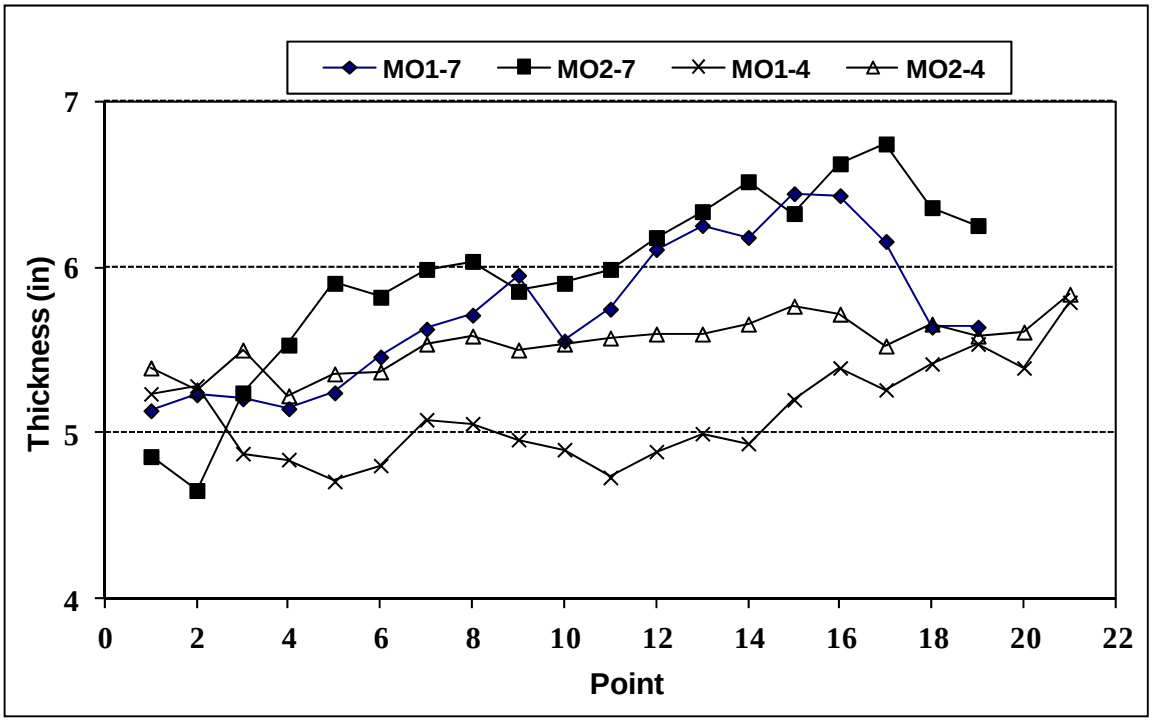

FIGURE 2.11: As-Constructed Thickness of Base Layer for Missouri Sections

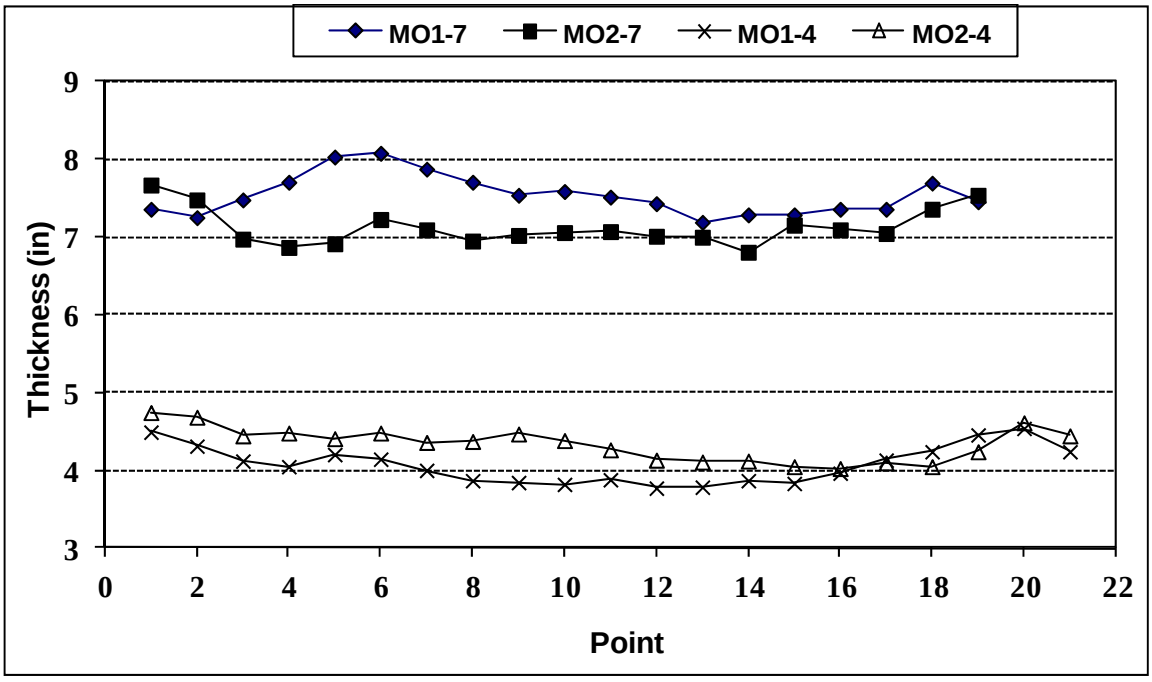

FIGURE 2.12: As-Constructed Thickness of HMA Layer for Missouri Sections

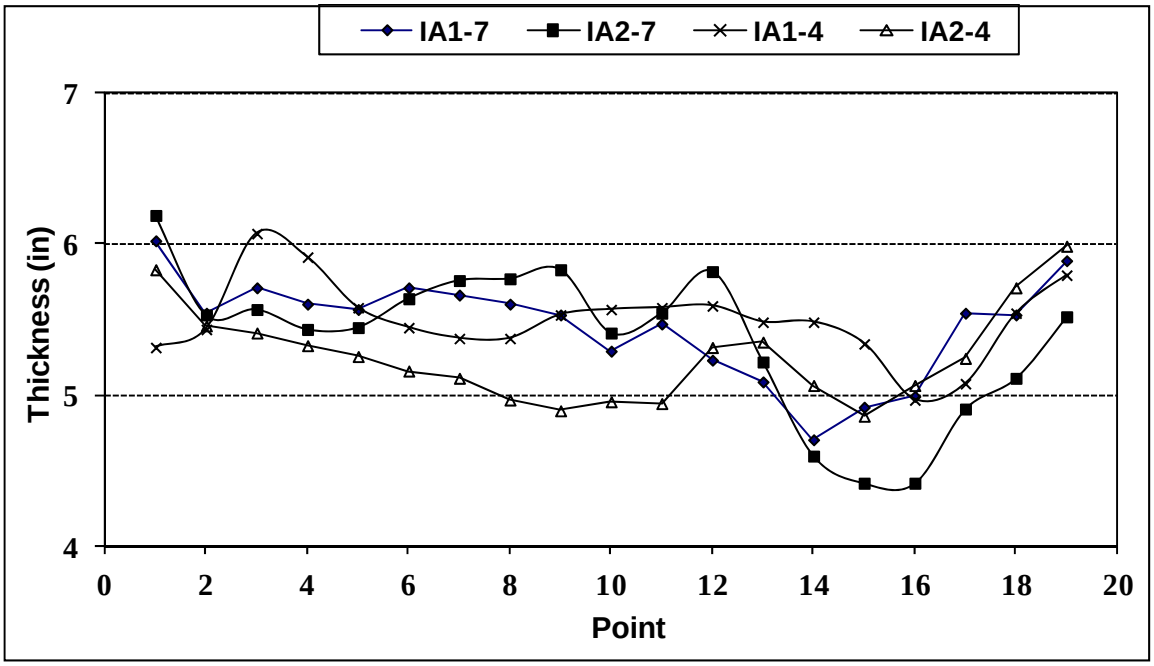

FIGURE 2.13: As-Constructed Thickness of Base Layer for Iowa Sections

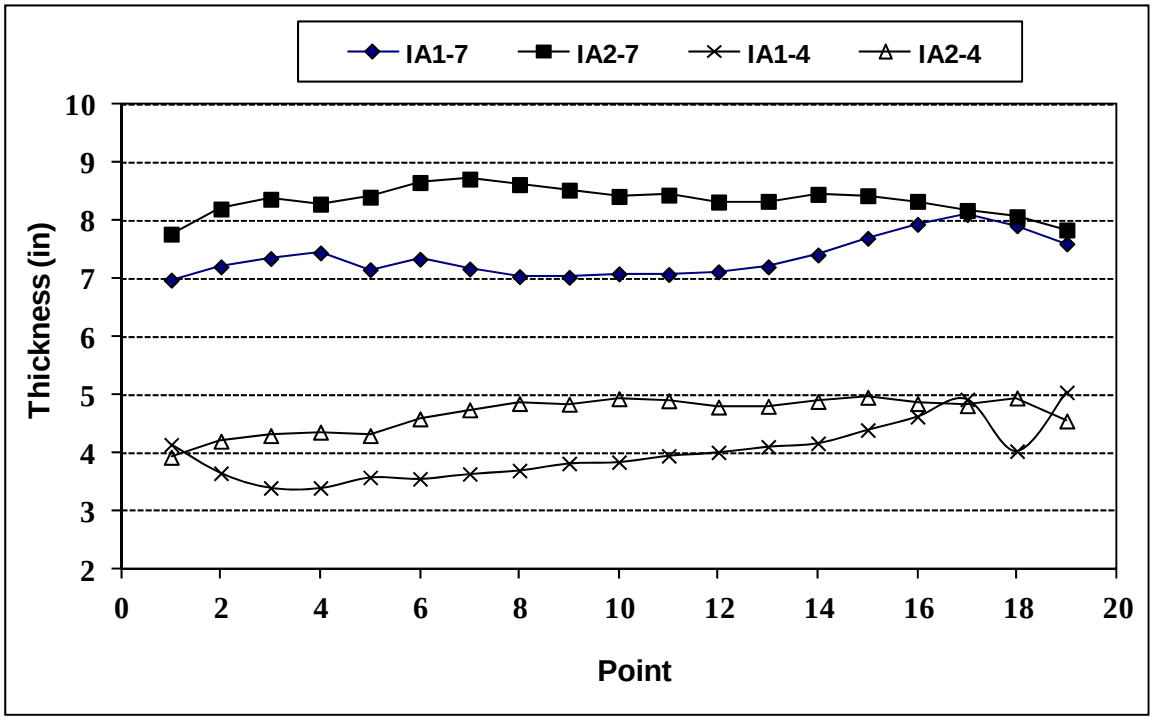

FIGURE 2.14: As-Constructed Thickness of HMA Layer for Iowa Sections

2.6. Instrumentation and Pavement Condition and Response Monitoring

Several sensors were placed in the test sections to monitor pavement response. In addition to complement measurements obtained from these sensors, falling-weight deflectometer (FWD) tests were also conducted.

2.6.1 Pressure Cells

Two stress cells (Geokon) were placed at the bottom of the base layer in the centerline of each pavement section to measure the vertical compressive stress at the top of the soil subgrade. Relative locations of the pressure cells are shown in Figure 2.15. One cell was placed in the western part of the lane and the other one in the eastern part. These 6-inch-diameter Geokon pressure cells were successfully used in previous projects and have shown good performance and acceptable results. These sensors were installed according to the manufacturer's guidelines. After the subgrade was compacted, holes were made to place the pressure cells. After the horizontal alignment was checked with a level, the cells were covered with a thin layer of sand.

2.6.2 Strain Gages

Strain gages were installed at the bottom of the asphalt concrete layer to measure transverse and longitudinal tensile strains. In each section, four strain gages were installed on the centerline of the lane, as shown in Figure 2.15. One gage was placed in the longitudinal direction and one in the transverse direction in the western part of the lane. Similarly one gage was placed in the longitudinal direction and one in the transverse direction in the eastern part of the lane.

The gages were constructed by attaching aluminum bars at the two ends of Tokyo Sokkai Kenkyujo (TML) strain gages. The H-Bars formed this way were fixed with short nails on top of the base layer after the layer was compacted, and before paving the asphalt concrete surface layer. During paving, asphalt mix was shoveled on top of the strain gages and the connection wires, and then lightly compacted to prevent deterioration of gages and wires during the paving operation. Five out of total 16 gages were lost during construction. It was presumed the gages became inoperable when the hot-asphalt mix melted their connection wires.

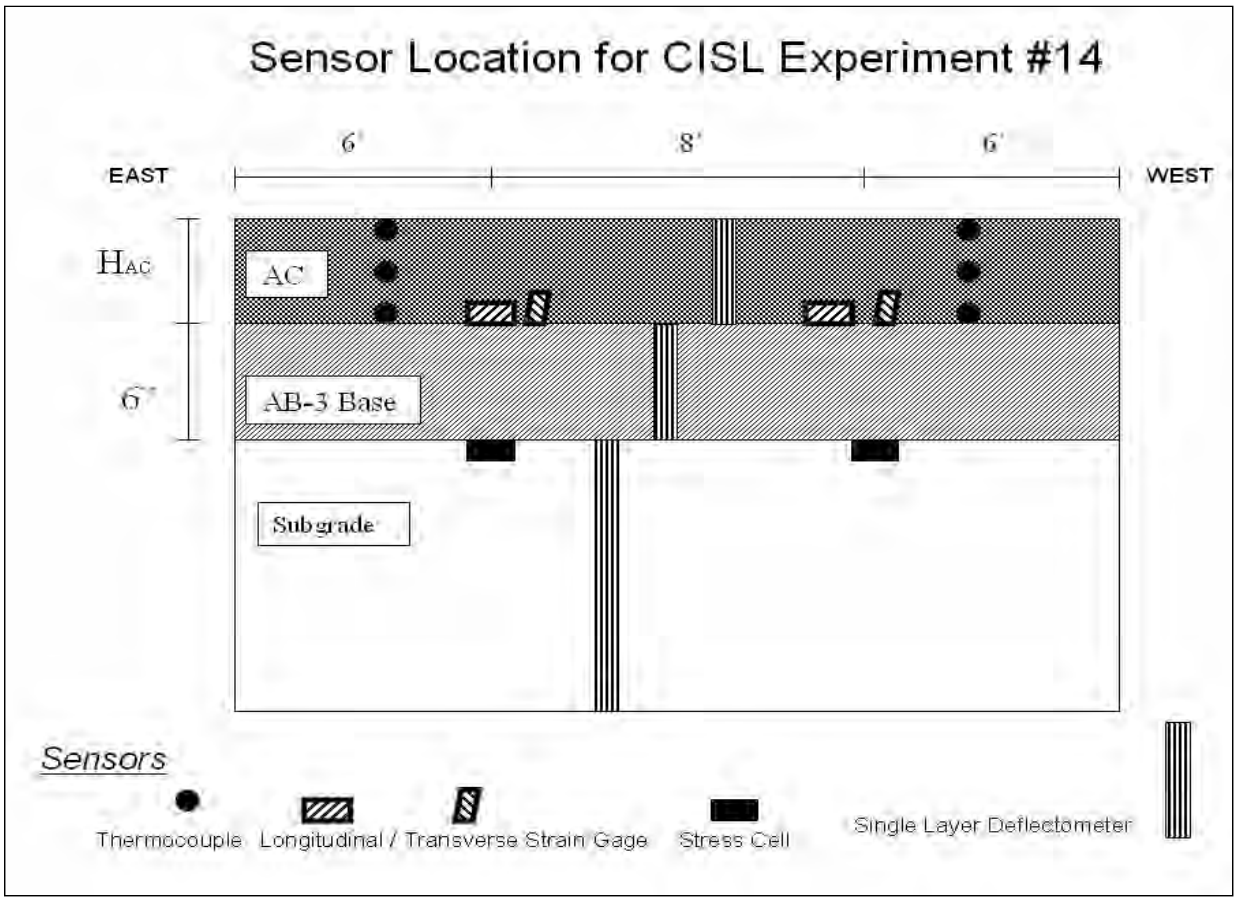

FIGURE 2.15: Location of Sensors Embedded in Pavement Structure

2.6.2.1 Single-Layer Deflectometer

In each pavement layer, a single-layer deflectometer devices were used to measure the dynamic deformation under the moving load as well as the permanent deformation. A single-layer Deflectometer (SLD) consists of a linear variable differential transformer (LVDT) fixed inside a short plastic tube underneath a circular plate (Figure 2.16). To measure the deformation in a pavement layer, the circular plate is glued to the top surface of the layer. The tip of the LVDT core is connected to a steel rod placed inside a steel tube that is driven in a vertical hole dug in the compacted layer; the rod moves freely inside the tube. The opposite end of the rod rests on a square steel plate placed underneath the layer before the material is placed and compacted.

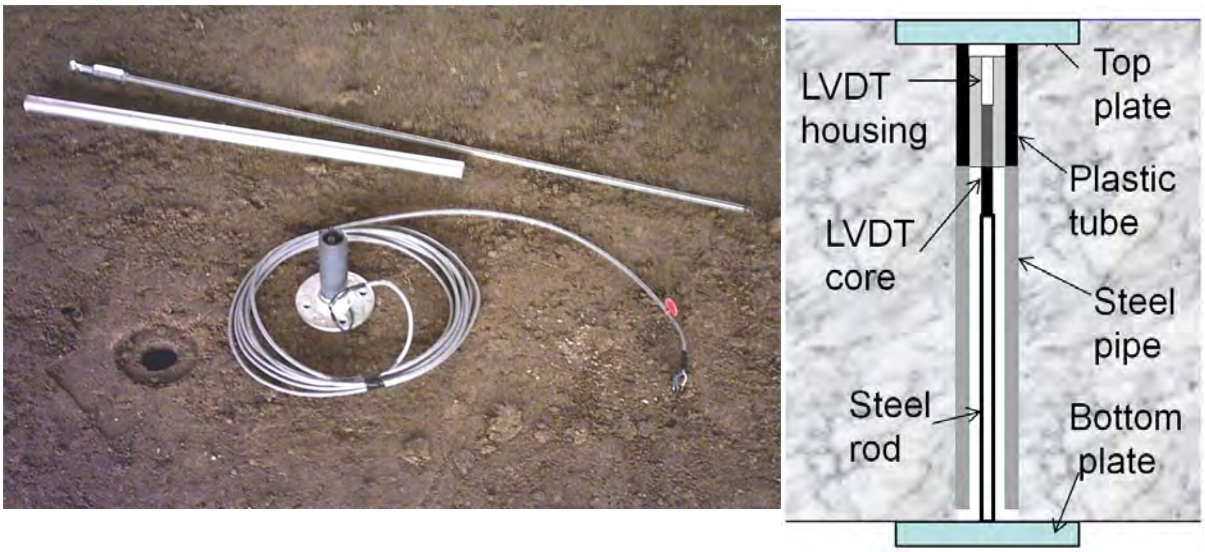

FIGURE 2.16: Single-Layer Deflectometer

The SLDs were not stacked but were placed in different locations (Figure 2.15). They functioned well with the exception of some SLDs mounted in the 4-inch asphalt concrete surface layer of the "fatigue-cracking" sections. Installation of the SLDs in the thin asphalt concrete layer was difficult since the length of the LVDT is about 3 inches with a fully retracted core.

2.6.3 Longitudinal Position of the CISL Load Assembly

A linear positioning gage, fixed to the east-north pole of the frame of the CISL machine, was used to record the longitudinal position of the loading bogie when strain/pressure measurements were performed.

The ATL load assembly position reading, dynamic wheel load, horizontal strains at the bottom of the asphalt surface layer, and vertical stress at the top of the subgrade were taken at a frequency of 100Hz by the same data acquisition system. Use of a single data acquisition system allowed all recording to be recorded on the same time basis in a single file.

2.6.4 Thermocouples

Four thermocouples were placed in each pavement structure, in the center location of each lane as shown in Figure 2.15. Two sensors were placed at the bottom of the asphalt concrete layer (3 inches from the surface) and two at the bottom of the base layer.

The thermocouples were manufactured in-house and their precision was verified before installation. Similar thermocouples were used in previous ATL experiments and produced acceptable results when compared with other conventional temperature-measurement devices. Temperature readings were taken monthly.

2.6.5 Falling-Weight Deflectometer Testing

Falling Weight Deflectometer (FWD) testing was performed by KDOT personnel on the constructed pavement structures before any APT loading was applied, at least once during the APT testing, and during the forensic analysis. The FWD tests were performed at three stations on each test lane as shown in Figure 2.17. For stations W and MW, the geophones were oriented toward the east. For stations ME and E, the geophones were oriented toward the west. Stations ME and MW were at the same location, in the center of the lane, but the geophones were directed to the East for station MW and to the west for station ME.

The FWD testing sequence consisted of three drops at the 6,000-lb load level followed by five drops at the 9,000-lb load level. The seven geophones were placed at: 0, 8, 12, 18, 24, 36 and 60 inches from the center of the FWD loading plate. The deflections recorded for the last drop at the 6,000-lb load level and the last two drops at the 9,000 lb-load level were used to back-calculate the elastic moduli of the pavement layers. These drops were selected since for the deflection measurements are the most reliable because the FWD loading plate should be in full contact with the pavement surface.

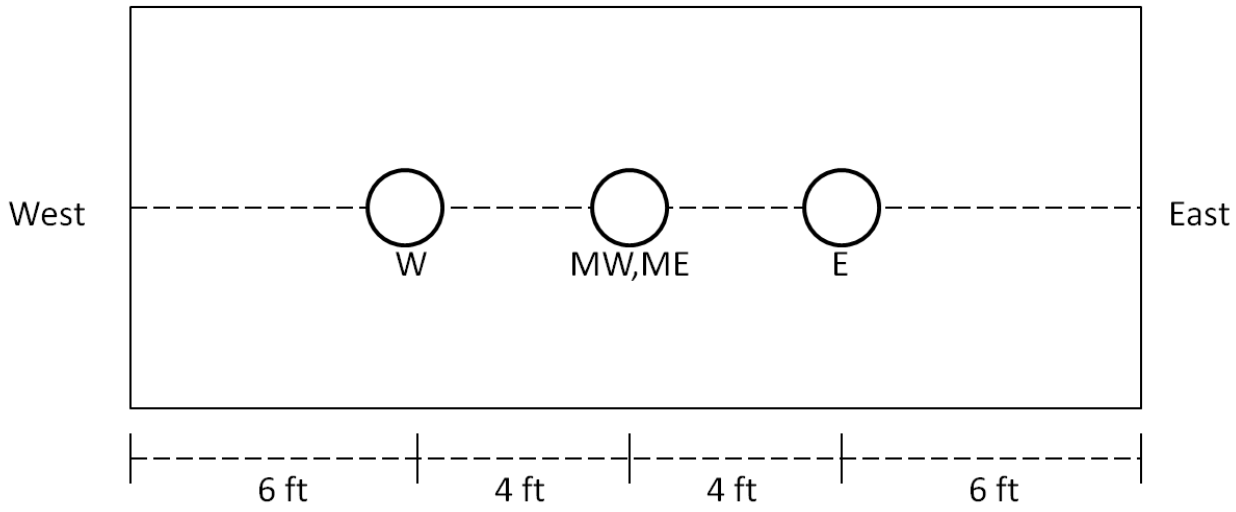

FIGURE 2.17: Location of Falling Weight Deflectometer Test Stations

TABLE 2.7: Falling Weight Deflectometer Test Dates

Test Sections	FWD testing Dates
KS1-7 and KS2-7	01/25/06; 05/23/06; 05/30/06; 10/09/07
KS1-4 and KS2-4	01/25/06; 03/28/06; 05/23/06; 10/09/07
MO1-7 and MO2-7	01/11/07; 07/09/07; 07/16/07; 10/09/07
MO1-4 and MO2-4	01/11/07; 10/09/07; 01/11/08; 06/16/08
IA1-7 and IA2-7	05/28/08; 06/16/08; 06/23/08
IA1-4 and IA2-4	05/28/08; 12/17/08; 06/15/09

2.7 Accelerated Pavement Testing Conditions

Test pavements were loaded in pairs using a single axle with a 23-kip (103 kN) load. Accelerated loading was done in bi-directional mode, at a speed of about 7 mph. The lateral wander applied in this experiment followed a truncated normal distribution with a standard deviation of 6 inches and maximum wander of 12 inches (Figure 2.18). Tire inflation pressure was maintained at 100 psi (690 kPa) and was verified weekly. The dynamic wheel load was monitored with load cells installed on each wheel; it was recorded at the same time as the response (stress, strain, and deformation) measurements.

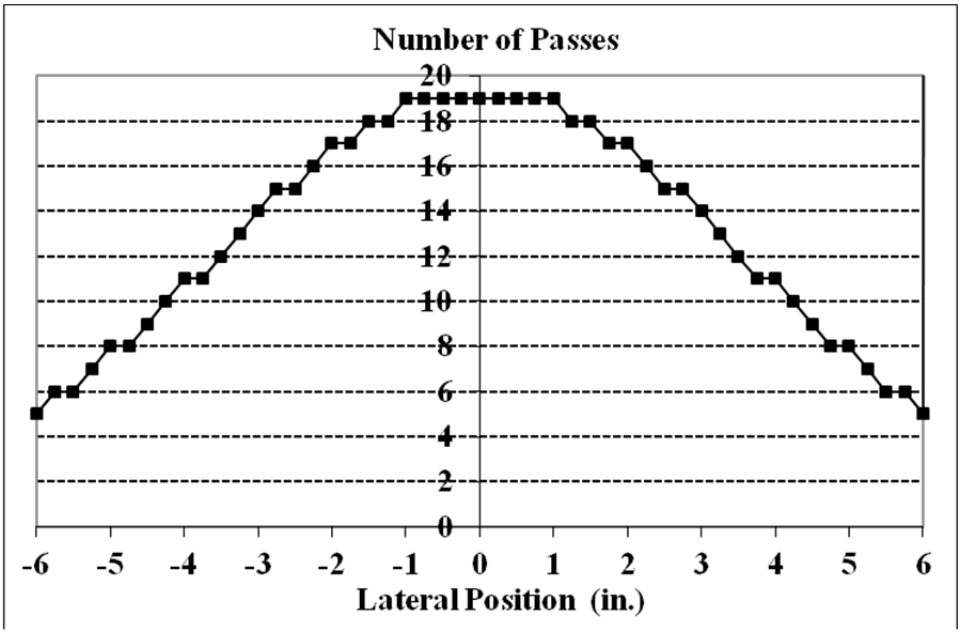

FIGURE 2.18: Number of Passes in Each Lateral Position of the Wheel

2.7.1 Testing Temperature

All testing was performed after the temperature-control chamber was built around the loading machine. Thermocouples embedded in the pavement structure indicated the corresponding pavement sections were tested under very similar temperature regimes (see Figures 2.19 to 2.24 and Appendix B). As expected, there were some deviations from the target temperatures (Table 2.1) since no air conditioning is available in the CISL laboratory where the tests were conducted.

2.7.2 Moisture Content

No water was added to the pavements during accelerated testing. Since the pavements were constructed in pits and the asphalt concrete surface layer was paved wall-to-wall, the moisture content in the subgrade soil remained relatively constant during accelerated testing. This was confirmed by time domain reflectometry (TDR) gages installed in the tested pavement structures, which indicated no change in volumetric moisture content.

2.8 Operating Schedule and Recording of Data

Appendix C includes the operating schedule of the project when test data was collected. Delays in the planned operating schedule were caused by delayed pavement construction and repairs to the APT machine.

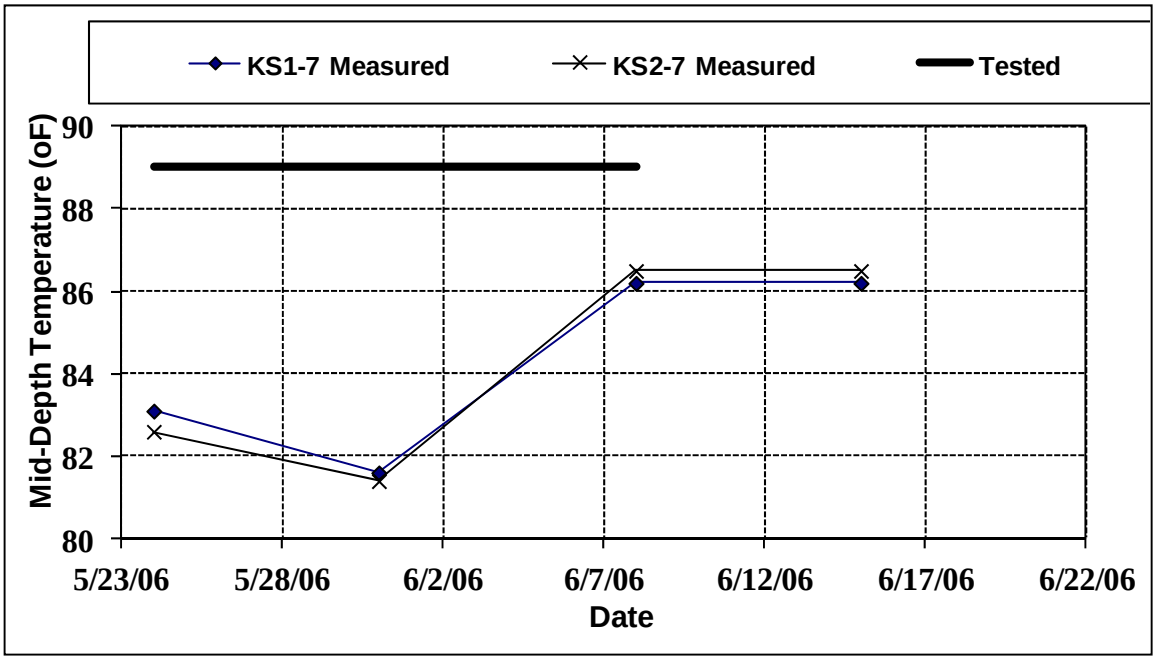

FIGURE 2.19: Mid-Depth Pavement Temperature for Kansas Rutting Sections

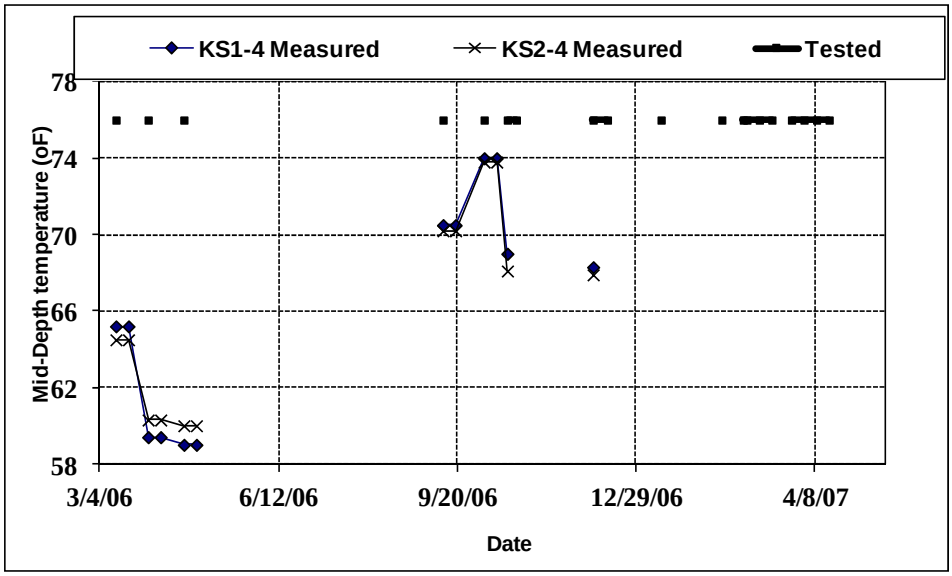

FIGURE 2.20: Mid-Depth Pavement Temperature for Kansas Fatigue-Cracking Sections

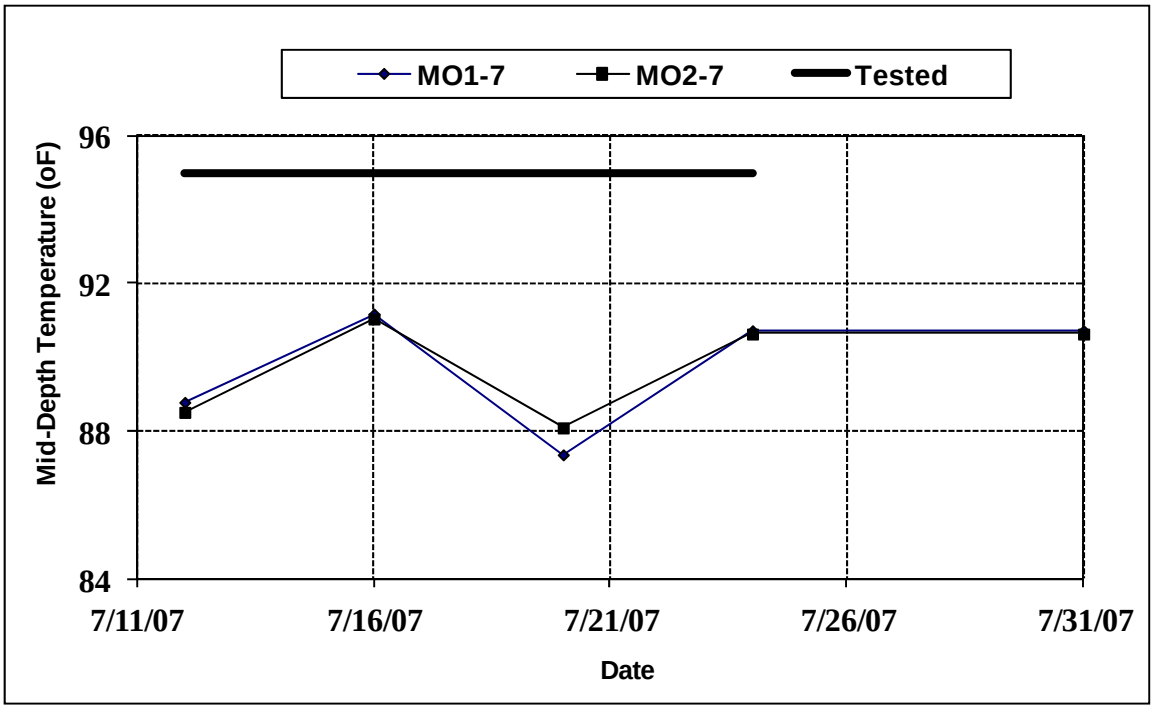

FIGURE 2.21: Mid-Depth Pavement Temperature for Missouri Rutting Sections

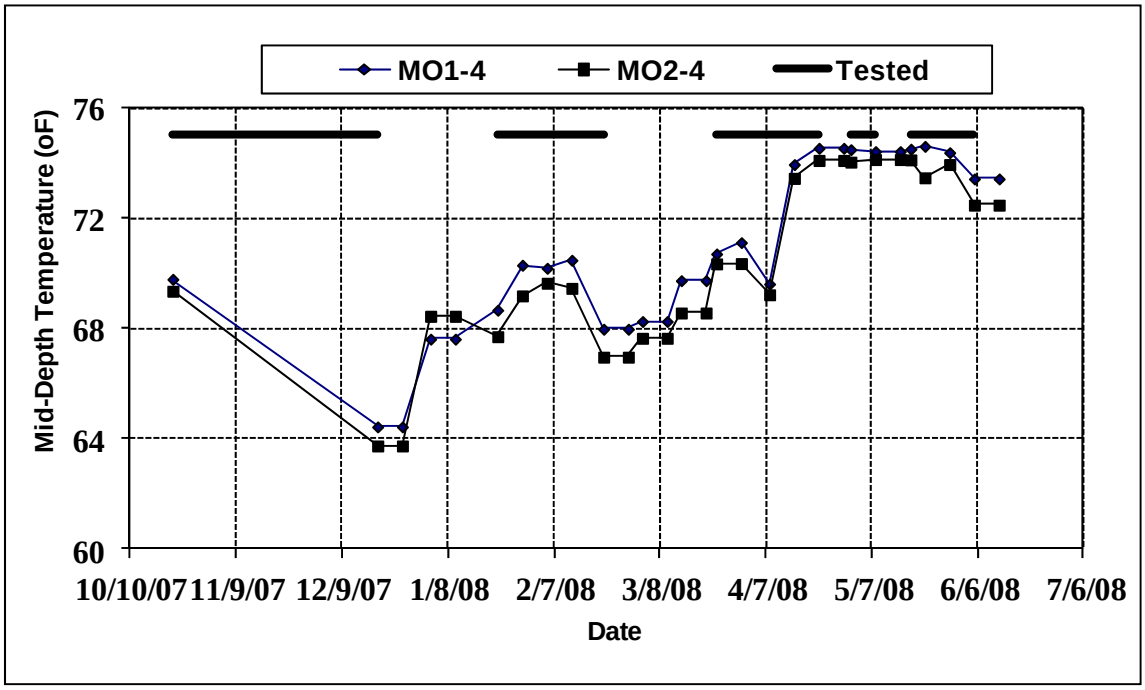

FIGURE 2.22: Mid-Depth Pavement Temperature for Missouri Fatigue-Cracking Sections

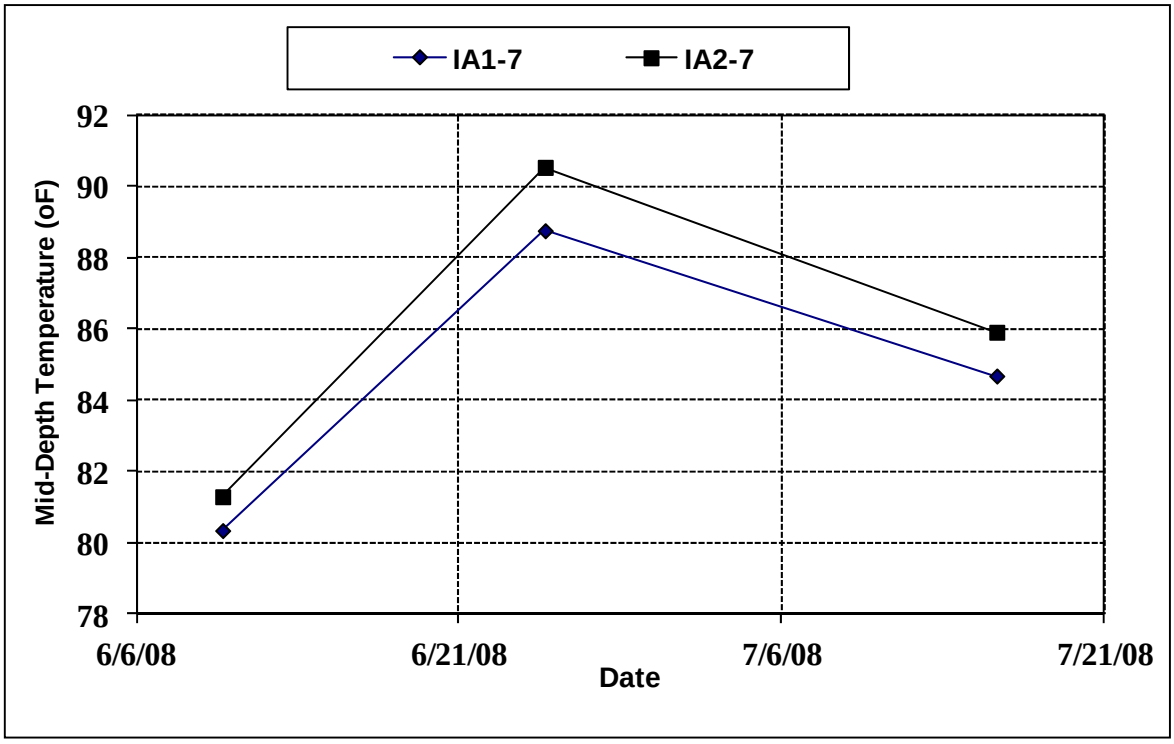

FIGURE 2.23: Mid-Depth Pavement Temperature for Iowa Rutting Sections

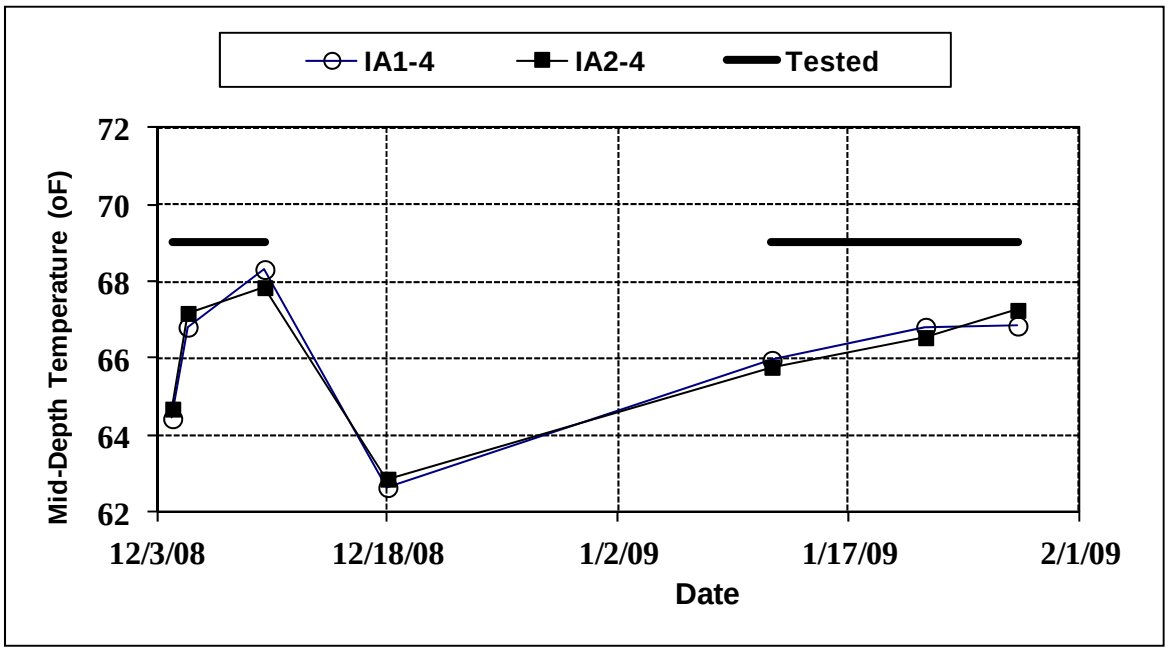

FIGURE 2.24: Mid-Depth Pavement Temperature for Iowa Fatigue-Cracking Sections

Chapter 3: Properties of the Asphalt Concrete Mixes

3.1 Asphalt Mix Designs and Testing

Asphalt mix designs for the six hot-mix asphalts were provided by the Kansas, Missouri, and Iowa Departments of Transportation. Two asphalt mix designs used in flexible pavement construction in each state were provided. The asphalt mix specifications and abbreviations are given in Table 3.1. The required mix design parameters for the asphalt mixes provided by the DOTs are given in Table 3.2. These mix designs were used by a local contractor to produce and construct pavement sections for APT in CISL. Table 3.3 summarizes as-built volumetric properties and in-place densities. The constructed mixes were somehow deviant from the asphalt mix design parameters provided. This affected the performance of some of the mixes. The tests performed to characterize asphalt mixes were used to evaluate mechanistic empirical material models and mechanistic permanent deformation prediction models. Laboratory tests for material characterization were performed on individual materials as well as on asphalt mixtures.

TABLE 3.1: Notations Used for HMA Mixes

	State	Asphalt mix type	Binder grade	Notation
1	Kansas	SM 19A	PG 64-22	KS1
2	Kansas	SM 12.5A	PG 64-28	KS2
3	Missouri	SP125C	PG 70-22	MO1
4	Missouri	SP125C	PG 64-22	MO2
5	Iowa	HMA 30M L-4	PG 64-22	IA1
6	Iowa	HMA 3M L-4	PG 64-22	IA2

TABLE 3.2: Mix Design Parameters

Parameter	Mix					
	KS1	KS2	MO1	MO2	IA1	IA2
NMAS	19.0	12.5	12.5	12.5	12.5	12.5
Design ESALs (million)	6.4	2.6	3.3	3.3	30.0	3.0
Ndesign	100	75	100	100	109	86
Binder	PG 64-22	PG 64-28	PG 70-22	PG 64 - 22	PG 64-22	PG 64-22
Design AC (%)	5.3	4.9	5.3	5.4	5.69	6.12

TABLE 3.3: Average As-Constructed Volumetric Properties of HMA Mixes

Parameter	Mix					
	KS1	KS2	MO1	MO2	IA1	IA2
AC (%)	5.61	5.2	5.3	5.4	7.5	7.0
AV @ N_{design} (%)	4.08	3.33	4.4	4.4	4.0	4.0
VMA	18.4	15.8	18.862	17.4	22.0	19.1
VFA	55.2	59.1	51.8	57.1	59.5	61.7
$\%G_{mm}@N_{ini}$	88.2	88.8	85.4	85.5	92.2	89.8
$\% G_{mm}@N_{des}$	96.1	95.6				
$\%G_{mm}@N_{max}$	97.2	99.9	97.2	97.3	99.6	99.4
Dust-binder ratio	1.0	0.9	1.1	1.1	0.5	0.5
In-place AV (%)	6.00±0.5	6.75±0.5	9.38±0.5	7.00±0.5	8.9±0.5	7.00±0.5

3.2 Properties of Constituent Materials

To verify Mechanistic-Empirical Pavement Design Guide (MEPDG) models, laboratory tests were performed on individual materials and on the asphalt mixtures from the three Midwest states, Kansas, Missouri and Iowa. The Kansas mixes were KS1 with a nominal maximum aggregate size (NMAS) of 19 mm, and asphalt binder grade PG 64-22 and KS2 with a NMAS of 12.5 mm and binder grade PG 64-28. Missouri mixes had NMAS of 12.5 mm, MO1 with PG 70-22 binder grade, and MO2 with PG 64-22 binder grade. Both Iowa mixes had NMAS of 12.5 mm and PG 64-22 binder grade; the difference was in the fine aggregate content (Table 3.2) and in cumulative design ESALs. Mix IA1 was designed for 30 million ESALs and IA2 for 3 million ESALs (Table 3.2).

Quality of materials is critical to the performance of asphalt mixes. Aggregates make up 80 to 85% of the mixture by volume. Therefore, aggregates characteristics are important for the performance of asphalt mixture. The Superpave asphalt mix design recommended tests that should be performed on aggregates to ensure that they meet required specifications, and they will result into asphalt mixtures with the desirable performance. Laboratory tests were performed on

aggregates and asphalt binder to ensure all materials used met specification requirements. The following tests were performed on aggregates:

- Gradation analysis (AASHTO T 27)
- Fine aggregate angularity (KT-50)
- Los Angeles abrasion test (ASTM C 131 method B)
- Flat and elongated particles (ASTM D 4791)
- Fractures particles (ASTM D 5821)

Asphalt binder is a viscoelastic material affected by loading time and temperature. Superpave uses performance grade (PG) asphalt to optimize its effect on the performance of asphalt pavement in a range of temperatures. The asphalt binders for this project were provided by the respective DOTs. The dynamic shear rheometer test was performed on asphalt binder to obtain shear modulus (G*) and phase angle (δ) for each binder used. These parameters were determined at seven different temperatures as required by AASHTO T 315 protocol. The test temperatures were 4, 13, 21, 29, 38, 46, and 54^{o}C. The tests were conducted on original binder, on reside after rolling thin film oven test (RTFO), and residue from pressure-aging vessels (PAV).

3.2.1 Gradation Analysis of Aggregates (AASHTO T 27)

This test was conducted in accordance with AASHTO T 27 to obtain particle-size distribution of individual aggregate samples as well as aggregate blends that met mix design specifications (job mix formula). The individual aggregate blend percentages are given in Tables 3.4 to 3.6; and the 0.45 power gradation charts of the job mix formulas for Kansas, Missouri, and Iowa aggregates are given in Figures 3.1 to Figure 3.4. The aggregate gradation of the six mixes met the Superpave gradation specification. Tables 3.5 to 3.9 give the gradation data for each mix and the grading band limits. These aggregate blend percentages were adopted for the laboratory sample fabrication.

TABLE 3.4: Aggregate Blends Used for Kansas Mixes

Mix	Aggregate designation	Source location	%	Mix	Aggregate designation	Source location	%
Kansas KS1	CS-1	3/4" Bayer Zeandale rock	31	Kansas KS2	CS-1	1/2" Bayer Zeandale rock	19
	CS-1A	Bayer Zeandale Man. sand	22		CS-1A	Bayer Zeandale Man. sand	16
	CS-2	Bayer Zeandale screenings	12		MSD 1	Bayer Zeandale Man Sand	16
	SH-1A	Bingham drag sand - chat	25		CG-5	MCM Crushed gravel	21
	SSG-1	MSM concrete sand*	10		SSG	MCM concrete sand *	28

* Kansas river sand

TABLE 3.5: Aggregate Blends Used for Iowa Mixes

Mix	Aggregate designation	Source location	%	Mix	Aggregate designation	Source	%
Iowa 30M ESALS (IA1)	A85006	1/2" minus - M.M. Ames	30	Iowa 3M ESALS (IA2)	A85006	1/2" cr. Limestone -M.M. Ames	35
	A85006	3/8" chip - M.M. Ames	20		A85006	3/8" chip - M.M. Ames	20
	A85006	Man. sand - M.M. Ames	40		A85006	Man. sand - M.M. Ames	20
	6A77502	Sand - M.M. Johnson	10		6A77502	Sand - M.M. Johnson	25

TABLE 3.6: Aggregate Blends Used for Missouri Mixes

Mix	Aggregate designation	Source location	%
Missouri Mix	64D1T037	3/4" APAC sugar creek rock	27
	64D1T038	3/8" APAC sugar creek rock	40
	64D1T040	Humble S & G flint chat	25
	64D1T039	APAC Sugar creek SG	8

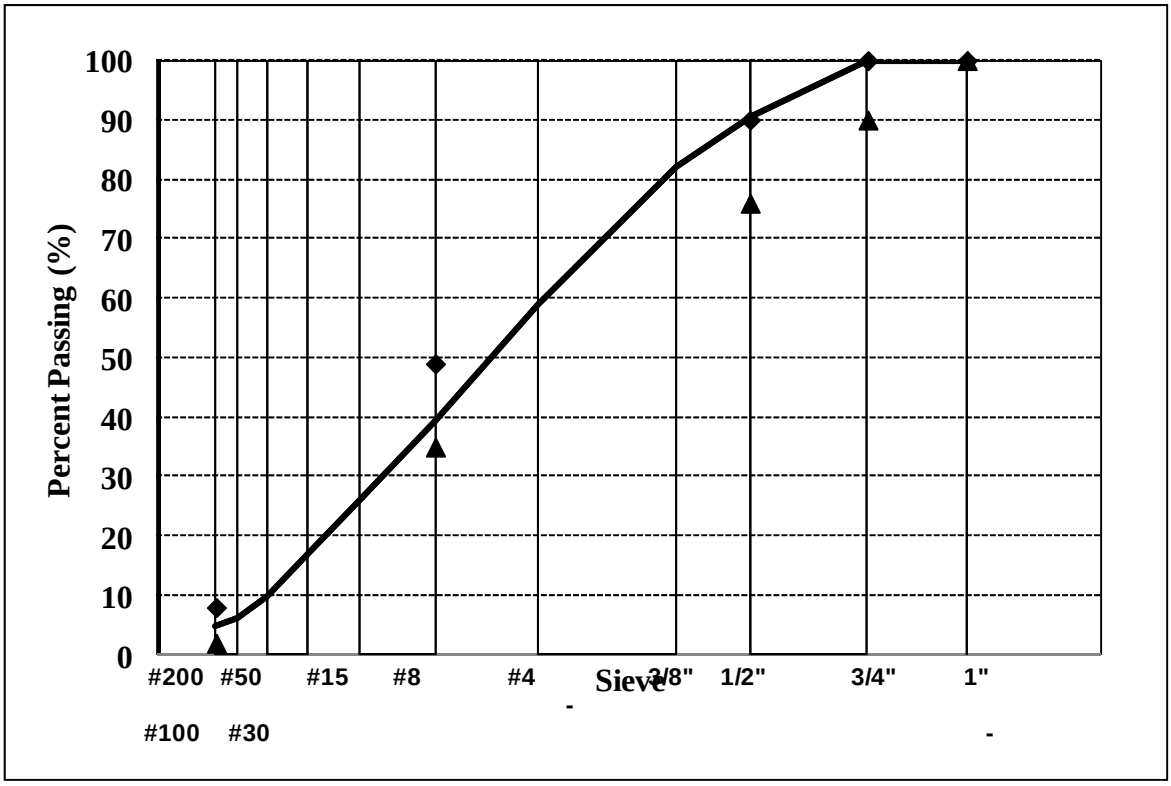

FIGURE 3.1: Aggregate Gradation with Control Points for KS1 Mix

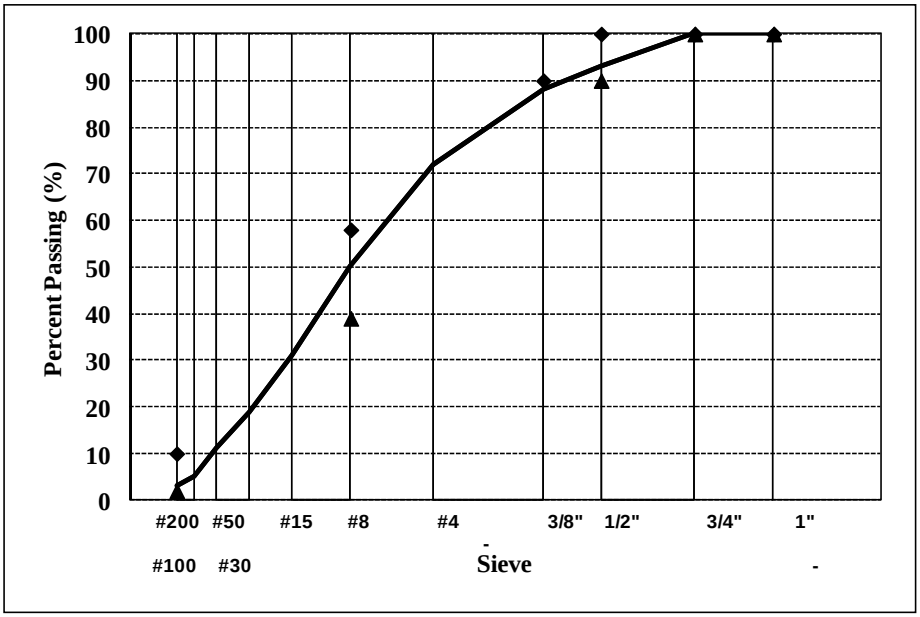

FIGURE 3.2: Aggregate Gradation with Gradation Band for KS2 Mix

TABLE 3.7: Gradation Data for Kansas Mixes

Sieve size (in)	Upper Limit	Gradation KS1	Lower Limit	Upper Limit	Gradation KS2	Lower Limit
1”	**100**	100	**100**	**100**	100	**100**
¾”	**100**	100	**90**	**100**	100	**100**
½”	**90**	90.3		**100**	93	**90**
3/8”		82.1		**90**	88	
#4		59.0			72	
#8	**49**	39.3	**35**	**58**	50	**39**
#16		25.9			31	
#30		17			19	
#50		10.1			11	
#100		6.0			5	
#200	**8**	4.7	**2**	**10**	3.2	**2**

TABLE 3.8: Gradation Data for Missouri Mixes

Sieve size (in)	Upper limit	Gradation MO	Lower limit
1”	**100**	100	**100**
¾”	**100**	100	**100**
½”	**100**	90.6	**90**
3/8”	**90**	79.8	
#4		49.3	
#8	**58**	31.8	**28**
#16		21.1	
#30		13.6	
#50		7.7	
#100		5.0	
#200	**10**	4.1	**2**

TABLE 3.9:Gradation Data for IA Mixes

Sieve size (in)	Upper limit	Gradation IA1	Lower limit	Upper limit	Gradation IA2	Lower limit
1”	**100**	100	**100**	**100**	100	**100**
¾”	**100**	100	**100**	**100**	100	**100**
½”	**100**	98	**91**	**100**	98	**91**
3/8”	**96**	89	**82**	**96**	89	**82**
#4	**69**	62	**55**	**69**	62	**55**
#8	**49**	44	**39**	**49**	44	**39**
#16		29			33	
#30	**22**	18	**14**	**24**	20	**16**
#50		9.2			9.5	
#100		4.5			4.4	
#200	**5.3**	3.3	**1.3**	**5.4**	3.4	**1.4**

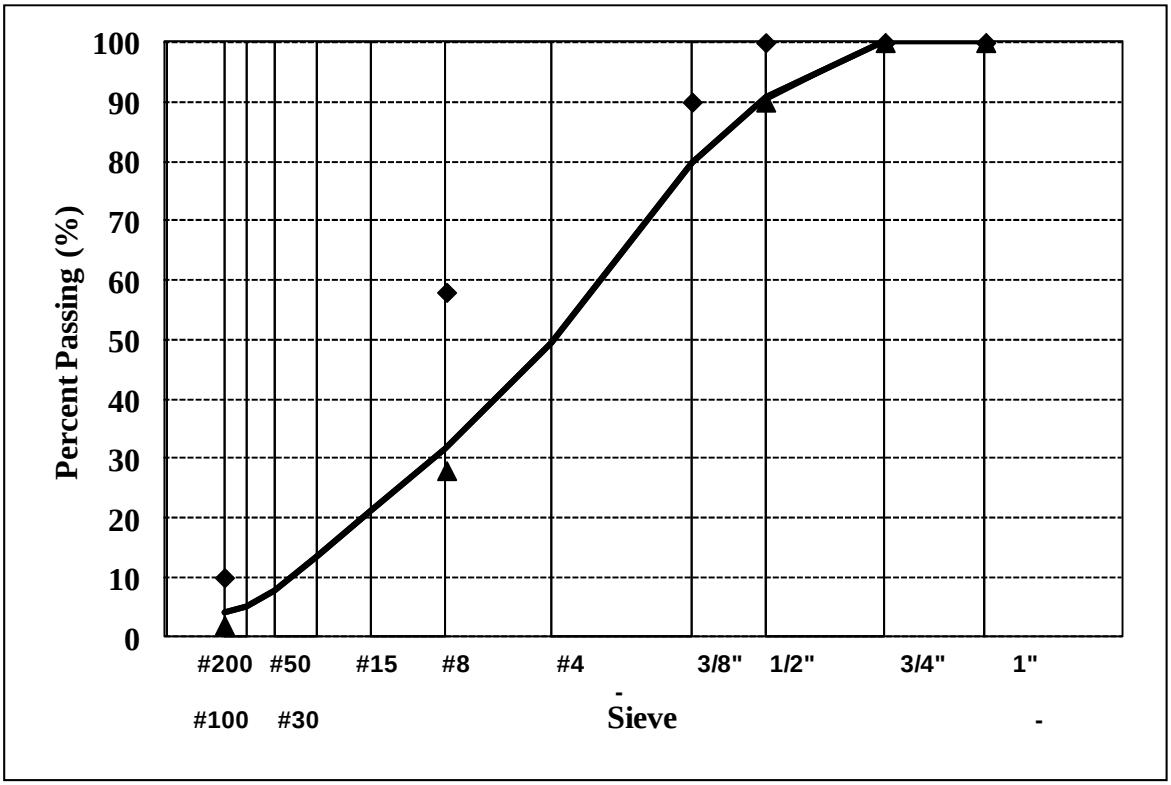

FIGURE 3.3: Aggregate Gradation with Gradation Band for MO1 and MO2 Mixes

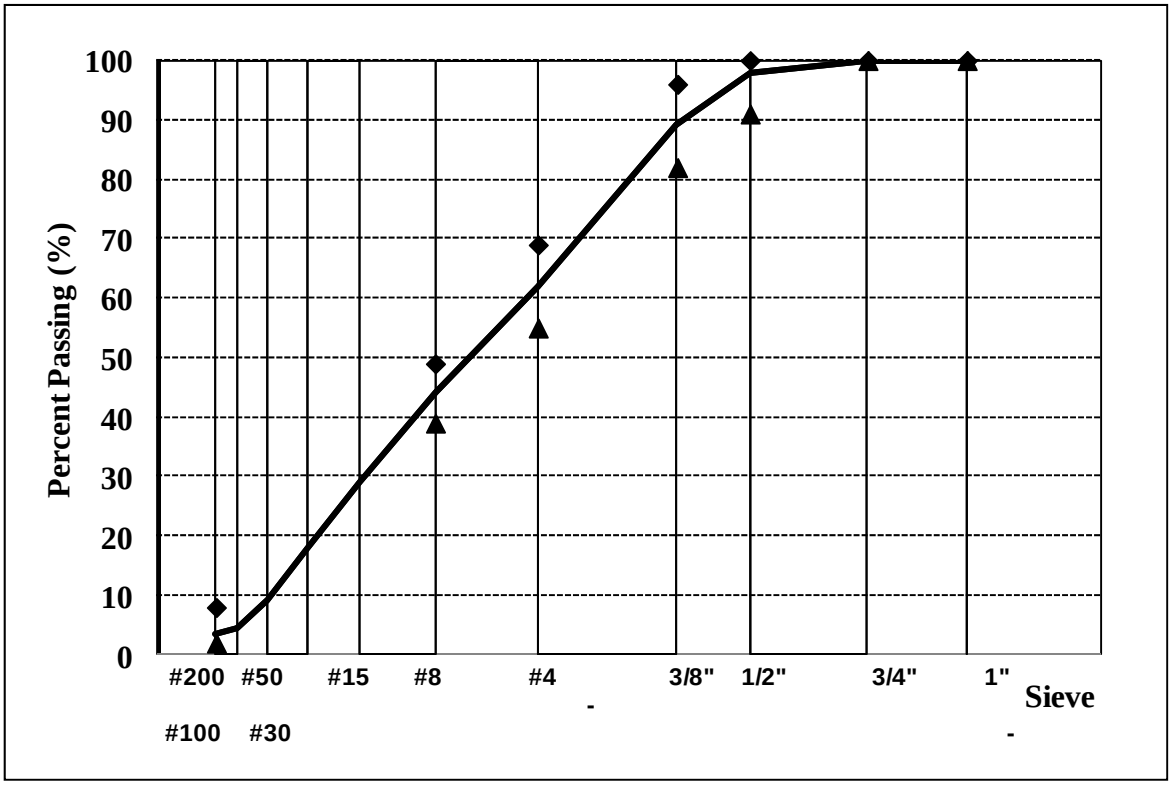

FIGURE 3.4: Aggregate Gradation with Gradation Band for IA1 and IA2 Mixes

3.2.2 Fine Aggregate Angularity – KT-50

The fine aggregate angularity (FAA) test was conducted to assess the texture of fine aggregates. Fine aggregate angularity is desired for formation of a strong aggregate skeleton that can resist permanent deformation. Angular aggregates have high friction between particles and therefore are desired over smooth aggregates due to its ability to resist deformation. This test was performed on individual fine aggregates passing a No.8 (2.36 mm) sieve following the KT-50 test procedure. D'Angelo et al. (2004) suggest that natural sand should have FAA less than 44, while manufactured (crushed) sand should have FAA more than 44. Results obtained for fine aggregates tested had FAA values greater than 44 for manufactured sand and FAA less than 44 for natural sand (SSG). Table 3.10 provides results from this test. It is expected natural sand will have lower values of FAA as compared with manufactured sand, because natural sand has fewer fractured faces and smoother texture.

TABLE 3.10: Fine Aggregates Angularity Test Results

Aggregate mix blend	Aggregate designation	FAA	Specification (AASHTO)
KS1	CS-1A	47.9	Min 40.00
	CS-2	47.25	
	SH-1A	48.55	
	SSG-1	38.00	
KS2	CS-1C	47.55	Min 40.00
	CG-5	44.4	
	SSG	38.38	
MO	64D1T040	48.35	Min 40.00
	64D1T039	48.15	
IA1	NMAS 12.5	44.2	Min 40.00
IA2	NMAS 12.5	45.2	Min 40.00

3.2.3 Los Angeles Abrasion Test

Aggregates are required to be hard and tough to resist crushing, degradation, and disintegration that occur when stockpiled or in the mixing, laying, and compaction process. They are also expected to provide internal friction that will transmit wheel loads to underlying layers and at the same time be resistant to abrasion and polishing due to traffic load. The Los Angeles abrasion test was carried out to obtain an indication of desired toughness and abrasion

characteristics of aggregates. This test was carried out on course aggregates in accordance with ASTM C 131 for Kansas and Missouri aggregates and method C for Iowa aggregates. The test was performed to determine aggregate toughness and resistance to abrasion. AASHTO recommends a maximum LAA value of 40% for aggregates used for surface course of high-type HMA pavements. Table 3.11 summarizes the test results and indicates that all coarse aggregates fulfilled the requirements for abrasion resistance.

TABLE 3.11: Results of Los Angeles Abrasion Tests

Aggregate mix blend	Aggregate designation	LAA (%)	Specification (AASHTO)
KS1	CS-1	26.1	Max 40.0
KS2	CS-1B	27.0	
MO	64D1T037	23.6	
IA1	12.5 NMAS	24.3	
IA2	12.5 NMAS	25.3	

3.2.4 Flat and Elongated Particles ASTM D 4791

Aggregate particles suitable for use in hot-mix asphalt should be cubical in shape rather than round, flat, thin, or elongated. Angular-shaped aggregates are desired in HMA because they exhibit greater interlock and internal friction. Rounded aggregates provide better workability but are prone to continual densification under traffic, ultimately leading to rutting. Flat, thin, and elongated particles are not desired in the mix because they form slip planes and reduce aggregate interlock. This test was performed according to ASTM D 4791 on material coarser than 9.5 mm. Flat (thickness to width) and elongated (width to length) aggregates were manually tested using a proportional caliper. Superpave recommends the percent of flat and/or elongated aggregates to be limited to 10%, using a length to width or thickness ratio of 5 to 1. Table 3.12 summarizes results from this test.

TABLE 3.12: Flat and Elongated Particles Test Results

Aggregate mix blend	Aggregate designation	Flat (%)	Elongated (%)	Flat and elongated (%)	Specification (AASHTO)
KS1	CS-1	0.48	0.09	1.47	Max 10.00
KS2	CS-1B	0.21	0.04	0.25	Max 10.00
	CS-1	0.16	0	0.16	
MO	64D1T040	0.07	0	0.07	Max 10.00
	64D1T039	0.38	0	0.38	
IA1	NMAS 12.5	0.16	0.34	0.5	Max 10.00
IA2	NMAS 12.5	0.11	0.18	0.29	Max 10.00

3.2.5 Percent of Fractured Particles in Coarse Aggregates ASTM D 5821

Fractured faces on aggregate particles increase aggregate interlock and hence improve mix stability and increase resistance of the mix to permanent deformation. This test was performed following ASTM D 5821 to determine the percent of aggregate particles having at least one fractured face and at least two fractured faces. The requirement is at least 95% and should have at least one fractured face. The results, tabulated in Table 3.13, show that all aggregate samples passed the fractured faces test. Superpave mix specifications for 9.5mm chips require particles with at least one fractured face to be 99%, and for particles with at least two fractured faces to be 95%.

TABLE 3.13: Percent Fractured Particles Test Results

Aggregate mix blend	Aggregate designation	Fractured faces		Specification (AASHTO)
		At least one	At least two	
KS1	CS-1	100	100	At least one fractured face Min 95% At least two fractured faces Min 90%
KS2	CS-1B	99.98	99.98	
	CS-1	99.95	99.95	
MO	64D1T040	100	100	
	64D1T039	100	100	
IA1	NMAS 12.5	99.36	99.47	
IA2	NMAS 12.5	100	99.28	

3.2.6 Dynamic Shear Rheometer Test on Asphalt Binders

The dynamic shear rheometer (DSR) test was performed on asphalt binder to characterize the viscous and elastic behavior of asphalt binders at high and intermediate (service) temperatures. The DSR test measures the complex shear modulus (G*) and phase angle (δ) of asphalt binder. The complex modulus, G*, is considered as the total resistance of binder to deformation when sheared repeatedly. It consists of two components: storage modulus G', which is elastic (recoverable) and loss modulus G", the viscous (non-recoverable). The phase angle delta (δ) is the time lag between applied stress and the resulting strain (D'Angelo 2004). For perfectly elastic materials, delta is zero, and for viscous materials like hot asphalt binder, delta is close to 90^{o}. At intermediate service temperature, asphalt binder is viscoelastic, possessing both elastic and viscous characteristics. It is therefore important to use both G* and δ to characterize the asphalt binders. For resistance to permanent deformation, a high-complex shear modulus (G*) and low- phase angle (δ) are desired because the higher the G* value, the stiffer the binder, and the lower the phase angle, the more elastic the asphalt binder (D'Angelo 2004). The test was performed at seven temperatures (4, 13, 21, 29, 38, 46, and 54^{o}C) on original binders and on the residual binders after the rolling thin film oven (RTFO) test and pressure-aging vessel (PAV). As expected, binder stiffness increased with binder aging, while binder stiffness decreased when the temperature increased. The DSR test results are given in Tables 3.14 to 3.18 and Figures 3.5 to 3.8.

TABLE 3.14: DSR Test Results on Kansas PG 64-22 Binder (KS1 Mix)

Temp °C	Original		RTFO		PAV	
	Shear mod. (G*) Pa	Phase angle δ (°)	Shear mod. (G*) Pa	Phase angle δ (°)	Shear mod. (G*) Pa	Phase angle δ (°)
4	1.40E+07	0	3.43E+07	41.31	NA	NA
13	1.02E+07	65.17	1.03E+07	45.2	NA	NA
21	1.76E+06	66.7	4.11E+06	54.3	7.15E+08	42
29	4.67E+05	72.04	1.13E+06	63.32	2.48E+08	48.52
38	89600	78.37	2.28E+05	70.64	5.97E+07	56.63
46	22120	82.31	57800	75.76	1.72E+07	62.85
54	5938	85.23	15420	80.03	5.12E+06	68.32

TABLE 3.15: DSR Test Results on Kansas PG 64-28 Binder (KS2 Mix)

Temp °C	Original		RTFO		PAV	
	Shear mod. (G*) Pa	Phase angle δ (°)	Shear mod. (G*) Pa	Phase angle δ (°)	Shear mod. (G*) Pa	Phase angle δ (°)
4	1.49E+07	180	NA	NA	NA	NA
13	3.94E+06	62.27	NA	NA	NA	NA
21	8.28E+05	67.95	NA	NA	NA	NA
29	2.20E+05	69.9	1.60E+05	63.95	NA	NA
38	51310	72.66	2.20E+05	67.22	2.88E+07	58.63
46	16080	74.88	49960	69.48	9.24E+06	62.06
54	5464	76.96	16580	71.76	3.17E+06	64.63

TABLE 3.16: DSR Test Results on Missouri PG 70-22 Binder (MO1)

Temp °C	Original		RTFO		PAV	
	Shear mod. (G*) Pa	Phase angle δ (°)	Shear mod. (G*) Pa	Phase angle δ (°)	Shear mod. (G*) Pa	Phase angle (°)
4	NA	NA	NA	NA	NA	NA
13	NA	NA	NA	NA	NA	NA
21	1.66E+06	65.75	3.97E+06	53	4.62E+08	41.95
29	3.82E+05	68.77	1.32E+06	59.97	1.61E+08	47.84
38	1.10E+05	71.19	3.04E+05	64.99	4.30E+07	54.29
46	31770	72.53	1.44E+05	66.69	1.44E+07	57.54
54	10280	73.23	52370	67.97	5.03E+06	60.48

TABLE 3.17: DSR Test Results on Missouri PG 64-22 Binder (MO2)

Temp °C	Original		RTFO		PAV	
	Shear mod. (G*) Pa	Phase angle δ (°)	Shear mod. (G*) Pa	Phase angle δ (°)	Shear mod. (G*) Pa	Phase angle δ (°)
4	NA	NA	NA	NA	NA	NA
13	NA	NA	NA	NA	NA	NA
21	2.02E+06	64.27	8.82E+06	56.1	4.85E+08	42.65
29	4.35E+05	71.44	1.00E+06	63.16	1.60E+08	48.48
38	78130	79.94	2.09E+05	70.07	4.06E+07	55.39
46	19270	81.61	55750	74.88	1.26E+07	59.83
54	5390	84.38	29760	77.14	4.00E+06	65.51

TABLE 3.18: DSR Test Results on Iowa PG 64-22 Binder (IA1 and IA2 mixes)

Temp °C	Original		RTFO		PAV	
	Shear mod. (G*) Pa	Phase angle δ (°)	Shear mod. (G*) Pa	Phase angle Δ (°)	Shear mod. (G*) Pa	Phase angle δ (°)
4	NA	NA	NA	NA	1.05E+08	26.77
13	NA	NA	NA	NA	3.91E+07	34.3
21	2.06E+06	65.7	7.03E+06	56.79	1.41E+07	41.57
29	4.11E+05	72.68	9.60E+05	62.81	4.39E+06	49.3
38	76150	78.53	1.93E+05	69.97	1.11E+06	57.31
46	19420	82.26	50710	74.78	3.32E+05	63.49
54	5566	85.04	14310	79.33	1.00E+05	68.7

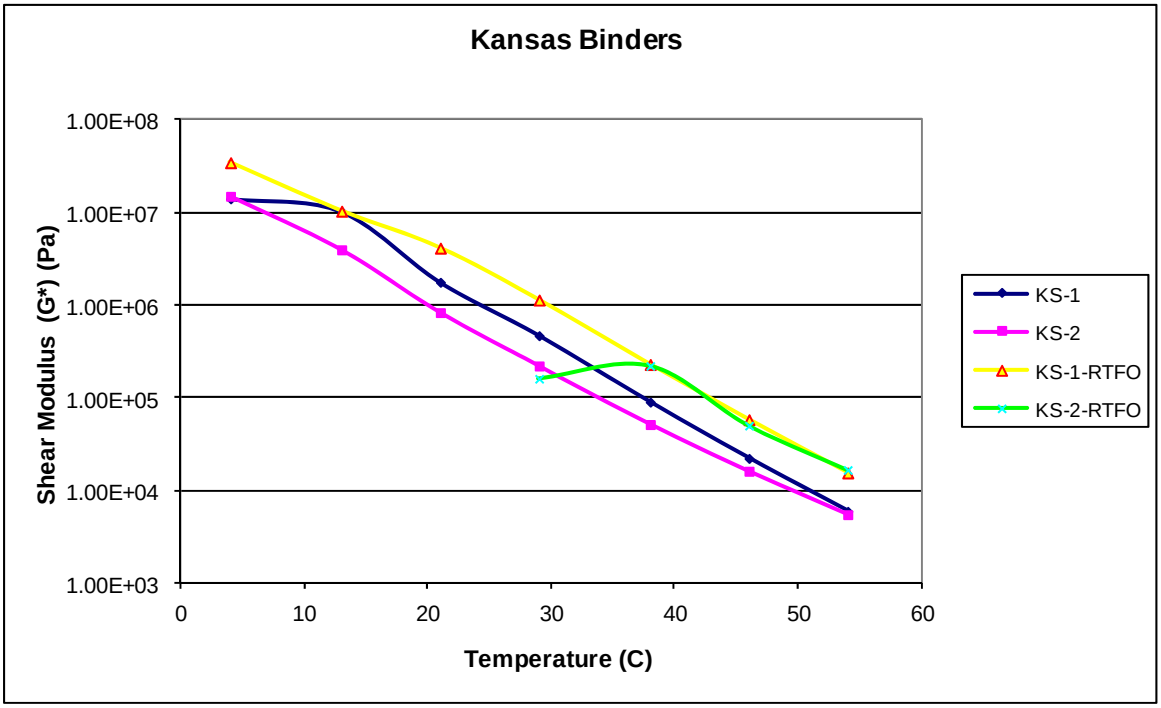

FIGURE 3.5: DSR Test Results on Original Binder and after TFOT for Kansas Binders

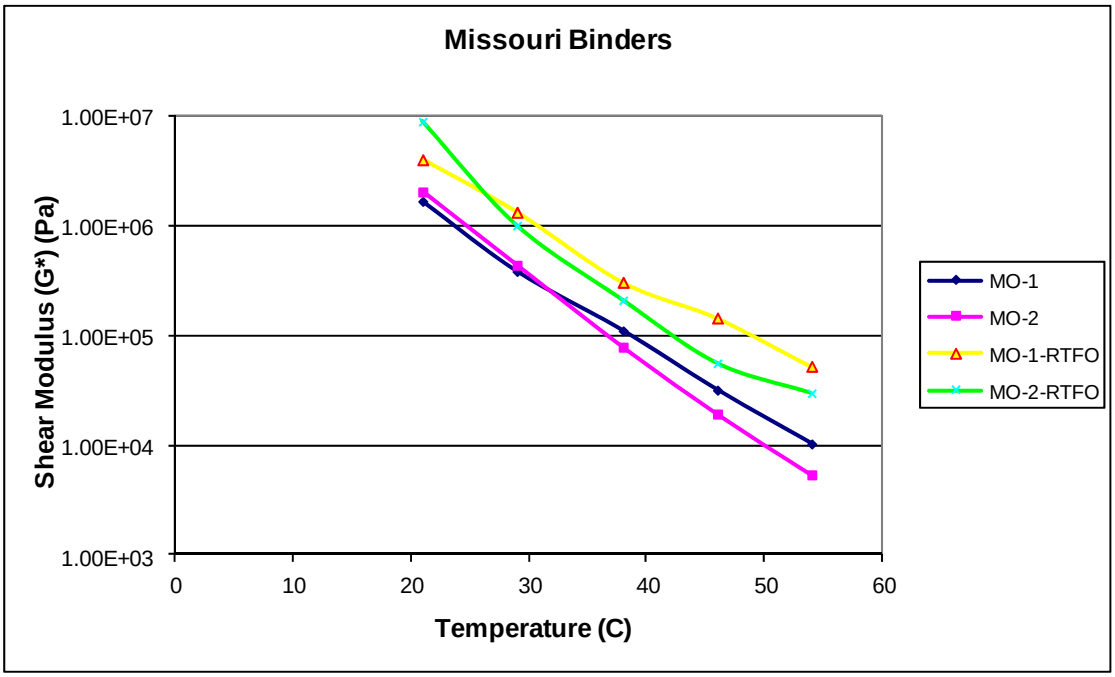

FIGURE 3.6: DSR Test Results on Original Binder and After TFOT for Missouri Binders

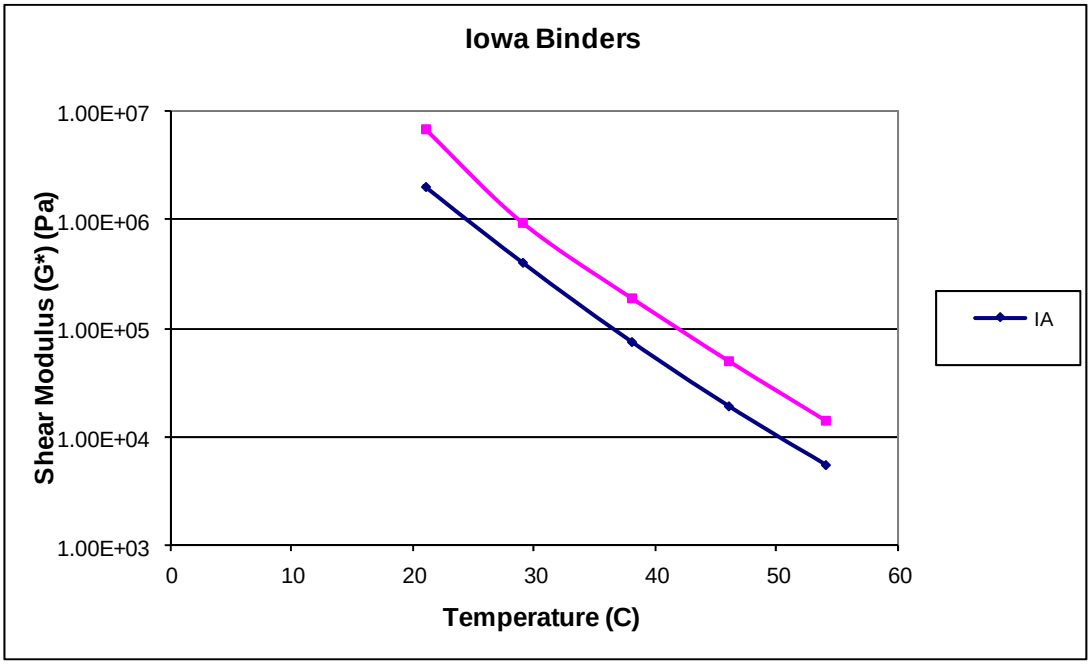

FIGURE 3.7: DSR Test Results on Original Binder and after TFOT for Iowa Binder

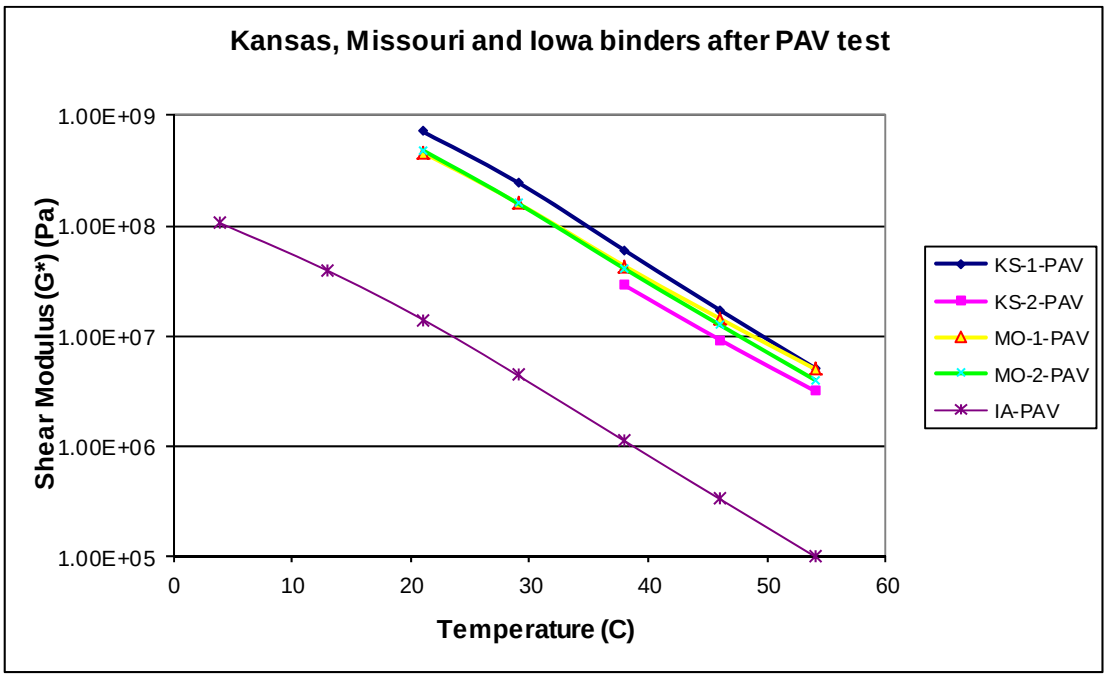

FIGURE 3.8: DSR Test Results on PAV Aged Binders

3.3 Laboratory Tests on Asphalt Mixes

A limited amount of materials was provided by Kansas, Missouri, and Iowa Departments of Transportation. These materials were used for construction of road sections in CISL, testing constituent materials, and testing asphalt mixes to obtain fundamental properties of materials. The asphalt mix designs were also provided by the DOTs for their respective asphalt mixes. A local contractor was employed to construct the pavement sections in the Civil Infrastructure Systems Laboratory (CISL) at Kansas State University. After the construction of pavement sections in CISL, cores were taken and *insitu* percent air voids were determined on each core. The contractor provided information on the mix quality control and actual binder content used. This information was used to fabricate samples in the laboratory.

3.3.1 Preparation of Test Samples

Samples for Kansas and Missouri mixes were fabricated in the laboratory using individual aggregate samples and asphalt binder that were provided for each mix. Aggregates were blended, heated, and mixed with heated asphalt at prescribed mixing temperature (Figure 3.9). Due to shortage of constituent materials, the specimens for Iowa mixes were prepared from plant-mixed, laboratory-compacted asphalt mixes. Mixes were collected during construction of the pavement sections at CISL.

The in-place (field) binder content provided by the contractor (Table 3.3) was used for the laboratory mixes. Superpave mix design procedure was followed. Asphalt mixes were aged in the oven at 135^{o}C for 3 hrs. Superpave specimens with 150 mm diameter and 170 mm height were compacted using the Superpave gyratory compactor (Figure 3.10). The cylinders were compacted at the field percent air voids and were left to cool down before they were extruded from the molds. Eighteen specimens with 100mm ± 1mm diameter and 150mm ± 2.5mm height were then cored and cut from the cylinders (Figure 3.11). These specimens were used to perform the dynamic modulus test. Twelve specimens for the Hamburg wheel tester and 12 specimens for asphalt pavement analyzer (APA) test were also fabricated for the CISL 14 project.

The specific gravity test was performed on each mix to obtain the theoretical maximum specific gravity. This value was used to calculate sample percent air voids when used with

sample bulk specific gravity (G_{mm}). For each fabricated sample, a bulk specific gravity (G_{mb}) was measured and percent air voids were calculated. Samples with air void within ± 0.5 percent of the target air void, were accepted for further testing Table 3.19 shows the summary of sample maximum specific gravity G_{mm}, binder content, and target percent air voids that were used for each asphalt mixture.

TABLE 3.19: Laboratory Volumetric Properties of Mixes Used for Sample Preparation

	Mix					
	KS1	**KS2**	**MO1**	**MO2**	**IA1**	**IA2**
% binder	5.61	5.2	5.3	5.4	7.5	7.0
% air voids	6.75±0.5	6.00±0.5	7.00±0.5	9.38±0.5	8.9±0.5	7.00±0.5
Gmm $_{Lab}$	2.4278	2.4586	2.473	2.4526	2.4370	2.439

FIGURE 3.9: Mixing of Asphalt Binder and Aggregates in the Laboratory

FIGURE 3.10: Compaction of Test Specimens Using the Superpave Gyratory Compactor

FIGURE 3.11: Cored and Trimmed Test Specimens

3.3.2 Dynamic Modulus Test

The dynamic modulus test was performed to measure the dynamic (complex) modulus (E*) and phase angle (δ) at several loading frequencies and temperatures. The dynamic modulus (E*) is among the tests recommended as simple performance tests (SPT). NCHRP Report 465 (Witczak, et al. 2002) defines simple performance tests as test methods that "accurately and reliably measures mixture response characteristic or parameter that is highly correlated to the occurrence of pavement distress (i.e. rutting and cracking) over a diverse range of traffic and climatic conditions." For permanent deformation, three tests are recommended as having a potential to correlate laboratory results to field performance. These tests are dynamic modulus (E*), Repeated load testing - flow number (F_n), and static creep - flow time (F_t). The repeated load and static creep tests results are reported in Chapter 4 of this report. The dynamic modulus test can be performed on laboratory- prepared samples or on cores from existing pavement with dimensions similar to laboratory- prepared samples (Roberts et al. 1996).

Dynamic modulus (|E*|) is the norm value of complex modulus obtained by dividing peak-to-peak stress by peak-to-peak strain for a material subjected to a sinusoidal (haversine) axial loading (Figure 3.12). The dynamic load ranges between 10 and 690 kPa (1.5 to 100psi); higher load is used for lower test temperatures. The effective temperature (T_{eff}) ranges between 25^{o}C and 60^{o}C (77 - 140^{o}F) and the design frequency ranges between 0.1 and 25 Hz. The dynamic load should be adjusted to obtain axial strains between 50 and 150 micro-strains. Specimen ends are treated to reduce friction. The specimen is then placed in the testing chamber at the desired test temperature, and it is left to stabilize before the sample is tested. The test specimen is first preconditioned with 200 cycles at 25 Hz using the target dynamic load. Then the specimen is loaded using specified temperature, frequency, and number of cycles. Loading stress and recoverable axial strain are computed for each frequency. Dynamic modulus and the phase angle are then calculated.

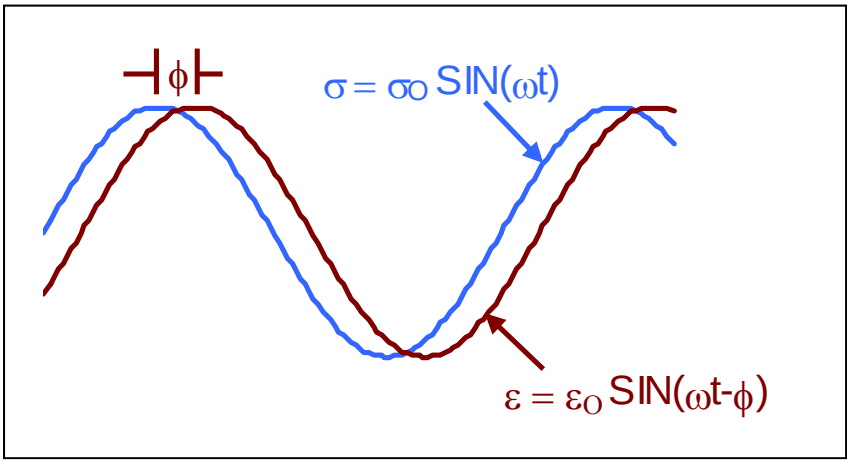

FIGURE 3.12: Sinusoidal Loading in the Dynamic Modulus Test

Measurement of the dynamic/complex modulus and phase angle represents one of the methods used to measure stress-strains relationship of visco-elastic materials. The modulus is a complex quantity, of which the real part represents the elastic stiffness and the imaginary part is the loss modulus, which characterizes the internal damping of the material. The absolute value of the complex modulus is commonly referred to as dynamic modulus (Huang 2004). Yoder and Witczak (1975) defined the sinusoidal stress as $\sigma = \sigma_o$ Sin (wt).

σ_o = stress amplitude (psi),

w = angular frequency (rad/sec), and

t = time in sec.

The resultants sinusoidal strain is given by $\varepsilon = \varepsilon_o$ Sin (wt – φ)

ε_o = recoverable strain amplitude (in/in);

φ = phase lag (degrees) is angle at which ε_o lags σ_o. $\varphi = t_i/t_p(360^o)$;

t_i = time lag between a cycle of sinusoidal stress and cycle of strain (sec); and

t_p = time for stress cycle (sec).

By definition, the complex modulus E* = E' + *i*E"

E' = $\sigma_o/\varepsilon_o \cos\varphi$ and refers to the real portion of the complex modulus;

E" = $\sigma_o/\varepsilon_o \sin\varphi$ and refers to the imaginary portion of the complex modulus; and

i = an imaginary number.

E* can also be written as $E^* = |E^*| e^{j\varphi}$

when φ = 0 (elastic material), $E^* = |E^*| = \sigma_o/\varepsilon_o$.

The elastic or dynamic modulus of material (ignoring the viscous effect) may be determined by the ratio of peak stress to strain amplitudes from the complex modulus test.

The dynamic modulus test was performed on the six asphalt mixes on laboratory-fabricated samples in accordance with AASHTO TP-62-03, at 20°C and 35°C. A sinusoidal vertical load with no rest periods was applied on cylindrical samples 100 mm in diameter by 150 mm in height, while measuring the corresponding vertical strain (deformation) and phase angle. The test was performed at six loading frequencies, 0.1, 0.5, 1, 5, 10 and 25 Hz. For this test, three linear variable differential transducers (LVDTs) were used for axial deformation data collection, providing an estimated limit of accuracy of 13.1%. Figure 3.13 shows a schematic diagram of a dynamic modulus test setup. Figure 3.14 presents the test setup at Kansas State University in the universal testing machine (UTM). Figure 3.15 shows specimen setup and LVDT connection. Three specimen replicas were tested for each asphalt mix. Test results from dynamic modulus tests at six frequencies and two test temperatures are given in Tables 3.20 to 3.22 and Figures 3.16 and 3.17.

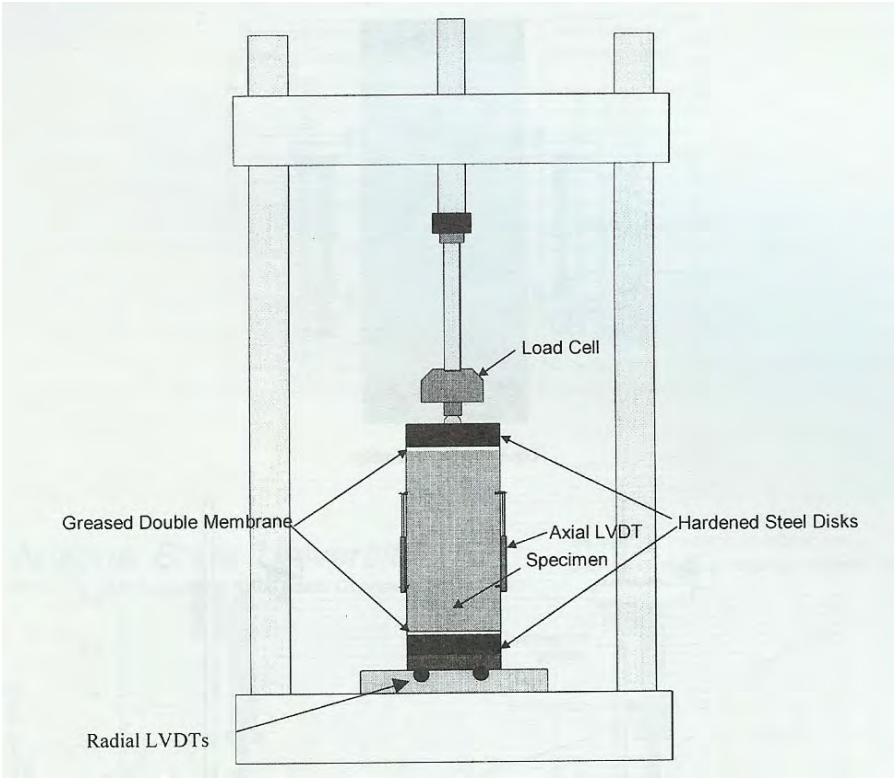

FIGURE 3.13: Schematic of Dynamic Modulus Test Device
Source: Witczak, et al. 2002

FIGURE 3.14: Universal Testing Machine (UTM)

FIGURE 3.15: Sample Setup with Attached LVDTs

TABLE 3.20: Dynamic Modulus (MPa) of KS1 and KS2 Mixes

		Temperature = 20º C							Temperature = 35º C					
	Sample ID	AV %	Frequency (Hz)						Frequency (Hz)					
			25	10	5	1	0.5	0.1	25	10	5	1	0.5	0.1
Dynamic Modulus (MPa)	KS1-07	6.74	11831	10047	8922	6414	5775	3859	5138	3929	3246	2018	1646	1067
	KS1-08	6.84	13201	11411	10459	8283	7403	5562	7323	5921	5053	3458	2857	1927
	KS1-09	6.68	10433	8997	7819	5661	5067	3456	4751	3716	3033	1860	1504	999
	Average	*6.75*	*11822*	*10152*	*9067*	*6786*	*6082*	*4292*	*5737*	*4522*	*3777*	*2445*	*2002*	*1331*
	SD	*0.08*	*1384*	*1210*	*1326*	*1350*	*1198*	*1118*	*1387*	*1216*	*1110*	*881*	*744*	*517*
	C.V.%	*1.20*	*11.71*	*11.92*	*14.62*	*19.89*	*19.70*	*26.04*	*24.17*	*26.90*	*29.38*	*36.01*	*37.13*	*38.86*
	KS2-05	6.93	8128	6374	5398	3581	3004	1903	5229	3192	2398	1426	1118	812
	KS2-06	6.84	7151	5989	5007	3358	2747	1753	2839	2095	1674	1042	848	620
	KS2-07	6.74	8433	6797	5863	4047	3415	2224	2702	2011	1633	1059	874	657
	Average	*6.84*	*7904*	*6387*	*5423*	*3662*	*3055*	*1960*	*3590*	*2433*	*1902*	*1176*	*947*	*696*
	SD	*0.10*	*670*	*404*	*429*	*352*	*337*	*241*	*1421*	*659*	*430*	*217*	*149*	*102*
	C.V.%	*1.39*	*8.47*	*6.33*	*7.90*	*9.60*	*11.03*	*12.28*	*39.58*	*27.09*	*22.63*	*18.45*	*15.73*	*14.63*
Phase Angle (Degrees)	KS1-07	6.74	11.08	15.38	17.86	22	27.78	32.45	22.03	24.54	26.12	28.32	34.39	31.57
	KS1-08	6.84	9.85	14.75	14.6	18.63	22.48	27.14	17.19	19.85	22.54	27.21	33.92	37.32
	KS1-09	6.68	11.84	15.81	16.34	21.91	27.7	32.58	22.04	25.06	27.03	28.23	33.96	30.36
	Average	*6.75*	*10.92*	*15.31*	*16.27*	*20.85*	*25.99*	*30.72*	*20.42*	*23.15*	*25.23*	*27.92*	*34.09*	*33.08*
	SD	*0.08*	*1.00*	*0.53*	*1.63*	*1.92*	*3.04*	*3.10*	*2.80*	*2.87*	*2.37*	*0.62*	*0.26*	*3.72*
	C.V.%	*1.20*	*9.19*	*3.48*	*10.03*	*9.21*	*11.69*	*10.10*	*13.70*	*12.40*	*9.41*	*2.21*	*0.76*	*11.24*
	KS2-05	6.93	17.53	20.92	23.14	27.17	34.78	36.97	24.04	25.84	26.99	26.67	31.2	27.86
	KS2-06	6.84	20.09	22.04	24.51	29.59	36.45	40.38	23.23	24.65	25.63	25.15	28.73	25.29
	KS2-07	6.74	12.6	18.38	21.37	26.26	33.08	36.67	23.51	24.49	25.21	24.22	27.56	23.87
	Average	*6.84*	*16.74*	*20.45*	*23.01*	*27.67*	*34.77*	*38.01*	*23.59*	*24.99*	*25.94*	*25.35*	*29.16*	*25.67*
	SD	*0.10*	*3.81*	*1.88*	*1.57*	*1.72*	*1.69*	*2.06*	*0.41*	*0.74*	*0.93*	*1.24*	*1.86*	*2.02*
	C.V.%	*1.39*	*22.74*	*9.17*	*6.84*	*6.22*	*4.85*	*5.42*	*1.74*	*2.95*	*3.59*	*4.88*	*6.37*	*7.88*

TABLE 3.21: Dynamic Modulus (MPa) of MO1 and MO2 Mixes

	Sample ID	AV %	Temperature = 20°C Frequency (Hz)						Temperature = 35°C Frequency (Hz)					
			25	10	5	1	0.5	0.1	25	10	5	1	0.5	0.1
Dynamic Modulus (MPa)	MO1-09	9.45	9045	7757	6615	4617	4034	2707	4024	3014	2533	1602	1334	934
	MO1-10	9.56	9315	7564	6434	4340	3767	2370	5036	3856	3146	1867	1534	1008
	MO1-11	9.29	8854	7326	6432	4528	3940	2563	3399	2526	1991	1226	1012	697
	Average	*9.43*	*9071*	*7549*	*6494*	*4495*	*3914*	*2547*	*4153*	*3132*	*2557*	*1565*	*1293*	*880*
	SD	*0.14*	*232*	*216*	*105*	*141*	*135*	*169*	*826*	*673*	*578*	*322*	*263*	*162*
	C.V.%	*1.44*	*2.55*	*2.86*	*1.62*	*3.15*	*3.46*	*6.64*	*19.89*	*21.48*	*22.6*	*20.58*	*20.36*	*18.47*
	MO2-02	6.99	6330	5248	4689	3457	3047	2083	3702	2690	2145	1295	1092	764
	MO2-07	7.09	8490	7075	6003	4004	3375	2159	3942	2990	2397	1488	1233	850
	MO2-10	7.19	7244	6023	5217	3568	3112	2043	3489	2562	2053	1246	1022	712
	Average	*7.09*	*7355*	*6115*	*5303*	*3676*	*3178*	*2095*	*3711*	*2747*	*2198*	*1343*	*1116*	*775*
	SD	*0.10*	*1084*	*917*	*661*	*289*	*174*	*59*	*227*	*220*	*178*	*128*	*107*	*70*
	C.V.%	*1.41*	*14.74*	*14.99*	*12.47*	*7.87*	*5.46*	*2.81*	*6.11*	*8.00*	*8.10*	*9.53*	*9.63*	*8.99*
Phase Angle (Degrees)	MO1-09	9.45	14.5	18.31	20.25	26.4	33.84	40.54	22.34	25.11	27	29.31	35	35.4
	MO1-10	9.56	15.9	18.9	22.69	28.7	36.51	42.94	21.95	25.29	27.76	29.95	36.14	36.61
	MO1-11	9.29	14.36	17.53	20.33	24.3	31.23	33.59	21.75	24.37	25.77	26.81	32.01	31.6
	Average	*9.43*	*14.9*	*18.2*	*21.1*	*26.5*	*33.9*	*39.0*	*22.0*	*24.9*	*26.8*	*28.7*	*34.4*	*34.5*
	SD	*0.14*	*0.9*	*0.7*	*1.4*	*2.2*	*2.6*	*4.9*	*0.3*	*0.5*	*1.0*	*1.7*	*2.1*	*2.6*
	C.V.%	*1.44*	*5.71*	*3.77*	*6.57*	*8.28*	*7.80*	*12.44*	*1.36*	*1.96*	*3.74*	*5.78*	*6.20*	*7.57*
	MO2-02	6.99	13.27	16.35	20.22	27.8	35.44	45.1	25.08	27.89	28.5	28.51	32.52	29.53
	MO2-07	7.09	15.85	19.45	22.79	27.3	35.07	38.54	22.77	25.42	26.87	27.3	31.35	27.61
	MO2-10	7.19	17.26	21.13	24.66	32.6	42.07	51.65	23.64	27.12	28.71	29.49	32.94	30.11
	Average	*7.09*	*15.5*	*19.0*	*22.6*	*29.2*	*37.5*	*45.1*	*23.8*	*26.8*	*28.0*	*28.4*	*32.3*	*29.1*
	SD	*0.10*	*2.0*	*2.4*	*2.2*	*2.9*	*3.9*	*6.6*	*1.2*	*1.3*	*1.0*	*1.1*	*0.8*	*1.3*
	C.V.%	*1.41*	*13.09*	*12.78*	*9.88*	*10.1*	*10.50*	*14.54*	*4.90*	*4.71*	*3.59*	*3.86*	*2.55*	*4.50*

TABLE 3.22: Dynamic Modulus (MPa) of IA1 and IA2 Mixes

			Temperature = 20º C						Temperature = 35º C					
			Frequency (Hz)						Frequency (Hz)					
	Sample ID	AV %	25	10	5	1	0.5	0.1	25	10	5	1	0.5	0.1
Dynamic Modulus (MPa)	IA1-01	8.71	5838	4790	4216	3035	2642	1719	1746	1203	970	570	480	336
	IA1-05	8.88	7773	6356	5372	3498	3046	1824	2124	1492	1206	738	594	383
	IA1-08	8.43	5479	4533	3882	2590	2252	1454	1885	1368	1088	642	528	354
	Average	*8.67*	*6363*	*5226*	*4490*	*3041*	*2647*	*1666*	*1918*	*1354*	*1088*	*650*	*534*	*358*
	SD	*0.23*	*1234*	*987*	*782*	*454*	*397*	*191*	*191*	*145*	*118*	*84*	*57*	*24*
	C.V.%	*2.62*	*19.39*	*18.88*	*17.41*	*14.93*	*15.00*	*11.45*	*9.97*	*10.71*	*10.85*	*12.97*	*10.72*	*6.63*
	IA2-02	7.13	9312	8161	7320	5586	4992	3501	3312	2617	2218	1416	1177	803
	IA2-04	7.49	8689	6934	5919	4080	3562	2242	2939	2314	1881	1260	1046	744
	IA2-05	7.17	6064	5089	4493	3255	2890	2011	3270	2446	2051	1436	1210	830
	Average	*7.26*	*8022*	*6728*	*5911*	*4307*	*3815*	*2585*	*3174*	*2459*	*2050*	*1371*	*1144*	*792*
	SD	*0.20*	*1724*	*1546*	*1414*	*1182*	*1074*	*802*	*204*	*152*	*169*	*96*	*87*	*44*
	C.V.%	*2.72*	*21.49*	*22.98*	*23.91*	*27.44*	*28.14*	*31.03*	*6.44*	*6.18*	*8.22*	*7.03*	*7.58*	*5.55*
Phase Angle (Degrees)	IA1-01	8.71	16.22	21.25	24.97	32.79	42.13	50.54	25.54	29.52	29.91	27.29	29.01	27.05
	IA1-05	8.88	15.78	19.61	21.9	28.56	36.73	44.39	26.1	28.8	30.76	31.99	37.77	38.04
	IA1-08	8.43	15.99	19.3	23.25	29.78	37.59	45.44	25.98	28.38	30.3	30.37	34.74	32.43
	Average	*8.67*	*16.00*	*20.05*	*23.37*	*30.38*	*38.82*	*46.79*	*25.87*	*28.90*	*30.32*	*29.88*	*33.84*	*32.51*
	SD	*0.23*	*0.22*	*1.05*	*1.54*	*2.18*	*2.90*	*3.29*	*0.29*	*0.58*	*0.43*	*2.39*	*4.45*	*5.50*
	C.V.%	*2.62*	*1.38*	*5.23*	*6.58*	*7.17*	*7.47*	*7.03*	*1.14*	*1.99*	*1.40*	*7.99*	*13.15*	*16.91*
	IA2-02	7.13	10.28	13.77	16.85	22.05	29.07	35.44	20.06	22.8	25.44	27.43	33.42	33.53
	IA2-04	7.49	15.89	18.16	21.56	27.33	34.5	40.35	23.01	25.51	27.52	28.59	33.31	31.75
	IA2-05	7.17	13.51	17.41	20.11	24.81	31.65	37.72	21.24	24.4	26.66	29.1	34.98	35.18
	Average	*7.26*	*13.23*	*16.45*	*19.51*	*24.73*	*31.74*	*37.84*	*21.44*	*24.24*	*26.54*	*28.37*	*33.90*	*33.49*
	SD	*0.20*	*2.82*	*2.35*	*2.41*	*2.64*	*2.72*	*2.46*	*1.48*	*1.36*	*1.05*	*0.86*	*0.93*	*1.72*
	C.V.%	*2.72*	*21.29*	*14.28*	*12.37*	*10.68*	*8.56*	*6.49*	*6.93*	*5.62*	*3.94*	*3.02*	*2.76*	*5.12*

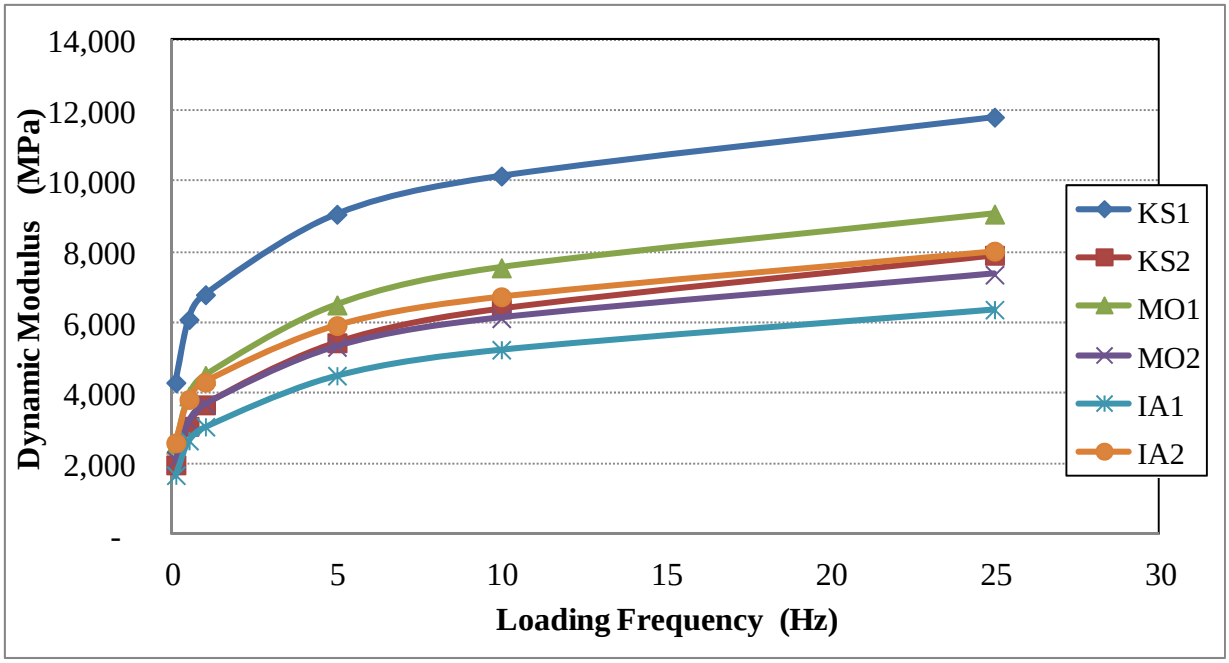

FIGURE 3.16: Dynamic Modulus at 20°C

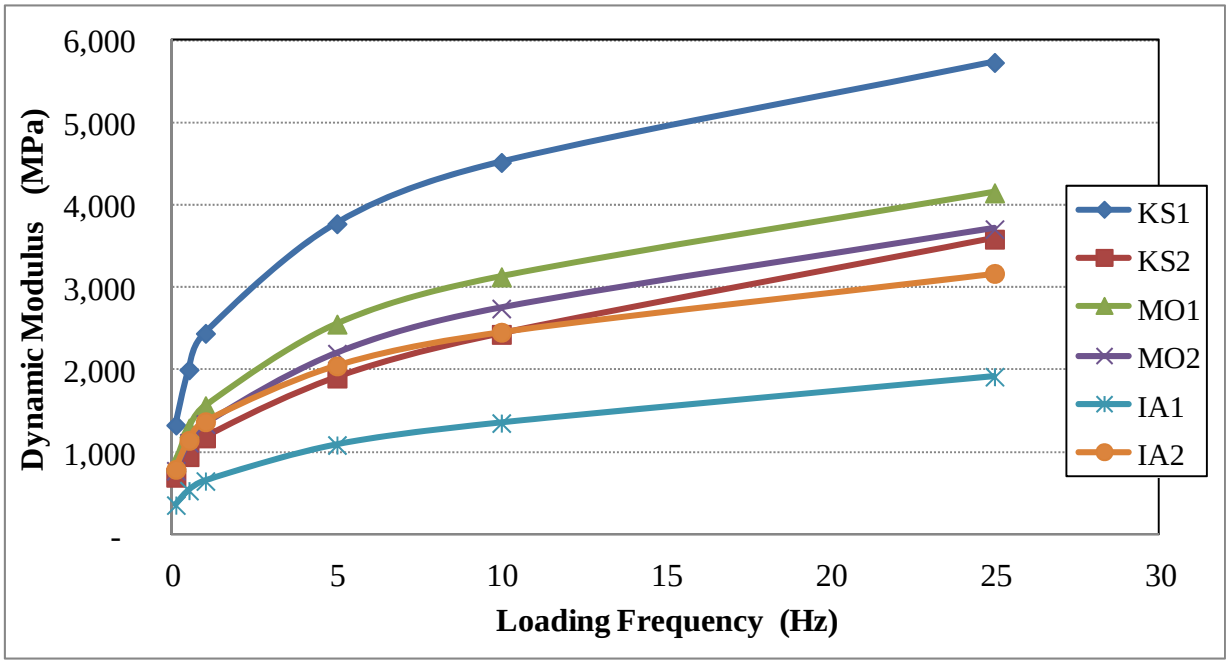

FIGURE 3.17: Dynamic Modulus at 35°C

The dynamic modulus test results (Figures 3.16 and 3.17) indicated that dynamic modulus values are higher at lower temperature and lower at higher temperature. From the same figures, it was observed that dynamic modulus is higher at higher loading frequencies.

Figures 3.26 and 3.27 summarize the results for all six mixes. Average values of the dynamic modulus were used for these plots. Kansas mix KS1 had the highest dynamic modulus, followed by Missouri mix MO1. Iowa mix IA1 had the lowest dynamic modulus. This is because Iowa 30M mix was constructed with a higher binder content and higher percent of air voids than the design requirements. The figures also show that for Kansas mixes, KS1 had higher values of dynamic modulus than KS2 mix. Missouri mix MO1 had higher average values of dynamic modulus than MO2 mix, while Iowa mix IA2 had higher values of dynamic modulus than IA1 mixes.

The dynamic modulus master curve parameters were calculated with 35°C as a reference temperature. The values obtained at 20°C were shifted to form a master curve at 35°C. Master Solver Version 2 was used for obtaining the parameters of the master curves. Equation 3.1 provides the sigmoid function (master curve equation) and Table 3.23 provides the sigmoid function parameters used for each mix. “Ea” stands for activation energy and it is used as a fitting parameter.

$$\log|E^*| = \delta + \frac{(Max - \delta)}{1 + e^{\beta + \gamma \log w_r}} \qquad \textbf{Equation 3.1}$$

where

|E*| = dynamic modulus;

ω_r = reduced frequency, Hz;

Max = limiting maximum modulus; and

δ, β and γ = fitting parameters.

From the master curves, the values of dynamic modulus at reference temperature, 35^{o}C were obtained for each frequency. Table 3.25 provides the dynamic modulus values (E*) measured from the dynamic modulus test.

The CISL testing speed was 7.6 mph. This vehicle travel speed induces a loading with a corresponding frequency of approximately 3.8 Hz (7.6/2). The E* values were then obtained from the master curves at a frequencies of 3.8 Hz, between 1.0 Hz and 5Hz. The values obtained in Table 3.25, were used for the calculation of theoretical pavement response.

TABLE 3.23: Fitting Parameters for Sigmoid Function

Fit Parameter	KS1	KS2	MO1	MO2	IA1	IA2
Delta (δ)	1.2777	1.2895	0.5248	0.7363	0.8027	1.7462
Beta (β)	-0.2000	0.3000	-0.5000	0.7340	0.7340	0.7340
Gamma (γ)	-0.5684	-0.5000	-0.5000	-0.5000	-0.5684	-0.5684
E_a	200000	200000	200000	200000	200000	200000

TABLE 3.24: Dynamic Modulus at 35°C

Frequency (Hz)	E* (ksi)					
	KS1	KS2	MO1	MO2	IA1	IA2
25.0	788.0	407.0	633.7	124.8	150.9	444.6
10.0	620.5	317.9	491.4	91.0	106.6	354.1
5.0	510.7	262.8	398.8	72.0	82.3	298.9
1.0	314.0	169.1	234.2	43.1	46.7	206.0
0.5	252.6	140.6	183.2	35.1	37.3	178.0
0.1	152.9	94.1	101.5	22.9	23.6	131.9
	E* (MPa)					
	KS1	KS2	MO1	MO2	IA1	IA2
25.0	5435.1	2806.8	4370.8	860.8	1040.7	3066.4
10.0	4279.3	2192.8	3388.9	628.0	735.4	2442.4
5.0	3522.0	1812.8	2750.3	496.9	567.7	2061.3
1.0	2166.0	1166.4	1615.2	297.0	321.8	1420.9
0.5	1742.4	970.0	1263.6	242.1	257.4	1227.4
0.1	1054.7	648.7	700.3	158.2	163.0	910.0

TABLE 3.25: Dynamic Modulus (E*) Values for APT Testing Conditions at 35°C

Mix	KS1	KS2	MO1	MO2	IA1	IA2
E* (ksi)	452	235	349	63	72	271
E* (MPa)	3115	1619	2410	437	494	1869

3.3.3 Rutting Resistance with Hamburg Wheel-Tracking Machine

The Hamburg wheel-tracking test was performed in accordance with AASHTO T324 to evaluate the rutting and moisture susceptibility of hot-mix asphalt (HMA). The test consists of two separate steel wheels moving back and forth on asphalt concrete specimens (Figure 3.18). The test was run simultaneously on two asphalt concrete slabs placed in a temperature-controlled water bath. The slabs were compacted at the desired density using a linear kneading compactor. Rut depth and number of passes were measured. Performance of the HMA was evaluated to determine failure susceptibility of the HMA due to weakness in the aggregate structure, inadequate binder stiffness, or moisture damage (Figure 3.19). The Hamburg test was performed at two temperatures, 35^{o}C and 50^{o}C, for each asphalt mix. Maximum number of 20,000 loads repetitions or maximum failure depth of 20mm was adopted as failure criteria. Results from this test are given in Table 3.26 and Figures 3.20 to 3.21.

TABLE 3.26: Hamburg Wheel Test Results

Mix	Lab prepared sample	Cored sample	Air voids (%)	Max. no. of passes	Max. depth (mm)	Tests temp (°C)
MO1	x		9.02	20,000	6.24	50
MO2	x		6.945	16,046	20.00*	50
KS1	x		6.02	20,000	2.38	50
KS2	x		6.76	11,350	20.00*	50
MO1		x	7.47	20,000	4.54	50
MO2		x	7.87	16,702	20.00*	50
KS1		x	6.63	10,006	20.00*	50
KS2		x	6.30	12,270	20.00*	50
MO1	x		9.61	20,000	3.72	35
MO2	x		7.33	20,000	3.75	35
KS1	x		6.17	20,000	2.38	35
KS2	x		6.85	20,000	3.40	35
MO1		x	7.63	20,000	3.47	35
MO2		x	7.86	20,000	3.96	35
KS1		x	6.14	20,000	4.69	35
KS2		x	5.80	20,000	4.21	35
IA1		x	8.86	3,324	20.00*	50
IA2		x	7.24	6,500	20.00*	50
IA1		x	9.02	20,000	10.15	35
IA2		x	8.16	20,000	5.31	35

* Sample failed

FIGURE 3.18: Hamburg Wheel-Tracking Machine

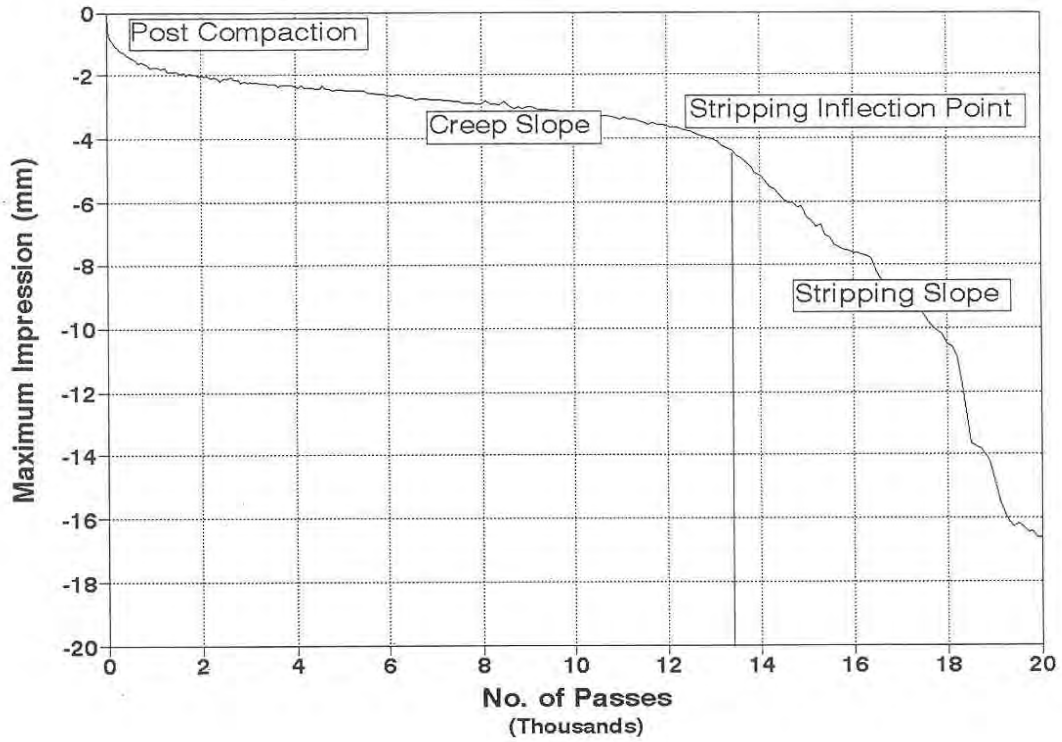

FIGURE 3.19: Typical Hamburg Test Curve and Its Major Characteristics

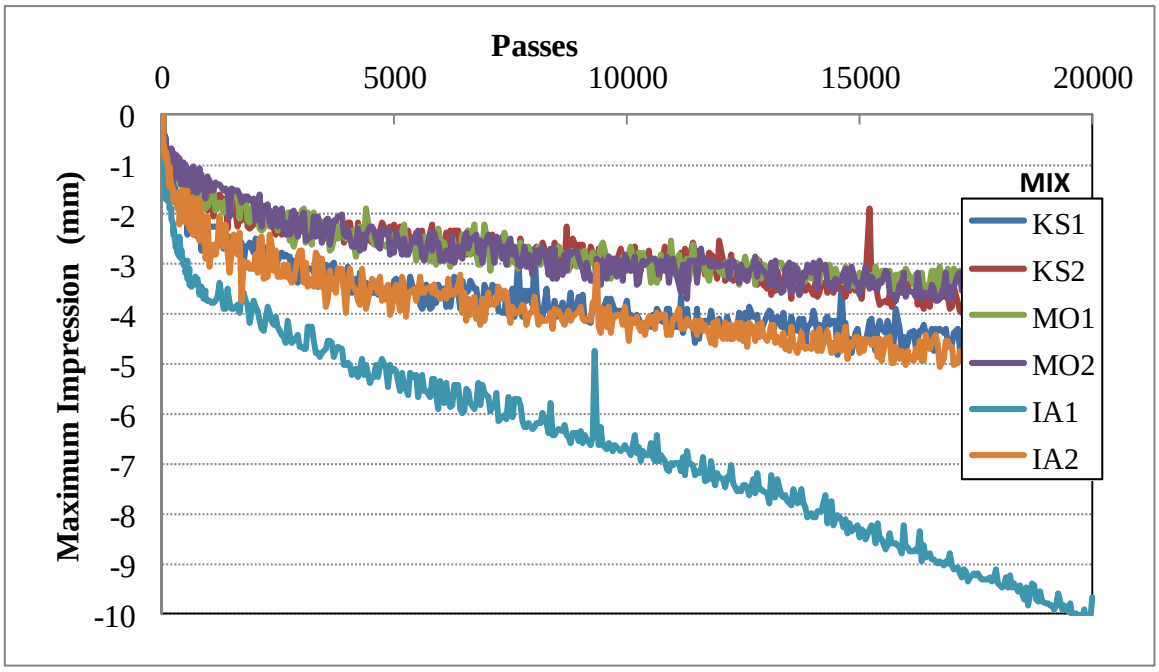

FIGURE 3.20: Hamburg Wheel Test Results for Mixes Tested at 35°C

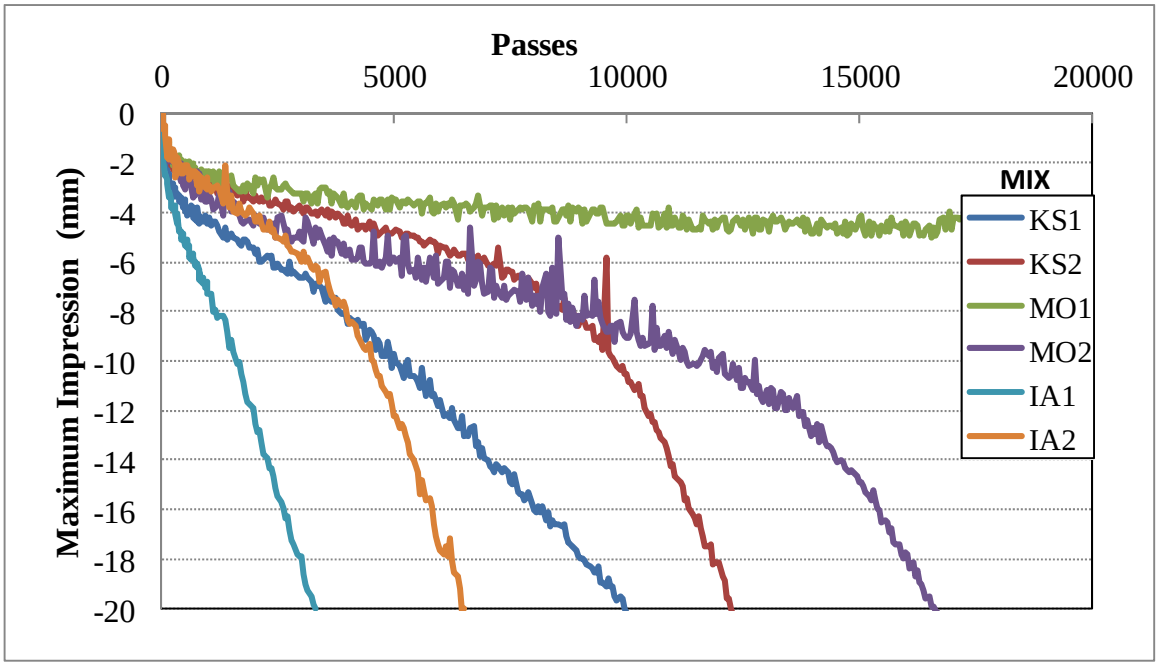

FIGURE 3.21: Hamburg Wheel Test Results for Kansas Mixes Tested at 50°C

Kansas mix KS2, Missouri mix MO2, and both Iowa mixes IA1 and IA2 failed after 11,350, 16,046, 3,324, and 6,500 repetitions, respectively, when tested at 50°C. KS1 and MO1 mixes did not fail at either 35°C nor 50°C, indicating they are more resistant to permanent deformation than the other

four mixes. At 35^{o}C, none of the six mixes had a permanent deformation more than 20mm after 20,000 load repetitions.

3.3.4 Rutting Resistance with the Asphalt Pavement Analyzer

Use of asphalt pavement analyzer (APA) started in the mid-1990s after the modification of the Georgia wheel load tester. APA evaluates fatigue cracking and rutting susceptibilities of asphalt concrete specimens or pavement samples. The APA is a multifunctional loaded-wheel tester that uses pneumatic cylinders on a concave metal wheel to apply repetitive load applications through a pressurized rubber hose. Typically, 8,000 repetitions or strokes are applied to the HMA specimens. Contact pressure of up to 1,378 kPa (200 psi) can be generated, but typically a contact pressure of 690 kPa (100 psi) contact pressure is used to simulate actual field loading conditions. Calibration of the applied load, contact pressure, and deformation measurement are built into the APA system and it is computer controlled. The APA can accommodate triplicate beam specimens (100 mm x 300 mm x 75 mm thick) or three sets of two cylindrical specimens. Cylindrical specimens are 150 mm in diameter with a standard thickness of 75 mm (Figure 3.42).

APA tests were performed on samples having a 150mm diameter and a 75 mm thickness fabricated in the KSU asphalt laboratory. The APA tests were performed at the Missouri Department of Transportation because Kansas State University does not own an asphalt pavement analyzer. The laboratory fabricated samples were tested at two temperatures, 35^{o}C and 64^{o}C, to a maximum number of passes of 8,000 while measuring rut depth. Results from the APA tests are given in Table 3.27 and Figures 3.23 to 3.26. Results provided are for Kansas and Missouri mixes. Iowa mixes were weaker than the other mixes and failed at a lower number of load repetitions. For instance, IA1 samples at 64^{o}C failed at sitting. Due to the difficulty in testing Iowa mixes, results were manually obtained and no plots are available for these samples.

FIGURE 3.22: Asphalt Pavement Analyzer Test

TABLE 3.27: Asphalt Pavement Analyzer Test Results

Mix	Tests temp (^{o}C)	Air voids (%)	Max. no. of passes	Max. depth (mm)
KS1	35	6.16	8,000	1.08
KS2		6.58	8,000	1.59
MO1		9.69	8,000	1.71
MO2		7.27	8,000	2.15
IA1		9.14	8,000	2.27
IA2		7.71	8,000	3.18
KS1	64	6.32	8,000	4.17
KS2		6.70	8,000	8.61
MO1		9.28	8,000	3.90
MO2		7.21	8,000	5.50
IA1		8.7	8,000	Failed
IA2		7.20	8,000	9.48

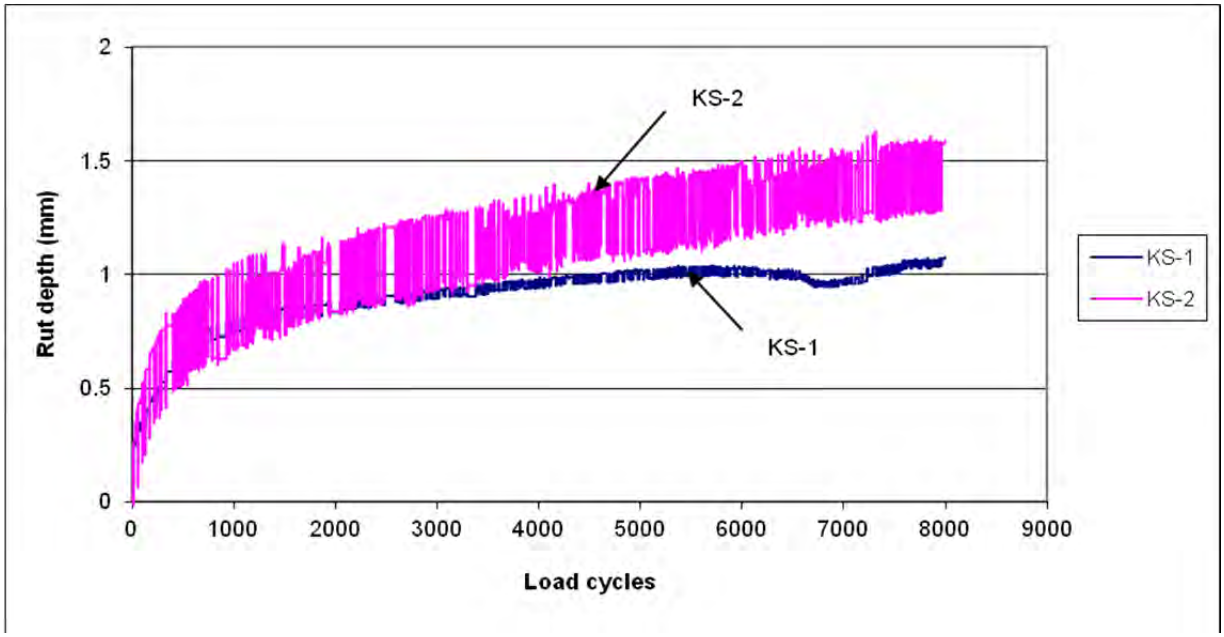

Figure 3.23 Asphalt Pavement Analyzer Test Results for Kansas Mixes at 35°C

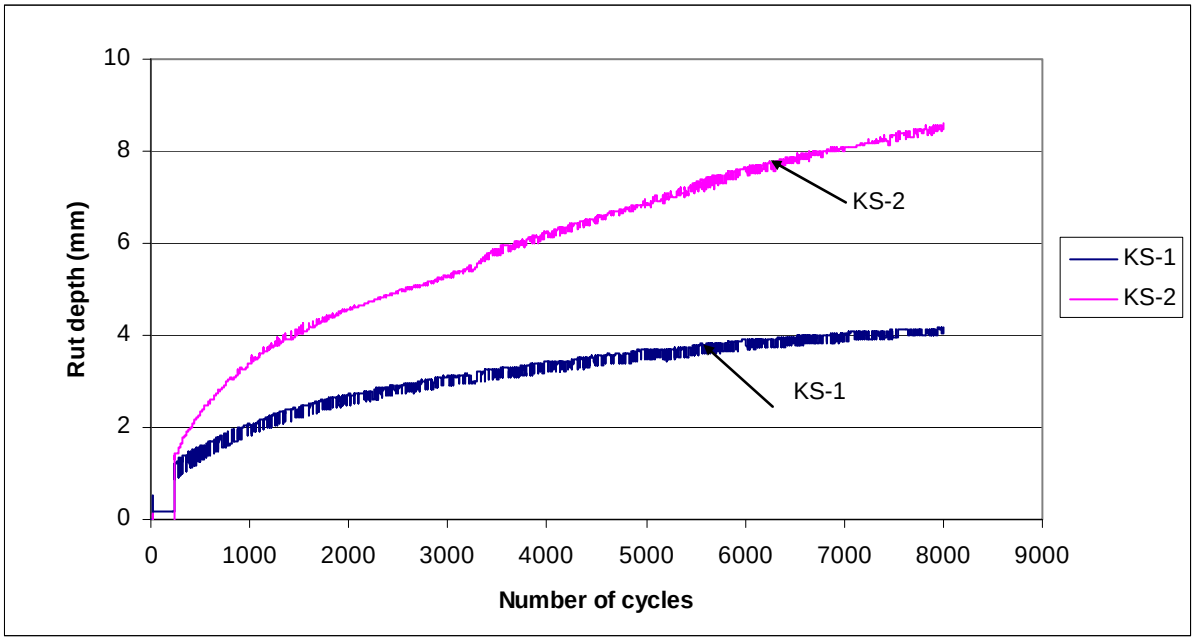

Figure 3.24Asphalt Pavement Analyzer Test Results for Kansas Mixes at 64°C

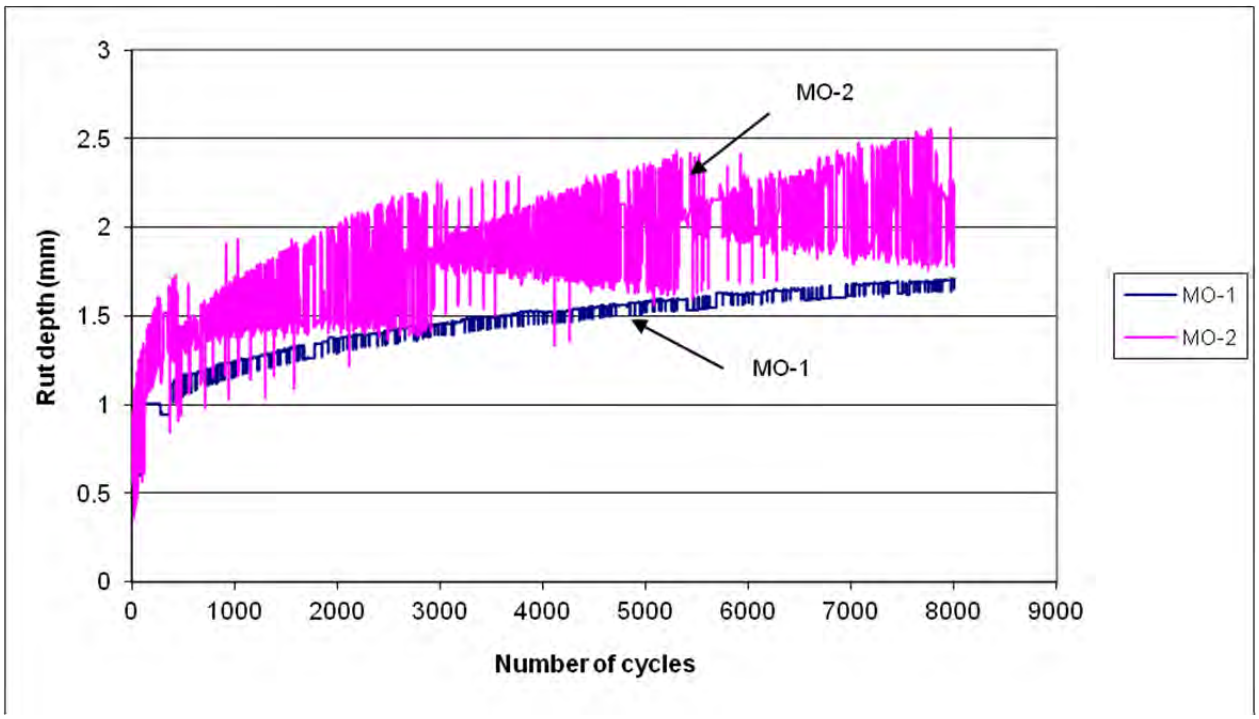

Figure 3.25 Asphalt Pavement Analyzer Test Results for Missouri Mixes at 35°C

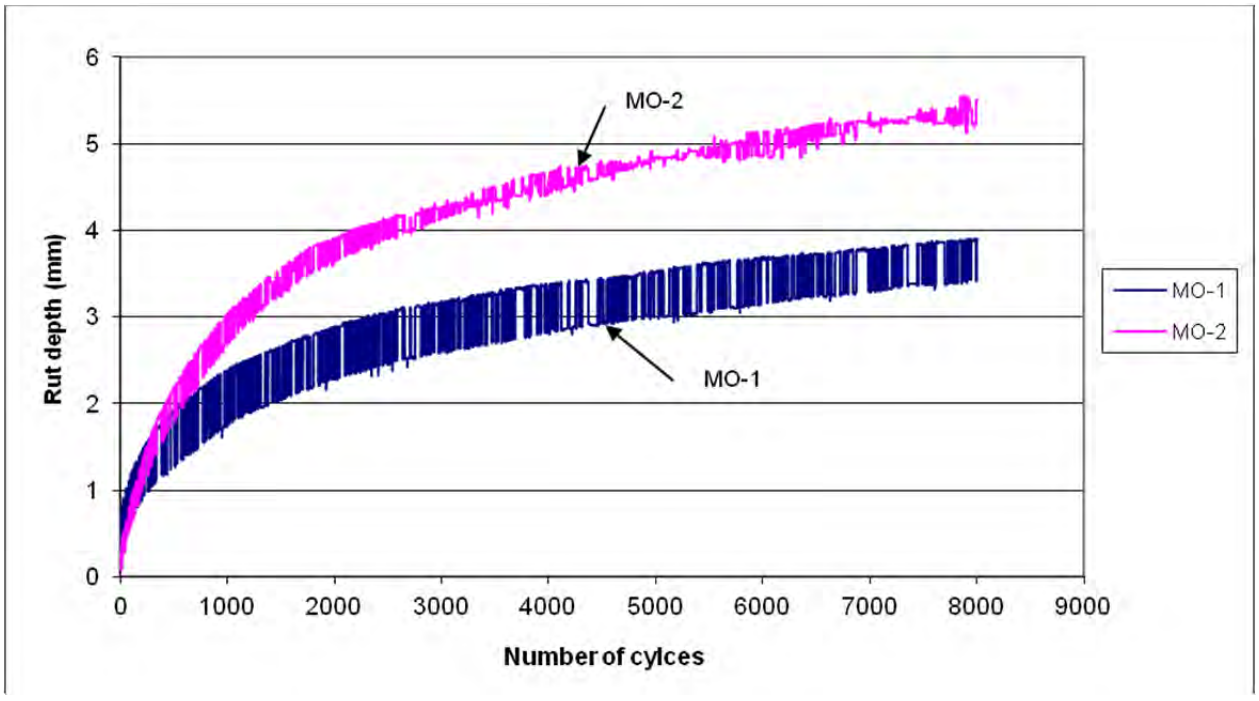

Figure 3.26 Asphalt Pavement Analyzer Test Results for Missouri Mixes at 64°C

Chapter 4: Advanced Testing of Asphalt Concrete

Advanced characterization of the mechanical properties of hot asphalt mixes were conducted in order to allow the verification and validation of mechanistic models for permanent deformation or rutting, and fatigue cracking of asphalt concrete layers. Such verification was conducted by Dr. Mbakisya Onyango as part of her doctoral research work (Onyango 2009). She verified selected mechanistic prediction models for permanent deformation by comparing the permanent deformations measured in the full-scale accelerated pavement test with those predicted by several mechanistic models integrated into the ABAQUS finite element software. Table 4.1 gives the tests performed and the number of replicate specimens tested per mix and test condition.

TABLE 4.1: Advanced Tests Conducted To Determine Mechanical Properties of Asphalt Concrete Mixes

	Test	**Test protocol**	**Measured Engineering Properties**	**Replicates per test condition**
1.	Dynamic modulus at 20 ^{o}C and 35 ^{o}C temp, and six frequencies (25; 10, 5; 1; 0.5; 0.1Hz)	AASHTO TP 62-03	Dynamic modulus |E*| and phase angle φ	3
2.	Static creep at 35^{o}C	NCHRP-465	Creep compliance and flow time, power law parameters at time T, D(T)	2
3.	Dynamic creep test at 35^{o}C	NCHRP-465	Creep compliance D and flow number	2
4.	Triaxial repeated load test at 35^{o}C, four confining pressures loaded with 0.1 sec loading and 0.9 sec unloading.	NCHRP-465	Elastic modulus |E*|, Drucker-Prager parameters angle of internal friction α, cohesion c, φ_p, and φ_{cv}.	4
6.	Uniaxial stain test (unconfined) at five strain rates and 35^{o}C	ASTM D 4123	Viscoplastic parameters	2
7.	Shear frequency sweep at constant height (FSCH) at 35^{o}C	AASHTO T320-07	Linear viscoelastic parameters, mix stiffness G*, phase angle φ	2
8.	Repetitive shear at constant height (RSCH) at 35^{o}C	AASHTO T320-07	Rutting susceptibility of mix, permanent shear stain	2
9.	Third-point beam fatigue at 20^{o}C and at least three strain levels	AASHTO T-321	The number of cycles to half of initial stiffness	At least 3

With the exception of tests 7 and 8, all tests were performed in the universal testing machine (UTM-25) at Kansas State University. The UTM-25, manufactured by Industrial Process Controls (IPC) of Melbourne, Australia, is a closed-loop, servo-control material testing system, designed as a versatile, high performance, and wide-ranging testing facility. The UTM-25 consists of four main components: personal computer (PC), computer data acquisition system (CDAS), hydraulic system, and environmental chamber.

The CDAS is a compact, self-contained unit that provides all critical control, timing, and data acquisition functions for the testing frame and transducers. It controls input and output data. It records signals from transducers, digitizes the information and passes it to the PC. It also controls the testing frame and transducers, and adjusts and applies the load through the actuator.

The hydraulic system consists of the hydraulic power packs, hydraulic service manifold, and hydraulic servo valve, which are controlled using pendant controls. The hydraulic system is connected to the actuator through an electrically controlled hydraulic servo valve. The hydraulic power pack is the energy source for the servo valve using high-pressure oil. The power pack provides low and high-pressure operating modes to the hydraulic service manifold, which are used during testing. The hydraulic servo actuator maintains high-frequency performance at significantly reduced pressures, supplies oil to the machine, eliminates hydraulic noise, and increases efficiency of the servo valve. The force applied to the sample is determined using a load cell mounted in line with the loading shaft.

The environmental chamber is provided to control test temperatures. It is comprised of a thermometer and a thermostat that controls and maintains the set temperature. Figure 3.14 in Chapter 3 shows a photo of the UTM-25 at KSU. Figure 3.15 shows the mounting of LVDT to the sample and the sample in the UTM-25 testing frame during the creep test.

4.1 Static Creep / Flow-Time Test

The static creep test is conducted to measure the resistance of asphalt concrete to flow. This is why this test is also known as the flow-time test. The test may be conducted in a uniaxial or triaxial state of compressive loading. The test is conducted in one cycle of load unload that provides information concerning the asphalt mixture response characteristics (elastic/plastic viscoelastic/viscoplastic). A test may be conducted at several temperature, stress, and confining

pressure levels. Effective temperatures range between 25°C and 60°C (77°F and 141°F). The design stress levels ranges between 69 and 207 kPa (10-30 psi) for unconfined tests, and 483 to 966 kPa for confined tests. Typical confinement levels range between 35 and 207 kPa (5-30 psi) (Witczak et al. 2002). The test is conducted on laboratory-prepared samples, having the diameter of 4 inches and the height of 6 inches, cored from Superpave gyratory compacted plugs.

The static creep test was conducted in accordance with NCHRP Report 465 - Appendix C (Witczak, et al. 2002). The axial load of 207 kPa (30 psi) was applied on the specimens for 10,000 seconds or until failure. When this test is performed, creep behavior exhibits three stages: primary, secondary, and tertiary. The primary and tertiary stages have a nonlinear relationship between strain and time. In the secondary stage, the relationship between strain and time is linear (Figure 4.1). Model parameters are obtained for the linear part of the relationship using plots of log strain vs log time. For this test, axial loads on some of the mixes were increased in order to obtain tertiary flow. This was because the specimens were tested at the APT test temperature of 35^{o}C, which is relatively low. Results are plotted as log strain vs log time or log compliance vs log time. From Figure 4.1, the three creep stages can be clearly seen and the creep model parameters, slope (m), intercept (d_o), flow time F_t and creep compliance (D) can be obtained. The creep compliance is calculated using a quasi-elastic method to approximate the linear viscoelastic convolution integral (Roberts et al. 1996).

$$D(t) = \varepsilon(t) / \sigma(t) \qquad \textbf{(Equation 4.1)}$$

Where :

D(t) is the creep compliance,

ε(t) is strain response, and

σ(t) is the applied stress.

From the plot of log compliance versus log time above (Figure 4.1), the compliance parameters d_o, d_1, and m are obtained from a linear portion of the creep compliance plot where:

- *Creep compliance* (D), in MPa-1, is the reciprocal of creep modulus and presented as a ratio of strain (ε) to stress (σ) for a viscoelastic material and is calculated with Equation 4.1;
- d_o is the instantaneous compliance and can be assumed to be the value of the total compliance at a time equal to 100 ms (if the load is applied rapidly at 50ms);
- d_1 (or sometimes "a") is the intercept of the creep compliance-time relationship, which is the estimated value of the total compliance at a time of one second; and
- *m* (or sometimes "b") is the slope of the creep compliance-time relationship and the *flow point* is the lowest point in the curve of rate of change in axial compliance versus loading time.

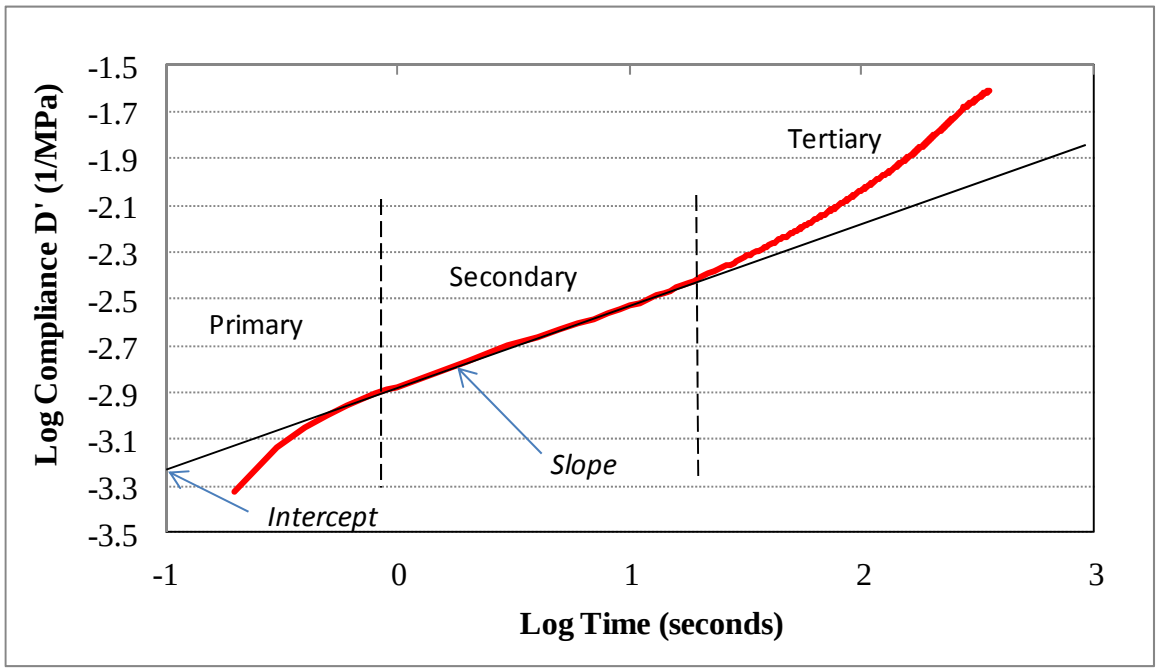

FIGURE 4.1: Creep Compliance vs. Time in a Static Creep Test

The Power law model is used to analyze creep test results and is mathematically expressed as shown in Equation 4.2:

$$\varepsilon_p = at^b \qquad \textbf{(Equation 4.2)}$$

Where:

ε is permanent strain,

t is time of loading cycle in seconds, and

a and b are the regression constants explained above.

The static creep test was conducted at 35^{o}C with uniaxial constant loading (without confinement) varying from 207 kPa to 690 kPa (30 to 100 psi). Asphalt mixes from Kansas KS1, Missouri MO1 and MO2, and Iowa IA2 did not fail after 10,000 seconds when tested at 207kPa (30psi). Therefore, the tertiary flow was not reached and hence flow time was not obtained. For these mixtures, either a higher load or longer loading time was required for tertiary flow time to be observed. Since the APT test was performed at 35^{o}C, it was logical to increase the load in order to obtain the tertiary flow and flow times. From this test, flow time, creep modulus, creep compliance and compliance, parameters, d_1, d_o, and m were obtained. Flow time is the time at which shear deformation under constant volume begins. The higher the flow time, the higher the asphalt resistance to permanent deformation is. d_1 and m are material regression coefficients, generally known as compliance parameters, where d_1 is the intercept and m is the slope (Figure 4.1); and d_o is instantaneous compliance. Power models are used to model the secondary (linear) phase of the creep compliance curve using this relationship:

$$D' = D(t) - d_o = d_1 t^m \qquad \textbf{(Equation 4.3)}$$

Table 4.2 gives the results of a static creep test for samples tested at 207, 345, and 609 kPa.

TABLE 4.2: Static Creep Test Results

Sample ID	Axial load (kPa)	D1 (1/Mpa)	m	Do (1/Mpa)	Flow time (sec.)	Creep modulus (MPa)	Creep compliance (1/Mpa)	Permanent deformation (mm)
IA1	207	0.000795	0.52665	0.00117	512.5	29.30	0.036275	0.76100
IA2	207	0.000578	0.20995	0.00073	1131.0	105.70	0.015105	0.07169
KS1	207	0.00058	0.2843	0.0004	7944.0	157.70	0.059400	0.12970
KS2	207	0.000252	0.3854	0.001045	3162.0	42.95	0.022310	0.47520
MO1	207	0.00075	0.3405	0.000675	7944.0	81.80	0.011515	0.25085
MO2	207	0.00099	0.2342	0.00084	5012.0	224.65	0.004375	0.10705
KS2	345	0.00102	0.2792	0.000775	1807.5	71.80	0.013580	0.49155
MO2	345	0.000209	0.2727	0.00079	5012.0	83.80	0.011144	0.44110
KS1	690	0.001325	0.13165	0.00045	7944.0	194.30	0.004725	0.35615
MO1	690	0.001495	0.32545	0.00051	1585.0	69.55	0.013890	0.97845
MO2	690	0.001333	0.348344	0.000725	566.0	77.80	0.012640	0.99944

The static creep test was performed on two replicates for each mix. Table 4.2 indicates that KS1 and MO1 samples had high flow-time values when tested at 207 kPa axial load, indicating that these mixes should have better rutting resistance as compared to the rest of the mixes. Mixes MO2 and KS2 were tested at 345 kPa, MO2 had a flow time of 5,012 seconds, indicating that it has a better rutting resistance than the KS2 mix. KS1, MO, and MO2 mixes were tested again at 690 kPa. KS1 had a flow time of 7,944 seconds, MO1 1,585 seconds, and MO2 an average of 566 seconds. Iowa mixes were tested at 207 kPa axial load and failed with flow times of 512 and 1131 seconds for IA1 and IA2, respectively. From this test, it was observed that KS1 and MO1 mixes have the highest rutting resistance, while IA1 has the lowest.

4.2 Dynamic Creep / Flow-Number Test

This test is conducted to measure the resistance of asphalt concrete to tertiary deformation (asphalt flow). The test can be conducted in a uniaxial or triaxial state of compressive loading. The test applies a repeated, pulsed, axial stress/load (cyclic); haversine loading with 0.1 sec loading and 0.9 sec

unloading, up to 10,000 cycles or until a specimen failure, whichever came first. The mixture's response characteristics (elastic/plastic viscoelastic/viscoplastic) are obtained. As in the static creep test, recommended test temperatures range from 25°C to 60°C (77°F to 141°F). The design stress levels ranges between 69 and 207 kPa (10-30 psi) for unconfined tests and 483 and 966 kPa (70-140 psi) for confined tests. Typical confinement levels range between 35 and 207 kPa (5-30 psi) (Roberts et al. 1996).

The test was conducted in accordance with NCHRP Report 465 Appendix B on laboratory-prepared samples with diameter of 100 mm (4 in) and heights of 150 mm (6 in), cored from Superpave gyratory-compacted plugs (Witczak, et al. 2002). The dynamic creep test setup is similar to the static creep test, but the loading is dynamic. The loading is applied for 0.1 sec. followed by 0.9 sec. of rest period for up to 10,000 repetitions or until failure, whichever comes first. The dynamic creep parameters, intercept (a), slope (b), and flow number $F_{n,}$ are obtained from the plots (Figure 4.4).

The dynamic creep test results are presented in cumulative permanent strain (ε_p) against number of loading repetitions. The permanent strain curves comprised of three zones: primary, secondary, and tertiary flow (Figure 4.2). The number of pulses (cycles) at which tertiary flow begins is known as the flow number F_n. A power law is used to model the secondary strain:

$$\varepsilon_p = aN^b \qquad \textbf{(Equation 4.4)}$$

The regression constants a, the intercept and b, the slope are obtained from the plots of permanent strain against the number of cycles. Figure 4.3 shows permanent strain against the number of cycles and Figure 4.4 shows strain slope against the number of cycles on linear scales. These are some of the typical dynamic creep test results obtained at the Kansas State University laboratory.

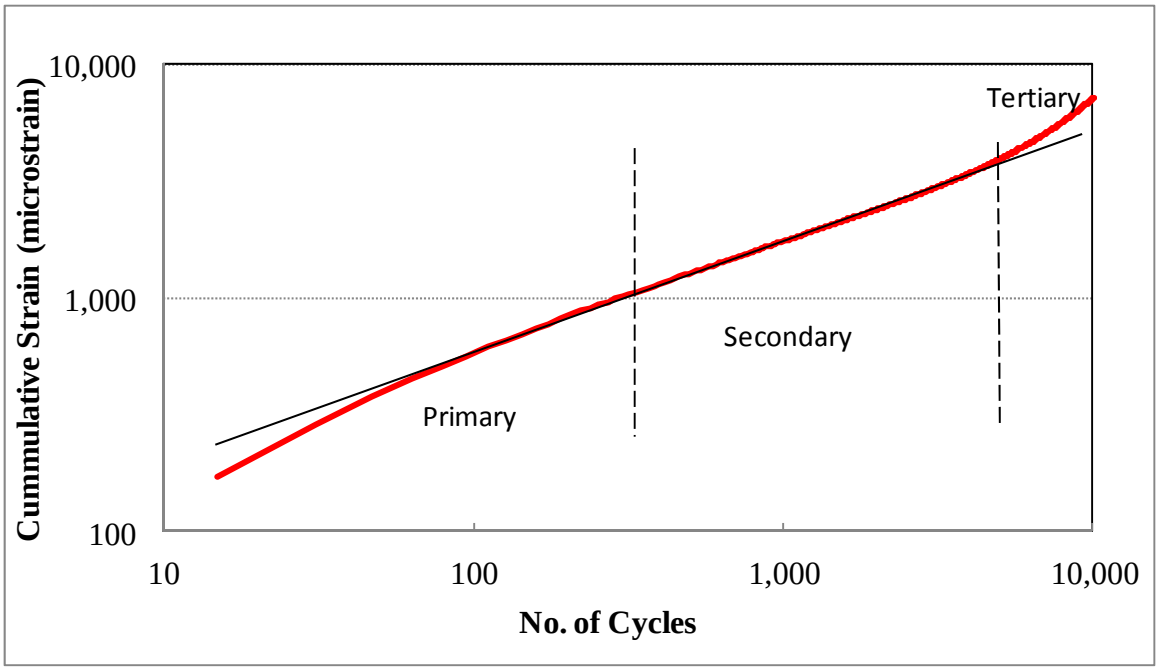

FIGURE 4.2: Permanent Strain vs Number of Cycles on Logarithmic Scale

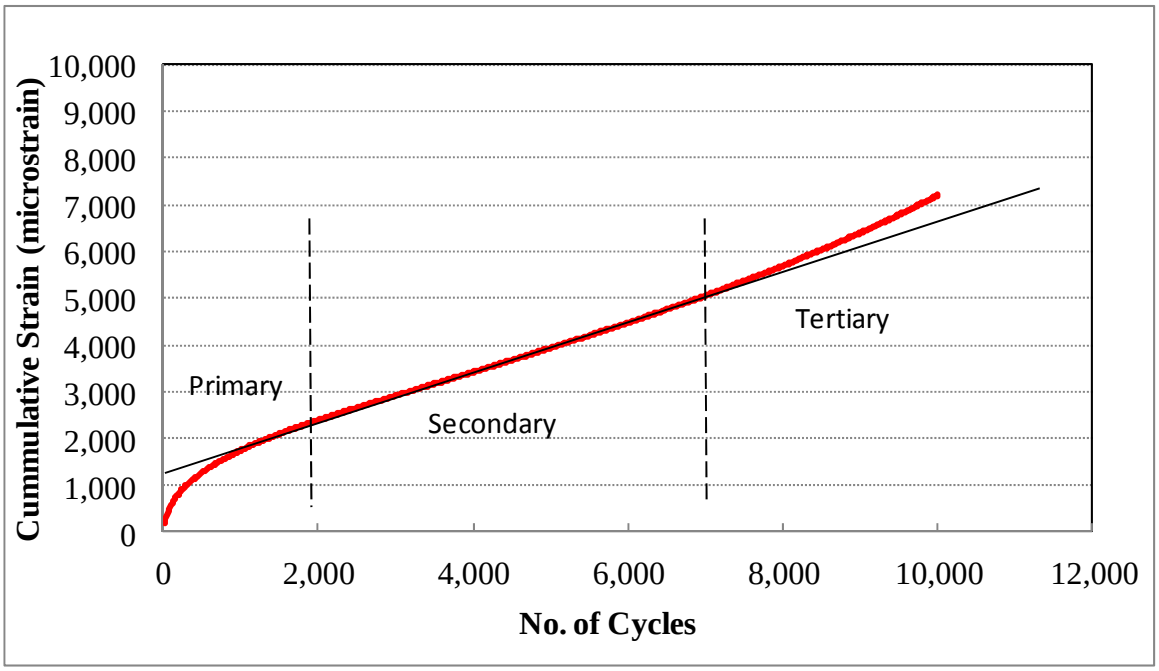

FIGURE 4.3: Permanent Strain vs Number of Cycles On Linear Scale

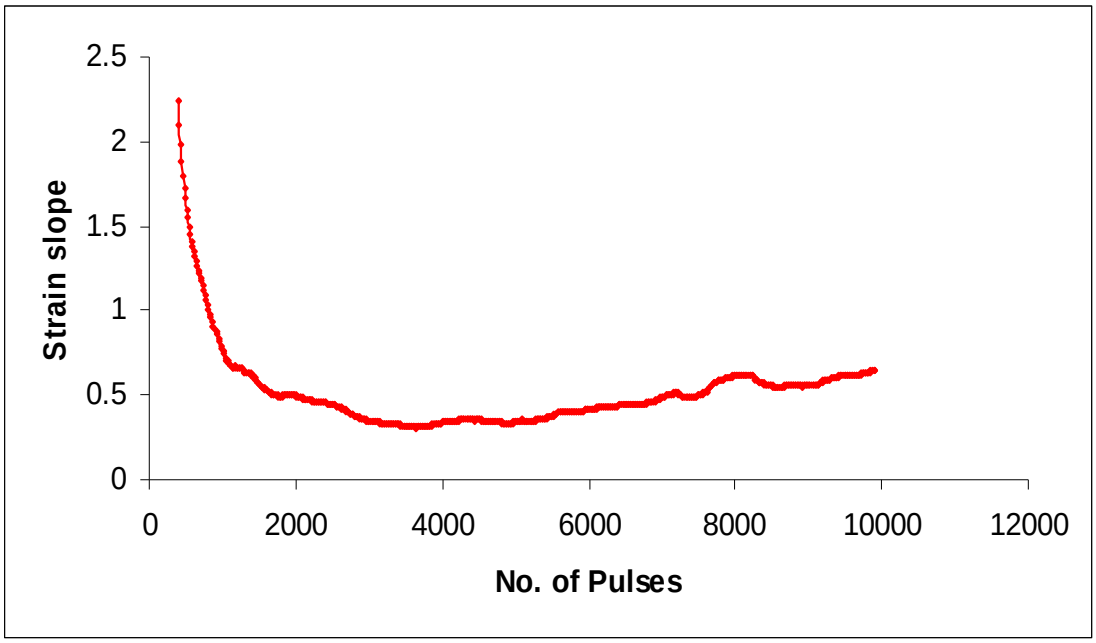

FIGURE 4.4: Strain Slope vs Number of Cycles

TABLE 4.3: Dynamic Creep Test Results

Mix	Test load	Dynamic creep parameters		
	(kPa)	a (x10^{-6})	b	FN
KS1	207	21.75	0.1506	10,000
KS2	207	105	0.60165	7,239
MO1	207	28.7	0.1642	10,000
MO2	207	53.1	0.4352	10,000
IA1	207	25.5	0.81465	2,500
IA2	207	25	0.01665	4,000
KS2	345	185	0.6128	3,000
MO2	345	275	0.5918	10,000
KS1	690	465	0.11665	10,000
MO1	690	595	0.6831	10,000
MO2	690	750	0.776867	7,639

The dynamic creep test was conducted at 207kPa, 345kPa, and 690kPa, as shown in Table 4.3. At 207 kPa KS1, MO1 and MO2 mixes did not fail. When tested at 345 kPa, KS2 failed at a 3,000 flow number and MO2 did not fail. At 690 kPa, MO1 and KS1 mixes did not fail and MO2 obtained a flow number of 7,639. From these results, KS1 and MO1 mixes are the most resistant to flow, indicating they have less potential for permanent deformation. Asphalt mix MO2 follows in the list, then KS2, IA2, and IA1.

4.3 Repeated Load Triaxial Compressive Strength Test

The repeated load triaxial strength tests were conducted on specimens having a 100 mm (4 in) diameter by 6 inches height, cored and sawed from gyratory compacted cylindrical plugs. The specimens were tested at four confining pressures, 0, 68.9, 137.9, and 206.7 kPa (0, 10, 15 and 30 psi, respectively). A haversine load was applied for 0.1 seconds loading and 0.9 seconds unloading at a strain rate of 0.0001 ε/s. Two replicate specimens were tested for each mix at every confining pressure, at 35^{o}C. The test is conducted typically to obtain viscoplastic (Druker-Prager) model parameters: cohesion (κ), internal angle of friction (α), and elastic modulus (E). The results obtained from the triaxial strength test are summarized in Table 4.4 and in Figures 4.5 to 4.10. It can be seen that for all mixes, the maximum strain increases with an increase in confining pressure.

TABLE 4.4: Results of the Triaxial Compressive Strength Test

Sample ID	% AV	Confining pressure (kPa)	Initial yield stress (kPa)	Failure strength (kPa)	Elastic modulus MPa
KS1	6.51	0	1094.50	1870.0	66.48
KS1	6.64	69	1486.66	1990.0	68.29
KS1	6.73	138	1567.62	2245.0	79.98
KS1	6.46	207	1650.02	2361.1	83.38
KS2	6.71	0	919.84	1145.5	57.14
KS2	6.49	69	975.01	1256.6	66.67
KS2	6.99	138	1120.44	1366.3	54.54
KS2	6.66	207	1200.77	1433.6	57.14
MO1	9.42	0	384.39	1211.4	90.45
MO1	9.57	69	617.43	1357.8	52.18
MO1	9.68	138	604.22	1459.4	66.50
MO1	9.61	207	864.76	1525.1	60.91
MO2	7.19	0	520.58	851.4	31.07
MO2	7.43	69	558.86	966.0	27.63
MO2	6.53	138	619.86	1123.5	34.68
MO2	6.93	207	792.47	1268.3	37.00
IA1	7.00	0	74.12	240.9	6.35
IA1	7.56	69	86.55	250.8	8.30
IA1	7.62	138	116.96	276.7	9.21
IA1	7.66	207	122.88	319.0	9.08
IA2	7.90	0	397.12	802.5	38.5
IA2	7.91	69	561.79	875.8	34.50
IA2	7.93	138	625.4	968.8	36.12
IA2	8.00	207	749.74	1095.6	41.54

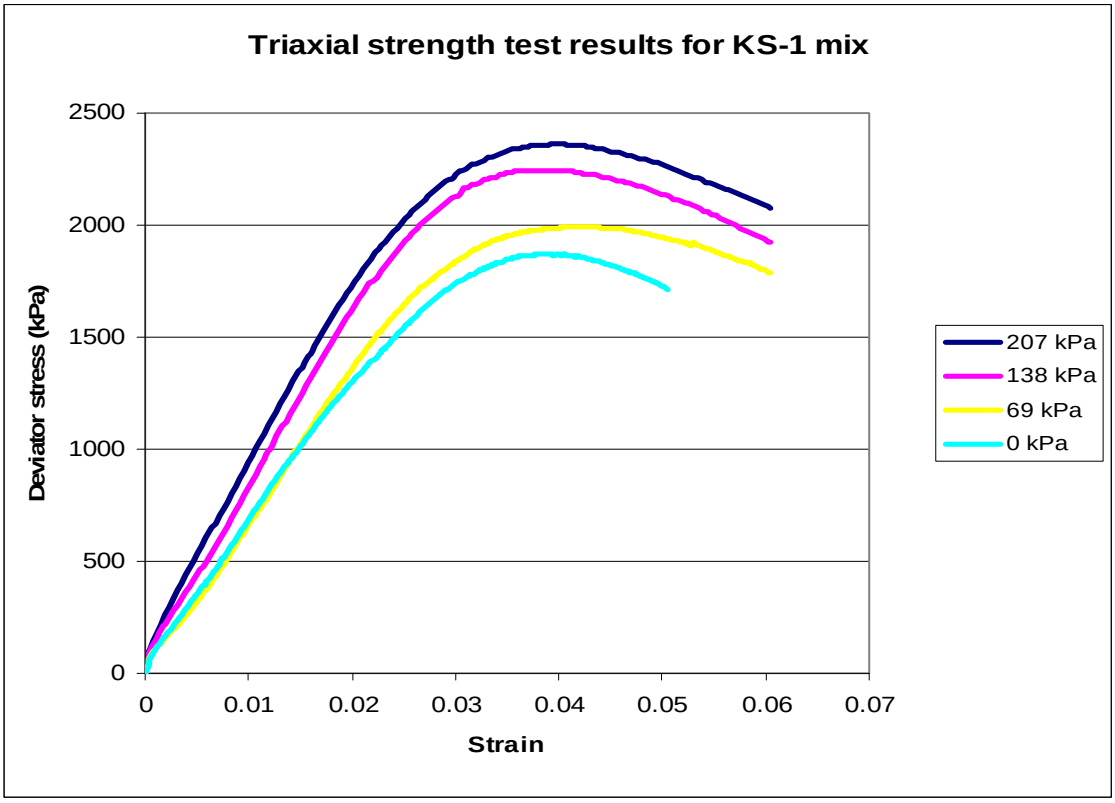

FIGURE 4.5: Triaxial Strength Test Results for KS1 Mix

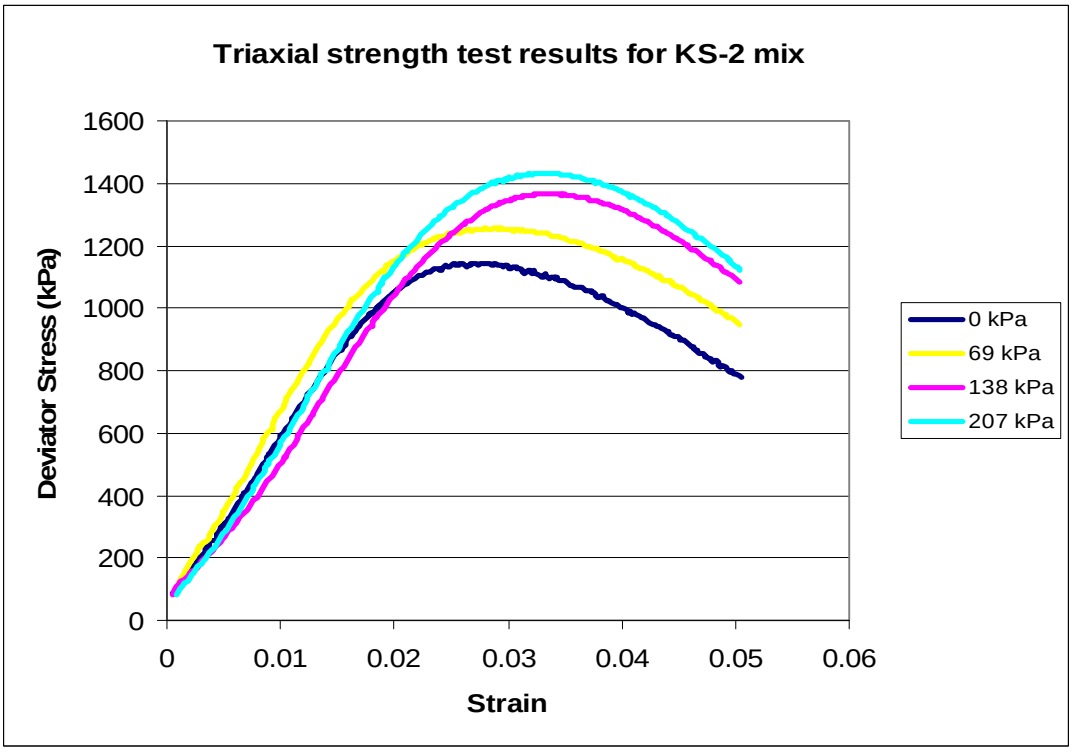

FIGURE 4.6: Triaxial Strength Test Results for KS2 Mix

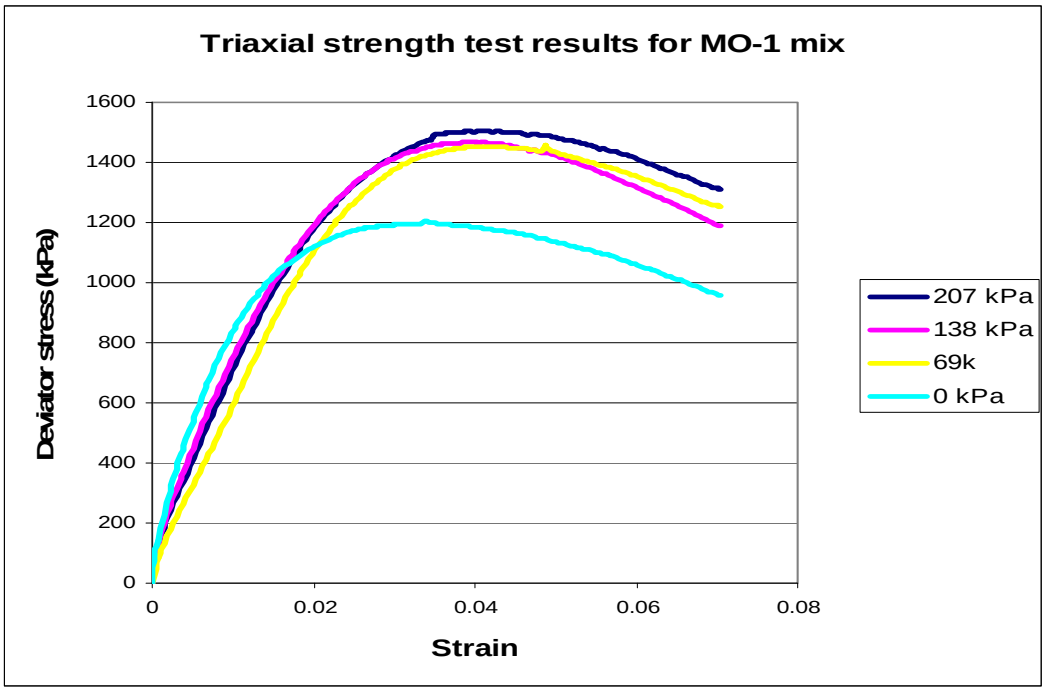

FIGURE 4.7: Triaxial Strength Test Results for MO1 Mix

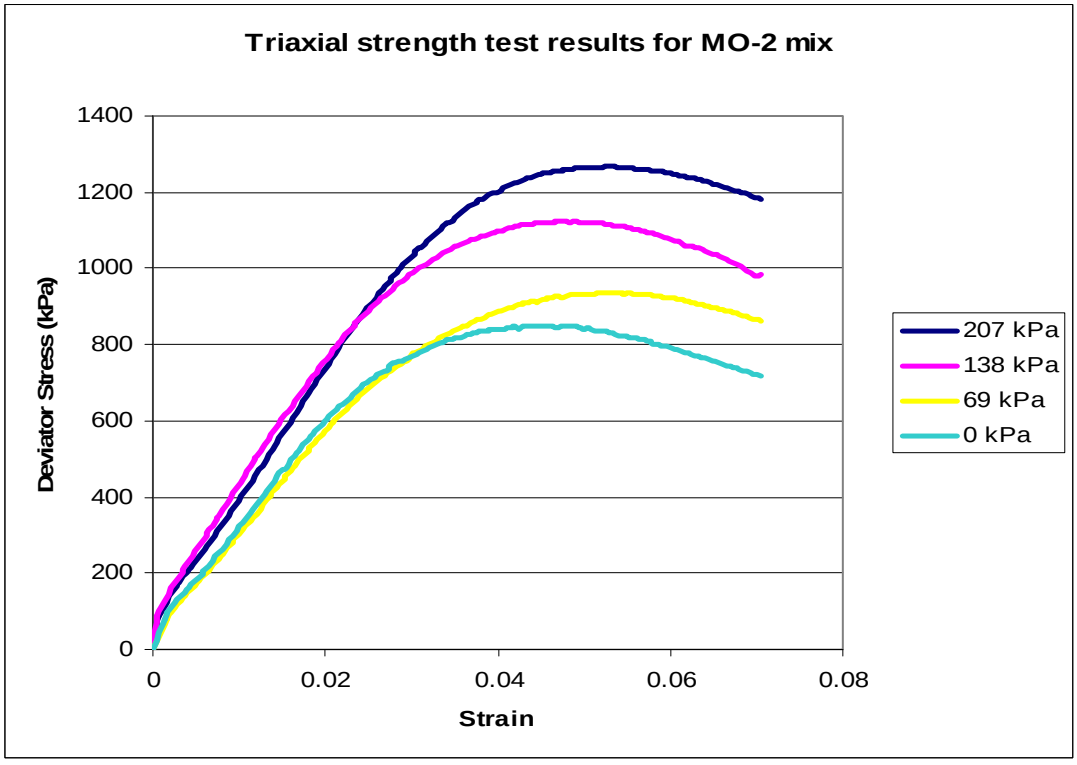

FIGURE 4.8: Triaxial Strength Test Results for MO2 Mix

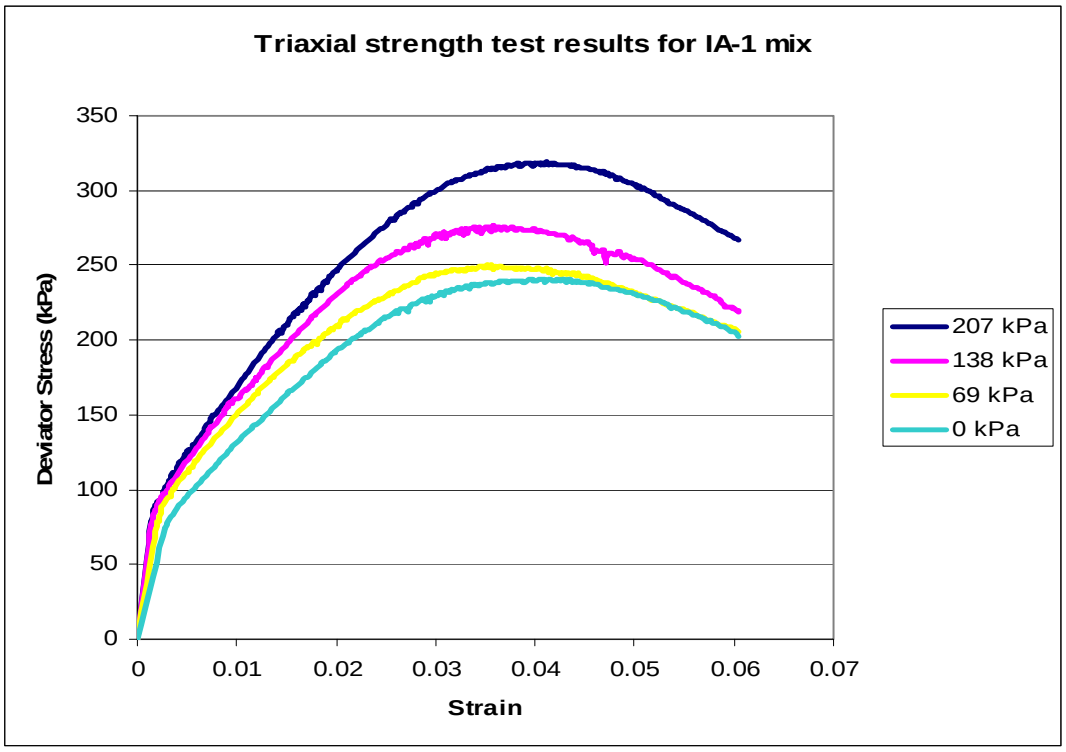

FIGURE 4.9: Triaxial Strength Test Results for IA1 Mix

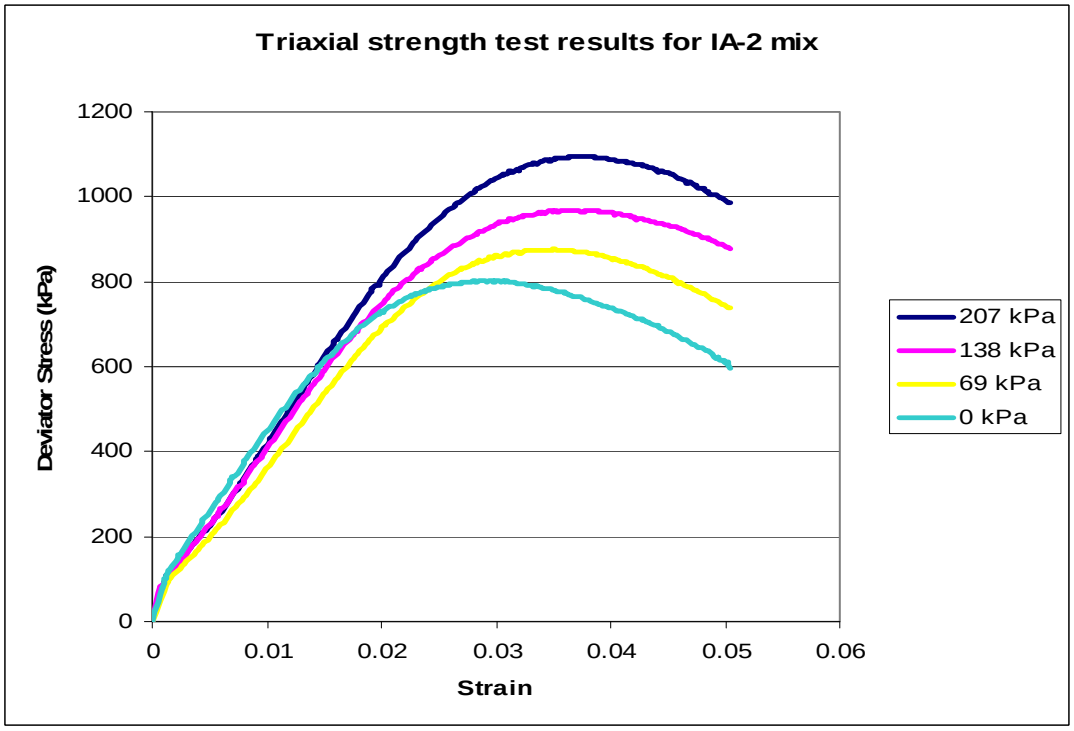

FIGURE 4.10: Triaxial Strength Test Results for IA2 Mix

4.4 Uniaxial (Unconfined) Strength Test at Five Strain Rates

The uniaxial strength test was conducted at five strain rates to obtain the elastic viscoplastic material parameters for the constitutive model and the initial elastic modulus. Two replicate specimens having 4 inches in diameter and 6 inches in height, cored out of compacted Superpave gyratory plugs, were prepared and tested at each strain rate. The test was conducted using the UTM-25, which has a load-cell capacity of 25kN. Two LVDTs with 100 mm gauge length were used to measure axial deformation. The test was conducted at 35 ± 0.5oC with a series of uniaxial compressive strength tests at five different strain rates: 0.00001, 0.0001, 0.002, 0.0042, and 0.072 ε/sec.

The uniaxial strength test was conducted at five strain rates to obtain the initial and yield strains for the viscoplastic model. The test was conducted at a range of strain rates to characterize the viscoplastic model at representative field vehicle speeds. The maximum vertical strain to be used in the test was obtained using the KENLAYER program (Witczak et al. 2002). The material properties, layer thickness, and loading conditions used for the strain analysis are given in Table 4.5.

TABLE 4.5: Loading Parameters Used in KENLAYER

Property	Asphalt	Base	Subgrade
Layer thickness (mm)	175	150	1475
Modulus (MPa)	250	80	8
Poisson's ratio (Assumed)	0.35	0.4	0.45
Loading	Single axle – dual wheel		
Tire radius	106.7 mm		
Tire pressure	690 kPa		
Tire spacing	360.68 mm		
Point of interest	50 mm below asphalt surface		

The KENLAYER program was used to obtain strain magnitude under the wheel after one load repetition. Input values given in Table 4.5 were used to obtain the maximum vertical strain of 0.001315 under the center of each tire. A triangular pulse-loading time was used to obtain the loading time with respect to speed travelled and depth below pavement surface. At a depth of 50 mm below pavement surface and a speed of 11.6 kph (7.2 mph) (the axle speed at CISL 14 experiment), an equivalent triangular loading time of 0.48 seconds was obtained (Witczak, et al. 2002). With these parameters, 0.24 sec is required to reach the maximum vertical strain. The strain rate was then

determined as a ratio of maximum vertical strain to the time required to reach the maximum vertical strain. Slow-moving vehicle speeds between 1.6 to 48 km/h (1 - 30 mph) were considered to obtain the strain rates used for testing. For each vehicle speed, the equivalent triangular loading time was obtained and the strain rate was determined. Table 4.6 gives the vehicle speed, loading time, and corresponding strain rate.

TABLE 4.6: Vehicle Speed and Corresponding Strain Rate

Vehicle speed km/h (mph)	1.6 (1)	8.08 (5)	11.6 (7.2)	16.1 (10)	32.2 (20)	48.3 (30)
Time (sec)	1.7	0.6	0.48	0.3	0.09	0.06
Strain rate (sec^{-1})	1.55 e-3	4.38 e-3	5.48e-3	8.77 e-3	2.92 e-2	4.38 e-2

The method explained above was used for an estimation of strain rates that can be used in the lab to obtain the initial and yield stress for the Drucker-Prager model. For laboratory tests, strain rates of 0.0001, 0.002, 0.0042, and 0.0071 strains per second were adopted representing vehicle speeds ranging from almost stationary to 10 mph. These are strain rates for slow-moving vehicles.

Table 4.7 and Figures 4.11 to 4.16 present results from the uniaxial strength test for the six mixes tested. From the figures it can be seen that asphalt mix at intermediate temperatures is strain-rate dependent, because maximum strain increased with an increase in strain rate. Kansas mix, KS, was not tested to failure at higher strain rates (0.0071 and 0.0042 sec^{-1}) because its material strength exceeded the capacity of the UTM-25 machine used for testing (25 kN).

TABLE 4.7: Results of Uniaxial Compressive Strength Tests

Sample ID	% AV	Strain rate (sec^{-1})	Initial yield stress (kPa)	Failure stress (kPa)	Elastic modulus (MPa)
KS1	6.12	0.00001	526.02	992.70	53.40
KS1	6.51	0.0001	1094.50	1870.00	74.03
KS1	6.26	0.0020	1504.73	2843.40	109.21
KS1	6.51	0.0042	1991.77	3058.50	102.65
KS1	6.46	0.0071	2027.94	3058.50	142.86
KS2	7.25	0.00001	484.76	664.10	36.2
KS2	6.71	0.0001	981.62	1145.50	57.14
KS2	6.56	0.0020	1493.95	2256.20	66.67
KS2	6.95	0.0042	1686.77	2672.50	54.54
KS2	6.50	0.0071	2152.66	2846.00	100
MO1	8.97	0.00001	416.16	721.50	27.40
MO1	9.42	0.0001	587.42	1211.40	106.81
MO1	9.08	0.0020	1063.93	2110.50	130.45
MO1	9.46	0.0042	1128.78	2365.00	110.00
MO1	9.16	0.0071	1932.00	2902.40	123.43
MO2	7.41	0.00001	343.49	784.00	31.44
MO2	7.19	0.0001	520.58	851.4	31.07
MO2	7.29	0.0020	688.83	1439.00	81.93
MO2	6.96	0.0042	994.65	1953.40	100.75
MO2	7.50	0.0071	1913.99	2577.50	131.97
IA1	7.00	0.0001	74.12	240.90	6.35
IA1	6.94	0.0020	230.23	665.70	40.94
IA1	6.72	0.0042	367.39	864.40	32.06
IA1	6.72	0.0071	544.29	986.70	32.97
IA2	7.38	0.00001	378.15	605.3	27.48
IA2	7.90	0.0001	397.12	802.50	38.5
IA2	7.63	0.0020	630.55	1561.60	71.8
IA2	7.38	0.0042	1145.11	2095.70	85.81
IA2	7.86	0.0071	1508.74	2368.00	88.66

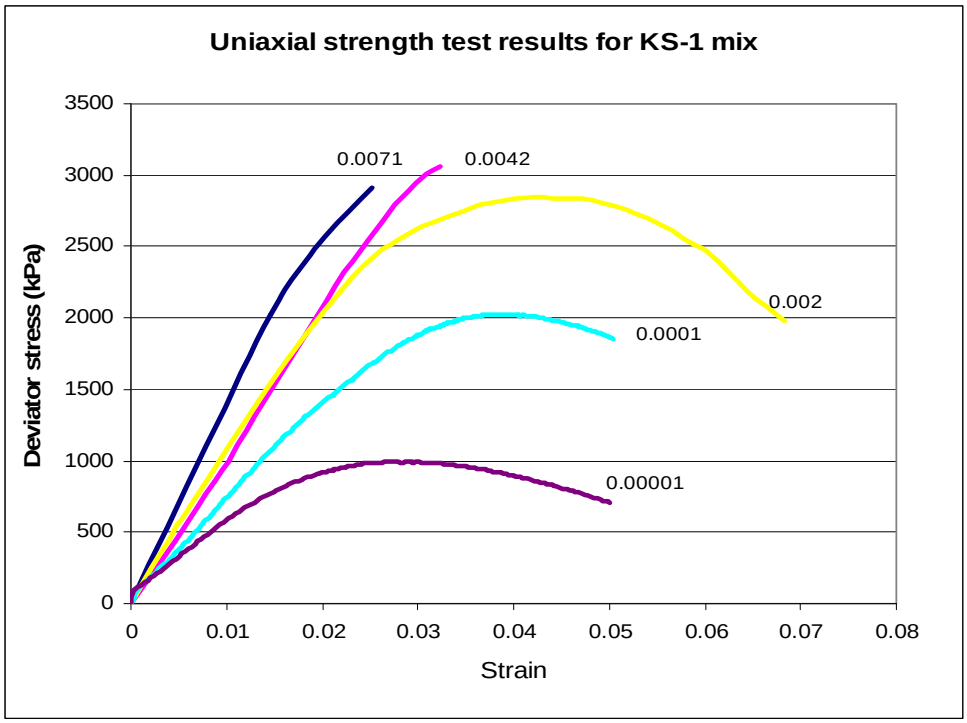

FIGURE 4.11 Uniaxial Strength Test Results for KS1 Mix

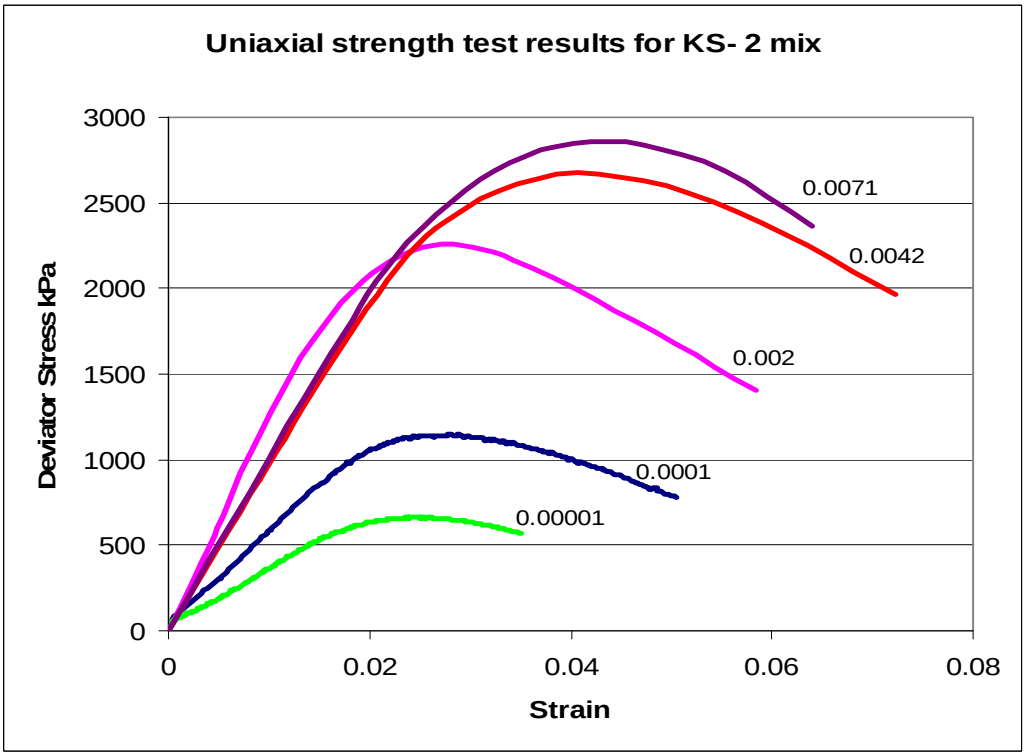

FIGURE 4.12 Uniaxial Strength Test Results for KS2 Mix

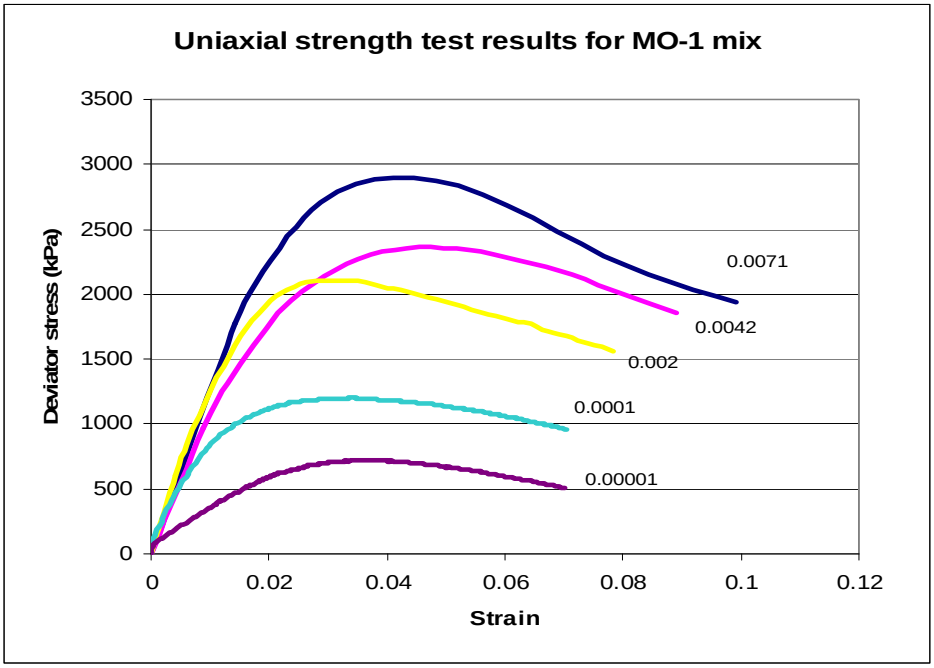

FIGURE 4.13: Uniaxial Strength Test Results for MO1 Mix

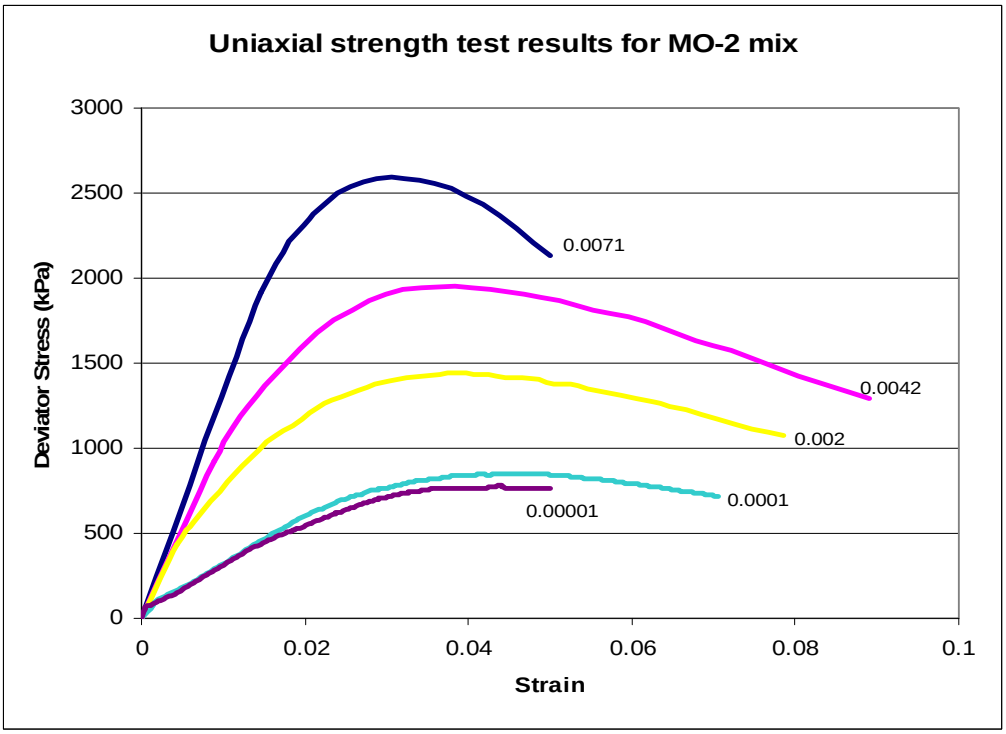

FIGURE 4.14 Uniaxial Strength Test Results for MO2 Mix

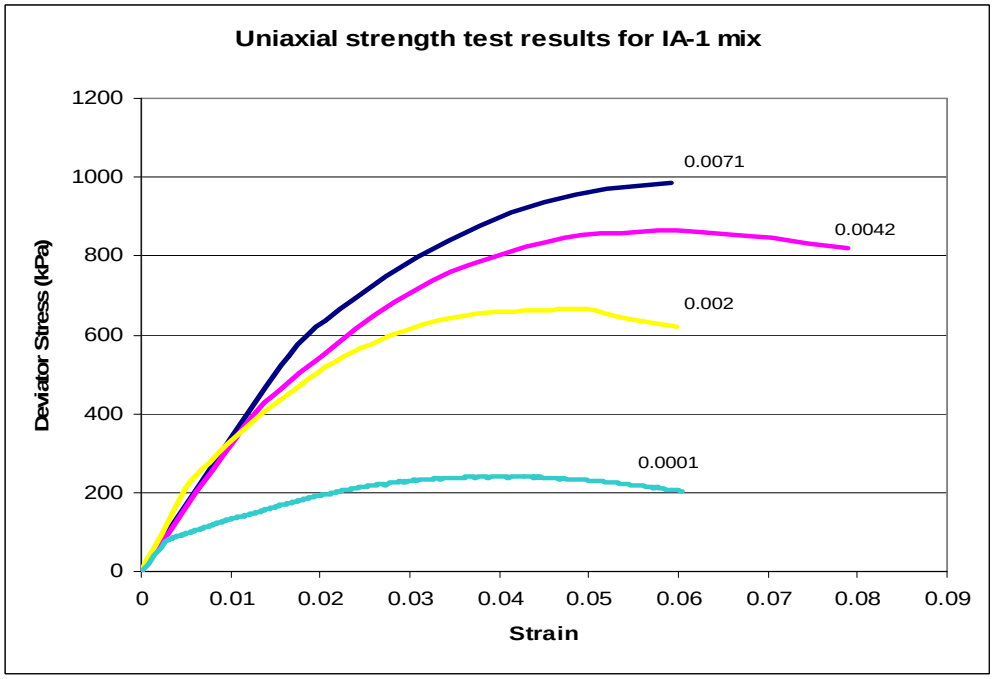

FIGURE 4.15 Uniaxial Strength Test Results for IA1 Mix

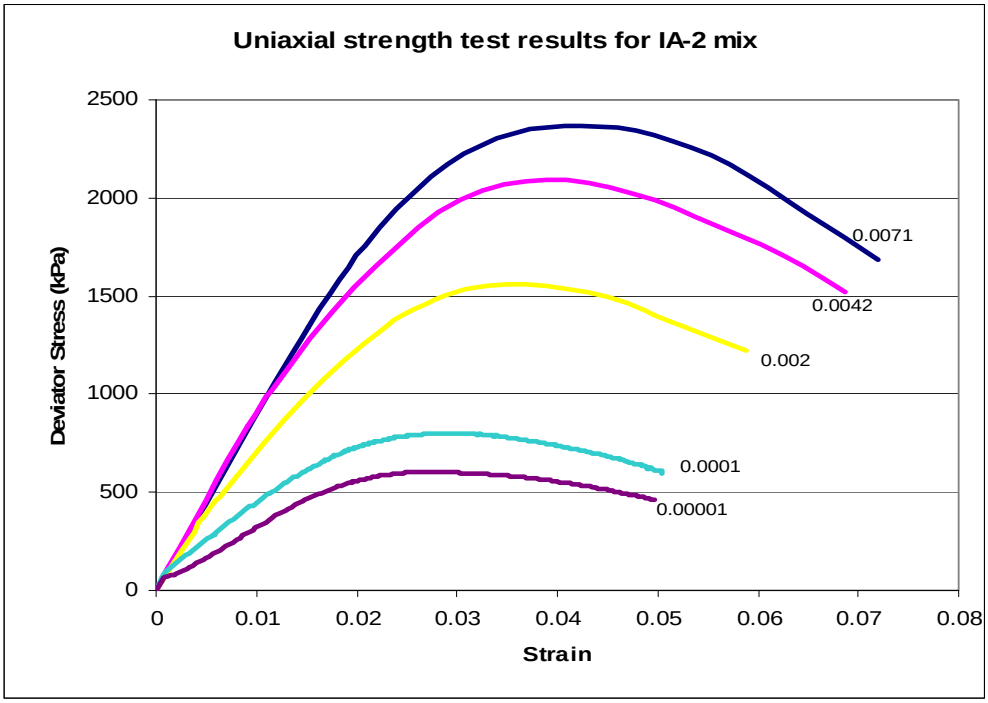

FIGURE 4.16 Uniaxial Strength Test Results for IA2 Mix

4.5 Superpave Shear Tests

Superpave shear tests (SST) were developed as a way to measure shear characteristics of HMA (Brown et al. 2001). The test system consists of a loading device, specimen deformation measurement, an environmental chamber, and a control and data acquisition system. The loading device is capable of applying both vertical and horizontal loads to the specimen. It is also capable of applying static, ramped (increasing or decreasing), and vertical and horizontal loads. It is controlled by closed-loop feedback using either stress control or strain control throughout the entire range of frequencies, temperatures, and confining pressures. The SST also simulates the high shear stresses (which lead to lateral and vertical deformation associated with permanent deformation in surface layers) that exist near the pavement surface at the edge of vehicle tires (Brown et al. 2001).

Six SST tests can be performed using the Superpave shear tester: simple shear, frequency sweep, uniaxial strain, volumetric shear, repeated shear at constant stress ratio, and repeated shear at constant height. These properties measure the resistance to permanent deformation and fatigue cracking in asphalt mixtures (Brown et al. 2001 and Huang 2000). Two SST tests were performed for this research; the simple shear test at constant height (SSCH) and repetitive shear at constant height (RSCH). The tests were performed at the Asphalt Institute Laboratory in Lexington, Kentucky.

The tests were conducted on 150-mm-diameter and 50.0 ±2.5-mm-tall specimens. These specimens were fabricated using the Superpave gyratory compactor at the KSU asphalt laboratory. The specimens were then sawn and accurately measured to make sure that the top and bottom faces were smooth and parallel. Specific gravity of the specimens was determined using AASHTO T166, Bulk Specific Gravity of Compacted Bituminous Mixtures test procedure. Specimens were then packed and shipped for testing to the asphalt institute.

4.5.1 Repeated Shear at Constant Height Test

The repeated shear at constant height (RSCH) test is performed by placing a pair of platens into a gluing jig provided with the shear test device (Figure 4.17). The platens are aligned and clamped into place. A thin coating of epoxy cement (~1.5 mm) is applied to each end of the dust-free test specimen. The epoxy coating should completely cover the specimen ends and should be of uniform thickness. Mounting screws are then attached with epoxy cement to the sides of the test specimen for

the horizontal LVDT(s). LVDTs are mounted on the sample in such a way that both vertical and horizontal deformations can be measured. The specimen is placed and secured tightly in the testing machine. The control chamber is adjusted to testing temperature. The specimen is preconditioned for 100 cycles with a shear stress of 69 ± 5 kPa. Each cycle is 0.7 seconds in duration and consists of the application of a 0.1-second haversine load followed by a 0.6-second rest period. The test is conducted until 5,000 cycles or a shear failure occurs, usually at 2.5mm or 5 percent shear strain. Axial deformation, shear deformation, axial load, and shear load at a rate of about 50 data points per second are recorded. The permanent shear strain is then computed. The repetitive simple shear test at constant height (RSST-CH) can also be used to obtain creep compliances D(t) and parameters to be used in the power law of the creep compliance equation, d_o, d_i, and m. For these samples, the shear load of 69 kPa was low because the samples were tested at 35^{o}C. Therefore the shear load was increased to 137.5 kPa (20 psi); the measured shear strains are provided in the results section (Chapter 5).

For this project, the SST repeated shear test at constant height (RSCH), AASHTO T320, Procedure C, was conducted at 35^{o}C with a shear load of 137.5 kPa (20 psi) and tested up to 50,000 number offload repetitions. Table 4.8 indicates that Iowa mix IA1 attained maximum permanent strain of 11.28% after 40,000 cycles. The rest of the samples had better resistance to permanent deformation. At 5000 cycles, all samples passes specification, having permanent strain less than 5% or 2.5mm deformation. After 10,000 cycles, Iowa mix IA1 showed the highest permanent shear strain of 11.28% at 40,000 cycles (Figure 4.19).

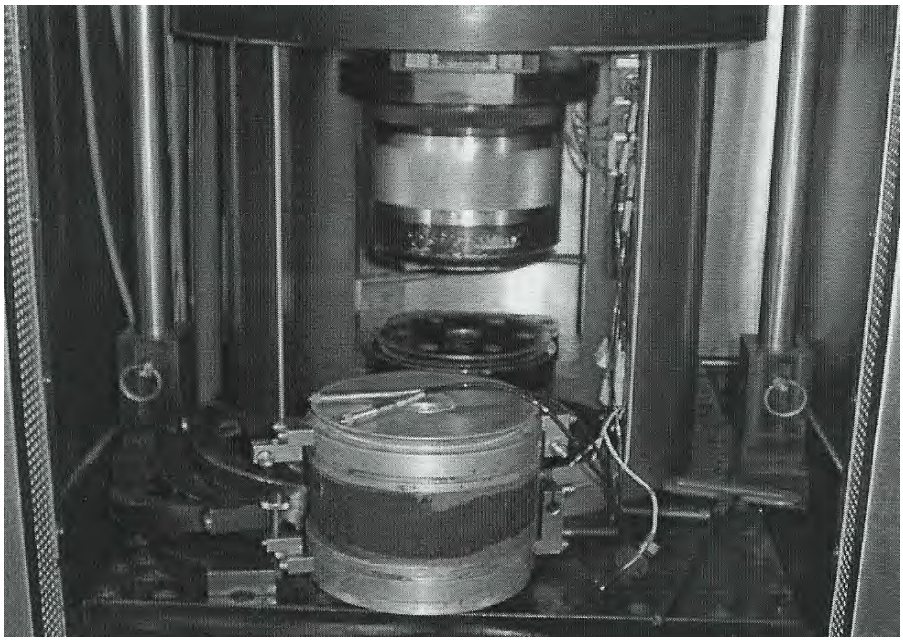

FIGURE 4.17: Superpave Shear Test (SST)

FIGURE 4.18: Cox SST Testing Machine

TABLE 4.8: Results of the SST Repeated Shear at Constant Height Test

Specimen	Mix ID	KS1	KS2	MO1	MO2	IA1	IA2
% Air Voids		6.49	6.59	8.63	6.82	9.18	7.75
	Cycles						
g_{perm} (strain) @ cycles	10	0.01%	0.08%	0.03%	0.04%	0.08%	0.05%
	50	0.04%	0.24%	0.08%	0.11%	0.23%	0.13%
	100	0.06%	0.35%	0.12%	0.17%	0.34%	0.19%
	500	0.15%	0.72%	0.26%	0.40%	0.70%	0.44%
	1,000	0.20%	0.94%	0.37%	0.55%	0.89%	0.59%
	5,000	0.39%	1.63%	0.75%	0.97%	1.61%	1.05%
	10,000	0.51%	1.92%	0.99%	1.17%	2.41%	1.30%
	20,000	0.63%	2.17%	1.27%	1.38%	4.76%	1.59%
	30,000	0.70%	2.29%	1.45%	1.50%	8.38%	1.78%
	40,000	0.75%	2.37%	1.58%	1.58%	11.28%	1.91%
	50,000	0.78%	2.43%	1.69%	1.65%	na	2.00%

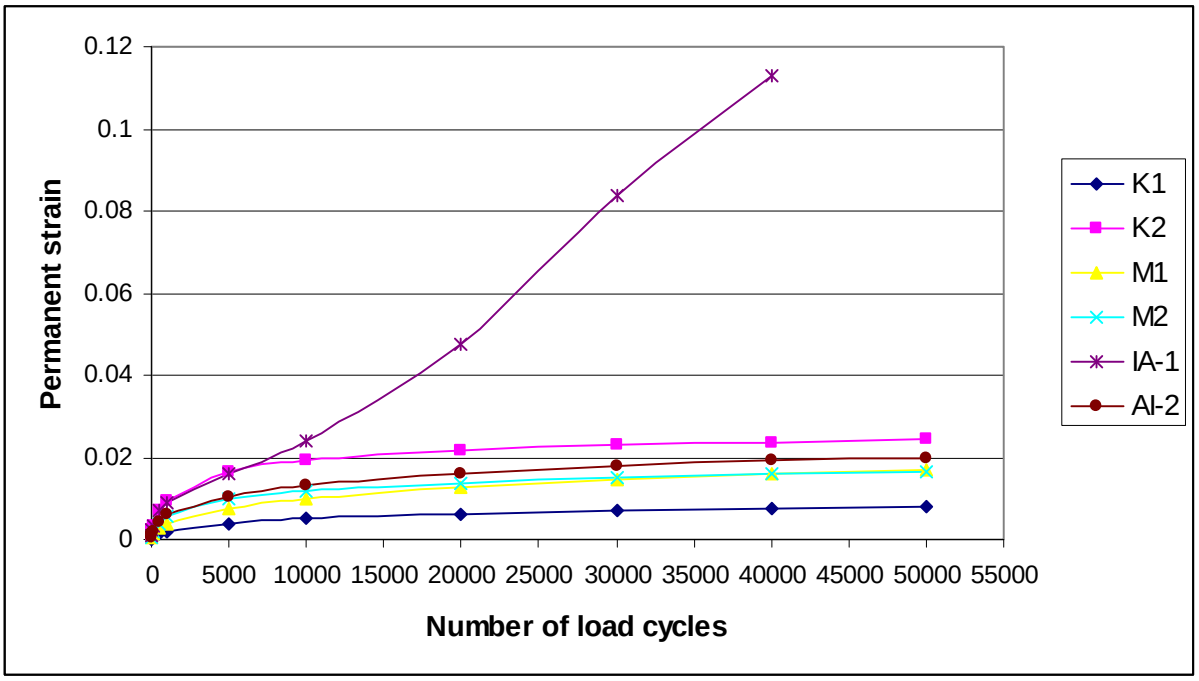

FIGURE 4.19: RSCH Test-Permanent Strain vs Number of Cycles

4.5.2 Frequency Sweep at Constant Height Test

The frequency sweep at Constant Height (FSCH) test was performed to obtain the dynamic shear modulus G*, storage modulus G' and loss modulus G" of asphalt mixtures. Storage and loss moduli represent the behavior of asphalt at intermediate temperatures, where G* = G' + iG". The storage modulus is elastic (recoverable) and the loss modulus is viscous and nonrecoverable. The dynamic modulus and phase angle are affected by both temperature and loading frequency. At low temperature and high loading frequency, the asphalt concrete is elastic and has a high dynamic modulus. At high temperature and low loading frequency, asphalt concrete is more viscous and has a low elastic modulus. Results from the FSCH test were used to construct master curves and obtain modulus values at a representative temperature of 35°C.

The dynamic shear modulus master curves were calculated using Mastersolver Version 2.0, developed by Ramon Bonaquist of Advanced Asphalt Technologies, LLC. Mastersolver has a capability to solve a modified version of the Mechanistic-Empirical Pavement Design Guide master curve equation, Equation 4.5.

$$\log|E^*| = \delta + \frac{(Max - \delta)}{1 + e^{\beta + \gamma \log w_r}} \qquad \textbf{(EQUATION 4.5)}$$

Where:

|E*| = dynamic modulus;

ω_r = reduced frequency, Hz;

Max = limiting maximum modulus; and

δ, β and γ = fitting parameters.

The reduced frequency is computed using the Arrhenius equation, Equation 4.6.

$$\log \omega_r = \log \omega + \frac{\Delta E_a}{19.14714}\left(\frac{1}{T} - \frac{1}{T_r}\right) \qquad \textbf{(EQUATION 4.6)}$$

Where:

ω_r = reduced frequency at the reference temperature

ω = loading frequency at the test temperature

T_r = reference temperature in ^oK

T = test temperature in ^oK, and

ΔE_a = activation energy (treated as a fitting parameter).

Substituting equation 4.2 into equation 4.1 yields the master curve that is used for dynamic modulus computation.

$$\log|E^*| = \delta + \frac{(Max - \delta)}{1 + e^{\beta + \gamma\left\{\log\omega + \frac{\Delta E_a}{19.14714}\left(\frac{1}{T} - \frac{1}{T_r}\right)\right\}}} \quad \textbf{(EQUATION 4.7)}$$

Temperature shift factors are given by Equation 4.8

$$\log a(T) = \frac{\Delta E_a}{19.14714}\left(\frac{1}{T} - \frac{1}{T_r}\right) \quad \textbf{(EQUATION 4.8)}$$

Where:

a(T) = shift factor at temperature T,

T_r = reference temperature in ^oK,

T = test temperature in ^oK, and

ΔE_a = activation energy (treated as a fitting parameter).

Bonaquist uses the Hirsch model and a limiting binder modulus of 1 GPa (145,000 psi) to estimate the maximum modulus from mixture volumetric properties, Equations 4.9 and 4.10.

$$|E^*|_{max} = P_c\left[4{,}200{,}000\left(1-\frac{VMA}{100}\right)+435{,}000\left(\frac{VFAxVMA}{10{,}000}\right)\right]+\frac{1-P_c}{\left[\frac{1-\frac{VMA}{100}}{4{,}200{,}000}+\frac{VMA}{453{,}000(VFA)}\right]}$$

(EQUATION 4.9)

Where:

$$P_c = \frac{\left(20+\frac{435{,}000(VFA)}{VMA}\right)^{0.58}}{650+\left(\frac{4355{,}000(VFA)}{VMA}\right)^{0.58}}$$

(EQUATION 4.10)

|E*| = limiting maximum mixture dynamic modulus;

VMA = voids in mineral aggregates, %; and

VFA = voids filled with asphalt, %.

These equations are used in the Mastersolve Version 2.0. The solver and results from the FSCH test were used to compute the dynamic shear modulus, storage modulus, and loss modulus.

The dynamic shear modulus (G*) values at 35^{o}C were obtained using Equation 4.5 and fitting parameters in Table 4.9. The dynamic shear modulus (G*) values at 35^{o}C (test temperature) and six loading frequencies are given in Table 4.10.

TABLE 4.9: Fitting Parameters for Dynamic Shear Modulus

Fit parameters	**Fit parameters for shear modulus G***					
	KS1	KS2	MO1	MO2	IA1	IA2
Delta (δ)	-0.4023	-0.5000	-0.7351	-0.9120	-0.4512	-0.5232
Beta (β)	-0.2000	0.1546	-0.2512	-0.3273	0.0892	-0.0720
Gamma (γ)	-0.3365	-0.3864	-0.3500	-0.3500	-0.3800	-0.3700
Ea	226928	202655	195866	189921	186672	211911
Max (MPa)	21584.62	21584.62	21584.62	21584.62	21584.62	21584.62

TABLE 4.10: Dynamic Shear Modulus at 35°C

	G* (MPa)					
Freq. (Hz)	**KS1**	**KS2**	**MO1**	**MO2**	**IA1**	**IA2**
25	1035.1	537.7	918.9	976.3	597.8	796.1
10	786.5	380.0	678.6	716.9	429.7	578.7
5	634.8	290.9	535.0	562.0	333.0	451.5
1	379.7	155.9	301.4	311.3	183.0	249.9
0.5	302.9	119.5	233.9	239.3	141.5	193.1
0.1	178.8	65.7	129.1	128.8	79.0	106.7

The storage modulus (G') values at 35°C were obtained using Equation 4.5 and the fitting parameters in Table 4.12. The storage modulus (G') values at 35°C (test temperature) and six loading frequencies are given in Table 4.12.

TABLE 4.11: Fitting Parameters for Storage Shear Modulus

Fit parameters	Fit parameters for storage modulus G'					
	KS1	KS2	MO1	MO2	IA1	IA2
Delta (δ)	-0.4064	-1.7980	-0.5588	-0.8128	-1.0203	0.1100
Beta (β)	-0.1000	-0.3065	-0.0686	-0.1775	-0.0899	0.4604
Gamma (γ)	-0.3500	-0.2984	-0.3800	-0.3800	-0.3274	-0.3787
Ea	246659	220776	199847	198340	205520	275157
Max (MPa)	21584.62	22775.03	21246.77	22051.59	20530.34	21651.54

TABLE 4.12: Storage Shear Modulus at 35°C

	G' (MPa)					
Freq. (Hz)	**KS1**	**KS2**	**MO1**	**MO2**	**IA1**	**IA2**
25	874.6	537.7	781.4	829.8	463.0	501.6
10	652.8	380.0	562.3	590.4	336.9	373.9
5	520.0	290.9	435.1	452.0	263.3	299.8
1	302.4	155.9	236.0	237.5	146.6	181.5
0.5	238.7	119.5	180.8	178.9	113.7	147.4
0.1	138.2	65.7	97.9	92.6	63.1	93.4

The fitting parameters used in Equation 4.1 to obtain the loss modulus (G") are given in Table 4.13.

TABLE 4.13: Fitting Parameters for Loss Shear Modulus

Fit parameters	Fit parameters for storage modulus G"					
	KS1	KS2	MO1	MO2	IA1	IA2
Delta (δ)	0.2253	-1.3920	-0.6030	-0.7013	-0.4052	0.4262
Beta (β)	0.5642	-0.0688	0.1087	0.0259	0.3796	0.9661
Gamma (γ)	-0.4000	-0.3000	-0.3000	-0.3500	-0.3500	-0.3500
Ea	144847	170924	165705	159777	161506	219532
Max (MPa)	21584.62	22775.03	21246.77	22051.59	20530.34	21651.54

The loss modulus (G") values at 35°C (test temperature) and six loading frequencies are given in Table 4.14.

TABLE 4.14: Loss Shear Modulus at 35°C

	G" (MPa)					
Freq. (Hz)	**KS1**	**KS2**	**MO1**	**MO2**	**IA1**	**IA2**
25	4.197	4.952	4.801	4.629	4.679	6.360
10	2.701	3.188	3.090	2.980	3.012	4.094
5	1.256	1.482	1.437	1.385	1.400	1.903
1	0.000	0.000	0.000	0.000	0.000	0.000
0.5	-1.139	-1.344	-1.303	-1.257	-1.270	-1.727
0.1	4.197	4.952	4.801	4.629	4.679	6.360

4.6 Flexural Fatigue of Asphalt Concrete Mixtures

In order to determine flexural fatigue properties of asphalt concrete mixes used for this research project, approximately 20-inch-square slabs were cut from slabs built outside of the CISL laboratory with the mixes at the same time the pavement test sections were built. The mix used in the pads was compacted with the same rollers and at the same density as the mix paved in the experimental pavement sections. A Troxler nuclear density gage was used to measure the as-compacted density.

The slabs were transported and stored at the KDOT Bureau of Materials and Research. Six beams were cut from each slab. Before testing, the beams were placed in the environmental chamber for at least 2 hours at 20°C, the test temperature. The 20°C temperature was controlled by the heating and cooling unit and was used for all tested samples.

The asphalt specimen was placed into the IPC beam-fatigue machine and was fixed in position with the clamps (Figure 4.20). After the input parameters were selected (dimensions of the beam, microstrain level) and all readings were zeroed, the fatigue test was started. Figure 4.21 shows the screen with the loading input data and Figure 4.22 shows the screen where the beam dimensions are inputted. After the test is initialized, the IPC beam-fatigue computer displays the initial stiffness, measured after 200 cycles, and computes the termination stiffness as half of the initial stiffness.

The applied cyclic load used was sinusoidal, with a frequency of 10 Hz and with no rest periods. The peak-to-peak load amplitude was recorded. The specimens were tested under controlled strain mode at three different strain levels: 100, 200, and 300 microstrain (10^{-6} in/in). Mixes KS1 and KS2 were also tested at 400 and 500 microstrain. Failure of the specimen was considered when the beam reached 50% of the initial stiffness.

The following data was recorded periodically during the test: test loading time, cycle number, maximum and minimum applied load and deflection, tensile stress, strain, phase angle, flexural stiffness, modulus of elasticity, and dissipated energy. The data for each fatigue test was saved in a binary file format and then in ASCII text files. The text files were then imported into Microsoft Excel for further numerical analysis. The typical output (Figure 4.23) shows that flexural stiffness decreases with an increasing number of loading cycles. This trend was observed for all beams tested in this experiment.

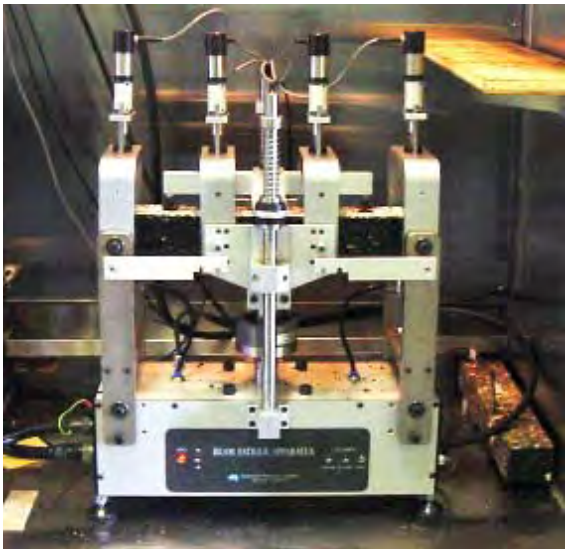

FIGURE 4.20: Beam Fatigue Testing Apparatus

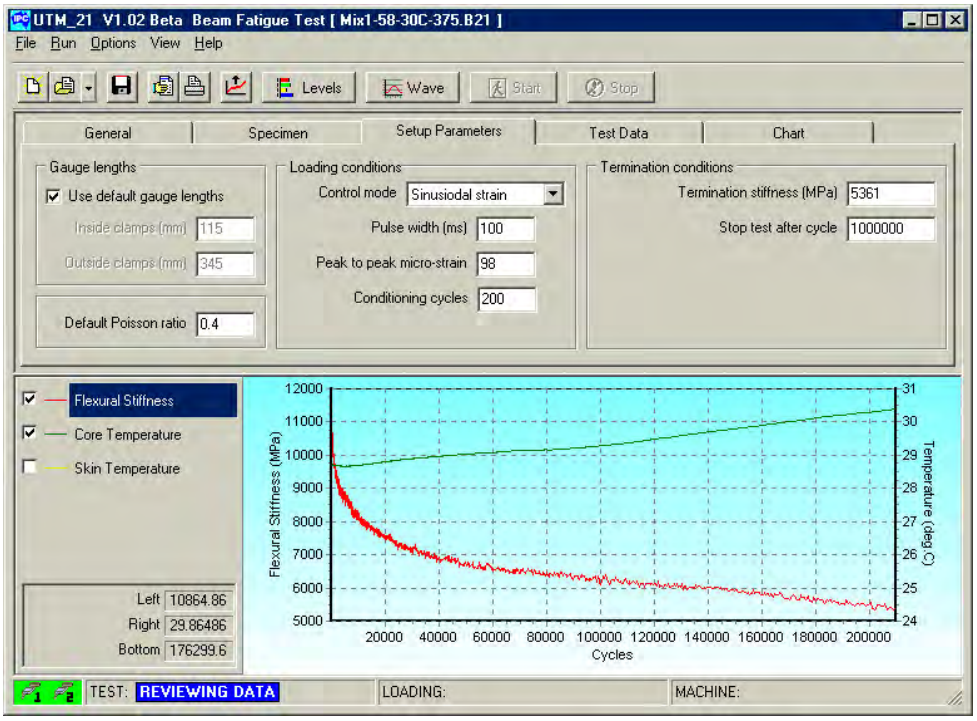

FIGURE 4.21: Input Screen for Loading Conditions

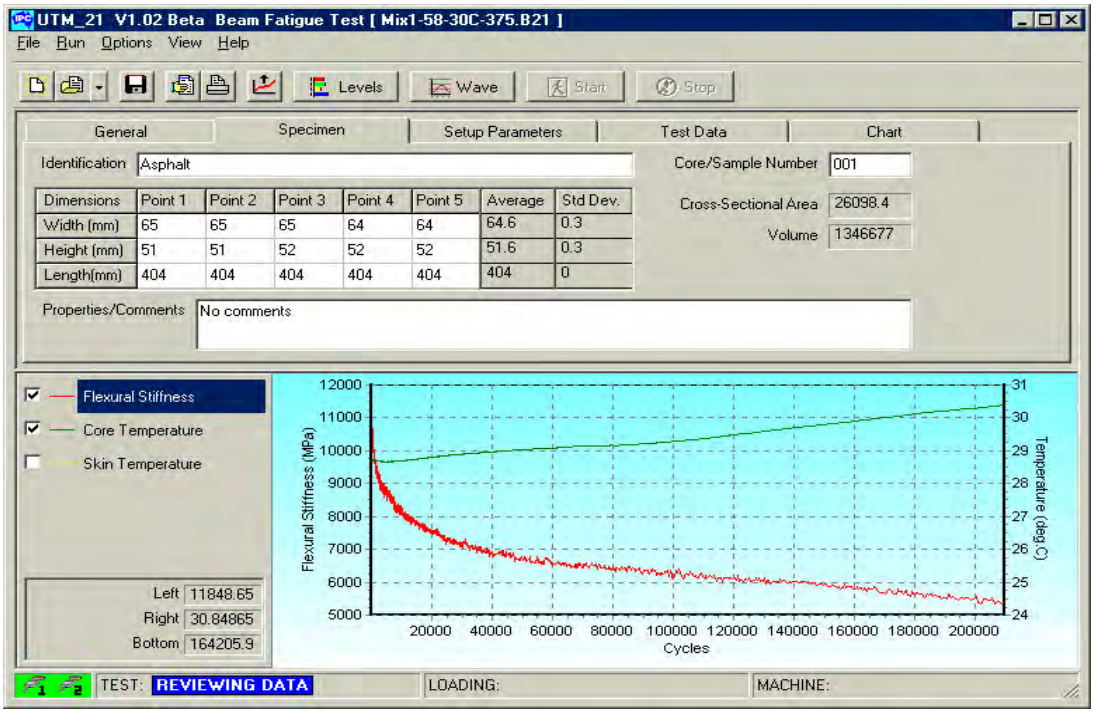

FIGURE 4.22: Input Screen for Specimen Dimensions

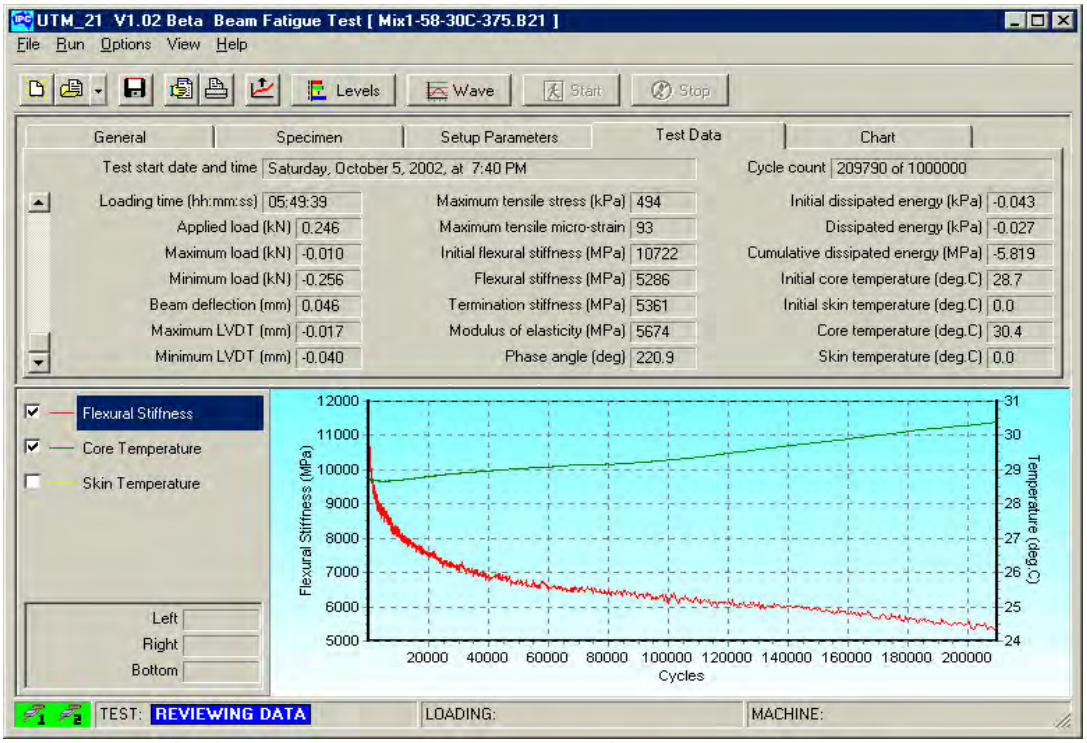

FIGURE 4.23 Typical Output Screen of Beam Fatigue Test

Some asphalt specimens in this test did not reach the termination stiffness of 50% of the initial stiffness after the maximum number of cycles of 2 million, especially the specimens tested at low strain levels. For time considerations, the tests were stopped after 2 million loading cycles. This limited cycle number was inputed in the UTM software as it was deemed that the stiffness data collected in the first 2 million cycles allowed the estimation of the number of cycles to failure, considered as the number of cycles where the stiffness reaches half of the initial values. For these specimens the assumption made was that after 500,000 load cycles, flexural stiffness decreases linearly with the number of applied cycles:

$$S = b_0 + b_1 N \qquad \textbf{(EQUATION 4.11)}$$

Where:

S = stiffness (MPa),

N = is the number of cycles,

b0 = is the intercept of the Y axis, and b1 is the slope.

The final modulus, which is half of the initial modulus, has the following equation:

Sfin = b0 + b1Nfin = 0.5 * Sinitial (EQUATION 4.12)

Therefore, the fatigue life N_{fin} was determined as follows:

Nfin = (Sfin - b0) / b1 (EQUATION 4.13)

The coefficients b0, b1, R2, and Nfin were computed using Microsoft Excel. A graphical example of the use of linear regression to estimate the number of cycles to failure for the specimens that did not fail up to 2 million cycles is shown in Figure 4.24. The number of cycles to failure, Nfin, are given in Tables 4.15 and 4.16.

The number of cycles to failure was also calculated considering an exponential evolution of the stiffness with the number of cycles, as follows:

S = c Nd (EQUATION 4.14)

The coefficients c and d were computed using Microsoft Excel from the stiffness data recorded in the first 2 million cycles. Then, the number of cycles to failure, Nfin , was calculated; results are given in Tables 4.15 and 4.16. However, it was visually found that the linear regression provided a much better fit than the exponential model, and therefore, the fatigue lives obtained with the linear model were retained for further analysis.

TABLE 4.15: Laboratory Fatigue Life of Kansas Mixes

Mix	Peak strain (microstrain)	Sample ID	Cycle count	Fatigue life (linear model)	Fatigue life (exponential model)
KS1		A-1-C	2,000,000	10,019,017	3,677,173
	100	A-1-D	2,000,000	8,679,003	36,404,789
		A-1-E	1,378,720	1,378,720	1,974,778
	200	A-2-A	2,000,000	4,236,160	2,777,032
		A-4-D	2,000,000	2,173,164	1,885,602
	300	A-4-E	2,000,000	2,475,927	5,742,727
		A-5-A	581,440	581,440	547,337
		A-2-D	713,405	713,405	780,483
		A-2-E	759,950	759,950	793,347
		A-6-D	840,220	840,220	851,951
	400	A-2-B	861,175	861,175	925,554
		A-1-A	223,205	223,205	257,197
		A-2-F	255,805	255,805	272,592
	500	A-4-C	277,590	277,590	286,578
KS2		B-7-A	2,000,000	8,814,827	9,316,494
		B-9-B	638,490	638,490	2,769,266
		B-7-B	2,000,000	6,253,127	4,575,229
		B-7-C	2,000,000	3,852,242	4,359,416
		B-8-A	2,000,000	4,856,483	50,410,704
		B-8-B	2,000,000	3,943,384	3,217,953
		B-9-A	2,000,000	8,503,710	8,718,832
		B-10-E	2,000,000	7,180,468	3,997,389
	100	B-10-F	2,000,000	17,530,371	7,303,975
		B-8-D	1,698,000	1,698,000	3,080,654
		B-7-D	2,000,000	4,945,782	3,522,089
		B-8-C	2,000,000	4,926,834	3,714,615
	200	B-9-D	2,000,000	6,794,876	5,523,085
	250	B-10-C	678,360	678,360	7,912,639
		B-7-E	1,642,050	1,642,050	2,524,207
		B-7-F	2,000,000	3,119,945	2,670,058
		B-8-E	2,000,000	2,329,442	2,478,181
		B-8-F	2,000,000	3,331,921	3,313,323
		B-9-E	2,000,000	2,421,425	2,233,077
	300	B-9-F	2,000,000	2,682,633	2,442,379
		B-11-A	823,960	823,960	948,218
	400	B-10-A	2,000,000	4,532,870	3,152,102
		B-11-C	462,500	462,500	531,963
		B-11-D	490,835	490,835	599,453
		B-11-B	554,555	554,555	621,211
	500	B-10-D	997,730	997,730	1,320,532

TABLE 4.16: Laboratory Fatigue Life of Missouri and Iowa Mixes

	Peak strain (microstrain)	Sample ID	Cycle count	Fatigue life (linear model)	Fatigue life (exponential model)
MO1		A-1A	2,000,000	18,287,878	27,182,242
	100	A-1B	2,000,000	37,305,628	9,640,434
		A-1C	2,000,000	38,422,994	5,776,227
		A-1D	1,727,975	5,982,926	3,455,370
	200	A-1E	2,000,000	11,043,358	4,816,867
		A-2A	2,000,000	5,016,405	3,371,338
		A-2B	2,000,000	3,222,254	2,621,585
		A-2C	2,000,000	6,578,289	3,565,572
	300	A-2D	2,000,000	5,347,120	2,960,902
MO2		B-3D	2,000,000	18,531,883	12,096,809
	100	B-3E	2,000,000	12,434,779	6,144,922
		B-3C	1,069,000	9,275,171	3,898,466
		B-3A	2,000,000	8,282,914	3,789,760
		B-3B	2,000,000	5,550,844	4,721,711
	200	B-4A	2,000,000	5,417,568	3,399,447
		B-4D	1,753,055	1,700,349	1,735,037
	300	B-4B	2,000,000	2,468,557	2,082,774
IA1		A-6	2,000,000	42,041,764	10,002,124
		A-11	2,000,000	23,290,630	10,208,353
	100	A-1	2,000,000	8,675,916	7,350,447
		A-7	2,000,000	5,173,506	4,578,251
		A-8	2,000,000	5,282,363	3,443,354
		A-15	2,000,000	4,435,707	3,585,862
	200	A-2	2,000,000	3,281,941	3,130,746
		A-19	413,455	468,428	473,785
		A-10	1,060,130	1,112,177	1,197,352
	300	A-3	2,000,000	2,168,180	2,131,449
IA2		B-4	2,000,000	6,213,807	8,599,841
		B-13	2,000,000	9,137,654	8,041,151
	100	B-14	2,000,000	7,010,069	10,813,529
		B-5	1,356,800	1,400,105	1,428,286
	200	B-16	1,369,415	1,498,402	1,853,830
		B-12	233,335	240,926	302,275
		B-18	270,240	287,902	406,085
		B-9	464,360	481,200	364,354
	300	B-17	762,655	906,128	835,923

Models expressing the relationship between the number of cycles to failure and loading strain were developed after the number of cycles to failure was determined for each tested sample. Table 4.17 presents, for each of the six mixes subjected to flexural fatigue tests, two models relating the number of cycles to failure and loading strain. The models are very similar from a mathematical standpoint. However, a slightly better fit is obtained with Model 1.

Figures 4.25 to 4.27 graph the number of cycles to failure versus strain for the six mixes. Figure 4.28 shows, on the same chart, the Model 1 fit curves for all six mixes. The figure indicates that at 20°C for loading stains higher than 100 micro-strain, Mix MO1, with a polymer- modified binder, has the highest fatigue life, while mix IA2 has the shortest fatigue life. The difference in fatigue life increases with the increased strain level.

In order to incorporate the effect of mix stiffness and volumetric properties, two overall fatigue models (Models 3 and 4) were developed from the fatigue data recorded on all samples.

These models are similar to Equation 1.7, the fatigue model incorporated in MEPDG, with $M = 4.84*[V_b / (V_a+V_b) – 0.69]$. A better fit of the overall model was obtained for Model 4.

TABLE 4.17: Models Relating the Number of Cycles to Failure and Loading Strain

Mix	a	b	c	R-Squared
Model 1: $N = a*(micro\text{-}strain)^b$				
KS1	1.61E+11	-2.10978		0.922867
KS2	9.41E+08	-1.06065		0.374794
MO1	3.71E+10	-1.53314		0.357193
MO2	4.77E+10	-1.72622		0.763139
IA1	1.09E+13	-2.82145		0.635796
IA2	1.29E+12	-2.61847		0.947428
Model 2: $log_{10}(N) = a + b*log_{10}(micro\text{-}strain)$				
KS1	11.19836	-2.07084		0.866162
KS2	8.963334	-1.0955		0.446746
MO1	10.57472	-1.54622		0.592261
MO2	10.68022	-1.7123		0.816795
IA1	13.03939	-2.83302		0.843026
IA2	12.0887	-2.60335		0.921726
Model 3: $N = 10^M * a * (strain)^b * (E^*)^c$				
	7.89	-1.59697	0.070324	0.09
Model 4: $log_{10}(N) = M + log_{10}(a) + b*log_{10}(strain) + c*log_{10}(E^*)$				
	8.44	-1.6095	0.045636	0.330
Note: E is measured in MPa*				

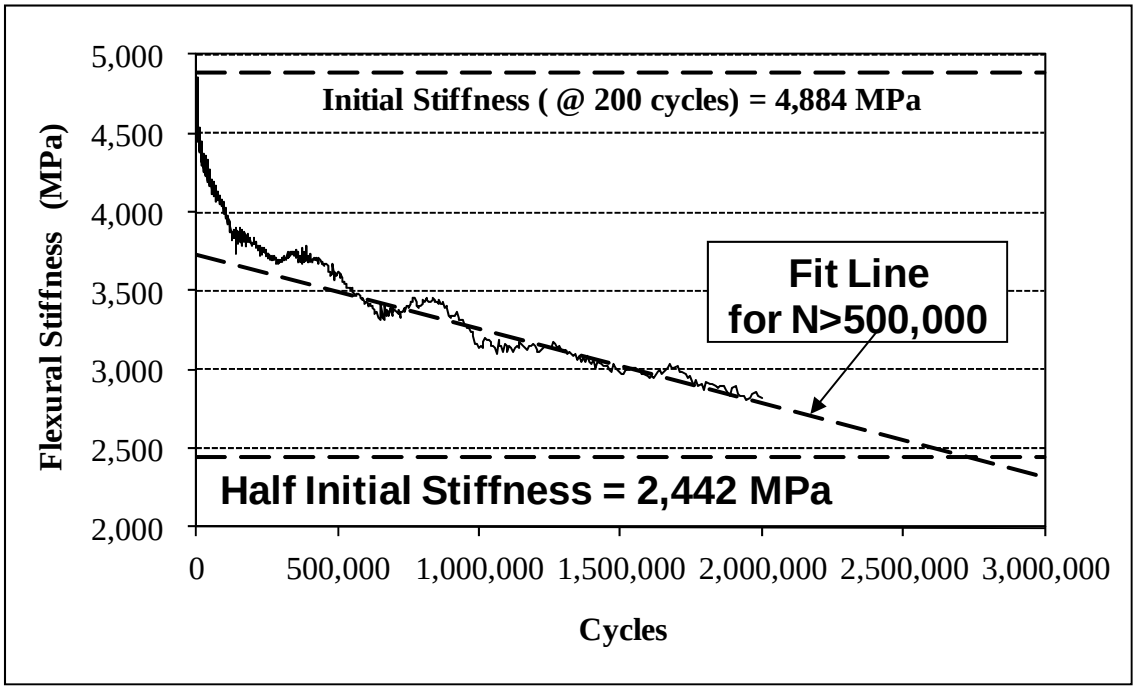

FIGURE 4.24: Estimation of Loading Cycles to Failure by Extrapolation

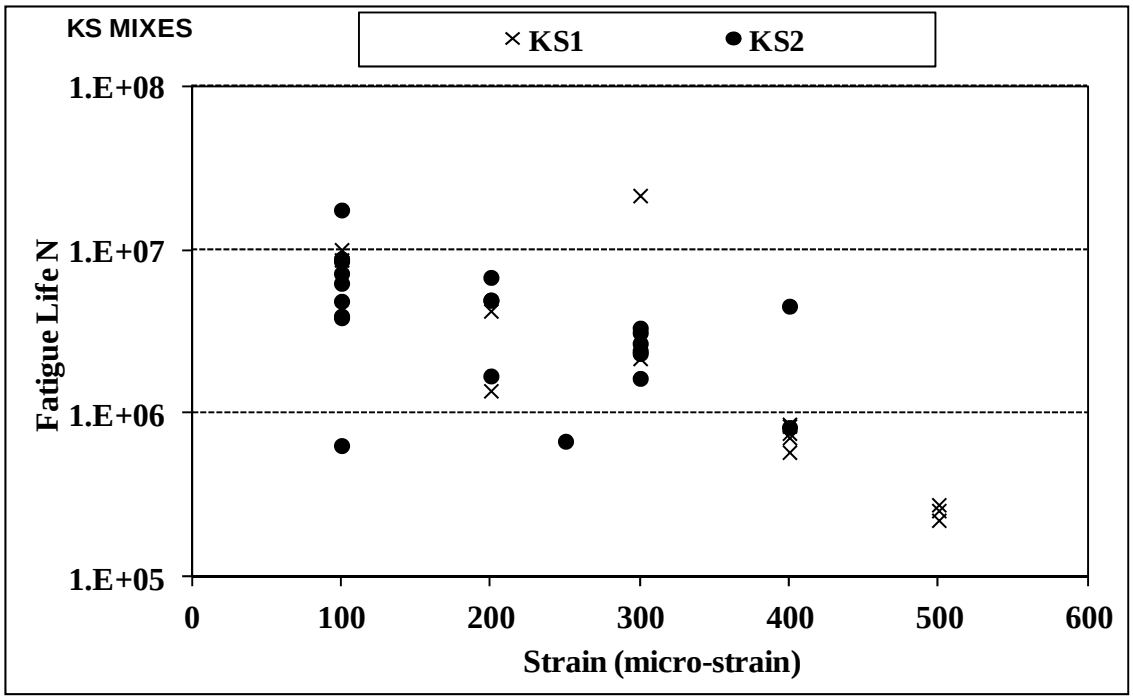

FIGURE 4.25 Flexural Fatigue Lives of Kansas Mixes

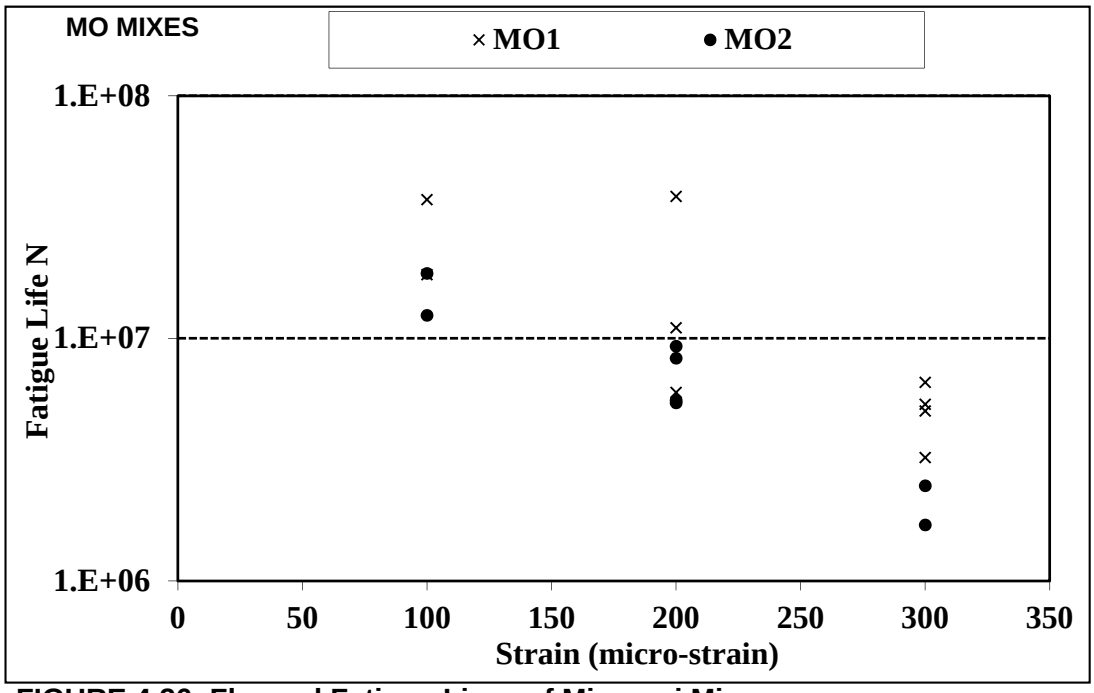

FIGURE 4.26: Flexural Fatigue Lives of Missouri Mixes

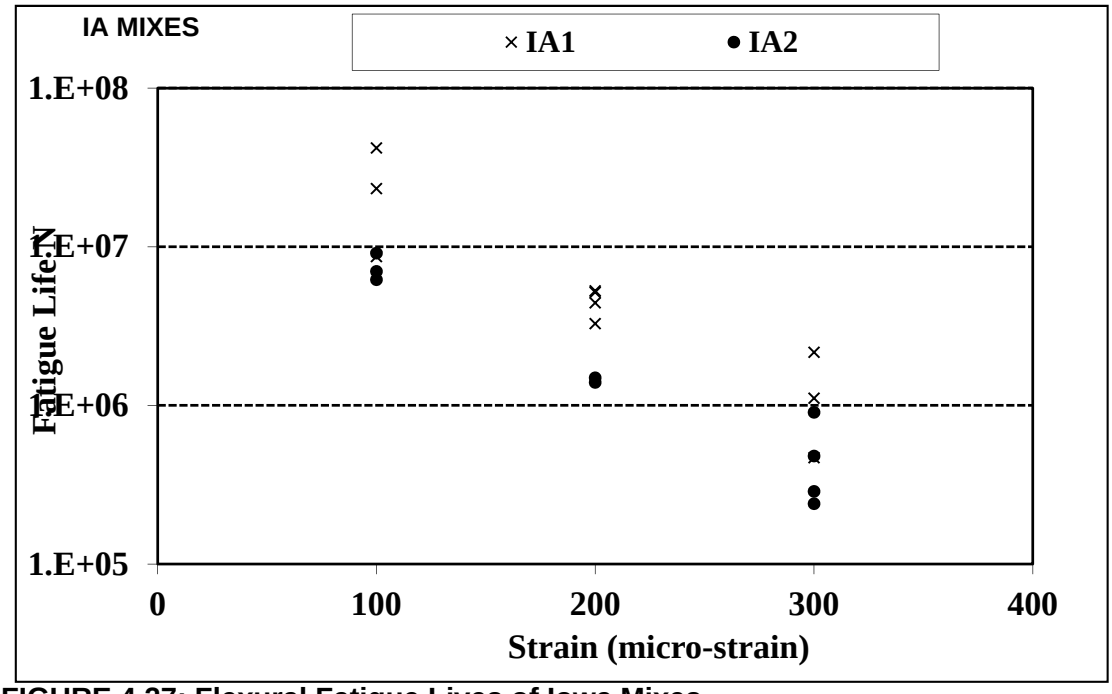

FIGURE 4.27: Flexural Fatigue Lives of Iowa Mixes

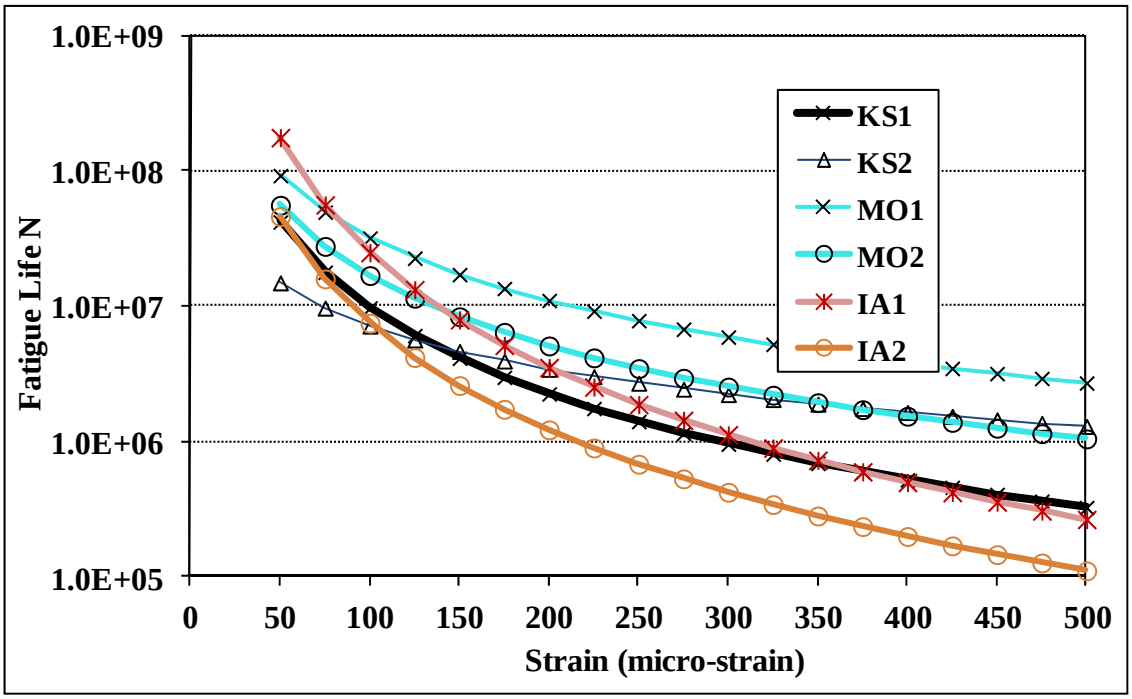

FIGURE 4.28: Flexural Fatigue Lives Predicted by Model 1

Chapter 5: Test Results and Observations

5.1 Transverse Profiles

Transverse profile measurements were performed periodically at the same time with the longitudinal profile and after strain/stress measurements. On each pair of pavement sections, transverse profiles were measured at three different spatial locations: at the middle of the lane, five feet west from the middle, and five feet east of the mid location. Each profile consists of elevation data at 210 points spaced at 0.5-inch intervals. For each profile, two steel balls were glued to the pavement outside the wheel paths (locations not trafficked by the APT machine), at transverse position of 36 and 72 inches. Steel balls were used as a reference since their elevations did not change during the APT loading. Movement of these balls was checked every time profile measurements were made using a reference elevation point at the base of the steel pole near the east entrance of the CISL.

Elevation data for the transverse profiles were assembled in a database in Excel spreadsheet format. Because of the large quantity, this data is being archived in electronic files on a CD-ROM that will be attached to this report.

Figure 5.1 illustrates two typical transverse profiles obtained from the elevation data on two adjacent pavement sections of the same pit. The initial profile is the profile measured before any APT load was applied. The profile showing a larger elevation variation is the profile after APT passes have been made on the pavements. Ruts caused by the passage of the APT load assembly at the pavement surface are clearly visible. Between the tires of the dual wheel, the asphalt concrete surface exhibited some heaving due to upward shoving of the materials.

Two major parameters were derived from the elevation data:

- *Permanent deformation* at the pavement surface was calculated first in each of the 105 (210/2) points of the profile by subtracting measured elevation after a given number of APT passes from the initial elevation data. The permanent deformation was positive when the current elevation of the point was lower than the initial elevation. Then, for each pavement, and for a particular transverse profile (west, middle, and east), the permanent deformation (PD) was computed as the maximum value obtained from the 105 points. The permanent deformation data is reported in Appendix D, in Tables D1 to D6.

- *Rut depth* (RD) for each pavement, and for a particular transverse profile (west, middle and east), was computed as the difference between the elevation of the highest and lowest points on that profile. Rut-depth data are reported in Tables D7 to D12. The initial value for the rut depth is not zero, since right after construction the pavement surface was not perfectly flat.

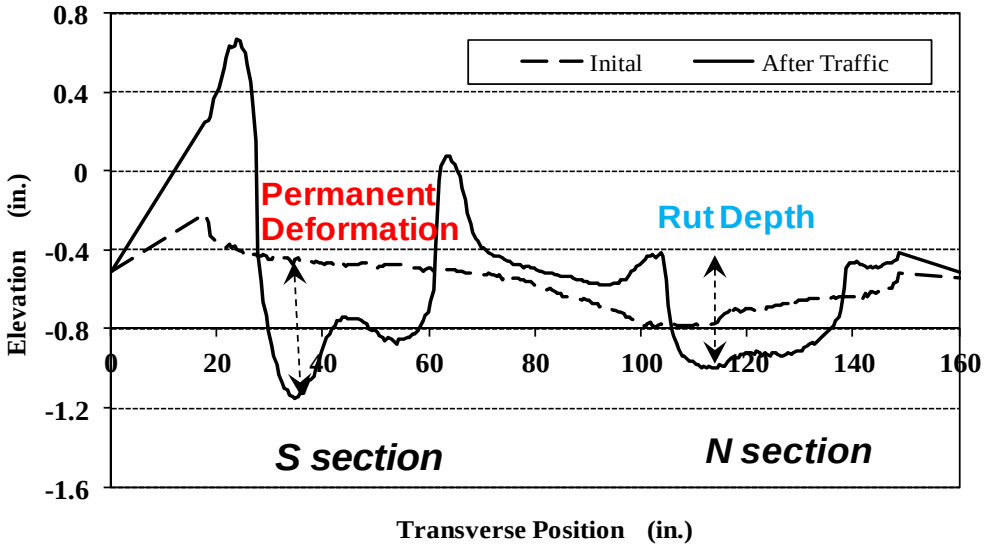

FIGURE 5.1: Example of Transverse Profile

The evolution of permanent deformation with the number of ATL load-assembly passes is plotted in Figures 5.2 through 5.4, while the evolution of rut depth with the number of applied APT load-assembly passes is plotted in Figures 5.5 to 5.7. The figures indicate the highest rut depths and permanent deformations values were recorded for the Iowa (IA) pavement sections that had binder content higher than the design values; the high binder content caused fast rutting failure of both rutting and fatigue cracking sections (Figures 5.4 and 5.7). As expected, KS1 mix (19mm NMAS) had a slightly lower rut depth and permanent deformation than KS2 mix (12.5mm NMAS). MO1 mix (30M design ESALS) had a better rutting resistance than MO2 mix (3M design ESALS). The rutting and permanent deformation of the KS and MO fatigue-cracking sections increased only during the first 200,000 passes; after that they remained relatively constant.

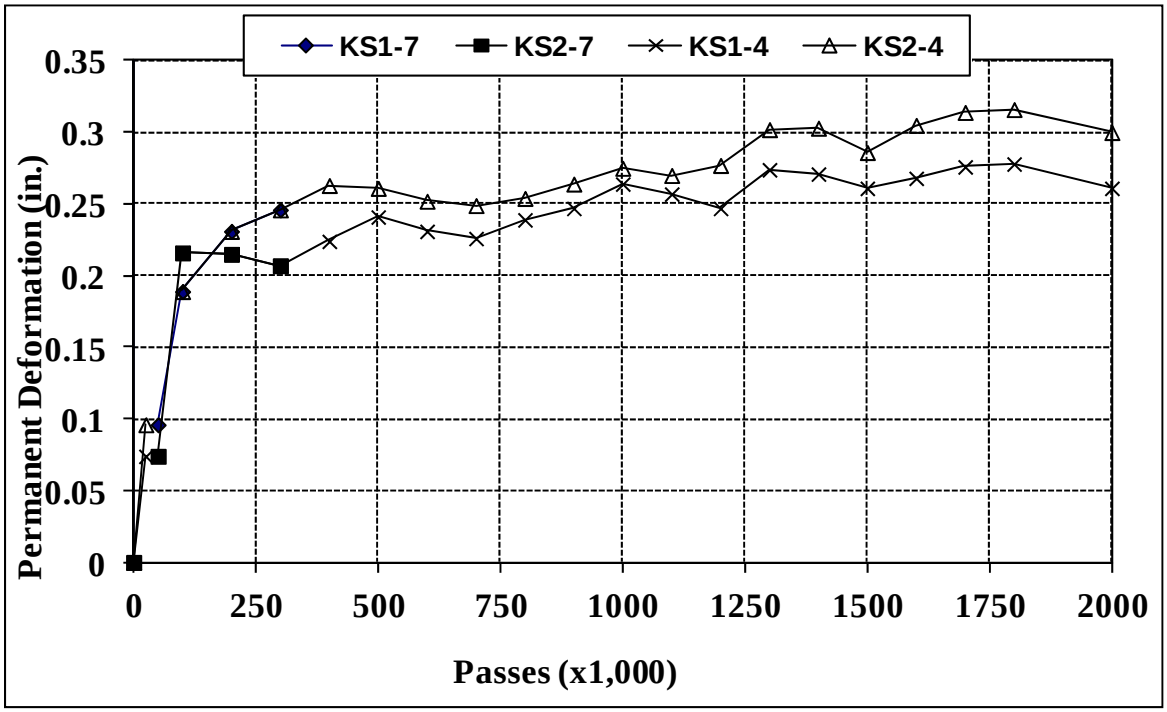

FIGURE 5.2: Evolution of Permanent Deformation for Kansas Sections

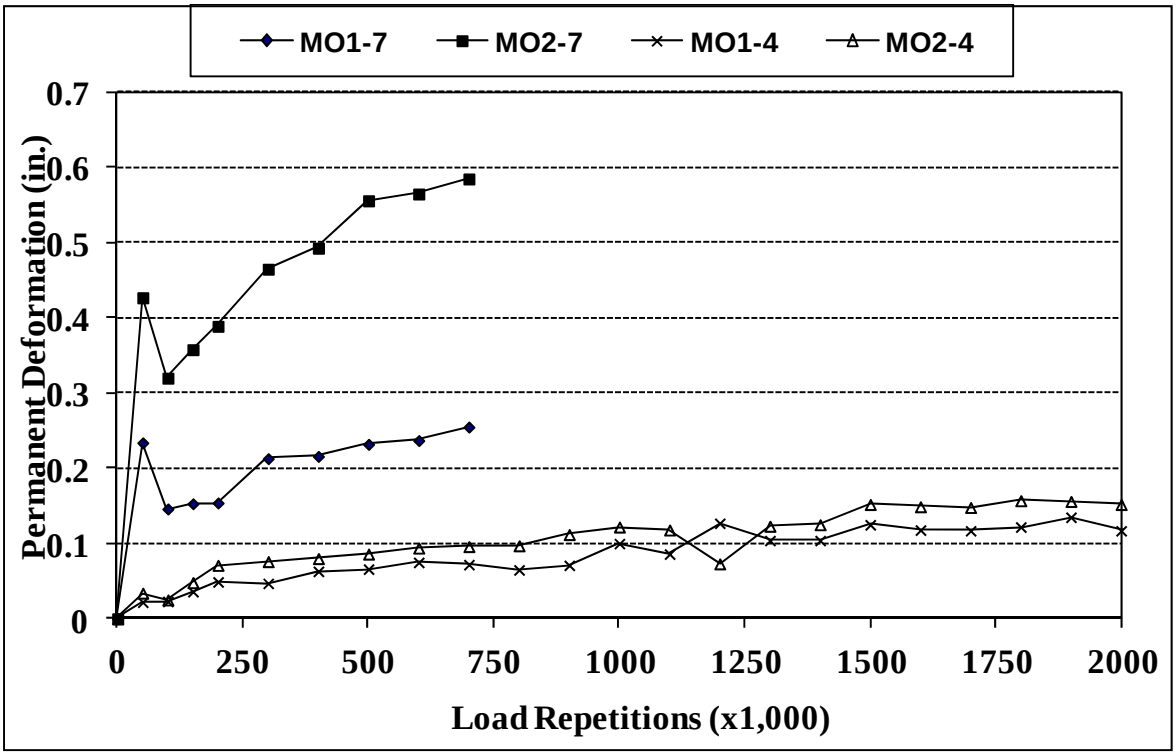

FIGURE 5.3: Evolution of Permanent Deformation for Missouri Sections

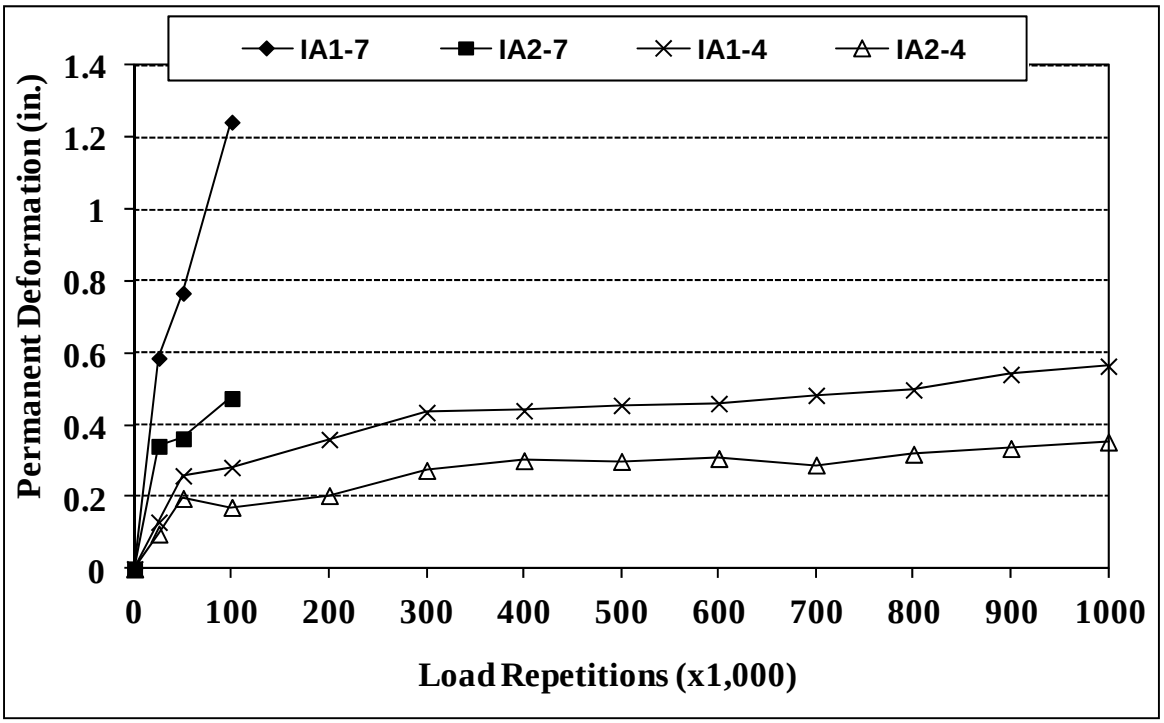

FIGURE 5.4: Evolution of Permanent Deformation for Iowa Sections

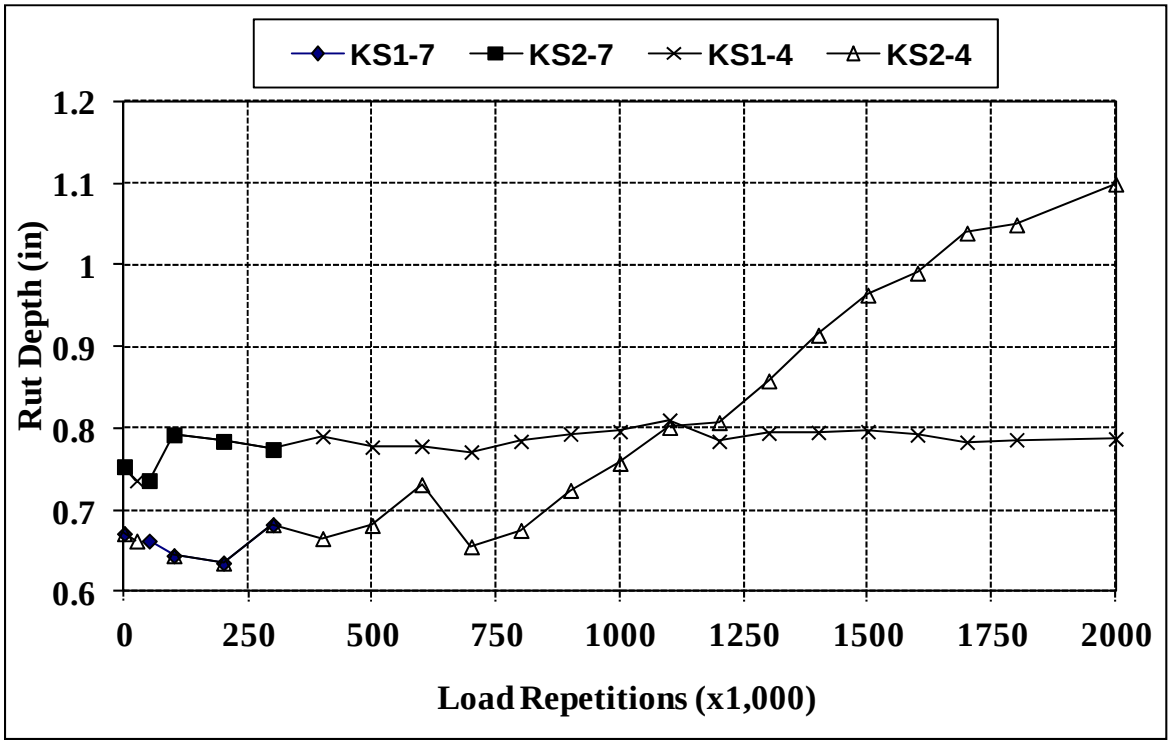

FIGURE 5.5: Evolution of Rut Depth for Kansas Sections

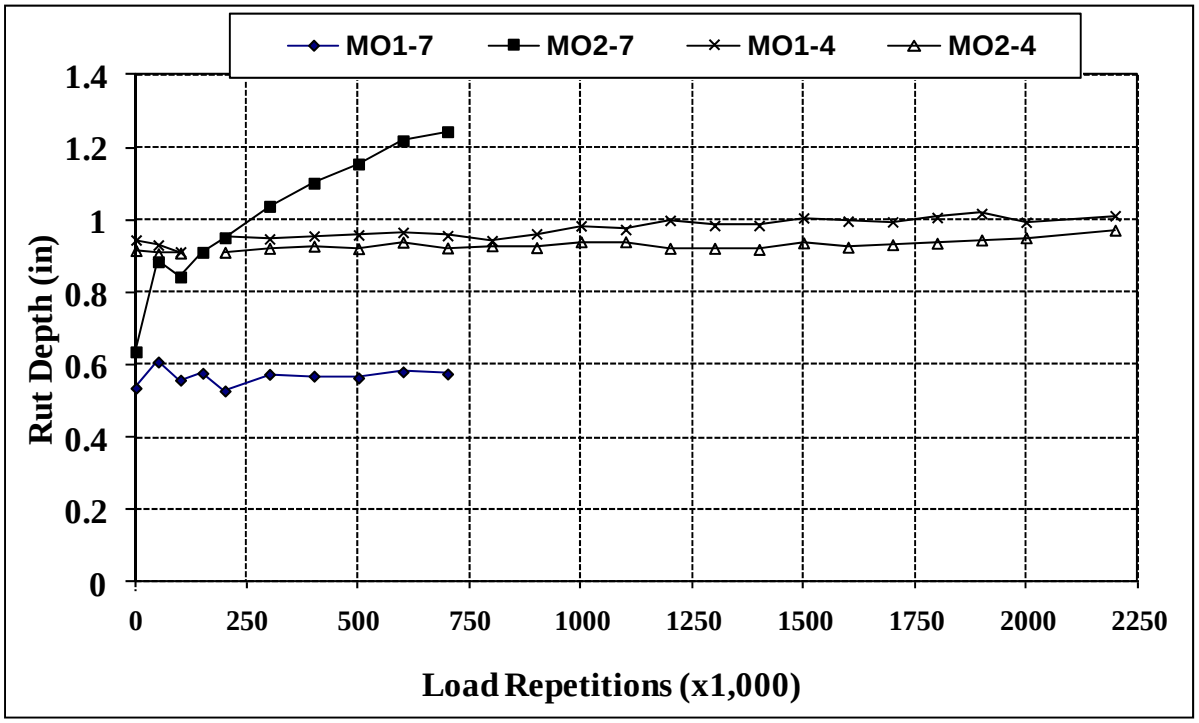

FIGURE 5.6 Evolution of Rut Depth for Missouri Sections

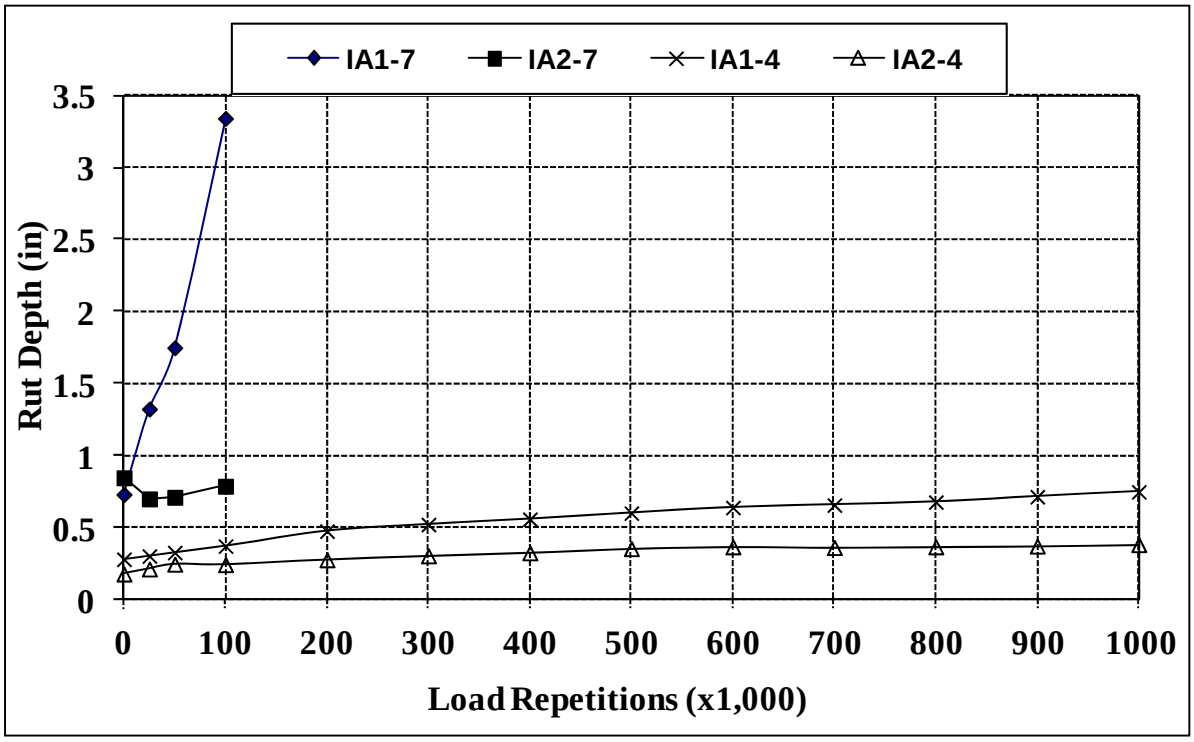

FIGURE 5.7 Evolution of Rut Depth for Iowa Sections

5.2 Longitudinal Profiles

The longitudinal profile of a pavement section was recorded by measuring the elevation of 19 points spaced at one-foot intervals on the outside wheel path with surveying equipment. The points were numbered from east to west, with the first point being at one foot west of the east wall of the pit. A fixed point at the base of a steel pole near the East entrance of the CISL was used as the reference. The longitudinal profile data is reported in Appendix E.

Roughness of the longitudinal profile was estimated from the elevation data, with the slope variance (SV) as the roughness statistic. SV was selected for this project because of its simplicity. Other indexes that are computed based on elevation data require a minimum length of pavement section. For example, to compute the International Roughness Index (IRI), the road section must be at least 33 feet (11 meters) long. The slope variance (SV) is computed as:

$$SV = [SUM (S_i - S_{avg})^2] / (N-1) \qquad \text{(EQUATION 5.1)}$$

Where:

N = number of segments where the slope is computed (N=18 for the CISL sections);

$S_i = 100*(h_{i+1} - h_i) / d$ - slope in point i, in percents;

h = elevation (in); and

d =spacing between points (d = 12 in).

It is important to note that the roughness statistic derived from the longitudinal profile is not a good indicator of pavement performance for the 20-ft-long pavement sections subjected to full-scale accelerated testing at the CISL, and it does not correlate well with the roughness of in-service pavements. The main reason is that the variability of material properties and layer thicknesses are different for such a short section than for an in-service pavement. Also, environmental factors that affect pavement performance are fully controlled in the CISL.

However, slope variance was computed here only to compare its evolution for the 12 pavement structures under study. Data for the longitudinal profile and slope variance values are given in Appendix E.

Figures 5.8 and 5.9 illustrate the evolution of slope variance and clearly indicate that SV values did not change with the number of accumulated APT load-assembly passes. This is probably due to the fact that the load applied by the APT machine is controlled to remain constant. The figures also indicate that the as-constructed roughness was better for the rutting sections than for the fatigue sections, which have thinner asphalt concrete layers.

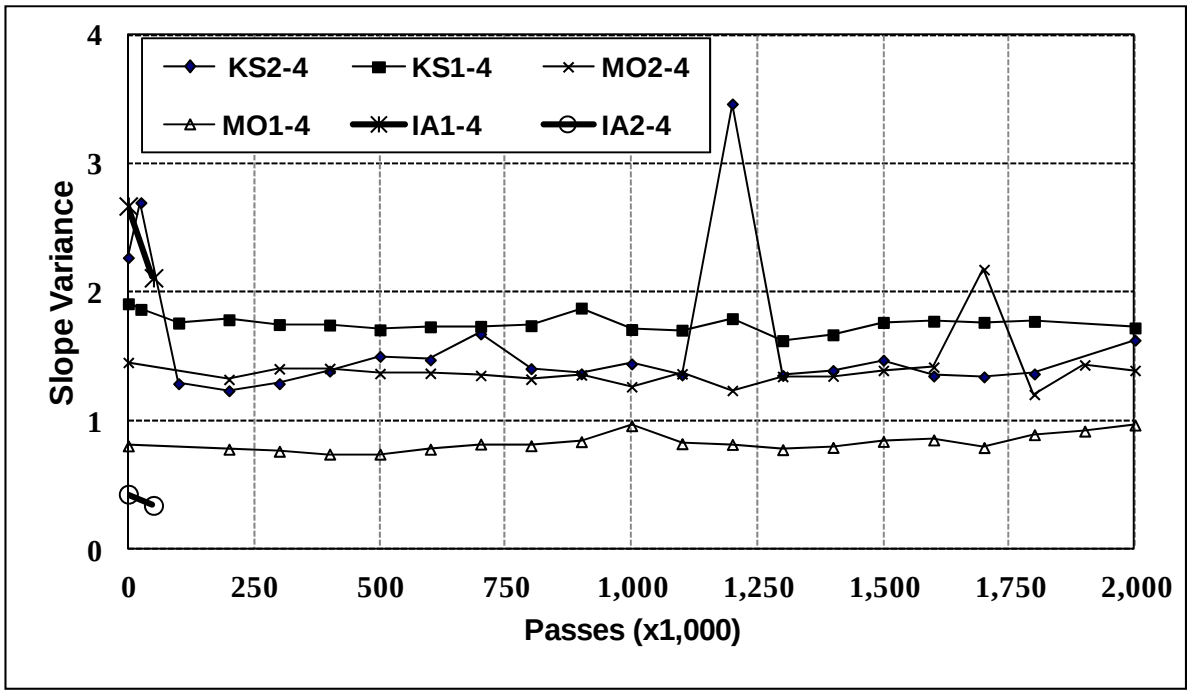

FIGURE 5.8: Evolution of Roughness for the Fatigue Cracking Sections

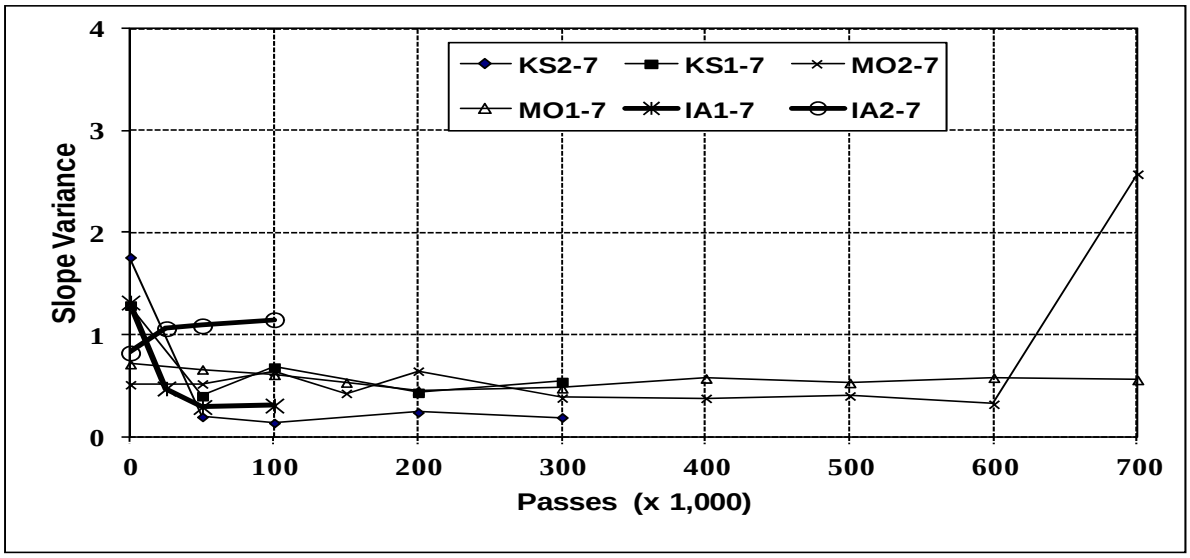

FIGURE 5.9: Evolution of Roughness for Rutting Sections

5.3 Fatigue Cracking

The pavement surface was monitored to observe surface cracking every time the pavement response and surface profile measurements were performed. The only crack observed was for section KS2-4 at 1,300,000 passes of the APT machine; no other cracks were observed in the other 11 sections tested. That crack was in the longitudinal direction, was located very close to the centerline of the section, and had a length of approximately 27 inches, as shown in Figures 5.10 and 5.11. The shaded area in Figure 5.10 represents the trafficked area. The crack grew to approximately 43 inches in the following 100,000 load repetitions, as shown in Figures 5.10 and 5.12. However, the crack was not observed anymore either when the next measurements were performed, at 1,500,000 load repetitions, or after that.

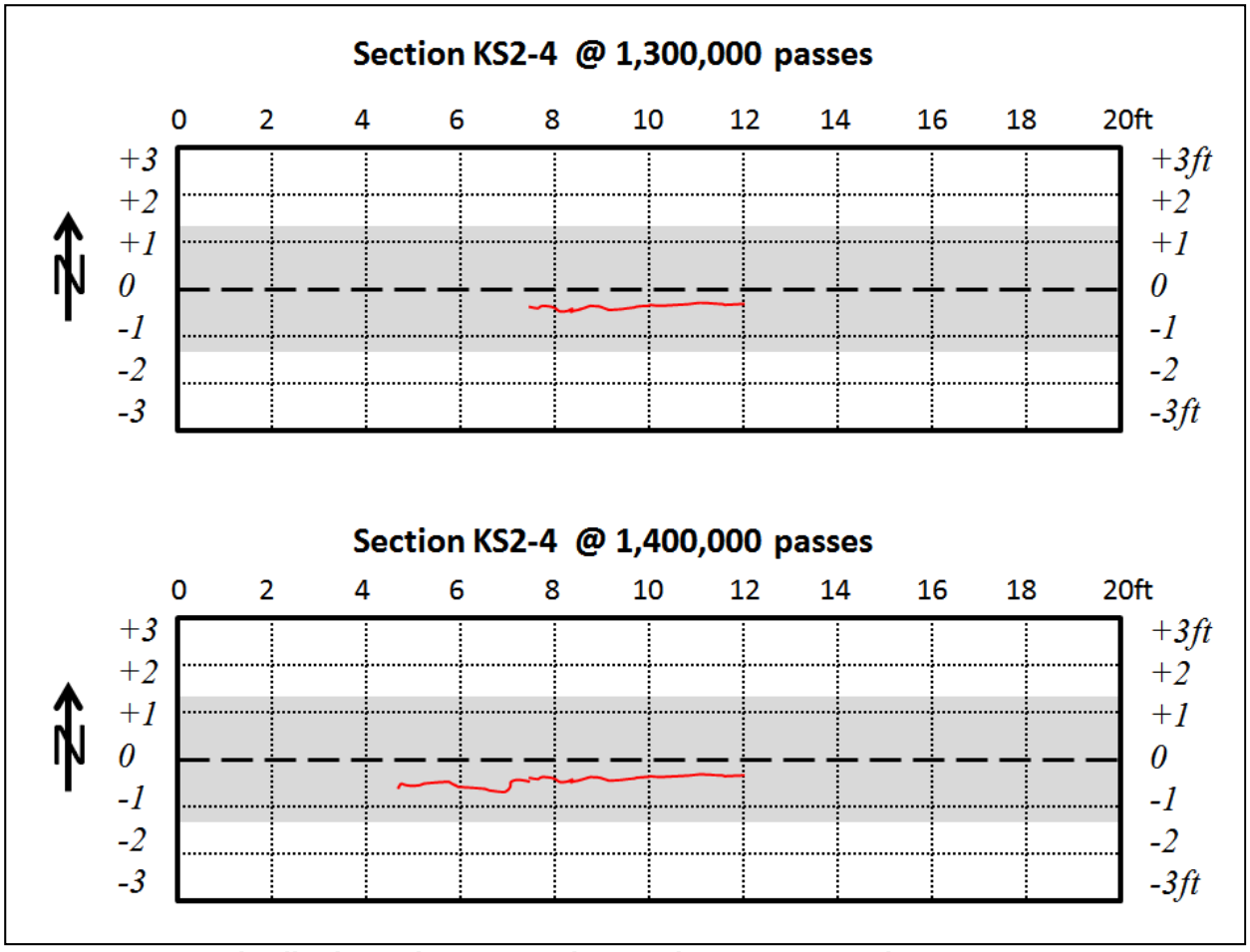

FIGURE 5.10: Longitudinal Crack Pattern Observed on KS2-4 section

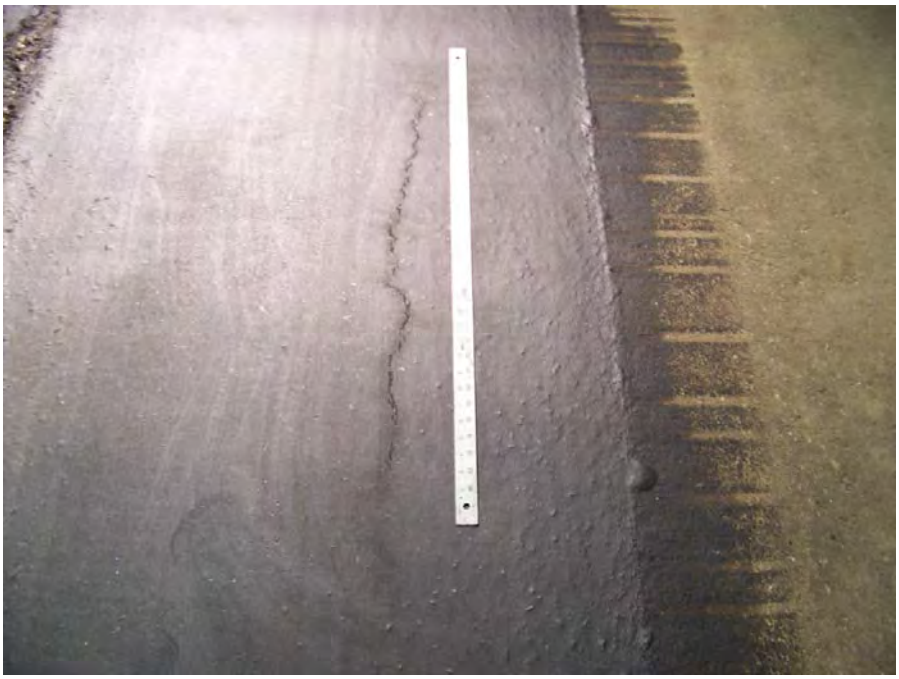

FIGURE 5.11: Longitudinal Crack on KS2-4 section at 1,300,000 Load Cycles

FIGURE 5.12: Longitudinal Crack on KS2-4 Section at 1,400,000 Load Cycles

5.4 Horizontal Strains at the Bottom of the Asphalt Concrete Layer

Strain and pressure values were recorded for at least four cycles (eight passes) of the CISL APT machine, at a sampling frequency of 100Hz. Recording was started when the axle was at the west end of the travel and had started traveling east. Strain measurements were performed for two lateral positions of the wheels:

i. Position 0" – The symmetry axis of the wheel was placed above the gages. In this position, the tires were straddling the gages, as shown in Figure 5.13.
ii. Position +6" - With one tire passing right above the strain gages, the symmetry axis of the wheel was 6 inches away, transversely from the gages (Figure 5.13).

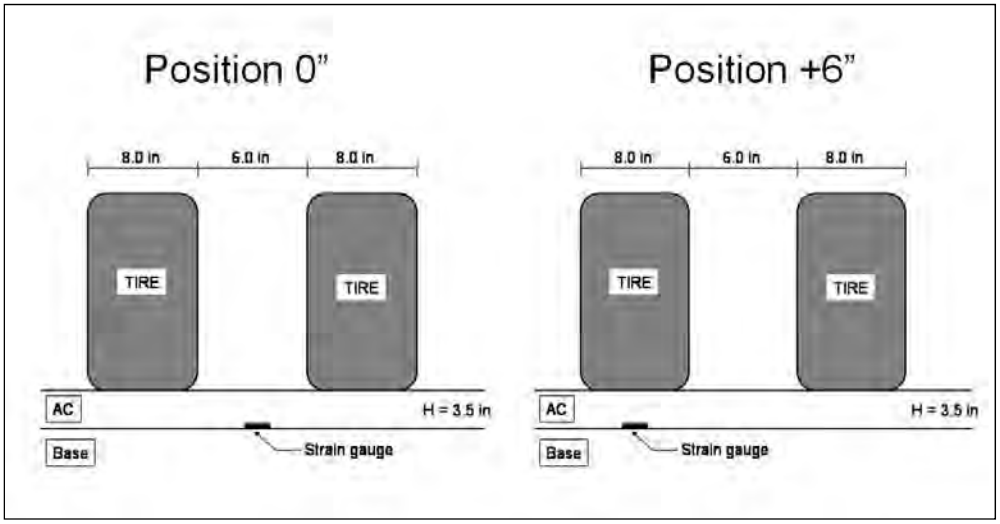

FIGURE 5.13: Position of the Wheel During Strain Measurements

The stress and strain data were stored in the same electronic file, in a spreadsheet format, along with the longitudinal position of the loading bogie. Figure 5.14 presents the six typical shapes of the strain signal that were observed for one pass (from the time the load assembly leaves one end of the travel until it arrives at the other end). Values A, B, and C recorded on the strain signals are given in Appendix F. Response values recorded for the gages that failed during asphalt layer paving due to high temperature of the asphalt mix, or erroneous values, were not included in the tables. No strain, stress, or displacement measurements were made for the IA1-4 and IA2-4 sections after the first 100,000 load applications, even though these sections were loaded up to 2,000,000 load applications.

From the recorded strain signals, two typical signal shape types were identified. Typical strain signal Type 1 was observed for the longitudinal strain, while typical strain signal Type 2 was observed for the transverse strain. For both cases, the strain values (S) were computed with the following formulas:

$$S = (A+C)/2 - B \qquad \text{(Equation 5.2)}$$

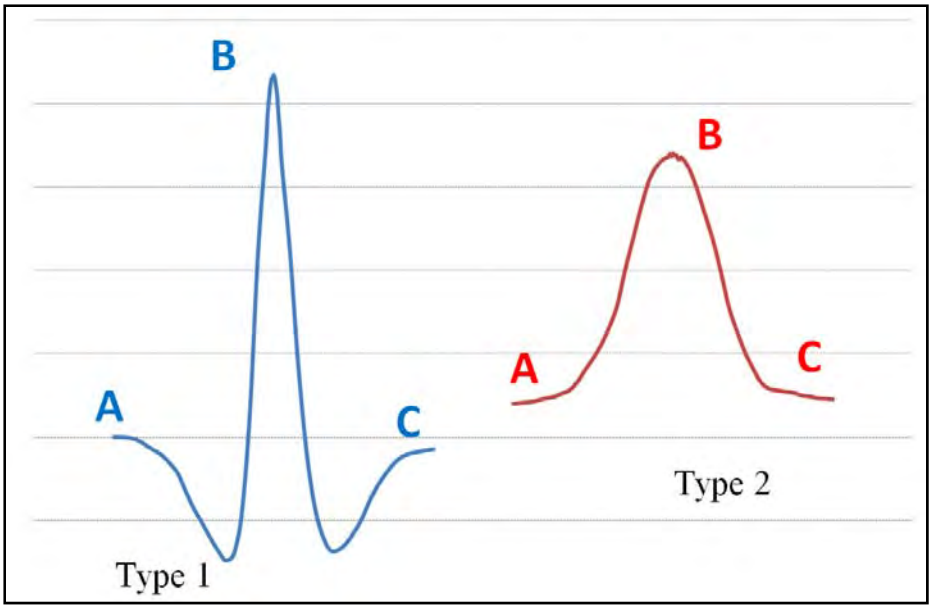

FIGURE 5.14: Types of Strain Signal Shapes

The values of measured horizontal strains at the bottom of the asphalt concrete layer obtained from typical signals are given in Appendix F. For measuring Position 0 only, Tables 5.1 to 5.4 summarize the values of the measured strains, while Figures 5.15 to 5.18 show the evolution of the measured strains with the number of applied passes.

TABLE 5.1: Longitudinal Strains for Rutting Sections (7-Inch HMA)

Passes (x1,000)	KS1-7 East	KS1-7 West	KS2-7 East	MO1-7 East	MO1-7 West	MO2-7 East	IA1-7 East	IA2-7 East
0	157.81	162.14	179.45	273.53	292.18	343.97	384.96	357.11
50	282.96	264.76	335.2	347.4	368.37	463.53		434.04
100		299.5	385.42	498.76		608.56		371.93
150				416.62		563.2		
200		345.47	401.87	451.95		583.21		
300		368.26	391.04	460.9		521.2		
400				478.55		576.25		
500				431.69	524.69	581.87		
600				363.09		520.75		
700				408.12		564.64		

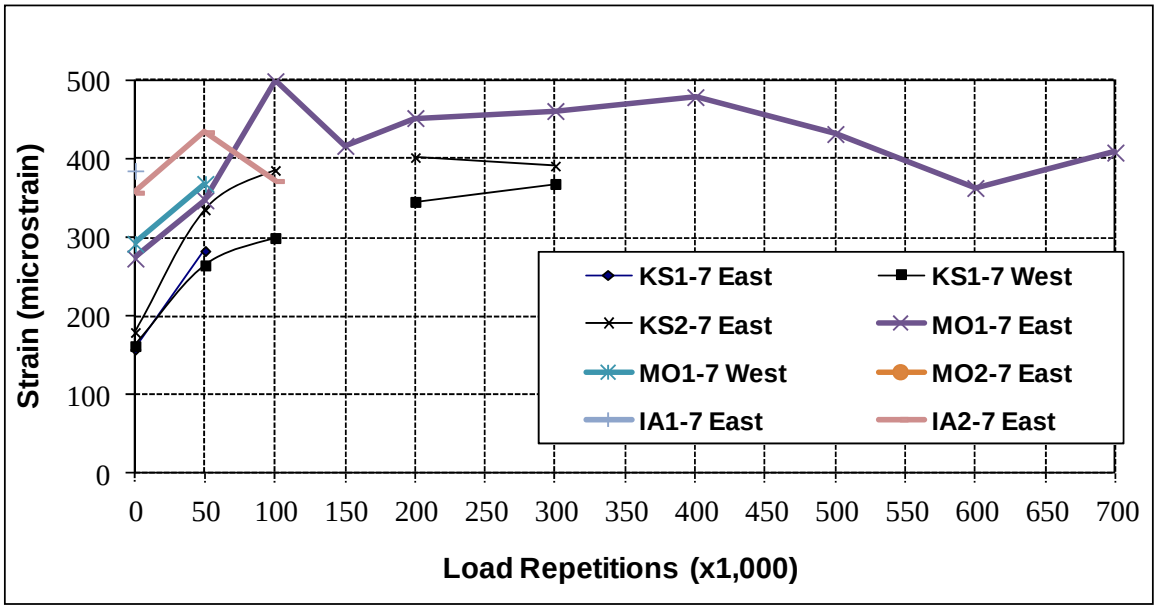

FIGURE 5.15: Longitudinal Strains for Rutting Sections (7-Inch HMA)

TABLE 5.2 Longitudinal Strains for Fatigue Cracking Sections (4-Inch HMA)

Passes (x1,000)	KS1-4 East	KS1-4 West	KS2-4 West	MO1-4 West	MO2-4 East	MO2-4 West	IA1-4 East	IA2-4 West	IA2-4 East
0	4956.22	4122.91	6622.01	296.44	213.84	235.69	306.24	437.66	258.78
25	195.34	252.06	377.12						304.39
50				266.7	201.27	216.19			243.43
70	253.92	300.57	489.08						
100	267.49	323.92	484.14	324.61	293.74	397.01			283.27
150	256.7	350.81	552.76	268.41	224.45	242.9			
200	290.93	369.82		264.55	249.57	185.65			
300	306.45	371.5		265.08	269.14	182.55			
400	301.11	372.15		270.38	279.73	188.63			
500	296.85	346.27		274.12	282.77				
600	304.95	369.44		243.91	279.6				
700	283.58	343.21		249.66	283.15				
800	310.45	366.06		253.35	289.97				
900	317.09	367.05		273.07	285.71				
1,000	338.85			249.84	269.22				
1,100	370.76			228.08	284.32				
1,200	379.87			226.03	268.84				
1,300	371.14			238.88	265.54				
1,400	371.05			253.51	286.4				
1,500	350.98			227.36	273.86				
1,600	375.63			227.36	293.35				
1,700	413.47			286.24					
1,800	408.65			203.21	286.54				
2,000	376.09			262.96	318.28				
2,100				155.03	273.06				

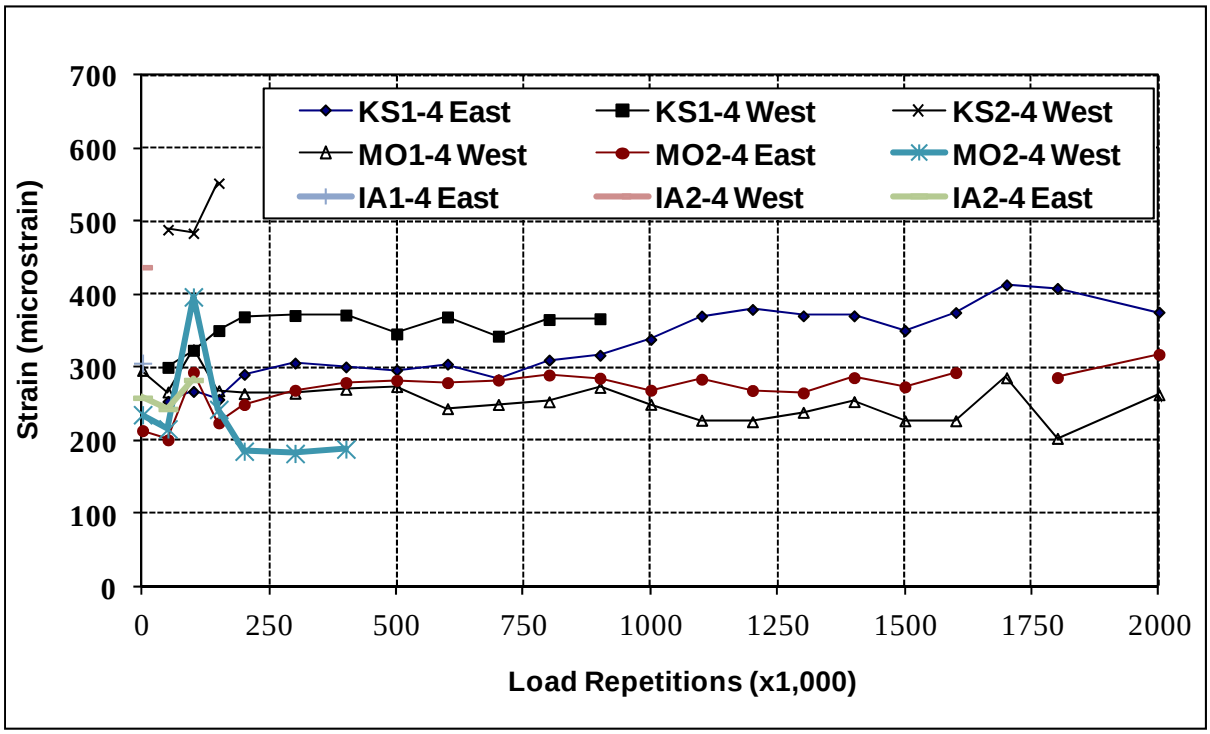

FIGURE 5.16 Longitudinal Strains for the Fatigue-Cracking Sections (4-Inch HMA)

TABLE 5.3 Transverse Strains for Rutting Sections (7-Inch HMA)

Passes (x1,000)	KS1-7 East	KS2-7 East	KS2-7 West	MO1-7 West	MO2-7 East	MO2-7 West	IA1-7 West	IA2-7 East	IA2-7 West
0	50.15	64.86	193.43	134.77	113.12	95.04	145.53	170.18	156.2
50	72.98	115.16	305.73	162.19		127.88	154.23	217.28	191.07
100	84.46	138.28	327.07	269.72		246.66	158.99	205.09	187.15
150				247.12	317.23	201.15			
200	100.99	147.8		213.07	421.76	178.27			
300	100.38	144		224.55		762.52			
400				254.36		244.89			
500				205.35	178.39	198.08			
600				178.97	189.56	155.57			
700				169.01	202.83	151.96			

TABLE 5.4 Transverse Strains for Fatigue-Cracking Sections (4-Inch HMA)

Passes (x1,000)	KS2-4 East	KS2-4 West	KS1-4 East	KS1-4 West	MO1-4 East	MO1-4 West	MO2-4 East	MO2-4 West	IA1-4 East	IA1-4 West	IA2-4 East	IA2-4 West
0	5,252	5,003	48.87	5,371	74.5	87.4	56.69	64.46	106.5	102.0	91.4	90.4
25	63.46	800.36	48.27	52.38					114.3	154.6	117.1	124.4
70	72.71	875.73	63.37	61.27	65.91	82.75	58.55	77.61	106.5	112.2	97.6	93.8
100	66.65	738.9	81.92	56.71					117.1	126.5	105.5	104.1
150			85.49	89.38								
200			83.68	99.74	68.49	91.83	62.5	87.71				
250			91.80	95.35								
300			84.16	103.56	79.21	101.58	69.21	95.32				
350			81.06	92.24								
400			80.78	89.13	83.36	102.28	75.89	99.86				
450			80.89									
500			73.02		82.52	102.89	78.33	104.9				
600			80.51		87	108.88	81.13	128.99				
700			68.88		79.23	97.04	73.78	107.55				
800			77.10		81.17	100.32	76.86	110.17				
900			75.62		77.84	103.28	74.99	109.22				
1,000			73.27		81.5	113.81	80.14	115.37				
1,100			87.54		83.16	118.62	84.77	138.14				
1,200			207.39		87.11	116.89	86.28	136.32				
1,300			85.71		88.79	134.73	91.65	134.5				
1,400			84.94		89.09	148.85	93.5	146.2				
1,500			79.85		92.9	145.72	95.22	139.07				
1,600			86.33		94.95	163	94.65	136.74				
1,700			189.63									
1,800			154.93		143.97	212.66		319.86				
1,900					106.4	172.11	102.98	131.39				
2,000					109.14	122.58	86.24	127.75				
2,100					160.39	247.29	114.13	145.95				

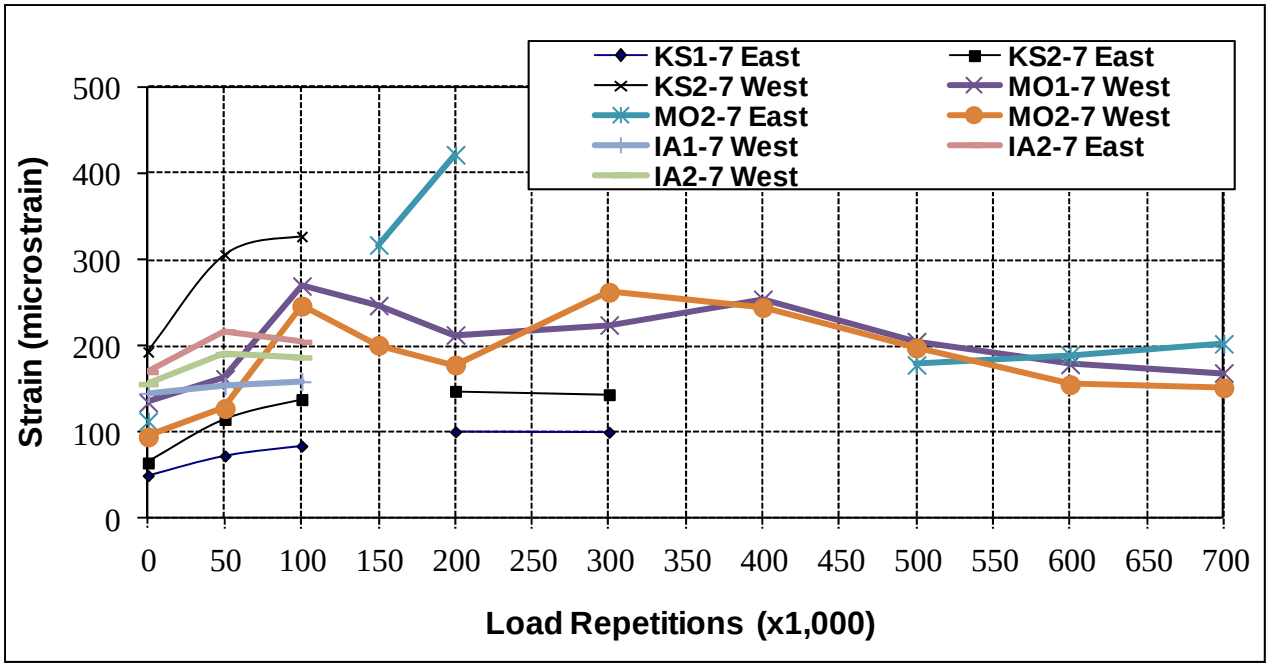

FIGURE 5.17 Transverse Strains for Rutting Sections

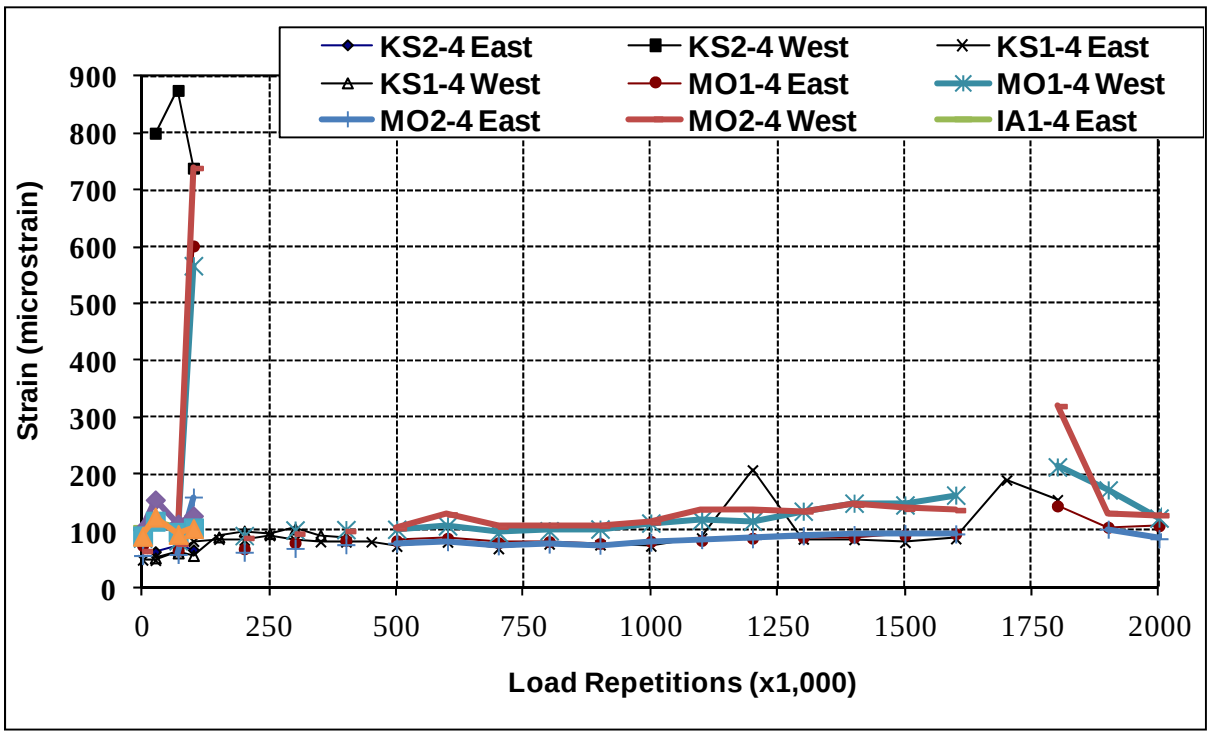

FIGURE 5.18 Transverse Strains for Fatigue Cracking Sections

A few observations can be made regarding the measured horizontal strains at the bottom of the asphalt layer:

- The measured longitudinal strains are almost always larger than the corresponding transverse strains.
- In the Kansas fatigue-cracking sections, the longitudinal strains recorded before loading commenced were very high. However, once loading commenced, the recorded strains were comparable to but remained higher than those recorded for the other fatigue-cracking sections.
- Differences between corresponding strains measured by replicate gages (east and west) installed in the same test sections can be significant, in many cases larger that the difference between corresponding strains measured on two sections with mixes from the same state. This can be justified by differences in layer thickness and material density at those two locations. However, in most cases, trends in the strains measured by the replicate sensors are similar.
- In general, when two mixes of the same state are compared, the ranking of the corresponding measured strains matches the expected ranking. Strains measured on the KS1, MO1, and IA1 sections are smaller than those measured on the KS2, MO2, and IA2 sections.
- For most cases, strains measured after the first 200,000 load repetitions seem to remain stable, exhibiting only small fluctuations after that.

5.5. Vertical Stresses at the Top of the Subgrade

Vertical compressive stresses at the top of the subgrade were measured for each pavement structure at two spatial locations (west and east) as shown in Figure 2.15. The stress measurements were performed at the same time with the strain measurements, on the dates indicated in the pavement monitoring plan given in Appendix C. In total, only eight out of 12 stress cells provided usable data; the cables connecting the remaining four stress cells were damaged during asphalt layer paving.

The measured compressive stresses are reported in Appendix G. The stress values measured by the two pressure cells for position “0” in the same lane are summarized in Table 5.5 and have been plotted in Figures 5.19 and 5.20. The data in Appendix G indicate the compressive stresses at the top

of the subgrade measured underneath a tire (wheel in position +6”) are always lower than the stresses recorded measured when the wheel straddles the gages (wheel in position “0”).

Figures 5.19 and 5.20 indicate the lowest vertical compressive stresses at the top of the subgrade were recorded for the MO sections, while the highest readings were obtained for the KS sections. However, the high difference between the stresses recorded for the corresponding KS and MO sections cannot be solely explained by the difference in asphalt mix properties. It is likely that the cells installed in the MO sections were not properly covered with wet sand during installation. This typically results in lower stress readings.

TABLE 5.5 Maximum Vertical Stresses on Top of Subgrade for Rutting Sections (psi)

Passes (x1,000)	KS1-7 East	KS1-7 West	KS2-7 East	KS2-7 West	MO1-7 East	MO2-7 West	IA1-7 East	IA2-7 West
0	-5.86		-5.89		-1.782	-1.395	-9.72	-6.75
50	-6.98		-6.82		-1.657	-1.633	-10.53	-5.7
100	-8.14		-7.76		-1.73	-1.866	-12.2	-12.88
150					-1.79	-1.925		
200	-9.74	-12.8	-13.63	-13.32	-2.108	-2.223		
300	-11.1	-13.46	-14.09	-13.29	-1.996	-2.199		
400					-2.16	-2.429		
500					-2.799	-2.695		
600					-2.576	-2.401		
700					-2.093	-2.505		

TABLE 5.6: Maximum Vertical Stresses on Top of Subgrade for Fatigue-Cracking Sections

Passes (x1,000)	KS1-4 East	KS1-4 West	KS2-4 East	KS2-4 West	MO1-4 West	MO2-4 West	IA1-4 West	IA2-4 East
0	-10.37	-10.05	-11.18	-10.31	-12.2	-9.1	-8.36	-6.23
25	-3.47	-6.57	-9.51	-8.44			-5.53	-1.7
50					-2.67	-0.89	-5.49	-2.26
70	-4.43	-9.11	-10.05	-10.14				
100	-5.16	-9.6	-10.91	-9.65	-3.36	-2.2	-5.89	-1.35
150	-6.47	-15.68	-17.77	-16.01				
200	-6.63	-17.51	-19.52	-17.75	-5.44	-2.19		
250	-6.71	-16.2	-19.2	-17.7				
300	-6.58	-15.68	-17.96	-16.98	-6.1	-2.96		
350	-7.05	-16.21	-17.72	-17.29				
400	-6.57	-16.02	-17.84	-16.73	-6.81	-3.48		
450	-6.84	-16.5	-18.02	-17.76				
500	-4.91	-15.71	-17.98	-15.62	-7.53	-3.76		
600	-7.05	-17.08	-18.51	-17.97	-7.96	-3.99		
700	-6.19	-15.94	-17.11	-15.93	-8.15	-3.73		
800	-7.76	-17.36	-19.14	-18.59	-8.24	-3.63		
900	-7.81	-17.68	-19.41	-18.51	-8.69	-3.79		
1,000	-8.08	-19.34	-21.55	-19.65	-9.17	-4.05		
1,100	-9.59	-20.93	-23.01	-22.71	-9.84	-4.89		
1,200	-9.47	-20.65	-22.64	-21.78	-10.05	-4.93		
1,300	-9.9	-21.44	-23.47	-22.43	-10.9	-5.4		
1,400	-10.06	-21.56	-23.52	-22.42	-11.08	-5.1		
1,500	-9.51	-20.3	-21.75	-20.78	-11.32	-5.02		
1,600	-10.31	-21.54	-22.9	-21.79	-11.86	-5.67		
1,700	-10.35	-22.05	-23	-21.79	-11.86	-5.67		
1,800	-10.45	-22.4	-23.98	-22.64	-12.46	-10.55		
1,900					-12.99	-6.47		
2,000	-10.02	-20.99	-22.74	-21.32	-15.68	-23.38		
2,100					-12.35	-7.22		

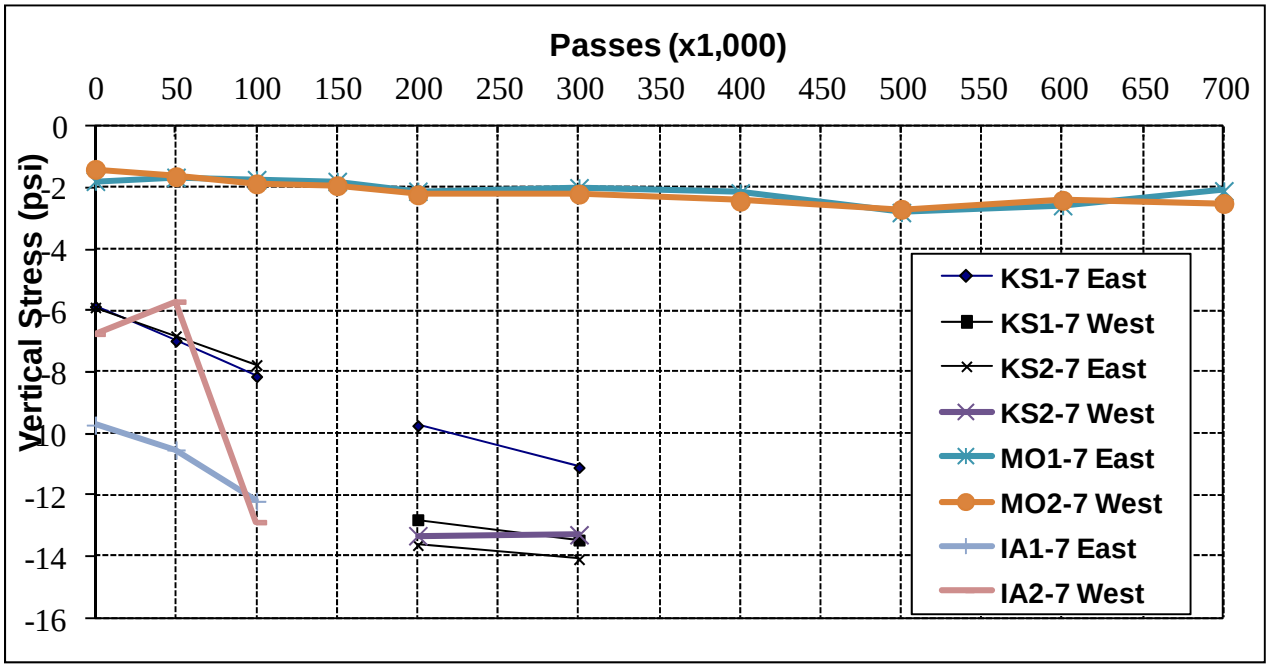

FIGURE 5.19: Maximum Vertical Stresses on Top of Subgrade for Rutting Sections

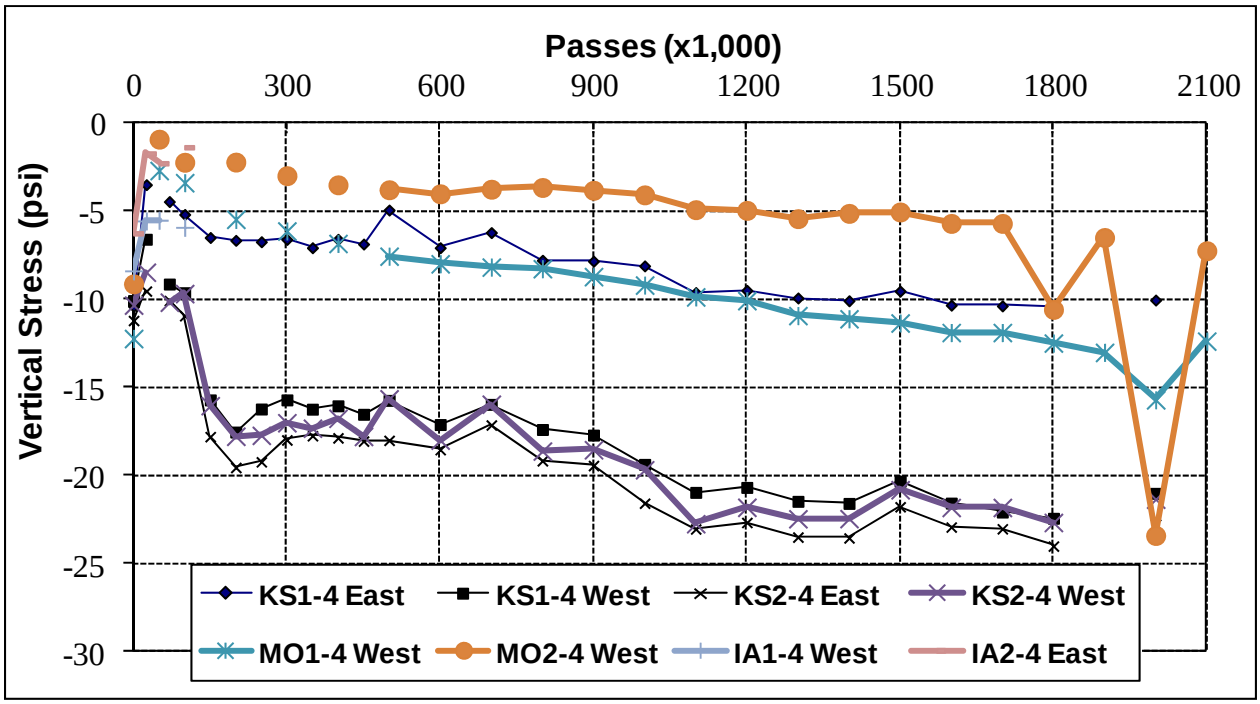

FIGURE 5.20: Maximum Vertical Stresses on Top of Subgrade for Fatigue-Cracking Sections

5.6 Dynamic and Permanent Deformation in Each Pavement Layer

The dynamic and permanent deformation in each pavement layer was measured with single-layer deflectometers (SLD) at the same time as the strain and stress measurements. The description of these sensors is given in Section 2.6.2.1. The dynamic and permanent deformation data are given in Appendix H, while a summary of the data is given in Tables 5.7 through 5.12.

TABLE 5.7 Permanent Deformations for Kansas Sections (microns)

Date	Passes (x1,000)	KS2-7				KS1-7			
		HMA	Base	Subgrade	Total	HMA	Base	Subgrade	Total
5/5/2006	0	0	*0*	0	**0**	0	*0*	0	**0**
5/24/2006	50	13.43	*24.34*	*99.18*	**136.95**	10.24	*-0.24*	*20.54*	**30.54**
5/31/2006	100	7.3	*35.35*	*170.16*	**212.81**	13.59	*-1.1*	*43.12*	**55.61**
6/8/2006	200	20.22	*43.78*	*183.29*	**247.29**	16.29	*-1.96*	*52.1*	**66.43**
6/19/2006	300	-16.37	*44.98*	*158.47*	**187.08**	15.9	*-0.86*	*57.77*	**72.81**
Date	**Passes (x1,000)**	**KS2-4**				**KS1-4**			
		HMA	**Base**	**Subgrade**	**Total**	**HMA**	**Base**	**Subgrade**	**Total**
3/13/2006	0	*0*	*0*	*0*	**0**	*0*	*0*	*0*	**0**
3/31/2006	25	*1.93*	*5.42*	*29.34*	**36.69**	*0.61*	*-0.07*	*8.93*	**9.47**
4/20/2006	70	*17.74*	*34.88*	*120.87*	**173.49**	*44.38*	*-1.96*	*15.03*	**57.45**
4/28/2008	100	*8.92*	*26.54*	*143.79*	**179.25**	*4.15*	*-1.06*	*5.44*	**8.53**
9/12/2006	100'	*15.87*	*33.56*	*45.05*	**94.48**	*0.28*	*20.06*	*22.27*	**42.61**
9/15/2006	150	*29.67*	*50.52*	*191.41*	**271.6**	*-65.58*	*96.49*	*28.54*	**59.45**
10/5/2006	200	*45.99*	*66.77*	*199.42*	**312.18**	*-195.15*	*147.28*	*39.33*	**-8.54**
10/10/2006	250	*50.01*	*58.62*	*189.12*	**297.75**	*-69.48*	*152.79*	*40.43*	**123.74**
10/18/2006	300	*47.33*	*62.08*	*144.24*	**253.65**	*-140.26*	*129.4*	*36.79*	**25.93**
10/23/2006	350	*47.32*	*62.41*	*163.01*	**272.74**	*-134.55*	*128.9*	*33.54*	**27.89**
10/30/2006	400	*52.51*	*62.11*	*138.08*	**252.7**	*-110.67*	*119.85*	*34.02*	**43.2**
11/3/2006	450	*54.93*	*62.35*	*169.44*	**286.72**	*-54.07*	*138.55*	*34.77*	**119.25**
12/5/2006	500	*55.34*	*59.36*	*172.8*	**287.5**	*-42.48*	*49.99*	*34.32*	**41.83**
12/13/2006	600	*63.9*	*64.62*	*148.15*	**276.67**	*10.15*	*109.77*	*33.51*	**153.43**
1/12/2007	700	*57.13*	*60.05*	*81.6*	**198.78**	*7.56*	*31.63*	*24.36*	**63.55**
1/19/2007	800	*69.94*	*69.62*	*169.22*	**308.78**	*7.3*	*126.72*	*36.7*	**170.72**
1/26/2007	900	*75.09*	*68.95*	*157.23*	**301.27**	*6.65*	*135.51*	*35.49*	**177.65**
2/15/2007	1,000	*82.46*	*85.48*	*155.24*	**323.18**	*-1.64*	*141.68*	*48.48*	**188.52**
2/22/2007	1,100	*94.72*	*101.48*	*265.35*	**461.55**	*-4.07*	*234.97*	*56.84*	**287.74**
3/1/2007	1,200	*89.72*	*98.86*	*251.71*	**440.29**	*-4.03*	*199.49*	*55.86*	**251.32**
3/8/2007	1,300	*100.43*	*101.4*	*271.91*	**473.74**	*-4.03*	*232.29*	*60.05*	**288.31**
3/15/2007	1,400	*100.25*	*104.46*	*280*	**484.71**	*0.31*	*241.09*	*58.32*	**299.72**
3/26/2007	1,500	*91.25*	*100.18*	*216.75*	**408.18**	*-5.49*	*183.34*	*48.88*	**226.73**
4/2/2007	1,600	*96.46*	*105.13*	*272.85*	**474.44**	*25.3*	*226.2*	*57.33*	**308.83**
4/9/2007	1,700	*93.05*	*116.2*	*280.9*	**490.15**	*-3.51*	*228.77*	*57.26*	**282.52**
4/16/2007	1,800	*102.59*	*120.68*	*279.01*	**502.28**	*-3.65*	*244.49*	*65.66*	**306.5**
5/3/2007	2,000	*105.91*	*110.84*	*258.3*	**475.05**	*-3.19*	*247.53*	*64.69*	**309.03**

Note: The shaded cells indicate data that is probably erroneous

TABLE 5.8 Permanent Deformations for Missouri Sections (micronss)

Date	Passes (x1,000)	MO2-7				MO1-7			
		HMA	Base	Subgrade	Total	HMA	Base	Subgrade	Total
6/20/2007	0		*0*	*0*		*0*	*0*		
7/12/2007	50		*6.75*	*-11.31*		*41.1*	*-12.55*		
7/16/2007	100		*1.34*	*-13.13*		*86.98*	*25.47*		
7/20/2007	150		*1.94*	*-18.93*		*96.38*	*19.8*		
7/24/2007	200		*2.32*	*-14*		*100.98*	*13.7*		
7/31/2007	300		*2.75*	*-23.13*		*118.52*	*2.25*		
8/10/2007	400		*1.23*	*-22.68*		*125.37*	*-16.64*		
8/21/2007	500		*3.16*	*-25.09*		*94.83*	*-13.51*		
9/4/2007	600		*8.07*	*-24.28*		*-0.18*	*1.14*		
9/14/2007	700		*6.66*	*-27.53*		*32.09*	*-32.99*		
Date	**Passes (x1,000)**	**MO2-4**				**MO1-4**			
		HMA	**Base**	**Subgrade**	**Total**	**HMA**	**Base**	**Subgrade**	**Total**
10/22/2007	0	*0*	*0*	*0*	**0**	*0*	*0*	*0*	**0**
12/17/2007	50	*33.17*	*-2.31*	*0.11*	**30.97**	*10.91*	*-0.03*	*0.11*	**10.99**
1/3/2008	100	*44.87*	*-4.08*	*-2.11*	**38.68**	*79.91*	*-1.33*	*-3.08*	**75.5**
1/14/2008	200	*57.16*	*-3.31*	*0.27*	**54.12**	*75.45*	*0.03*	*0.07*	**75.55**
1/22/2008	300	*70.83*	*-3.27*	*0.02*	**67.58**	*99.92*	*0.8*	*0.11*	**100.83**
1/29/2008	400	*81.13*	*-2.84*	*0.14*	**78.43**	*114.06*	*2.2*	*0.29*	**116.55**
2/5/2008	500	*103.59*	*-3.02*	*0.19*	**100.76**	*128.5*	*2.99*	*0.05*	**131.54**
2/12/2008	600	*120.46*	*-3.16*	*0.02*	**117.32**	*136.29*	*1.96*	*0.03*	**138.28**
2/21/2008	700	*125.44*	*-3.09*	*0.1*	**122.45**	*131.15*	*3.52*	*0.14*	**134.81**
3/3/2008	800	*137.71*	*-2.75*	*0.36*	**135.32**	*140.57*	*3.48*	*0*	**144.05**
3/14/2008	900	*144.82*	*-3.24*	*0*	**141.58**	*148.74*	*4.55*	*0.1*	**153.39**
3/24/2008	1,000	*163.04*	*-3.3*	*0.18*	**159.92**	*147.72*	*3.13*	*-0.04*	**150.81**
3/31/2008	1,100	*163.91*	*-2.97*	*-0.04*	**160.9**	*161.6*	*2.89*	*0.08*	**164.57**
4/8/2008	1,200	*160.65*	*-2.91*	*0.12*	**157.86**	*158.5*	*2.78*	*0.08*	**161.36**
4/15/2008	1,300	*176.42*	*-3.11*	*0.1*	**173.41**	*167.36*	*-3.96*	*0.09*	**163.49**
4/22/2008	1,400	*173.92*	*-3.11*	*0.02*	**170.83**	*175.96*	*-3.67*	*0.17*	**172.46**
5/1/2008	1,500	*182.07*	*-2.17*	*0.15*	**180.05**	*173.94*	*3.16*	*0.25*	**177.35**
5/8/2008	1,600	*184.33*	*-2.94*	*-0.05*	**181.34**	*180.38*	*-3.25*	*0.03*	**177.16**
5/15/2008	1,700								
5/22/2008	1,800	*185.65*	*-4.23*	*-1.64*	**179.78**	*173.48*	*13.1*	*-6.92*	**179.66**
5/29/2008	1,900	*195.48*	*-2.9*	*0.32*	**192.9**	*200.64*	*5.96*	*0.24*	**206.84**
6/5/2008	2,000	*244.7*	*-3.9*	*-2.15*	**238.65**	*243.87*	*20.87*	*-7.13*	**257.61**
9/15/2008	2,000	*158.19*	*-2.06*	*0.14*	**156.27**	*147.55*	*2.78*	*0.47*	**150.8**
10/22/2008	2,100	*204.5*	*-3.13*	*-0.06*	**201.31**	*245.1*	*1.27*	*0.08*	**246.45**

Note: The shaded cells indicate data that is probably erroneous

TABLE 5.9 Permanent Deformations for Iowa Sections (microns)

Date	Passes (x1,000)	IA2-7				IA1-7			
		HMA	Base	Subgrade	Total	HMA	Base	Subgrade	Total
6/10/2008	0	*0*	*0*	*0*	**0**	*0*	*0*	*0*	**0**
6/25/2008	50	*-6.91*	*11.48*	*64.59*	**69.16**	*13.7*	*-6.87*	*107.21*	**114.04**
7/16/2008	100	*-21.08*	*-24.02*	*6.28*	**-38.82**		*-8.38*	*7.064*	
Date	**Passes (x1,000)**	**IA2-4**				**IA1-4**			
		HMA	**Base**	**Subgrade**	**Total**	**HMA**	**Base**	**Subgrade**	**Total**
12/4/2008	0	*0*	*0*	*0*	**0**	*0*	*0*	*0*	**0**
12/5/2008	5	*1.14*	*-0.34*	*23.97*	**24.77**	*4.18*	*36.99*	*18.76*	**59.93**
12/10/2008	30	*-1.44*	*8.5*	*37.31*	**44.37**	*6.12*	*75.3*	*31.05*	**112.47**
12/18/2008	50	*-0.21*	*-9.72*	*0.41*	**-9.52**	*4.16*	*63.47*	*28.43*	**96.06**
1/12/2009	100	*1*	*-6.38*	*12.04*	**6.66**	*12.56*	*70.56*	*33.11*	**116.23**

Note: The shaded cells indicate data that is probably erroneous

TABLE 5.10 Dynamic Deformations for Iowa Sections (microns)

Date	Passes (x1,000)	IA2-7			IA1-7		
		HMA	Base	Subgrade	HMA	Base	Subgrade
6/10/2008	0	-28.95	-46.53	-409.70	-19.55	-17.69	-332.90
6/25/2008	50	-37.21	-70.66	-471.12	-40.85	-18.58	-436.62
7/16/2008	100	-35.89	-46.89	-418.38		-12.49	-405.18
Date	**Passes (x1,000)**	**IA2-4**			**IA1-4**		
		HMA	**Base**	**Subgrade**	**HMA**	**Base**	**Subgrade**
12/4/2008	0	-1.79	-103.45	-290.60	-3.45	-27.35	-296.56
12/5/2008	5	-3.19	-105.13	-309.6	-4.01	-66.76	-314.53
12/10/2008	30	-4.75	-112.94	-324.19	-15.88	-105.56	-326.70
12/18/2008	50	-2.25	-92.84	-285.63	-11.39	-93.44	-324.04
1/12/2009	100	-2.56	-95.92	-294.22	-21.02	-100.68	-327.67

The following can be concluded regarding the SLD measurements:

- It was the first time these deformations were measured at the KSU APT facility. Difficulties during installation were encountered, especially for the SLDs installed in the asphalt layers. The shaded cells in the tables indicate likely unreliable data. Therefore, the installation and data recording, and interpretation for these sensors, must be revised.
- When compared with the permanent deformation recorded from the surface profiles for the KS and MO "fatigue cracking" sections (Figures 5.2 to 5.5), the total permanent deformation recorded by the SLD sensors has the same ranking; the highest total deformation was recorded for the KS2-4 section, while the smallest was recorded for the MO1-4 section. However, the SLD-measured permanent deformations are more than one order of magnitude smaller than the deformations estimated from the surface profile measurements.

- The dynamic deformations values seem more reasonable than the permanent deformations in terms of magnitude.
- The dynamic and the permanent deformation readings recorded by the SLD sensors installed in the MO1-4 and MO2-4 sections are very low, much lower than those recorded in the KS1-4 and KS2-4 sections.

TABLE 5.11 Dynamic Deformations for Kansas Sections (microns)

Date	Passes (x1,000)	KS2-7			KS1-7		
		HMA	Base	Subgrade	HMA	Base	Subgrade
5/5/2006	0	-18.09	-37.19	-66.02	19.01	-23.11	-73.63
5/24/2006	50	-29.86	-61.15	-74.82	-30.70	-19.54	-89.98
5/31/2006	100	-37.67	-72.85	-78.16	-2.94	-23.07	-116.57
6/8/2006	200	-40.42	-81.97	-70.21	3.87	-21.83	-124.4
6/19/2006	300	-39.76	-82.88	-87.42	5.43	-23.08	-128.6
Date	**Passes (x1,000)**	**KS2-4**			**KS1-4**		
		HMA	**Base**	**Subgrade**	**HMA**	**Base**	**Subgrade**
3/13/2006	0	-30.51	-91.40	-479.45	-6.79	-456.94	-66.02
3/31/2006	25	-33.41	-97.75	-507.95	1.00	-456.41	-74.82
4/20/2006	70	-48.68	-127.18	-603.05	-39.05	-448.59	-78.16
4/28/2008	100	-40.02	-116.68	-630.71	-3.53	-454.76	-70.21
9/12/2006	100'	-52.36	-122.53	-521.23	1.57	-471.08	-87.42
9/15/2006	150	-66.39	-147.06	-672.80	68.90	-545.65	-92.73
10/5/2006	200	-77.76	-161.00	-679.09	194.47	-597.31	-104.49
10/10/2006	250	-82.78	-153.71	-661.97	71.28	-601.24	-103.56
10/18/2006	300	-83.00	-154.30	-623.43	143.22	-585.60	-102.20
10/23/2006	350	-82.17	-153.91	-642.63	140.51	-587.91	-99.96
10/30/2006	400	-86.58	-153.96	-615.41	126.77	-573.11	-102.32
11/3/2006	450	-89.23	-155.29	-645.87	63.17	-593.71	-102.57
12/5/2006	500	-88.36	-152.37	-648.32	52.46	-504.88	-100.57
12/13/2006	600	-96.81	-156.47	-631.52	-9.96	-567.33	-104.07
1/12/2007	700	-90.17	-151.90	-554.26	-5.85	-488.77	-93.24
1/19/2007	800	-104.17	-162.46	-644.16	-6.34	-580.94	-110.87
1/26/2007	900	-108.72	-161.75	-636.12	-5.47	-588.37	-111.55
2/15/2007	1,000	-117.48	-178.5	-631.58	15.97	-611.33	-119.63
2/22/2007	1,100	-131.05	-195.14	-741.57	6.64	-682.27	-134.34
3/1/2007	1,200	-127.23	-193.75	-730	6.23	-663.29	-132.88
3/8/2007	1,300	-135.11	-199.1	-740.18	6.65	-689.32	-139.65
3/15/2007	1,400	-135.92	-201.52	-746.85	1.57	-696.16	-141
3/26/2007	1,500	-124.59	-191.51	-680.75	10.92	-638.85	-128.82
4/2/2007	1,600	-134.2	-78.34	-740.8	-28.33	-683.56	-141.4
4/9/2007	1,700	-132.02	-210.73	-752.24	5.51	-682.47	-142.34
4/16/2007	1,800	-142.89	-214.4	-754.45	5.46	-711.15	-150.21
5/3/2007	2,000	-138.42	-202.81	-721.32	5.41	-683.7	-143.29

Note: The shaded cells indicate data that is probably erroneous

TABLE 5.12 Dynamic Deformations for Missouri Sections (mils)

Date	Passes (x1,000)	MO2-7			MO1-7		
		HMA	Base	Subgrade	HMA	Base	Subgrade
6/20/2007	0	-43.75	49.40	-6.13	-129.81	11.88	
7/12/2007	50		50.29	8.75	-170.97	50.29	
7/16/2007	100		59.10	12.14	-217.68	-24.79	
7/20/2007	150		59.94	16.23	-226.8	-26.32	
7/24/2007	200		58.38	16.76	-231.61	-26.32	
7/31/2007	300		59.11	24.77	-250.66	-27.32	
8/10/2007	400		58.93	25.44	-261.81	38.23	
8/21/2007	500		53.00	25.64	-242.74	22.86	
9/4/2007	600		43.44	23.05	-211.975	20.53	
9/14/2007	700		49.12	27.14	-142.135	29.53	
Date	**Passes (x1,000)**	**MO2-4**			**MO1-4**		
		HMA	**Base**	**Subgrade**	**HMA**	**Base**	**Subgrade**
10/22/2007	0	-22.88	-3.12	0.65	-7.25	-0.53	0.60
12/17/2007	50	-57.24	-0.59	0.70	-18.18	-0.55	0.70
1/3/2008	100	-74.31	2.50	3.74	-90.60	1.62	3.82
1/14/2008	200	-83.62	1.00	0.62	-85.70	-0.66	0.71
1/22/2008	300	-97.97	0.83	0.64	-110.36	-2.11	0.73
1/29/2008	400	-112.69	0.64	0.64	-129.58	-3.21	0.59
2/5/2008	500	-136.96	0.80	0.63	-143.05	-4.42	0.61
2/12/2008	600	-157.88	0.76	0.77	-151.98	-4.94	0.73
2/21/2008	700	-163.75	0.97	0.64	-147.92	-4.57	0.52
3/3/2008	800	-179.46	0.68	0.66	-156.31	-4.61	0.64
3/14/2008	900	-187.56	1.00	0.58	-163.99	-5.62	0.61
3/24/2008	1,000	-202.88	0.91	0.62	-163.89	-5.41	0.52
3/31/2008	1,100	-205.29	0.67	0.56	-174.58	-5.85	0.63
4/8/2008	1,200	-202.9	0.63	0.64	-173.19	-6.41	0.52
4/15/2008	1,300	-217.21	0.65	0.61	-182.90	-6.79	0.59
4/22/2008	1,400	-220.22	0.68	0.67	-192.46	-7.08	0.60
5/1/2008	1,500	-223.56	-0.71	0.60	-192.18	-6.61	0.36
5/8/2008	1,600	-226.51	0.72	0.65	-198.52	-7.70	0.64
5/15/2008	1,700			0.65		-7.00	
5/22/2008	1,800	-255.77	2.32	3.66	-201.70	-17.83	12.24
5/29/2008	1,900	-235.16	0.80	0.66	-219.94	-7.49	0.62
6/5/2008	2,000	-300.61	2.65	3.98	-257.90	-22.84	17.40
9/15/2008	2,000	-194.96	-0.82	0.84	-164.90	-3.51	0.87
10/22/2008	2,100	-395.7	0.92	0.72	-261.51	-3.73	0.59

Note: The shaded cells indicate data that is probably erroneous

5.7 Backcalculation of Layer Moduli from the FWD Deflections

The backcalculation analysis was performed using the MODULUS 6.0 backcalculation program (Scullion and Michalak 2006). The measured FWD deflections along with the backcalculated layer moduli are reported in the Appendix I. In the backcalculation process, thicknesses obtained from the rod-and-level measurements in the same spot where FWD tests were performed were used (Figures 2.9 to 2.13). The backcalculated asphalt layer moduli were then corrected to the standard temperature of 68°F, because the temperature recorded at the mid-depth of the asphalt layer during FWD tests varied significantly between 60°F and 94° F.

The backcalculated moduli are reported in Appendix I for each of the four test locations only for the last drop at the 9,000 lb load level (Drop 3). Average values for the four locations are reported in Table 5.13. The table contains only the temperature-corrected HMA layer moduli; the moduli values before temperature correction are given in Appendix I.

Table 5.13 indicates that the backcalculated moduli exhibited large variations along the same test section. Subgrade and base moduli varied from section to section despite the fact that the same granular base and subgrade soils were used in the construction of all test sections. This large variation cannot be attributed to the variation of layer thickness of the constructed pavements since the thicknesses used in the backcalculation process were obtained from the rod-and-level measurements in the same spot where the FWD tests were performed.

The table, as well as Figures 5.21, 5.24, and 5.27, indicate that the backcalculated HMA layer moduli before APT loading was applied had the same relative ranking as the dynamic moduli measured in the laboratory at 25 Hz loading frequency (Tables 3.20 to 3.22); the stiffness values of the KS1, MO1, and IA2 mixes were higher than that of the corresponding mixes from the same state (KS2, MO2, and IA1). All layer moduli changed during APT loading. However, as expected, the subgrade moduli seemed to exhibit the smallest changes with the number of load repetitions. For the asphalt and base layer moduli, no clear trend for this change can be observed.

TABLE 5.13: Average Back-Calculated Moduli (ksi)

Section	Passes (x1,000)	HMA*	Base	Subgrade
	0	571.08	315.73	6.68
	50	762.27	209.5	7.17
KS1-7	100	577.2	143.65	7.4
	0	341.9	294.73	9.2
	50	692.96	150.2	9.5
KS2-7	100	406.64	88.38	9.48
	0	587.01	84.55	10.75
	25	484.16	109.08	9.58
	100	712.57	66.43	11.15
KS1-4	2,000	721.42	237.75	11.68
	0	444.18	87.45	10.48
	25	333.74	41.9	9.65
	100	468.25	33.88	10.33
KS2-4	2,000	437.9	79.4	11.43
	0	708.11	141.45	7.5
	50	727.68	171.25	8.08
	100	671.74	86.75	7.73
MO1-7	700	730.64	183.98	7.8
	0	447.03	156.38	6.4
	50	495.71	142.93	6.73
	100	451.59	87.55	6.58
MO2-7	700	556.99	174.98	6.38
	0	382.98	125.63	8.33
	200	366.65	171	7.4
MO1-4	2,000	517.81	71.08	7.35
	0	319.8	116.23	7.98
	200	277.53	133	6.68
MO2-4	2,000	435.65	66.63	6.78
	0	249.26	166.85	7.1
	25	374.83	129	6.83
IA1-7	50	203.07	81.4	7.17
	0	358.5	77.88	8.13
	25	897.05	59.65	7.75
IA2-7	50	634.2	48.3	8.3
	0	182.95	98.2	10.2
IA1-4	50	476.62	85.53	8.3
	0	246.59	58.3	10.95
IA2-4	50	179.46	148.65	9.6

* after temperature correction

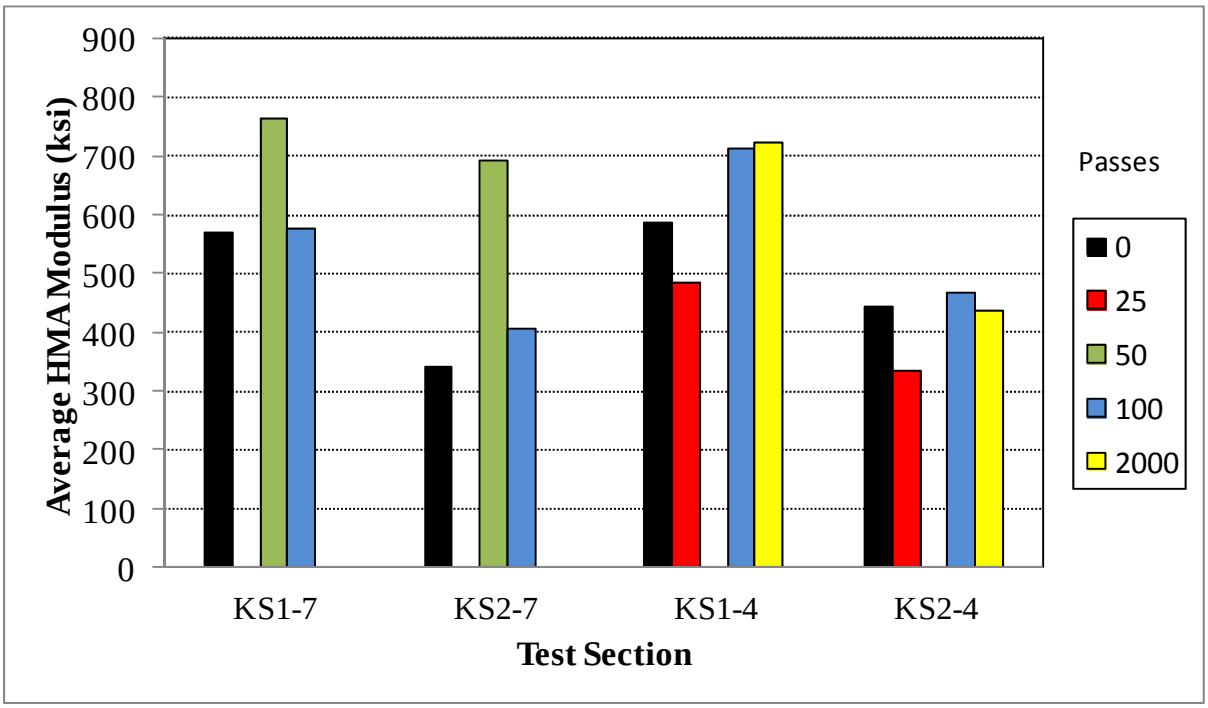

FIGURE 5.21: Back-Calculated AC Modulus for Kansas Sections

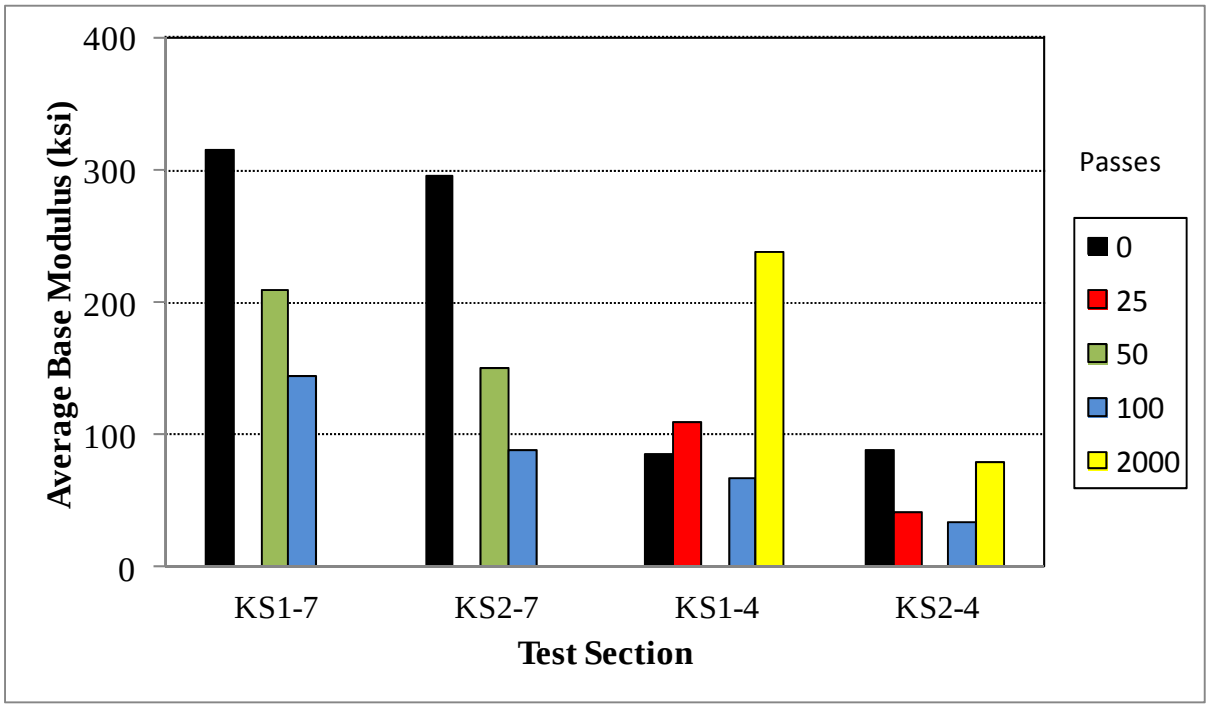

FIGURE 5.22: Back-Calculated Base Modulus for Kansas Sections

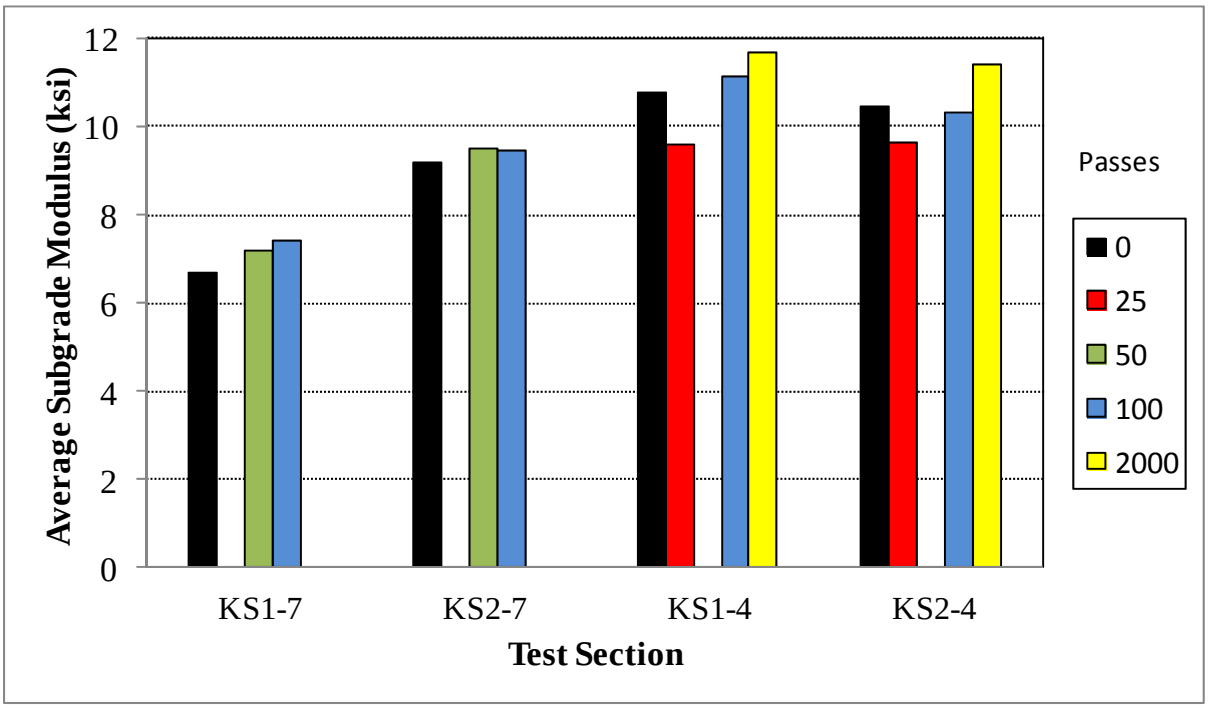

FIGURE 5.23: Back-Calculated Subgrade Modulus for Kansas Sections

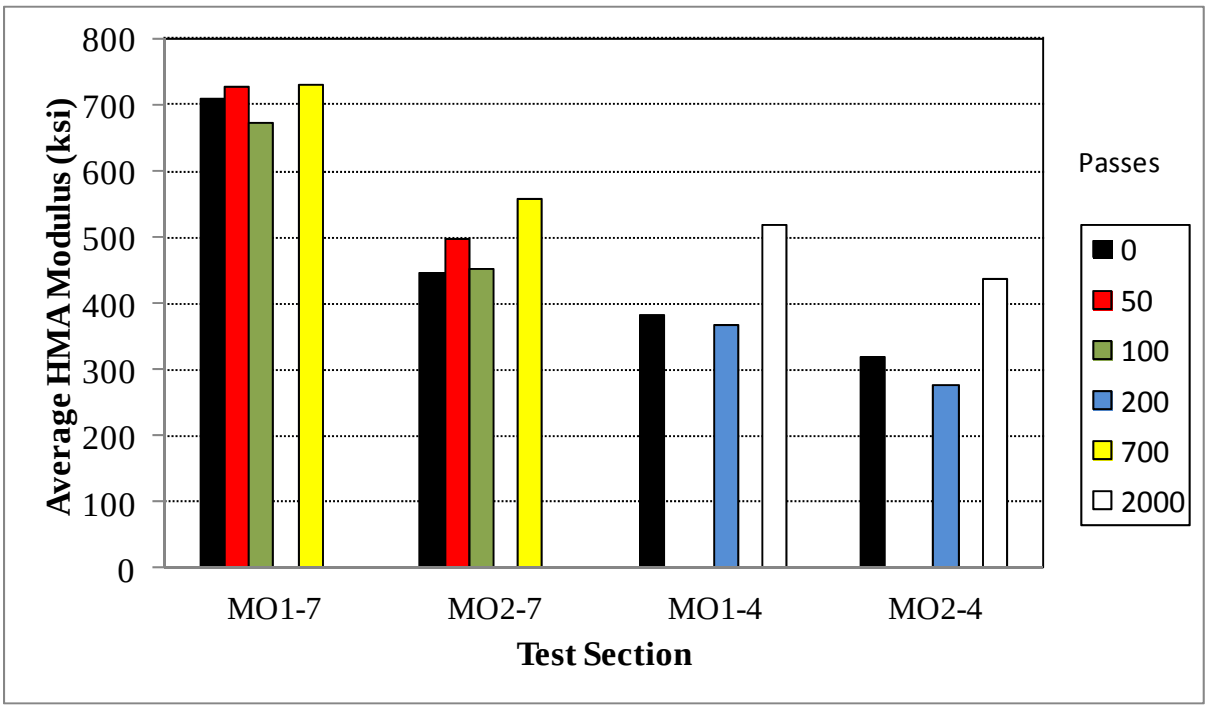

FIGURE 5.24: Back-Calculated AC Modulus for Missouri Sections

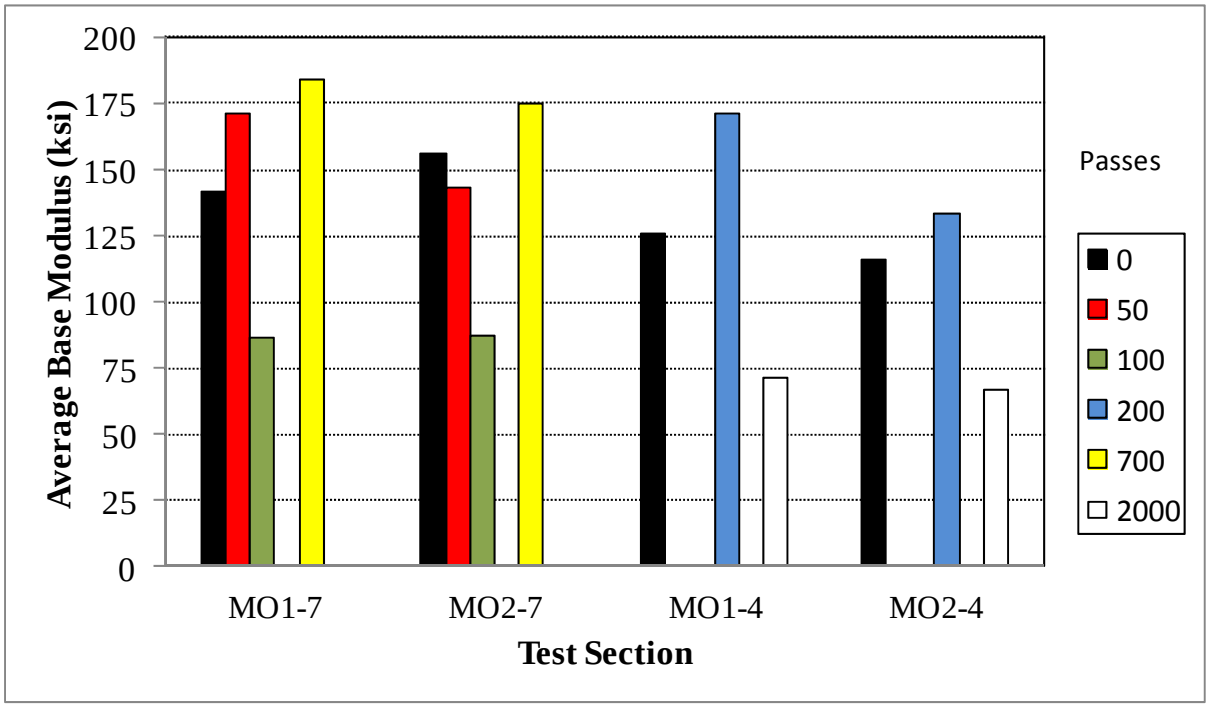

FIGURE 5.25: Back-Calculated Base Modulus for Missouri Sections

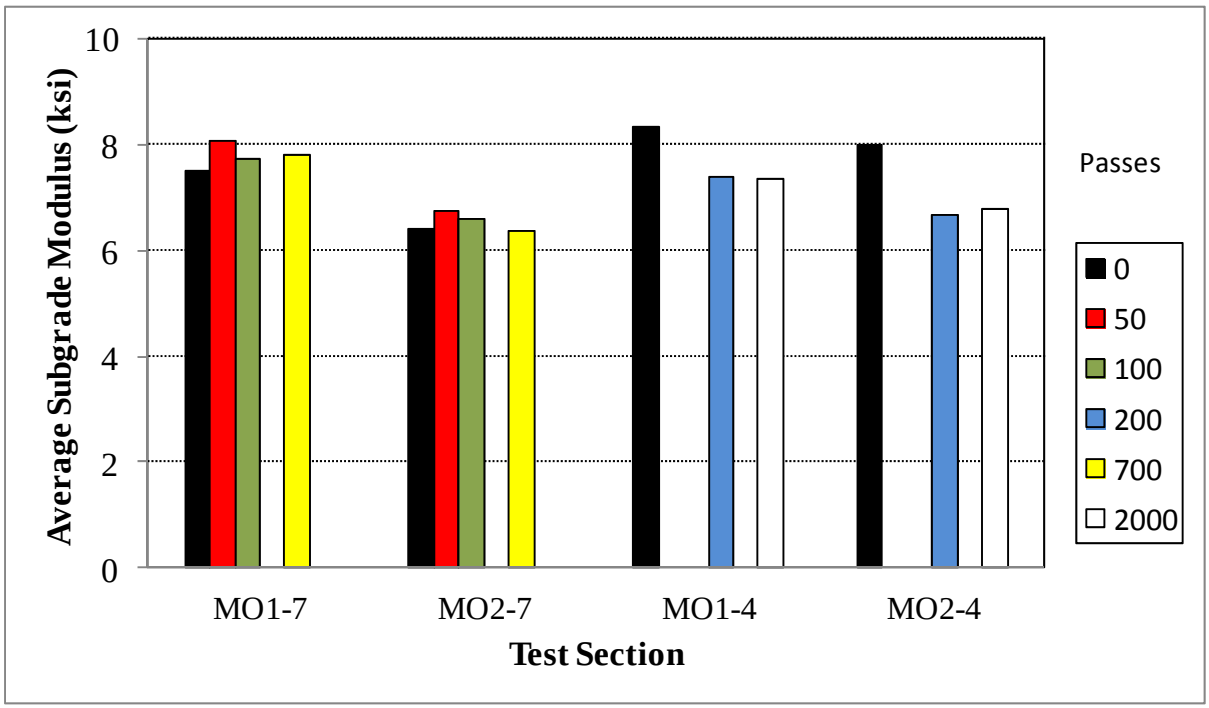

FIGURE 5.26: Back-Calculated Subgrade Modulus for Missouri Sections

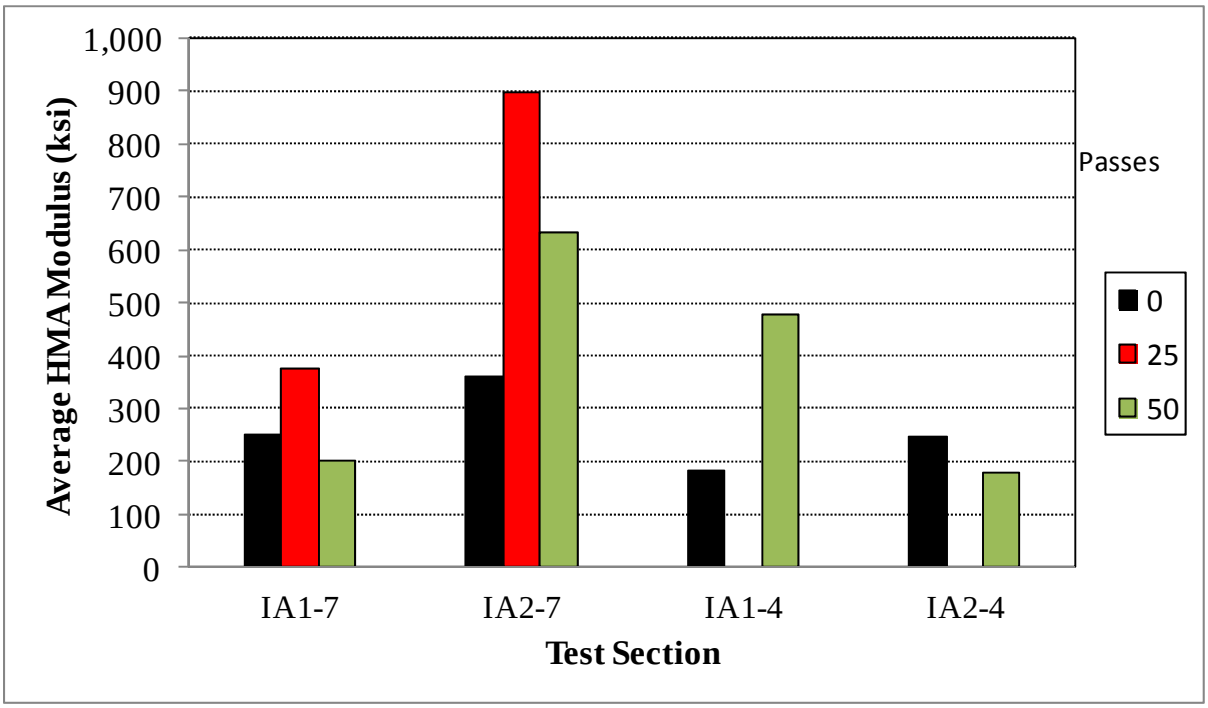

FIGURE 5.27: Back-Calculated AC Modulus for Iowa Sections

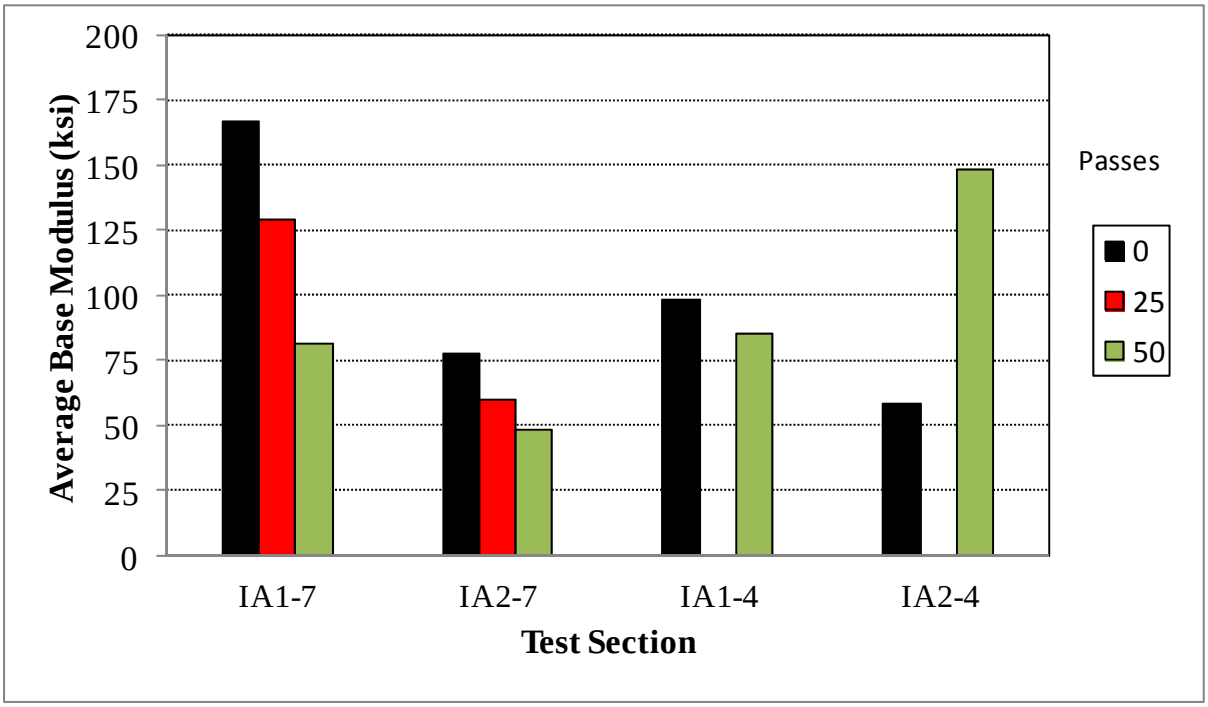

FIGURE 5.28: Back-Calculated Base Modulus for Iowa Sections

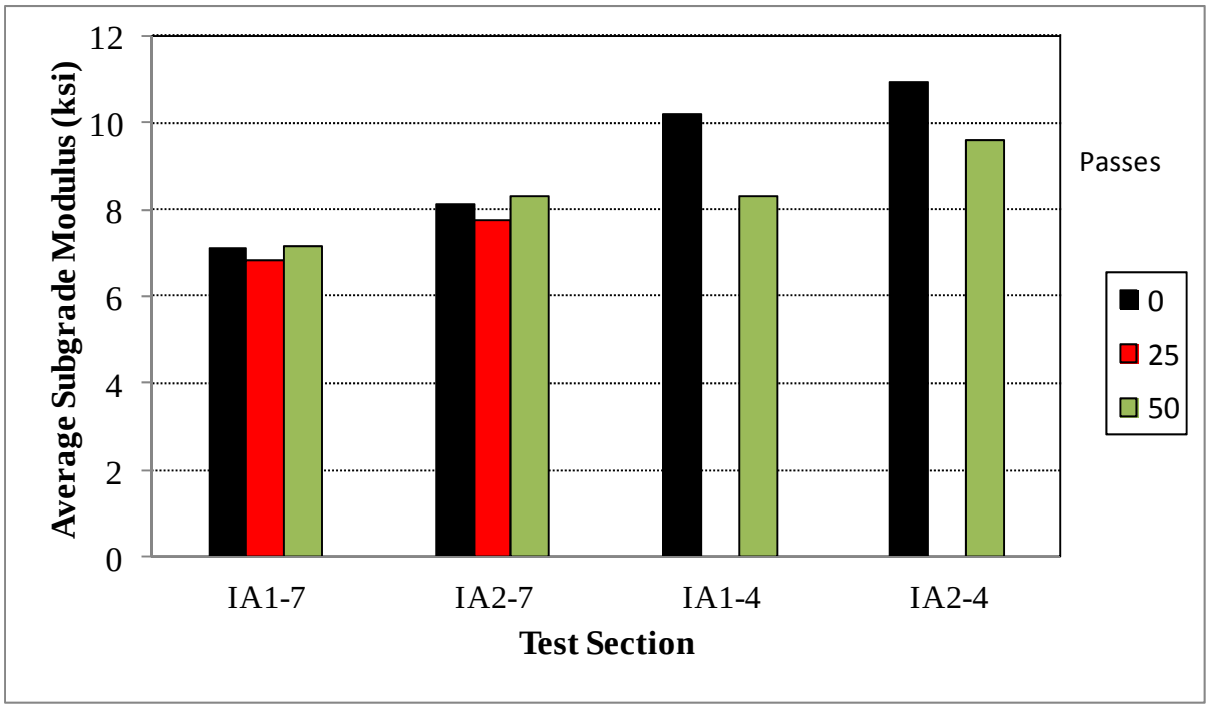

FIGURE 5.29: Back-Calculated Subgrade Modulus for Iowa Sections

5.8. Forensic Evaluation

After the accelerated pavement testing was finished, 6-inch and 4-inch-diameter asphalt cores were taken by Kansas DOT from the wheel path and outside the wheel path areas on each lane. However, only data measured on the cores extracted in the Kansas sections are available. Data for the other sections were lost, even though coring was done in these sections as well. Table 5.11 and Figure 5.30 show the thicknesses of the asphalt concrete layers determined by cores, while Figures 5.31 and 5.32 indicate the exact locations where the cores were extracted. Table 5.12 gives the *insitu* air voids measured on cores extracted from outside wheel path of the "rutting" sections. The data suggests that, except for the MO1 and IA1 mixes, the *insitu* air voids were around 7.0 percent.

TABLE 5.14 HMA Thickness (inches) for Kansas Sections (from cores)

Core No	KS1-7	Core No	KS2-7	Core No	KS1-4	Core No	KS2-4
5	6.92	9	6.50	7	4.12	1	4.00
6	6.88	10	6.65	8	4.09	2	4.17
7	6.98	11	6.94	9	3.95	3	3.96
8	7.48	10	6.68	10	4.08	4	4.13
				11	3.45	5	4.30
				12	3.48	6	3.88
Average Thickness							
	7.06		6.69		3.86		4.08

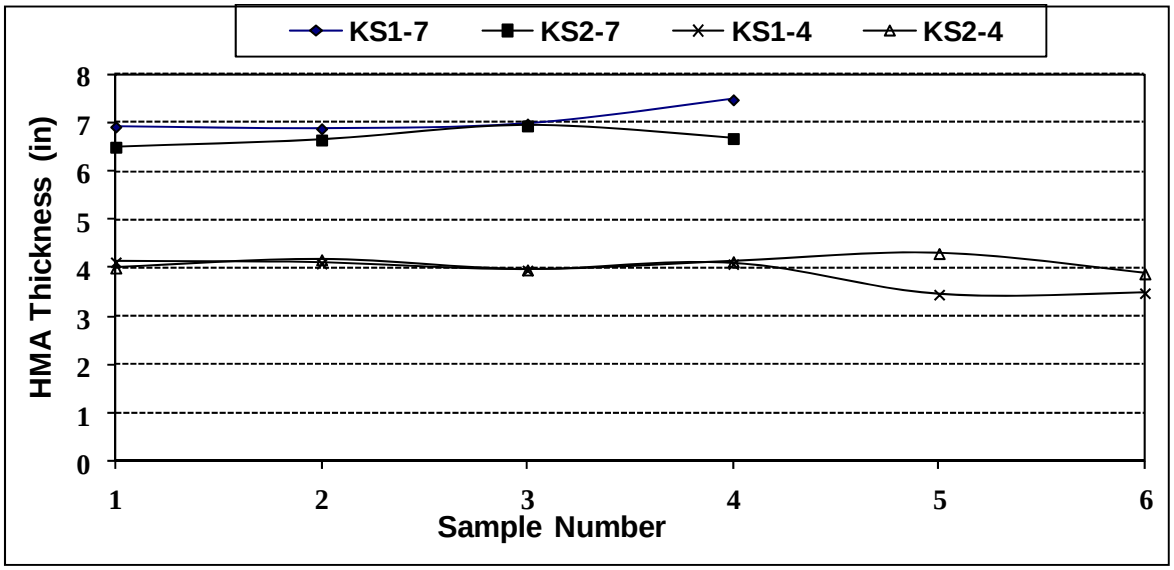

FIGURE 5.30: HMA Thickness for Kansas Sections (from cores)

TABLE 5.15 HMA Core Air Voids (percent) for Rutting Sections

Sample ID	AV %	Sample ID	AV %	Sample ID	AV %
KS1-7 : 07	6.74	MO1-7 : 09	9.45	IA1-7 : 01	8.71
KS1-7 : 08	6.84	MO1-7 : 10	9.56	IA1-7 : 05	8.88
KS1-7 : 09	6.68	MO1-7 ; 11	9.29	IA1-7 : 08	8.43
Average	*6.75*	*Average*	*9.43*	*Average*	*8.67*
KS2-7 : 05	6.93	MO2-7 : 02	6.99	IA2-7 : 02	7.13
KS2-7 : 06	6.84	MO2-7 : 07	7.09	IA2-7 : 04	7.49
KS2-7 : 07	6.74	MO2-7 : 10	7.19	IA2-7 : 05	7.17
Average	*6.84*	*Average*	*7.09*	*Average*	*7.26*

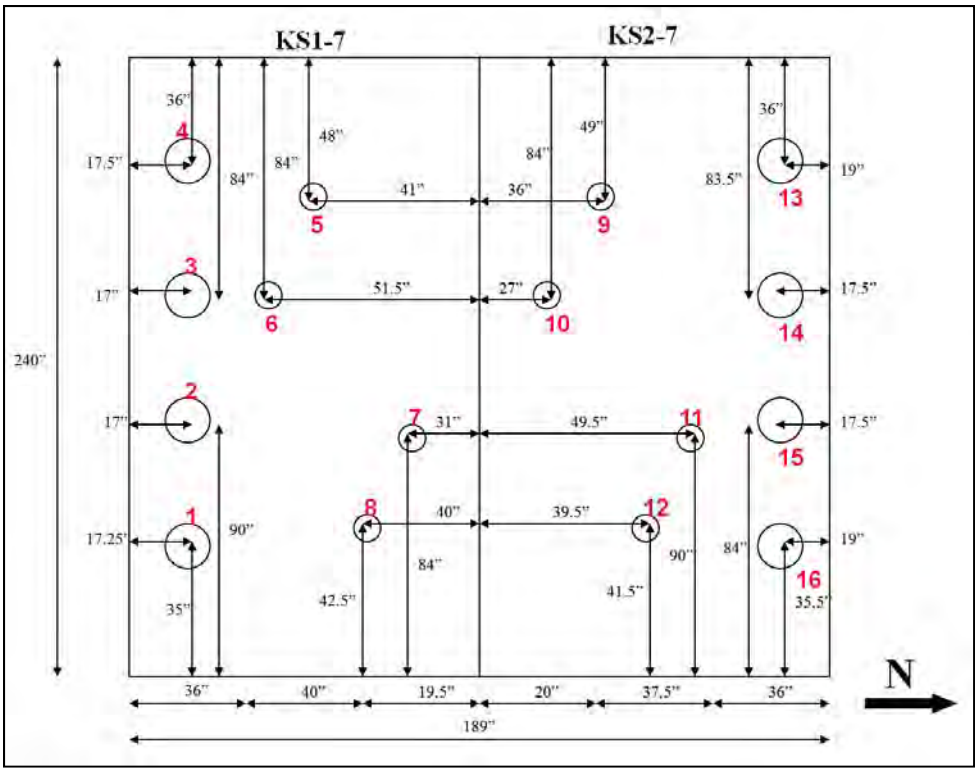

FIGURE 5.31: HMA Layer Thickness from Cores – NN and NS sections

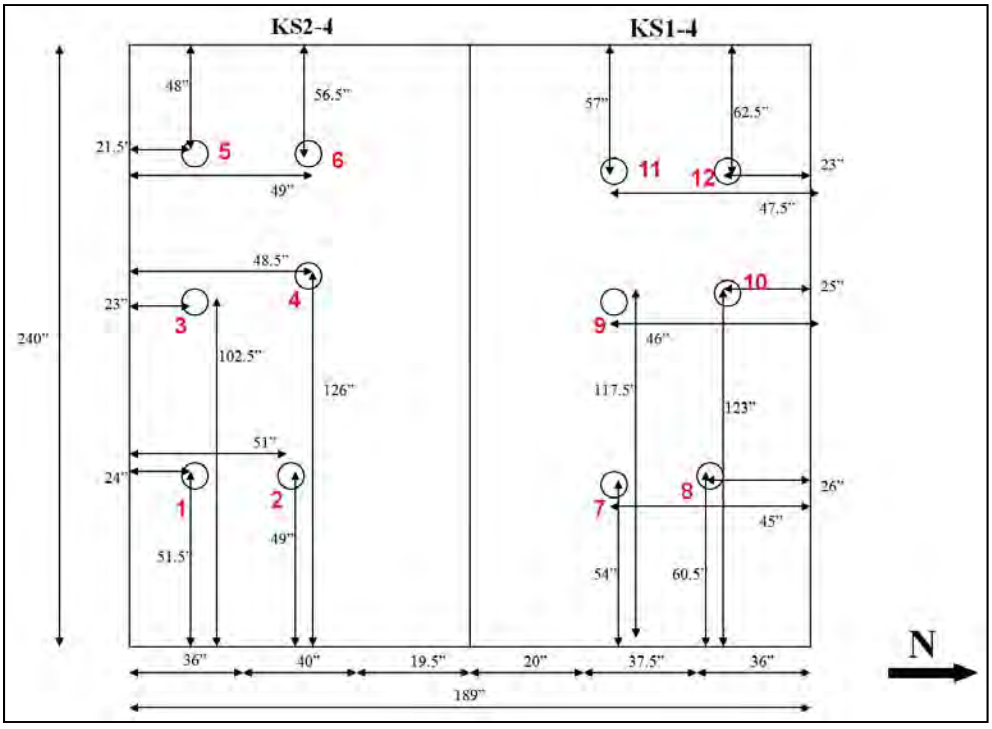

FIGURE 5.32: HMA Layer Thickness from Cores – SN section

Chapter 6: Verification of MEPDG Models for New Flexible Pavement Structures

6.1 Verification of Dynamic Modulus Prediction Model

The NCHRP 1-37A mechanistic-empirical design methodology has a hierarchical approach for specifying design inputs. The dynamic modulus values for Level 1 analysis must be obtained from the testing of asphalt mixtures. However, for level 2 and level 3 analysis, the dynamic modulus is predicted using the Witczak model (NCHRP 2004) and with the revised Witczak model (Bari and Witczak 2006). The later model is preferred since the shear modulus and phase angle of the asphalt binder, values more commonly measured in the United State, are used. The dynamic modulus values can be predicted over a range of temperatures and rates of loading using Equation 6.1 (Bari and Witczak 2006):

$$\log_{10} E^* = -0.349 + 0.754\left(|G_b^*|^{-0.0052}\right)\left(\begin{array}{l} 6.65 - 0.032\rho_{200} + 0.0027\rho_{200}^{\ 2} + 0.011\rho_4 + 0.0001 - 0.011\rho_4^{\ 2} \\ + 0.006\rho_{38} - 0.00014\rho_{38}^{\ 2} - 0.08V_a - 1.06\left(\frac{V_{bef}}{V_a + V_{bef}}\right) \end{array}\right)$$

$$+\left(\frac{2.558 + 0.032V_a + 0.713\left(\frac{V_{bef}}{V_a + V_{bef}}\right) + 0.0124\rho_{38} + 0.0001\rho_{38}^{\ 2} - 0.0098\rho_{34}}{1 + e^{(-0.7814 - 0.5785\log|G_b^*| + 0.8834\log\delta_b)}}\right)$$

(EQUATION 6.1)

Where:

E* = dynamic modulus, psi ;

Gb* = asphalt/bitumen shear modulus, psi;

Va and Vbef = volume of air void and the effective volume of binder, %;

ρ200 = % passing the # 200 (0.075 mm) sieve, by weight;

ρ4, ρ38 and ρ34 = % retained on the # 4 (4.75 mm), 3/8" (9.5 mm) and ¾" (19 mm) sieves; and

δb = Phase angle of asphalt binder /bitumen, degrees.

The revised Witczak model was used to predict the dynamic modulus at five loading frequencies and two temperatures (20oC and 35oC), and the values obtained were compared to the dynamic moduli measured in the laboratory. The comparison, illustrated in Figure 6.1, clearly

demonstrates that the predicted moduli were reasonably close to the measured moduli, the difference being less than 20% for almost all cases. Therefore, the laboratory test results validate the revised Witczak model for dynamic modulus (Equation 6.1).

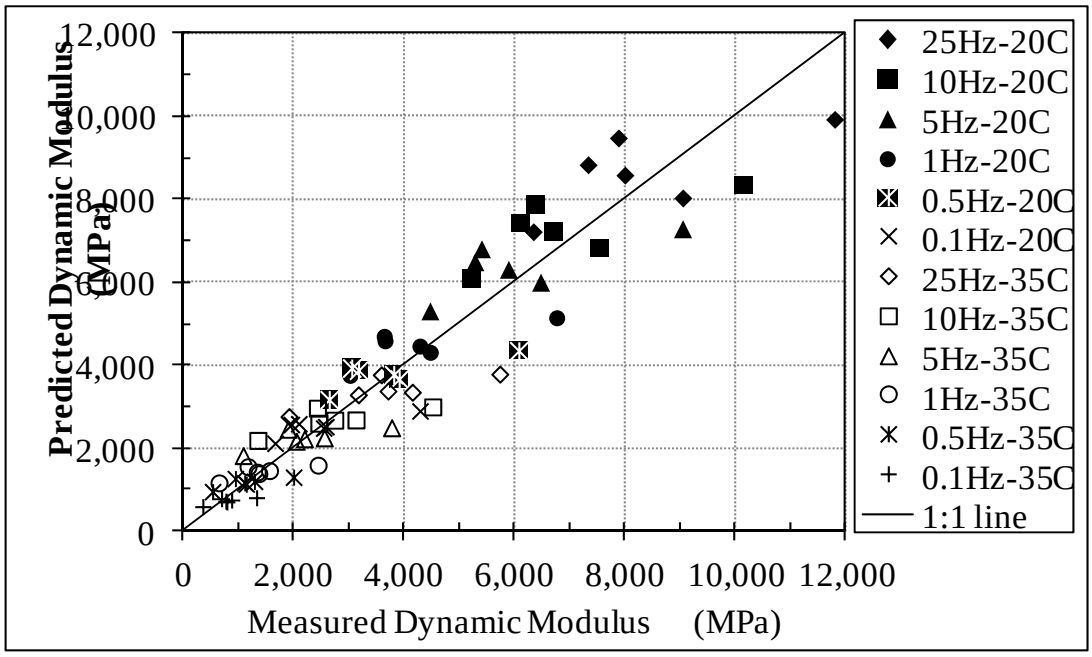

FIGURE 6.1: Predicted vs. Measured Dynamic Moduli

6.2 Verification of Permanent Deformation Prediction Model

The APT experiment at CISL allows for evaluation of the model for predicting the permanent deformation in flexible pavement structures. For all experimental sections, transverse surface profile data recorded several times during accelerated loading was used to measure the permanent deformation at the pavement surface. To validate the prediction model for permanent deformation used in MEPDG, runs of the MEPDG software were done using the pavement materials data and layer thicknesses measured on the 12 experimental sections at 50% reliability level. A new MEPDG climatic file was generated with all temperatures being kept constant and at the temperatures used during the APT testing. No precipitation and 100% cloud cover were also included in the climatic file. For each section, two MEPDG input files were created as follows:

- level 1 input file, in which the laboratory-measured dynamic modulus and phase angle of the asphalt concrete were incorporated

- level 3 input file, in which the binder grade and aggregate gradation data were used as inputs for characterization of asphalt concrete.

The input file included the traffic only with type-5 trucks that have only single axles with dual tires for the rear axles. The analysis period was for 12 months. For each section, traffic volume was calculated such that the total number of axle repetitions in the analysis period would be equal to the number of load repetitions applied in the APT experiment. The same axle load, speed, and standard deviation for the lateral wheel wander as those used in the APT experiment were specified in the file.

Table 6.1 tabulates the computed permanent deformation at the pavement surface by the MEPDG software. Figure 6.2 plots the evolution of the total measured and computed permanent deformation in the Missouri (MO) pavement structures. The R and F that follows the mix code indicate the ‘rutting’ and the “fatigue cracking” sections for that mix, respectively. It can be observed from the chart that the permanent deformation predicted by the MEPDG model for level 1 analysis is typically about three times the corresponding measured deformation. This suggests that the MEPDG model over-predicts permanent deformation.

At level 3 analysis, the MEPDG model indicated the same rutting performance for the two Missouri mixes. However, the mix with the polymer-modified binder (MO1) had a much better performance in the APT rutting experiment than the mix with unmodified binder (MO2). This suggests that the level 3 analysis cannot capture the effect of binder stiffness on the rutting performance of the mix, especially the difference between the unmodified and the polymer-modified binders, since these mixes had the same aggregate structure.

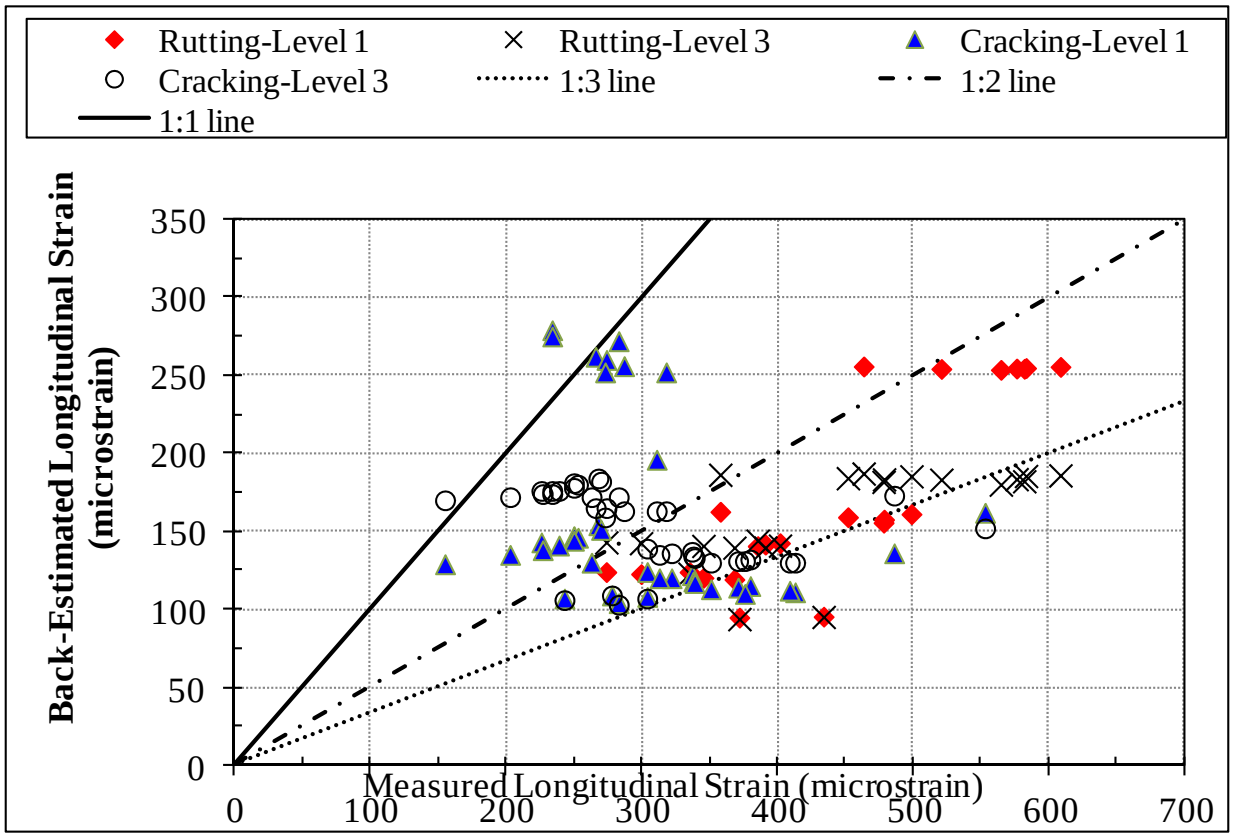

FIGURE 6.2: Measured and Computed Total Permanent Deformation in the Missouri Sections

TABLE 6.1: MEPDG-Computed Permanent Deformation

Section	MEPDG Design Level	MONTH											
		1	**2**	**3**	**4**	**5**	**6**	**7**	**8**	**9**	**10**	**11**	**12**
		Passes											
		25,020	**50,039**	**75,059**	**100,079**	**125,098**	**150,118**	**175,137**	**200,157**	**225,177**	**250,196**	**275,216**	**300,236**
KS1-7	1	0.1626	0.192	0.2113	0.226	0.238	0.2482	0.257	0.2649	0.2721	0.2785	0.2845	0.29
	3	0.1914	0.2291	0.2547	0.2744	0.2906	0.3045	0.3167	0.3275	0.3373	0.3463	0.3546	0.3623
KS2-7	1	0.2162	0.2613	0.2919	0.3158	0.3357	0.3528	0.3681	0.382	0.3947	0.4063	0.4171	0.4271
	3	0.1942	0.2325	0.2581	0.2778	0.294	0.3079	0.32	0.3308	0.3406	0.3496	0.3578	0.3655
		Passes											
		166,798	**333,595**	**500,393**	**667,190**	**833,988**	**1,000,790**	**1,167,580**	**1,334,380**	**1,501,180**	**1,667,980**	**1,834,770**	**2,001,570**
KS1-4	1	0.2515	0.287	0.3098	0.327	0.341	0.3525	0.3622	0.371	0.3789	0.3858	0.3922	0.3982
	3	0.2665	0.3057	0.3311	0.3503	0.3659	0.3791	0.3906	0.4008	0.41	0.4184	0.4264	0.4339
KS2-4	1	0.2929	0.338	0.3675	0.39	0.4084	0.4241	0.4378	0.4501	0.4612	0.4713	0.4807	0.4894
	3	0.2999	0.3451	0.3756	0.3984	0.4169	0.4324	0.446	0.458	0.4688	0.4786	0.4876	0.496
		Passes											
		58,379	**116,758**	**175,137**	**233,517**	**291,896**	**350,275**	**408,654**	**467,033**	**525,412**	**583,791**	**642,170**	**700,550**
MO1-7	1	0.2284	0.2698	0.2972	0.3182	0.3353	0.3498	0.3625	0.3737	0.3838	0.393	0.4014	0.4092
	3	0.2646	0.3166	0.3519	0.3795	0.4023	0.422	0.4394	0.4555	0.4702	0.4836	0.4961	0.5078
MO2-7	1	0.5698	0.7225	0.8301	0.9153	0.9866	1.048	1.102	1.151	1.195	1.236	1.273	1.308
	3	0.2653	0.3173	0.3536	0.3817	0.4049	0.4249	0.4424	0.4581	0.4724	0.4854	0.4975	0.5087
		Passes											
		166,798	**333,595**	**500,393**	**667,190**	**833,988**	**1,000,790**	**1,167,580**	**1,334,380**	**1,501,180**	**1,667,980**	**1,834,770**	**2,001,570**
MO1-4	1	0.2831	0.3232	0.3485	0.3675	0.383	0.396	0.4074	0.417	0.4256	0.4335	0.4403	0.4466
	3	0.3106	0.3572	0.3875	0.4105	0.4293	0.4453	0.4593	0.4718	0.4831	0.4934	0.5029	0.5117
MO2-4	1	0.4112	0.4826	0.53	0.5665	0.5963	0.6217	0.6439	0.6636	0.6814	0.6977	0.7126	0.7264
	3	0.3038	0.3489	0.3782	0.4004	0.4185	0.4338	0.4471	0.459	0.4698	0.4795	0.4885	0.4969
		Passes											
		8,340	**16,680**	**25,020**	**33,360**	**41,699**	**50,039**	**58,379**	**66,719**	**75,059**	**83,399**	**91,739**	**100,079**
IA1-7	1	0.2831	0.350	0.3955	0.4307	0.4598	0.4846	0.5063	0.5256	0.5429	0.5588	0.5733	0.5867
	3	0.1629	0.197	0.2198	0.2378	0.2525	0.2651	0.2761	0.286	0.2949	0.303	0.3105	0.3174
IA2-7	1	0.1319	0.1594	0.1778	0.1919	0.2037	0.2137	0.2225	0.2304	0.2375	0.244	0.2499	0.2555
	3	0.1355	0.1642	0.1838	0.1989	0.2114	0.222	0.2313	0.2396	0.2471	0.254	0.2603	0.2662
		Passes											
		8,340	**16,680**	**25,020**	**33,360**	**41,699**	**50,039**	**58,379**	**66,719**	**75,059**	**83,399**	**91,739**	**100,079**
IA1-4	1	0.1256	0.147	0.1606	0.1707	0.1788	0.1856	0.1916	0.1968	0.2014	0.2056	0.2094	0.213
	3	0.1525	0.1783	0.1947	0.207	0.2167	0.2249	0.232	0.2383	0.2438	0.2489	0.2535	0.2578
IA2-4	1	0.1256	0.147	0.1606	0.1707	0.1788	0.1856	0.1916	0.1968	0.2014	0.2056	0.2094	0.213
	3	0.1251	0.1464	0.1599	0.17	0.1781	0.1849	0.1907	0.1959	0.2005	0.2047	0.2085	0.212

A similar conclusion was reached in local calibration and validation of MEPDG for the state of Utah (Darter et al. 2009). Rutting data on in-service pavement sections were extracted from the Utah Department of Transportation's (UDOT) Pavement Management System database and from the LTPP database of flexible pavements in the state. The study found the following:

- The nationally calibrated MEPDG model predicted adequately rutting only for older pavements constructed using viscosity binder grade (AC-10 and AC-20), before the SuperPave mix design methodology was adopted by UDOT.
- For the newer flexible pavements built using the SuperPave HMA mixes, the nationally calibrated models over-predicted the surface rutting by a factor of 3 (regression slope = 2.922).

6.3 Verification of Pavement Response Model

The model that calculates the stresses and strains that develop in the pavement structure under truck wheel loading is a component of paramount importance in the MEPDG model since distresses and thus, pavement performance, are estimated based on the computed stresses and strains. The MEPDG software does not yield computed stresses and strains as outputs. Rather the software output contains accumulated fatigue-damage parameters for bottom-up fatigue cracks. This fatigue damage is calculated from the value of the longitudinal strain found at the bottom of the asphalt concrete layer in incremental fashion using Miner's law (NCHRP 2004). The fatigue model calculates the allowable repetitions to failure as:

$$N_f = 0.00432 * k_1' * C (1/\varepsilon_t)^{3.9492} (1/E)^{1.281} \quad \textbf{(EQUATION 6.2)}$$

Where:

ε_t = longitudinal strain at the bottom of the asphalt concrete layer;

E – stiffness of the asphalt concrete;

$C = 10^M$ and $M = 4.84*[V_b / (V_a+V_{bef}) – 0.69]$;

V_a and V_{bef} = air voids and effective binder volumetric content (%); and

k_1' = a parameter that depends only on the thickness of the asphalt layers.

For each of the 12 months, the total duration of simulated APT trafficking used in this study, the MEPDG output obtained lists the fatigue damage in percentages, the number of trucks passing over the designed pavement structure, and the estimated stiffness of the asphalt concrete layers. Since the number of trucks in the simulations was the same as the number of axle passes in the APT experiment, it was possible to compute the damage calculated by the MEPDG model for a single pass of the APT axle for each month and then to "back-estimate" the longitudinal strain at the bottom of the asphalt concrete with Equation 6.2. The back-estimated longitudinal strains are given in Table 6.2, while the measured longitudinal strains are given in Table 6.3.

Figure 6.3 shows the correspondence between the measured longitudinal strains and the corresponding values "back-estimated" from the MEPDG output in the level 1 and level 3 analysis. The figure suggests that for the "rutting" sections, the measured strains were between two and three times higher that the computed strains, at both levels 1 and 3. For the thinner sections, the computed strains were closer to the measured strains in some cases, but in many cases were two to three times higher that the measured strains. This suggests the algorithms for computing the response in the MEPDG model should be revised and further validated; the under-prediction of strains may result in under-designed pavement structures for fatigue resistance.

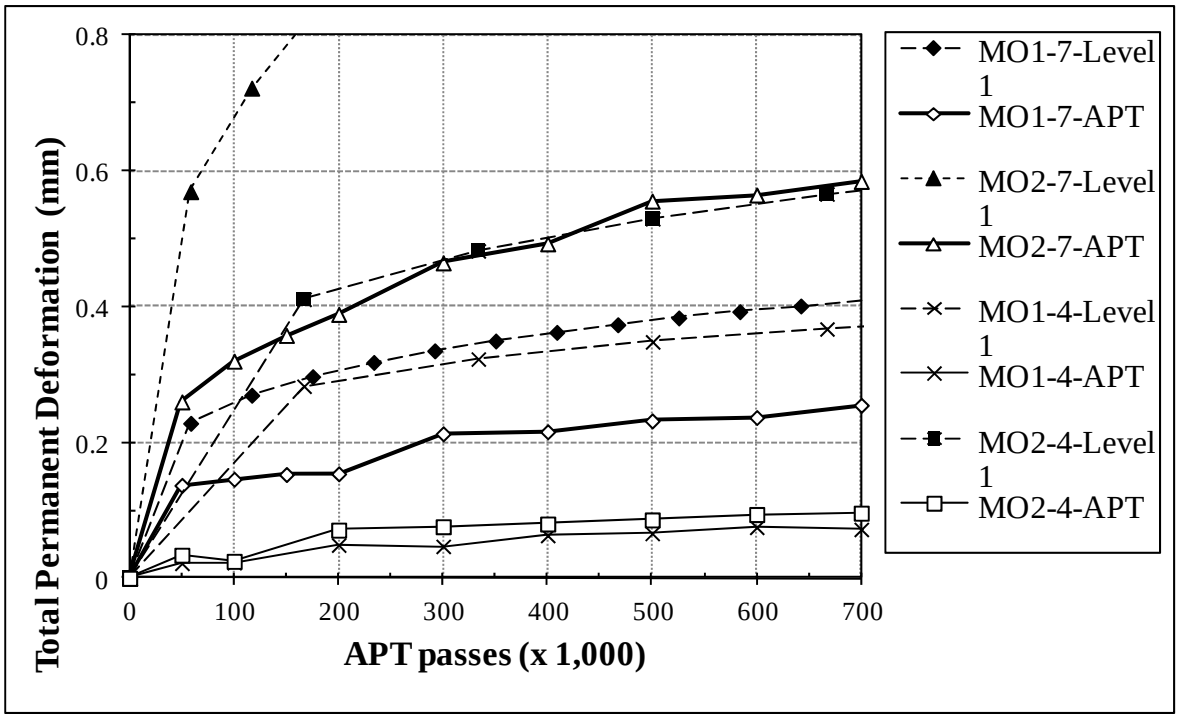

FIGURE 6.3 Measured and Back-Estimated Longitudinal Strains

In addition to back-estimating the longitudinal strains from the MEPDG software output, the MEPDG- calculated pavement response was obtained by performing runs with JULEA software. JULEA is the linear-elastic model incorporated in the MEPDG software for computing response of new flexible pavement structures. The JULEA software models the wheel load as uniformly distributed over circular areas.

TABLE 6.2: Back-Estimated Longitudinal Strains (microstrains) - MEPDG

	Month	1	2	3	4	5	6	7	8	9	10	11	12
KS1-7	**Traffic**	**25,020**	**50,039**	**75,059**	**100,079**	**125,098**	**150,118**	**175,137**	**200,157**	**225,177**	**250,196**	**275,216**	**300,236**
	Leve1	124.90	124.22	123.55	122.72	122.09	121.67	120.51	120.31	119.95	119.60	119.26	119.26
	Leve3	143.97	143.46	142.96	142.48	142.02	141.58	141.16	140.75	140.36	137.97	139.62	139.62
KS2-7	Leve1	134.44	139.69	139.30	140.65	141.94	139.93	141.25	142.52	140.62	141.91	141.62	141.62
	Leve3	145.43	144.85	144.16	144.09	142.38	143.06	141.40	140.93	140.49	141.23	139.66	139.66
KS1-4	**Traffic**	**166,798**	**333,595**	**500,393**	**667,190**	**833,988**	**1,000,790**	**1,167,580**	**1,334,380**	**1,501,180**	**1,667,980**	**1,834,770**	**2,001,570**
	Leve1	123.69	121.55	120.44	120.38	118.27	116.97	114.86	114.42	113.17	111.07	111.58	110.11
	Leve3	138.56	137.30	136.21	134.60	133.90	132.51	131.89	131.30	130.03	129.51	130.44	131.14
KS2-4	Leve1	162.21	161.16	159.99	158.78	158.04	157.34	155.84	155.63	154.62	154.06	153.12	152.26
	Leve3	151.65	153.36	149.45	140.22	132.47	124.80	118.60	112.40	107.90	102.07	98.62	95.34
MO1-7	**Traffic**	**58,379**	**116,758**	**175,137**	**233,517**	**291,896**	**350,275**	**408,654**	**467,033**	**525,412**	**583,791**	**642,170**	**700,550**
	Leve1	162.64	161.12	159.15	158.43	157.62	155.64	153.67	152.97	152.31	151.68	149.83	149.04
	Leve3	186.38	185.38	184.18	183.91	183.43	181.83	181.39	182.11	180.57	180.18	179.81	179.29
MO2-7	Leve1	255.78	255.55	254.81	255.15	254.47	254.33	254.22	253.64	255.04	252.09	251.13	254.65
	Leve3	187.14	185.95	185.57	184.68	183.56	182.20	183.22	180.07	179.57	181.70	178.63	178.00
MO1-4	**Traffic**	**166,798**	**333,595**	**500,393**	**667,190**	**833,988**	**1,000,790**	**1,167,580**	**1,334,380**	**1,501,180**	**1,667,980**	**1,834,770**	**2,001,570**
	Leve1	154.10	150.84	147.23	145.75	143.98	143.15	141.13	137.81	135.82	135.23	130.40	129.47
	Leve3	183.99	182.30	180.96	179.57	177.70	175.86	176.22	174.47	172.75	172.15	171.58	169.62
MO2-4	Leve1	278.55	275.42	272.22	269.90	265.89	265.94	261.57	259.60	257.76	256.04	252.16	252.16
	Leve3	175.98	174.15	172.39	170.68	169.28	168.45	165.35	164.62	163.93	163.28	162.67	159.10
IA1-7	**Traffic**	**8,340**	**16,680**	**25,020**	**33,360**	**41,699**	**50,039**	**58,379**	**66,719**	**75,059**	**83,399**	**91,739**	**100,079**
	Leve1	262.00	261.67	260.97	260.31	260.06	259.83	258.54	257.31	259.66	255.00	257.41	256.05
	Leve3	156.42	155.85	155.56	155.55	155.04	154.54	154.07	153.61	153.18	153.27	152.88	151.82
IA2-7	Leve1	95.58	95.43	95.63	95.28	95.21	95.40	95.08	95.03	94.99	94.96	93.44	94.82
	Leve3	95.58	95.65	95.55	95.51	95.49	95.19	95.46	95.46	95.19	95.21	95.23	93.82
IA1-4	**Traffic**	**8,340**	**16,680**	**25,020**	**33,360**	**41,699**	**50,039**	**58,379**	**66,719**	**75,059**	**83,399**	**91,739**	**100,079**
	Leve1	195.76	193.97	191.71	190.65	188.88	188.37	185.68	184.23	184.00	181.61	180.43	179.85
	Leve3	162.84	161.53	160.59	158.74	157.91	157.13	156.39	155.69	153.96	154.42	152.77	151.89
IA2-4	Leve1	109.41	108.77	107.90	107.63	107.40	106.75	106.59	106.45	105.92	105.42	104.95	104.23
	Leve3	108.61	107.85	107.49	106.90	106.79	105.81	105.75	104.84	104.84	104.42	103.59	103.42

TABLE 6.3: Measured Longitudinal Strain (microstrain)

Section	KS1-7		KS2-7	KS1-4		KS2-4	IA1-7	IA2-7		IA1-4		IA2-4	MO1-7		MO2-7	MO1-4		MO2-4	
Passes (x 1,000)	East	West	East	East	West	West	East	East	West	East	West	East	East	West	East	East	West	East	West
0	158	162	179				385	357		306		259	274	292	344	264	296	214	236
5											311	278							
25				195	252	377													
30												304							
50	283	265	335					434	834			243	347	368	464	106	267	201	216
70				254	301	489													
100		300	385	267	324	484		372		2933		283	499		609				
150				257	351	553							417		563				
200		345	402	291	370								452		583		268	224	243
250				290	355	109							961		1121		265	250	186
300		368	391	306	371								479		576		265	269	183
350				301	374								432	525	582		270	280	189
400				301	372								363		521		274	283	
450				302	372								408		565		244	280	
500				297	346												250	283	
600				305	369												253	290	
700				284	343												273	286	
800				310	366												250	269	
900				317	367												228	284	342
1,000				339													226	269	
1,100				371													239	266	
1,200				380													254	286	
1,300				371													227	274	
1,400				371													227	274	
1,500				351													486	1248	
1,600				376													203	287	
1,700				413													598	2475	
1,800				409													263	318	
2,000				376													155	273	

The calculation of the theoretical strains with the JULEA software was done assuming the loading configuration shown in Figure 6.4. The figure also shows the points where the stresses and strains were computed (output points). The layer moduli were the same as those used in the MEPDG inputs for Level 3 design analysis and are given in Table 6.4.

Results of the JULEA calculations are given in Tables 6.5 to 6.7. They suggest the following:

- The computed maximum longitudinal strains at the bottom of the HMA layer are not always in between the two wheels. Depending on pavement layer thicknesses and stiffnesses, they can also develop right underneath the center of one circular loading area.
- Longitudinal strains computed by the JULEA model are different from those back-estimated from the MEPDG output. This suggests that the MEPDG software code should be verified for accuracy.
- With a very few exceptions, the longitudinal strains computed by the JULEA model and back-estimated from the MEPDG output are smaller than the corresponding measured strains. This can lead to severe under-estimation of the fatigue damage for the bottom-up cracking and thus, to over-estimation of the fatigue cracking lives of the flexible pavement structures.
- Vertical stresses computed by JULEA at the top of the subgrade layer were very different from the measured values (given in Tables 5.5 and 5.6). The measured values were almost twice the JULEA-computed values for the “fatigue cracking” sections.

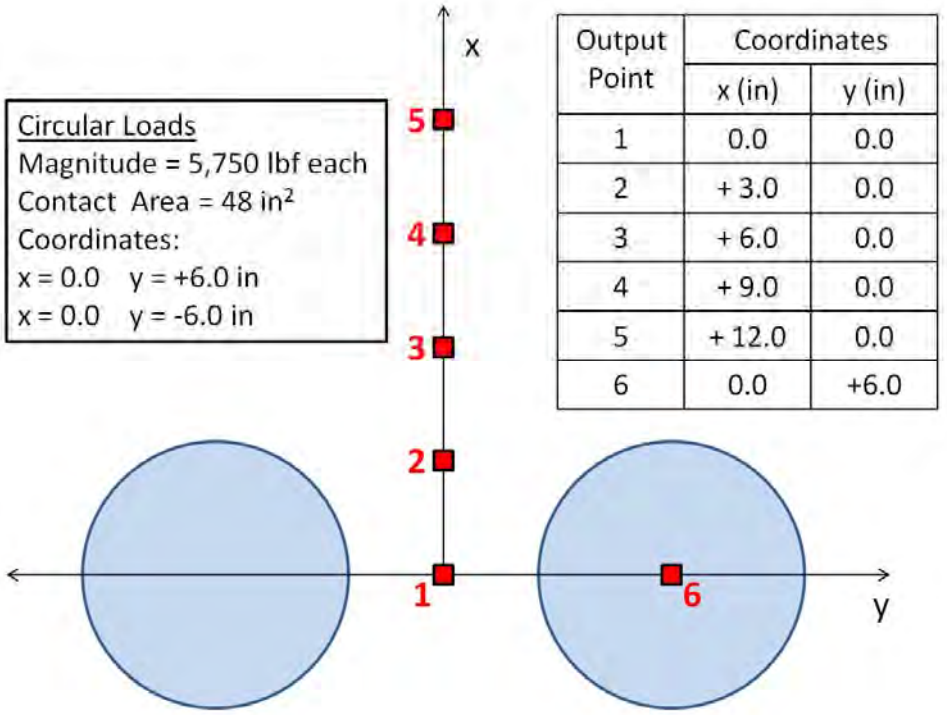

Output Point	Coordinates	
	x (in)	y (in)
1	0.0	0.0
2	+ 3.0	0.0
3	+ 6.0	0.0
4	+ 9.0	0.0
5	+ 12.0	0.0
6	0.0	+6.0

FIGURE 6.4: Loading Model for JULEA Calculations

TABLE 6.4: Modulus of Elasticity Used in the JULEA Calculations (ksi)

Layer Number	1	2	3	4	5	6	7	8	9
Layer type	AC1	AC2	AC3	AC4	AC5	AC6	Top base	Bottom base	Subgrade
Thickness	0.5	0.5	1	1	1	3	2	4	
KS1-4	1,933.6	1,613.0	1,370.4	1,193.9	1,085.6	-	82.19	82.29	7.14
KS2-4	1,808.6	1,488.5	1,248.2	1,074.7	968.99	-	48.57	48.63	7.14
MO1-4	1,491	1,262.6	1,087	957.84	877.96	-	48.57	48.63	7.14
MO2-4	1,662.9	1,391.4	1,184.7	1,033.8	941.13	-	48.57	48.63	7.14
IA1-4	978.14	768.12	608.96	495.69	428.52	-	82.19	82.29	7.14
IA2-4	1,549.7	1,298.5	1,106.6	966.41	880.14	-	152.63	152.82	7.14
KS1-7	657.01	550.22	464.0	400.03	360.78	312.71	82.19	82.29	7.14
KS2-7	657.76	546.67	457.6	391.94	351.9	303.29	82.19	82.29	7.14
MO1-7	583.53	495.46	423.26	368.96	335.27	293.87	48.57	48.63	7.14
MO2-7	583.53	495.46	423.26	368.96	335.27	293.87	48.57	48.63	7.14
IA1-7	470.47	396.66	336.11	290.7	262.67	228.80	82.19	82.29	7.14
IA2-7	561.1	471.41	398.44	344.02	310.54	270.15	152.63	152.82	7.14

TABLE 6.5: JULEA Computed Horizontal Strains at the Bottom of the HMA Layer

Test Section	Test Temp. (°C)	Longitudinal Strain (microstrain)						Transverse Strain (microstrain)					
		Output Point (see Figure 6.4)						Output Point (see Figure 6.4)					
		1	2	3	4	5	6	1	2	3	4	5	6
KS1-4	20	178	136	66.3	21.8	-0.79	182	44.9	54.2	66.3	66	58.6	129
KS2-4	20	222	177	89.4	30.4	-1.58	232	67.8	76.7	89.4	87.3	76.8	162
MO1-4	20	241	185	90	27.2	-5.64	246	63.5	75.2	90	88.6	77.7	171
MO2-4	20	233	179	89.5	29.2	-3.07	237	65.3	76	89.5	87.6	76.9	165
IA1-4	20	236	165	57	0.24	-20	254	8	28	57	64	57	180
IA2-4	20	133	95.3	37.5	6.59	-5.49	143	11.2	22.1	37.5	40.8	36.9	103
KS1-7	35	185	148	78.4	30.2	6.05	183	71.6	74.7	78.4	75.8	67.8	127
KS2-7	35	187	149	78.6	30	5.72	185	71.6	74.8	78.6	76	68	128
MO1-7	35	246	199	109	43.2	8	242	102	105	109	104	91.9	167
MO2-7	35	246	199	109	43.2	8	242	102	105	109	104	91.9	167
IA1-7	35	200	156	75.8	22.9	-1.13	200	65.7	70	75.8	74.4	66.4	138
IA2-7	35	121	92.4	42	11.3	-0.52	122	33.5	36.9	42	42.5	38.6	85.3

TABLE 6.6: JULEA-Computed Vertical Compressive Stress at the Top of the Subgrade Layer

Test Section	Test Temperature (°C)	Stress (psi)	
		Point 1	Point 6
KS1-4	20	5.66	5.34
KS2-4	20	6.54	6.17
MO1-4	20	6.9	6.47
MO2-4	20	6.7	6.29
IA1-4	20	6.93	6.57
IA2-4	20	4.95	4.71
KS1-7	35	4.5	4.25
KS2-7	35	4.53	4.27
MO1-7	35	5.2	4.89
MO2-7	35	5.2	4.89
IA1-7	35	5.01	4.72
IA2-7	35	4.02	3.8

TABLE 6.7: Summary of Computed and Measured Longitudinal Strains (microstrain)

Section	Predicted			Measured	
	MEPDG		JULEA	Sensor	
	Level 1	Level 3	Level 3	E	W
KS1-7	125	144	185	158	162
KS2-7	134	145	187	179	
KS1-4	124	139	182	195	252
KS2-4	162	152	232		377
MO1-7	163	186	246	274	292
MO2-7	256	187	246	344	
MO1-4	154	184	246	264	296
MO2-4	279	176	237	214	236
IA1-7	262	156	200	385	
IA2-7	96	96	122	357	
IA1-4	196	163	254	306	311
IA2-4	109	109	143	259	

6.4 Evaluation of Laboratory Rutting Tests

The Hamburg wheel-tracking device (HWTD), the asphalt pavement analyzer (APA), and the repetitive shear at constant height (RSCH) tests were conducted to evaluate the rutting performance of the six asphalt mixes in the laboratory. These tests are used by several state agencies in the United States to screen out the mixes with high rutting susceptibility.

Test specimens were compacted with a Superpave gyratory compactor. Target densities of the specimens were those corresponding to the in-place densities obtained during construction of the CISL test sections. HWTD sample size was 6 inches in diameter and 2.44 inches in thickness, whereas APA sample size was 6 inches in diameter and 2.95 inches in thickness. The RSCH test samples are nominally 2 inches in height and 6 inches in diameter. The HWTD tests were conducted at Kansas State University whereas the bituminous research section of the Missouri Department of Transportation (MODOT) conducted the APA tests. Superpave Shear Tester RSCH tests for rutting at 35°C were conducted by the Asphalt Institute up to 50,000 cycles per AASHTO T 320-07 protocol

A summary of performance ranking of each test is presented in Table 6.8. The ranking suggests that results of the Hamburg wheel-tracking device (HWTD) correlate the best with

results of the APT experiment, followed by those from APA. A poor correlation can be observed between results from the RSCH test and results of the other three tests.

It is important to note here that the conclusions on the comparison with the laboratory rutting tests are valid only for 95°F (35°C) test temperature, since the APT experiment and all the laboratory rutting tests were performed at this temperature to obtain a direct comparison. The test samples were also fabricated at the same air voids as measured in the as-constructed APT sections (before any loading). All three laboratory tests are typically done at higher temperatures: HWTD at 122°F (50°C) and APA at 131°F (55°C), and at different air voids.

TABLE 6.8: Rutting Performance Ranking of Six Asphalt Concrete Mixes

Mix ID	Repeated load tests, all performed at 35°C				Ranking			
	APT Perm. Def. (mm) @ 100,000 passes	HWDT depth (mm) @ 20,000 cycles	APA depth (mm) @ 8,000 cycles	RSCH g_{perm} (mm) @ 50,000 cycles	APT	HWDT	APA	RSCH
KS-1	4.8	4.69	1.08	0.79	2	4	1	1
KS-2	5.5	4.21	1.59	2.47	3	3	2	6
MO-1	3.7	3.47	1.71	1.72	1	1	3	3
MO-2	8.1	3.96	2.15	1.68	4	2	4	2
IA-1	31.1	10.15	2.27	2.31	6	6	5	5
IA-2	11.8	5.31	3.18	2.03	5	5	6	4

Chapter 7: Conclusions and Recommendations

The Midwest States Accelerated Pavement Testing Pooled-Funds program, financed by the transportation departments of four Midwestern states, sponsored one accelerated pavement testing (APT) project aimed to validate the response and distress models in the Mechanistic-Empirical Pavement Design Guide (MEPDG) using accelerated pavement testing (APT). Twelve pavement sections were constructed with six different Superpave asphalt mixes. Each section was loaded by an APT machine with a 23-kip (103 kN), single-axle load in bi-directional mode at a constant speed of approximately 7 mph (12 km/h). The lateral wheel wander followed a truncated normal distribution with a standard deviation of 6 inches. The tire inflation pressure was maintained at 100psi (690 kPa).

Six pavement sections were tested in a "rutting" experiment conducted at 95ºF (35ºC) and six sections were tested in a "fatigue-cracking" experiment conducted at 68ºF (20ºC). The sections were instrumented with strain gages, pressure cells, and displacement sensors to measure pavement response under APT loading. An extensive laboratory testing program was conducted to determine properties of the materials used in the construction of the experimental sections. Simulation of the APT testing was conducted with MEPDG software for level 1 and 3 analyses, at a 50% reliability level. The material properties, loading, and climatic conditions during the APT test were used in the MEPDG input and the results of the simulations were compared with the results of the APT test.

Major findings of this research study are as follows:

- The revised Witczak model (Bari and Witczak 2006) predicts with adequate accuracy the dynamic modulus of asphalt concrete mixes at the studied range of loading frequency (0.1 to 25 Hz) and temperatures (20 to 35ºC)**.**
- The MEPDG structural response model for flexible pavements under-predicts the longitudinal strains at the bottom of the asphalt concrete layers, the structural response used for predicting alligator cracking. The computed strains were two to three times smaller than the measured strains.

- The laboratory beam-fatigue tests performed at 68ºF (20°C) indicate that a single model for the fatigue life of asphalt concrete, such as the one incorporated in MEPDG, does not effectively predict the fatigue life of all mixes.
- The experiment could not verify either the bottom-up or top-down fatigue-cracking models incorporated in the MEPDG, since only one of the twelve tested sections exhibited cracking. Moreover, the longitudinal crack that appeared in that section healed before the load repetitions ended.
- The MEPDG model predicted about three times higher total permanent deformation at the pavement surface than the measured permanent deformation. This is because the MEPDG prediction model was calibrated with data collected on in-service asphalt pavements built before the Superpave design method was implemented in the United States. Introduction of this mix design significantly reduced the rutting of asphalt mixes.
- MEPDG level 3 analysis does not capture the effect of binder stiffness on the rutting performance of the mix. This is especially true for rutting performance of mixes with polymer- modified binders.
- The longitudinal strains computed by the JULEA linear-elastic model were different from those back-estimated from the MEPDG outputs. Since the MEPDG software uses the JULEA model for pavement response calculations, it is suggested that the MEPDG software code be verified for accuracy.
- With a very few exceptions, the longitudinal strains computed by the JULEA model and back-estimated from the MEPDG output were smaller than the corresponding measured strains. This can lead to severe under-estimation of the fatigue damage for the bottom-up cracking and to over-estimation of the fatigue-cracking lives of the flexible pavement structures.
- Vertical stresses computed by JULEA at the top of the subgrade layer were very different from the measured values. The JULEA-computed values were about half of the measured values for the “fatigue-cracking” sections. This can

lead to under-prediction of rutting in the subgrade layers of flexible pavement structures.

- Laboratory rutting tests performed at 95°F (35°C) indicate results of the Hamburg wheel- tracking device (HWTD) test correlate the best with results of the APT experiment, followed by those from the asphalt pavement analyzer (APA). It is important to note here that conclusions on the comparison with the laboratory rutting tests are valid only for 95°F (35°C) test temperature, since the APT experiment and all laboratory rutting tests were performed at this temperature to obtain a direct comparison. All three laboratory tests are typically done at higher temperatures: HWTD at 122°F (50^{o}C) and APA at 131°F (55^{o}C).

The following recommendations can be made based on the results obtained in this study:

- The MEPDG model for permanent deformation in flexible pavement structures should be calibrated only with *insitu* data collected on asphalt pavements designed and built after adoption of the Superpave binder specifications and mix design. This is needed since it appears the current nationally calibrated rutting model over-predicts the permanent deformation by a factor of two to three.
- It is recommended that the MEPDG structural response and performance models be further revised, evaluated, and validated with results from a wider spectrum of instrumented APT and in-service pavement sections, since the accuracy of the response model is critical for achieving an efficient design of flexible pavement structures.
- The MEPDG software code should be verified for accuracy since it appears the computed strains are different than the strains computed by the JULEA software.
- The detailed database of material properties and response and performance of full-scale asphalt pavement structures under-accelerated testing assembled in

this research should be used for the validation of other models for predicting response and distress in flexible pavements.

- As a screening test, results of the Hamburg wheel tracking device (HWTD) test are better related to the *insitu* rutting performance of asphalt mixes than results of the asphalt pavement analyzer (APA). Therefore, HWTD is recommended as a better tool for studying rutting performance of asphalt mixtures.

References

AASHTO. 2008. *Mechanistic-Empirical Pavement Design Guide: A Manual of Practice*. Interim Edition, Washington, D.C.

AASHTO T 27. 2002. Standard Method of Test for Sieve Analysis of Fine and Coarse Aggregates. Washington, D.C.

AASHTO T 166. 2000. Standard Method of Test for Bulk Specific Gravity of Compacted Asphalt Using Saturated Surface-Dry Specimens. Washington, D.C.

AASHTO T 307-99. 1999. Standard Method of Test for Determining the Resilient Modulus of Soils and Aggregate Materials. Washington, D.C.

AASHTO T 315. 2008. Standard Method of Test for Determining the Rheological Properties of Asphalt Binder Using a Dynamic Shear Rheometer (DSR). Washington, D.C.

AASHTO T 324. 2004. Standard Method of Test for Hamburg Wheel-Track Testing of Compacted Hot-Mix Asphalt (HMA). Washington, D.C.

AASHTO TP-62-03. 2003. Standard Method of Test for Determining Dynamic Modulus of Hot-Mix Asphalt Concrete Mixes. Washington, D.C.

ASTM C 131. 1996. Standard Test Method for Resistance to Degradation of Small-Size Coarse Aggregate by Abrasion and Impact in the Los Angeles Machine. ASTM International, West Conshohocken, PA.

ASTM D 698-00. 2000. Standard Test Methods for Laboratory Compaction Characteristics of Soil Using Standard Effort (12,400 ft-lbf/ft3 (600 kN-m/m3)). ASTM International, West Conshohocken, PA.

ASTM D 4318-00. 2000. Standard Test Methods for Liquid Limit, Plastic Limit, and Plasticity Index of Soils. ASTM International, West Conshohocken, PA.

ASTM D 4791. 1999. Standard Test Method for Flat Particles, Elongated Particles, or Flat and Elongated Particles in Coarse Aggregate. ASTM International, West Conshohocken, PA.

ASTM D 5821. 1995. Standard Test Method for Determining the Percentage of Fractured Particles in Coarse Aggregate. ASTM International, West Conshohocken, PA.

Bari, J. and M. W. Witczak. 2006. "Development of a New Revised Version of the Witczak E* Predictive Model for Hot-Mix Asphalt Mixtures." *Journal of the Association of Asphalt Paving Technologists.* Vol. 75, pp 381-423, Savannah, GA.

Brown, E. R., S. P. Kandhal, and J. Zhang. 2001. *Performance Testing for Hot-Mix Asphalt. National Center for Asphalt Technology (NCAT)*. Report No. 01-05, Auburn University, Auburn, AL.

D'Angelo, J., S. Vanikar, and K. Petros. 2004. "Designing Tomorrow's Pavements: The New Guide and Software May Become the National Approach for Creating and Rehabilitating Roadway Surfaces." *Public Roads*. Volume 68 (2), Federal Highway Administration, Washington, D.C.

Darter, M., L. Titus-Glover, and H. L. Von Quintus. 2009. *Implementation of the Mechanistic-Empirical Pavement Design Guide in Utah: Validation, Calibration, and Development of the UDOT MEPDG User's Guide.* Utah Department of Transportation Research Division.

Huang, B. 2000. *Fundamental Characterization and Numerical Simulation of Large Stone Asphalt Mixtures.* Ph.D. dissertation, Louisiana State University, Baton Rouge.

Huang, Y. H. 2004. *Pavement Analysis and Design*. Prentice Hall, Upper Saddle River, N.J.

KT-50. 2005. Kansas Test Method. *Uncompacted Void Content of Fine Aggregate.* Kansas Department of Transportation, Topeka, KS.

Kansas Department of Transportation. 1990. *Standard Specifications for State Road and Bridge Construction, Metric Version*. Topeka, KS.

McGee, K. H. *Overview of the AASHTO 2002 Guide.* http://www.2002guide.com/ Accessed May 2004.

Melhem, H. G. 1997. *Development of an Accelerated Testing Laboratory for Highway Research in Kansas*, Report No. FHWA-KS-97/5, Kansas Department of Transportation, Topeka, KS.

Melhem, H. G. 1999. *Accelerated Testing for Studying Pavement Design and Performance (FY97-98)*, Report No. FHWA-KS-99-2, Kansas Department of Transportation, Topeka, KS.

Melhem, H. G. and F. Sheffield. 2000. *Accelerated Testing for Studying Pavement Design and Performance (FY 99)*, Report No. FHWA-KS-99-7, Kansas Department of Transportation, Topeka, KS.

Melhem, H. G., R. Swart and S. Walker. 2003a. *Accelerated Testing for Studying Pavement Design and Performance (FY 2000): Effectiveness of Fiber-Reinforced and Plain, Ultra-Thin Concrete Overlays on Portland Cement Concrete Pavement (PCCP).* Report No. FHWA-KS-02-6, Topeka, KS.

Melhem, H. G., R. Swart and S. Walker. 2003b. *Accelerated Testing for Studying Pavement Design and Performance (FY 2001): Evaluation of the Performance of Permeable and Semi-Permeable Unbound Granular Bases under Portland Cement Concrete Pavement (PCCP) Slabs and Alternate Load Transfer Devices for Joint Repair.* Report No. FHWA-KS-02-7, Topeka, KS.

NCHRP. *Guide for Mechanistic-Empirical Design of New and Rehabilitated Pavement Structures: Final Report*. 2004. NCHRP Project 1-37A. Transportation Research Board, National Research Council, Washington, D.C.

Onyango, M. 2009. *Verification of Mechanistic Prediction Models for Permanent Deformation in Asphalt Mixes Using Accelerated Pavement Testing,* Doctoral Dissertation, Kansas State University, Manhattan.

Roberts, F. L., P. S. Kandhal, E. R. Brown, D. Y. Lee and T. W. Kennedy. 1996. *Hot-Mix Asphalt Materials, Mixture Design, and Construction*. National Asphalt Pavement Association, Lanham, MD.

Romanoschi, S. A., M. Hossain, P. Lewis and O. Dumitru. 2003. *Performance of Foamed Asphalt Stabilized Base In Full-Depth Reclaimed Asphalt Pavement* (CISL EXPERIMENT NO. 11), Final Report, Midwest States Accelerated Pavement Testing Pooled Fund Program.

Romanoschi, S. A., M. Hossain, P. Lewis and O. Dumitru. 2008. *Evaluation of The Chemical Stabilized Subgrade Soil.* (CISL EXPERIMENT NO. 12), Final Report, Midwest States Accelerated Pavement Testing Pooled Fund Program.

Romanoschi, S. A., C. Dumitru, P. Lewis and M. Hossain. 2009. *Thin-Bonded Rigid Overlays on PCC and HMA*. (CISL EXPERIMENT NO. 13), Final Report, Midwest States Accelerated Pavement Testing Pooled Fund Program.

Scullion, T. and C. H. Michalak. 2006. *MODULUS 6.0 User's Manual*. Texas Transportation Institute, College Station, TX.

Von Quintus, H. and L. Scofield. 2003. *2002 Design Guide – Implementation*. Presented at the Workshop on 2002 AASHTO Design Guide, 82nd Annual Meeting of the Transportation Research Board, January 11, 2003.

Witczak, M. W., K. Kaloush, T. Pellinen, M. El-Basyouny and H. Von Quintus. 2002. *Simple Performance Tests for Superpave Mix Designs*. Report 465. National Cooperative Highway Research Program, Transportation Research Board, National Research Council, Washington, D.C.

Yoder, E. J. and M. W. Witczak. 1975. *Principles of Pavement Design*. Wiley, New York.

AD ASTRA PER ASPERA

Kansas

Department of Transportation